

# **Conversion of Biocompounds to Methane using Advanced Reforming Processes**

Hafizah Binti Abdul Halim Yun

Submitted in accordance with the requirements for the degree of  
Doctor of Philosophy

The University of Leeds  
School of Chemical and Process Engineering

July 2017

The candidate confirms that the work submitted is her own, except where work which has formed part of jointly-authored publications has been included. The contribution of the candidate and the other authors to this work has been explicitly indicated below. The candidate confirms that appropriate credit has been given within the thesis where reference has been made to the work of others.

The following jointly authored publications are based on Chapter 3, 4, 5 and 6 within this thesis. The candidate Hafizah Binti Abdul Halim Yun performed the experimental and modelling work, and writing up the initial draft of the publications. Dr. Valerie Dupont was co-supervisor of the research work and made suggestions and involved in editing to the draft papers.

1. Hafizah Abdul Halim Yun and Valerie Dupont. Thermodynamic analysis of methanation of palm empty fruit bunch (PEFB) pyrolysis oil with and without in situ CO<sub>2</sub> sorption. *AIMS Energy*, 2015. 3(4): 774-797.
2. Valerie Dupont, Hafizah A. H. Yun, Robert White and Lifita Tande. High methane conversion efficiency by low temperature steam reforming of bio-feedstock. In: 4<sup>th</sup> International Conference on Renewable Energy Gas Technology, 22-23 May 2017, Pacengo (Verona), Italy.
3. Hafizah Abdul Halim Yun and Valerie Dupont. Plant modelling for bio-methane production from palm empty fruit bunch (PEFB). Poster published in: 4<sup>th</sup> International Conference on Renewable Energy Gas Technology, 22-23 May 2017, Pacengo (Verona), Italy.

4. Hafizah Abdul Halim Yun and Valerie Dupont. Experimental studies on methanation of acetic acid as bio-oil surrogate in a packed bed reactor.  
[To be submitted].

This copy has been supplied on the understanding that it is copyright material and that no quotation from the thesis may be published without proper acknowledgement.

The right of Hafizah Binti Abdul Halim Yun to be identified as Author of this work has been asserted by her in accordance with the Copyright, Designs and Patents Act 1988.

© 2017 The University of Leeds and Hafizah Binti Abdul Halim Yun

## **Acknowledgements**

In the name of Allah, the Almighty, for giving me His blessing and granting me the strengths, patience and capabilities to accomplish my studies successfully. I would like to express my gratitude to my supervisor, Dr. Valerie Dupont for the encouragement and guidance for me to accomplish my thesis. Without her continued support and interest, this thesis would not have been the same as presented here. I am also thankful to the technicians and the entire staffs of School of Chemical and Process Engineering (SCAPE). I would like to show my appreciation to all of my colleagues in the Energy Research Institute for your warm welcoming, encouraging and friendliness, especially to Dr. Zaheer Abbas, Dr. Zainab Ibrahim, Oluwafemi, Lifita Tande and Sergio Ramirez who were also doing their research works supervised by Dr. Valerie Dupont.

I am also very grateful to my friends, Ella Karim, Su Sanip, Juniza, Zatul Iffah, Fatimah Ibrahim, Juliana, Nor Zalina, Ummi Hani, Nurshafawati, Nur Zaima, Shazana Hilda, Sharifah Alawieyah, Farhanis, Kamla and Yee Sing for always being there for me, when I really need your supports. Not to be forgotten, I would like to acknowledge my financial support for this research, Ministry of Education Malaysia, as well as to Universiti Malaysia Sarawak (UNIMAS) for giving me the opportunity to pursue my PhD study in the University of Leeds. I owe my loving thanks to my parents for their patience and for loving me endlessly. Without their understanding, it has been impossible for me to complete this thesis.

## Abstract

The conversion of biomass to synthetic natural gas (SNG) draws great interest in the world because it is a sustainable energy resource, where it can replace the fossil natural gas and reduce environmental problems. Common technologies for CH<sub>4</sub> production are based on the gasification of biomass at high temperature followed by CO and CO<sub>2</sub> methanation, but it is energetically costly and complex, requiring separate reforming stages due to the heavy tar production from the gasification process, and multiple cooling stages of the methanation due to the large exothermicity of this equilibrium driven reaction.

Therefore, the main focus of this research was to attempt to address these issues by introducing the low temperature steam reforming (LTSR) process of bio-oil for CH<sub>4</sub> production via fast pyrolysis of biomass using palm empty fruit bunch (PEFB) as the biomass feedstock, a significant renewable waste of the palm oil industry, currently underexploited. One advantage of proposing the pyrolysis route vs. gasification, was the conversion of PEFB into bio-oil without generation of heavy tars, and at lower temperature than gasification due to the lower endothermicity of the chemical process favouring oil product rather than gas. Another advantage was the lower exothermicity of the subsequent methanation step by using bio-oil as feed rather than CO and CO<sub>2</sub>. It was intended that bringing closer the enthalpy changes of the gasification by pyrolysis and of the methanation by feedstock substitution, would improve the efficiencies of heat transfers between the two.

Chemical Equilibrium and Applications (CEA) program was used to analyse thermodynamic equilibrium for conversion PEFB bio-oil to CH<sub>4</sub> using LTSR process. It was found that CH<sub>4</sub> production was favoured in the 130–330 °C range and at around molar steam to carbon ratio of 3 at atmospheric pressure. Using the optimum conditions observed from the thermodynamic equilibrium calculations, the experimental feasibility of CH<sub>4</sub> production from acetic acid as single compound bio-oil surrogate via LTSR was performed at bench scale by using nickel-calcium aluminate (Ni/Ca-Al<sub>2</sub>O<sub>3</sub>) catalyst in a packed bed reactor. The optimum conditions for CH<sub>4</sub> production were obtained at 400 °C and S/C of 2 with 15.7 wt.% at atmospheric pressure. As undesirable carbon formation on the catalyst was observed during the experiments, it is suggested to operate at higher pressure (20–30 bar), which is commonly used in the CO and CO<sub>2</sub> methanation industrial processes. Based on the Aspen Plus simulation results for the full flow biorefinery of CH<sub>4</sub> production from PEFB via fast pyrolysis followed by LTSR of the bio-oil, the estimated thermal efficiencies were 74.3% (net power and heat demand not included in the process) and 81.1% (net power and heat demand included in the process) were comparable to the current biomass gasification technology to CH<sub>4</sub> production via syngas followed by CO and CO<sub>2</sub> methanation.

## Table of Contents

<b>Acknowledgements.....</b>	<b>iv</b>
<b>Abstract.....</b>	<b>v</b>
<b>Table of Contents.....</b>	<b>vii</b>
<b>List of Tables.....</b>	<b>x</b>
<b>List of Figures.....</b>	<b>xiv</b>
<b>Abbreviations.....</b>	<b>xix</b>
<b>Nomenclature.....</b>	<b>xxii</b>
<b>Formulae.....</b>	<b>xxiv</b>
<b>Chapter 1 .....</b>	<b>1</b>
1.1 Global energy consumption .....	1
1.2 Environmental impact .....	6
1.3 Synthetic Natural Gas (SNG) production .....	9
1.4 Palm oil biomass as a modern fuel .....	12
1.5 Research aims and objectives .....	16
<b>Chapter 2 .....</b>	<b>20</b>
2.1 Introduction .....	20
2.2 SNG production from coal and fossil fuel .....	21
2.2.1 Coal as feedstock .....	22
2.2.2 Fossil fuel as the feedstock .....	27
2.3 Current technologies for synthetic natural gas (SNG) production .....	28
2.3.1 Lurgi process .....	28
2.3.2 TREMP process of Haldor Topsøe .....	30
2.3.3 RMP process .....	31
2.3.4 Non-adiabatic process (IRMA cooled reactor) .....	33
2.4 Techniques for CH <sub>4</sub> product stream purification.....	36
2.4.1 Physical and chemical absorption .....	37
2.4.2 Pressure swing adsorption (PSA) .....	39
2.4.3 Membrane separation .....	39
2.4.4 Cryogenic separation.....	40
2.4.5 Comparison between the upgrading techniques.....	40

2.5	Thermochemical conversion of biomass to SNG production .....	42
2.5.1	Bio-oil production from pyrolysis.....	46
2.5.2	Properties of bio-oil.....	49
2.5.3	Palm empty fruit bunch (PEFB) pyrolysis oil.....	53
2.6	Methanation catalyst.....	55
2.7	Summary .....	63
<b>Chapter 3</b>	<b>.....</b>	<b>64</b>
3.1	Introduction.....	64
3.2	Modelling approach.....	65
3.2.1	Chemical Equilibrium and Applications (CEA) program.....	65
3.2.2	Aspen Plus program .....	66
3.3	Experimental approach.....	73
3.3.1	Research materials.....	73
3.3.2	Experimental set-up.....	75
3.3.3	Solids and liquids characterization .....	80
<b>Chapter 4</b>	<b>.....</b>	<b>85</b>
4.1	Introduction.....	85
4.2	Methane production from bio-oil via steam reforming process.....	86
4.3	Thermodynamic equilibrium calculations for CH <sub>4</sub> production from PEFB bio-oil.....	89
4.4	PEFB bio-oil composition and choice of model bio-oil .....	94
4.5	Thermodynamic equilibrium analysis of direct CH <sub>4</sub> production from PEFB bio-oil by LTSR with and without in situ CO <sub>2</sub> sorption .....	99
4.5.1	Expected outputs from stoichiometry of LTSR and SE- LTSR reactions and relevance to LTSR process design.....	99
4.5.2	Temperature and S/C effects on the equilibria of isothermal LTSR and SE-LTSR of PEFB bio-oil model.....	104
4.5.3	Pressure effects in the equilibria of isothermal LTSR and SE-LTSR of PEFB bio-oil model .....	110
4.5.4	Enthalpy balances for the equilibria of isothermal LTSR and SE-LTSR of PEFB bio-oil model .....	111
4.5.5	Comparison between isothermal and adiabatic LTSR processes for CH <sub>4</sub> production from PEFB bio-oil model ....	117
4.6	Conclusion .....	122
<b>Chapter 5</b>	<b>.....</b>	<b>124</b>
5.1	Introduction.....	124
5.2	CH <sub>4</sub> production from acetic acid by LTSR.....	125



5.3	Experimental procedure.....	127
5.4	Calculations of process outputs .....	129
5.5	Influence of process parameters on CH <sub>4</sub> production from acetic acid by LTSR .....	132
5.5.1	Temperature effect .....	133
5.5.2	Steam to carbon ratio (S/C) effect .....	136
5.6	Catalyst characterization.....	138
5.6.1	Catalyst phases and crystallite size with X-ray diffraction (XRD).....	139
5.6.2	Carbon in the catalyst by TGA and elemental analysis ...	140
5.6.3	Morphology and elemental composition of catalyst with SEM-EDX .....	144
5.7	Product distributions of acetic acid conversion via LTSR.....	147
5.8	Conclusion .....	151
<b>Chapter 6</b>	<b>.....</b>	<b>152</b>
6.1	Introduction .....	152
6.2	Process description.....	153
6.3	Biomass pre-treatment and characterisation in the model .....	154
6.4	Bio-oil production modelling.....	159
6.5	Methanation reactor modelling.....	166
6.6	CH <sub>4</sub> stream purification modelling.....	168
6.7	Heat integration.....	174
6.7.1	Process 1 (air-preheater integration) .....	174
6.7.2	Process 2 (steam integration).....	178
6.7.3	Process 3 (vaporized bio-oil integration).....	179
6.7.4	Process 4 (air-preheater, steam and re-vaporized bio-oil integration).....	180
6.8	Process performance .....	181
6.9	Conclusion .....	198
<b>Chapter 7</b>	<b>.....</b>	<b>199</b>
7.1	Introduction .....	199
7.2	Conclusions .....	200
7.2.1	Conclusion of experimental results.....	201
7.2.2	Conclusion of plant scale modelling results .....	202
7.2.3	Final conclusions .....	203
7.3	Recommendations for future work .....	204

## List of Tables

Table 1.1	Primary energy supply share in Malaysia [5]. (ktoe are kilotons of oil equivalent).....	4
Table 1.2	Natural gas compositions in volume percentage in Europe's gas fields [6].....	4
Table 1.3	The average daily activity of a fossil fuel 2000 MW power plant [6].....	7
Table 1.4	The top holders of world conventional natural gas reserves in 2015 [15]. ....	10
Table 1.5	Share percentage (%) of natural gas consumption by sectors in 2013. ....	11
Table 1.6	Comparative cost for palm oil compared to soybean and rapeseed in December 2016 [31].....	14
Table 1.7	Palm oil biomass components and quantity produced in Malaysia [36-38]. ....	15
Table 2.1	Compositions of gas produced in volume percentage (vol.%) from different type of coal. ....	24
Table 2.2	Commercial Lurgi plants for coal gasification process [49].....	26
Table 2.3	The operating temperatures between several type of processes in converting to SNG production from crude [40].....	27
Table 2.4	Operating parameters and gas compositions in the pilot plant of the Lurgi process at 17.7 bar [51, 53].....	29
Table 2.5	Operating parameters and gas compositions of the TREMP of Haldor Topsoe process (ADAM and EVA project) [57]. ....	31
Table 2.6	Operating parameters and gas compositions of the RMP process [58]. ....	32
Table 2.7	Comparison between common CO <sub>2</sub> separation techniques [61, 68, 69].....	41
Table 2.8	Pyrolysis for bio-oil production in 2012 from white wood [94].....	49

Table 2.9	Product of pyrolysis from three main components in biomass [95].	50
Table 2.10	Production of several compounds in bio-oil production from biomass pyrolysis [95, 96].	50
Table 2.11	The main compounds of bio-oil from three different type of biomass [97].	51
Table 2.12	Composition of functional group of PEFB bio-oil [98].	53
Table 2.13	Main chemical compounds in PEFB bio-oil in area percentage (%).	54
Table 2.14	Characteristics of PEFB bio-oil [98, 99, 102, 103].	55
Table 2.15	Current research for using different type of catalyst in methanation process.	58
Table 2.16	Several type of adsorbent used in gas purification [40].	58
Table 3.1	Description of unit operation blocks in Aspen Plus software.	70
Table 4.1	Characteristics of PEFB bio-oil [98, 102].	95
Table 4.2	Estimation for three different PEFB bio-oil compositions based on the intended elemental formula $C_{0.3238}H_{0.4957}O_{0.1798}N_{0.0007}$ .	98
Table 4.3	Molar inputs of reactants in mixture M3 based on 3000 of total moles of carbon input.	104
Table 4.4	Reaction of enthalpy ( $\Delta H_R$ ) for main global reactions that are related to LTSR for methane production at 298 K (M3 = $C_{0.3368}H_{0.482}O_{0.1789(G)}$ ).	112
Table 4.5	Enthalpy change terms for 1 mole of $CH_4$ produced by isothermal LTSR at S/C of 3 and isothermal SE-LTSR with Ca:C of 0.5:1 (with CaO and $Ca(OH)_2$ as sorbents) at 1 atm. All calculations were done at 450 K and $\Delta H$ terms were given in kJ/mol of $CH_4$ .	116
Table 5.1	The effect of reaction temperature towards $CH_4$ production at constant S/C of 2 using 4 grams of Ni/Ca- $Al_2O_3$ catalyst.	134
Table 5.2	The effect of steam to carbon ratio towards $CH_4$ production at constant 400 °C using 4 grams of Ni/Ca- $Al_2O_3$ catalyst.	136

Table 5.3	Comparison of components (C, H, N and S) of used catalysts (Ni/Ca-Al <sub>2</sub> O <sub>3</sub> ) for different reaction temperature. The catalysts were used in LTSR process at constant S/C of 2.....	143
Table 5.4	Comparison of components (C, H, N and S) of used catalysts (Ni/Ca-Al <sub>2</sub> O <sub>3</sub> ) for different steam to carbon ratio (S/C). The catalysts were used in LTSR process at constant 400 °C.....	143
Table 5.5	Total carbon balance of LTSR experiments using Ni/Ca-Al <sub>2</sub> O <sub>3</sub> catalyst with different of reaction temperatures. The value of steam to carbon ratio of 2 was used at atmospheric pressure. ....	147
Table 5.6	Total carbon balance of LTSR experiments using Ni/Ca-Al <sub>2</sub> O <sub>3</sub> catalyst with different of steam to carbon ratio, S/C. The operating temperature was set at 400 °C and atmospheric pressure.	147
Table 5.7	Re-calculated C in gas and on catalyst from carbon balance of LTSR experiments using Ni/Ca-Al <sub>2</sub> O <sub>3</sub> catalyst with different of reaction temperatures. The value of steam to carbon ratio of 2 was used at atmospheric pressure. ....	149
Table 5.8	Re-calculate the total carbon balance of LTSR experiments using Ni/Ca-Al <sub>2</sub> O <sub>3</sub> catalyst with different of steam to carbon ratio, S/C. The operating temperature was set at 400 °C and atmospheric pressure. ....	149
Table 5.9	The amount of carbon deposition on the catalyst at the beginning of the reaction in 2 hours of experiment. ....	150
Table 6.1	Proximate and ultimate analyses (mf wt.%) of PEFB [98] which is defined in Aspen Plus. ....	155
Table 6.2	Product distributions for pyrolysis process.....	160
Table 6.3	Ultimate analysis of bio-char from the pyrolysis of PEFB [151].....	161
Table 6.4	Model mixture of bio-compounds for PEFB bio-oil based on DTG analysis Figure 6.6 with ultimate analysis [154].....	162
Table 6.5	Dry gas products from methanation process. ....	168
Table 6.6	Parameters values for HPWS simulation for biogas production from anaerobic process [129] and comparison of the results between literature and our simulations results. ....	170
Table 6.7	Parameters values for HPWS simulation and compositions of the upgraded bio-methane production from PEFB bio-oil.....	173

Table 6.8	Gas compositions of the upgraded bio-methane production before and after splitting 3.1% of upgraded bio-methane production. ....	175
Table 6.9	Gas compositions of the upgraded bio-methane production before and after splitting 10.6% of upgraded bio-methane production. ....	177
Table 6.10	Comparison of heat and power demand for different levels of process integration (Feedstock for methanation process = Bio-oil).....	185
Table 6.11	Comparison of heat and power demand for different levels of process integration (Feedstock for methanation process = Bio-oil and non-condensable pyrolysis gas).....	186
Table 6.12	Comparison of the process performance between the two different feedstocks options in the methanation process. ....	188
Table 6.13	Comparison of the process performance between the two different feedstocks options which includes heat and power demand in the methanation process. ....	188
Table 6.14	Comparison of the process performance of our work with other biomass gasification systems to CH <sub>4</sub> production. ....	192
Table 6.15	Comparison of heating values (HHV and LHV) by using Channawala and Parikh (Eq. 6.3) and Lind (Eq. 6.4–6.5) for different of biomass.....	196
Table 6.16	Gas compositions, pressures, temperatures and flow rates of the process streams based on 3000 kg/hr of raw PEFB. ....	197
Table 6.17	Efficiencies at the two main conversion stages, and overall efficiency of PEFB to pure CH <sub>4</sub> process.....	197

## List of Figures

Figure 1.1	Global natural gas consumption in 1965, 1985 and 2003 [4]. Source: BP (2004) .....	3
Figure 1.2	Natural gas consumption by sector in Malaysia from 1990–2014 [7]. Source: PETRONAS, Gas Companies, Power Utilities, IPPs and Self-Generation Plants.....	5
Figure 1.3	Natural gas consumption by sector in Italy from 1960–1995 [4]. Source: IEA (2003) .....	6
Figure 1.4	Total percentage of Greenhouse Gases (GHG) that contribute to global warming [10]. .....	8
Figure 1.5	Worldwide carbon dioxide emissions from 1980–2014 [11]. .....	8
Figure 1.6	Worldwide vegetable oil demand in 2015 [27]. .....	13
Figure 1.7	Comparison palm oil efficiency with other major oil crops (soybean, sunflower and rapeseed) [29]. Source: Oil World 2013.....	14
Figure 1.8	World palm oil production in 2009 [39]. .....	16
Figure 2.1	Flow diagram of general processes in SNG production from coal [43]. .....	23
Figure 2.2	Flow diagram of fixed bed methanation process (Lurgi process) in SNG production from coal [40]. .....	25
Figure 2.3	Simplified flow process diagram for the Lurgi process with adiabatic fixed bed methanation reactor [52]. .....	29
Figure 2.4	Simplified flow process diagram for the TREMP process of Haldor [55, 56]. .....	30
Figure 2.5	Simplified flow process diagram for the RMP process [58, 59]. .....	32
Figure 2.6	Simplified flow process diagram for non-adiabatic process by using IRMA cooled reactor [60]. .....	33
Figure 2.7	Temperature profiles in the IRMA reactor for three different gas flows of syngas [60]. .....	34

Figure 2.8	Common techniques used for CO <sub>2</sub> removal.....	37
Figure 2.9	Schematic diagram of membrane separation for biogas upgrading process [74]. .....	40
Figure 2.10	Thermochemical processes of biomass conversion to energy production [39]. .....	43
Figure 2.11	General gasification process of wood to SNG production [91]. .....	45
Figure 2.12	Process flow for production of SNG from lignocellulosic biomass gasification technology [92]. .....	45
Figure 2.13	General applications for fast pyrolysis products [93]. .....	47
Figure 2.14	Fast pyrolysis process for fluidized bed [101]. .....	48
Figure 2.15	The minimum methanation temperature as a function of elements periodic group number [114]. .....	56
Figure 2.16	The effect of surface area of catalyst by varying nickel concentration [115]. .....	57
Figure 2.17	Simplified flow diagram of (a) the conventional and (b) the single step of steam methane reforming processes [128]. .....	60
Figure 3.1	Simplified process flowsheet of bio-methane production from biomass via fast pyrolysis process. ....	67
Figure 3.2	Unit operation block of a heat exchanger in Aspen Plus software. ....	72
Figure 3.3	Ni/Ca-Al <sub>2</sub> O <sub>3</sub> catalyst from TST Ltd in form of (a) as-received pellet and (b) after crushing and sieving (250–355 µm of particle size). .....	74
Figure 3.4	Schematic diagram of experimental set-up for bio-oil conversion into CH <sub>4</sub> production via LTSR. ....	77
Figure 3.5	Photograph of experiment rig for bio-oil conversion into CH <sub>4</sub> production via LTSR. ....	78
Figure 3.6	Photograph of micro-GC (CP 4900). .....	79
Figure 3.7	Photograph of TGA (Stanton Redcroft TGA1000) for TPO analysis. ....	82
Figure 3.8	Photograph of SEM (Carl Zeiss EVO MA15) coupled with EDX (Oxford Instruments AZtecEnergy). .....	83

Figure 4.1	CH <sub>4</sub> yield (wt. %) for three different PEFB bio-oil mixture compositions listed in Table 4.2 for S/C from 3 to 7 and 1 atm. ....	98
Figure 4.2	CH <sub>4</sub> production vs. temperature from M3 mixture (Table 4.3) without (a) and with Ca(OH) <sub>2(S)</sub> (b) at 1 atm. The top horizontal line is the theoretical maximum production via (R4.13). ....	106
Figure 4.3	Production of (a) carbon graphite, (b) CO, (c) CO <sub>2</sub> and (d) H <sub>2</sub> between 400 and 800 K at 1 atm for LTSR (solid lines) and SE-LTSR (dashed lines) processes. ....	107
Figure 4.4	CH <sub>4</sub> production within 300–800 K at S/C = 3.0 for total pressures between 1 and 30 atm. The top horizontal line is the theoretical maximum production via (R4.13). ....	111
Figure 4.5	Total enthalpy ( $\Delta H_{Tot}$ ) for producing 1 mole of CH <sub>4</sub> from bio-oil steam reforming for LTSR in the range of S/C = 2–7, SE-LTSR using Ca(OH) <sub>2</sub> :C = 0.5:1 (no inlet steam) and CaO:S:C = 0.5:0.5:1 for reformer temperatures of 400–600 K at 1 atm. (S = steam). ....	114
Figure 4.6	CH <sub>4</sub> production for adiabatic LTSR within 300–800 K at 1 atm. This figure is to be compared to Figure 4.1(a) of the isothermal case. ....	118
Figure 4.7	Temperature output of the process for different values of S/C ratio (1–3) within 300–800 K of input temperature at 1 atm. ....	119
Figure 4.8	CH <sub>4</sub> production (a) and CaCO <sub>3</sub> production and equilibrium temperature (b) in the isothermal (tp) and adiabatic (hp) cases for SE-LTSR using CaO as CO <sub>2</sub> sorbent within 300–800 K at 1 atm. The top line in (a) is the theoretical maximum. The format of molar ratio is presented in CaO:H <sub>2</sub> O:C. (S = steam) ....	120
Figure 5.1	Production of gases (CH <sub>4</sub> , CO <sub>2</sub> , CO and H <sub>2</sub> ) at (a) 350 °C, (b) 400 °C and (c) 450 °C. The value of steam to carbon ratio of 2 was used at atmospheric pressure. ....	135
Figure 5.2	Production of gases (CH <sub>4</sub> , CO <sub>2</sub> , CO and H <sub>2</sub> ) at S/C of (a) 1, (b) 2 and (c) 3. The operating temperature was set at 400 °C atmospheric pressure. ....	137
Figure 5.3	XRD patterns of fresh and used Ni/Ca-Al <sub>2</sub> O <sub>3</sub> catalysts. ....	140
Figure 5.4	TPO results of the used catalysts (Ni/Ca-Al <sub>2</sub> O <sub>3</sub> ) (a) TGA-TPO and (b) DTG-TPO for different reaction temperatures under air flow (50 ml/min) at a heating rate of 10 °C/min. The catalysts were used in LTSR process at constant S/C of 2. ....	141



Figure 5.5	TPO results of the used catalysts (Ni/Ca-Al <sub>2</sub> O <sub>3</sub> ) (a) TGA-TPO and (b) DTG-TPO for different steam to carbon ratio (S/C) under air flow (50 ml/min) at a heating rate of 10 °C/min. The catalysts were used in LTSR process at constant 400 °C.....	142
Figure 5.6	SEM image of fresh Ni/Ca-Al <sub>2</sub> O <sub>3</sub> catalyst at 10.00 K mag.	144
Figure 5.7	EDX mapping for elemental distribution (a) Al, (b) O, (c) Ca and (d) Ni elements of fresh Ni/Ca-Al <sub>2</sub> O <sub>3</sub> catalyst. ....	145
Figure 5.8	SEM image of used Ni/Ca-Al <sub>2</sub> O <sub>3</sub> catalyst at 10.00 K mag. The catalyst was used in LTSR process at 400 °C and S/C of 2. ....	145
Figure 5.9	EDX mapping for elemental distribution (a) Al, (b) O, (c) Ca and (d) Ni elements of used Ni/Ca-Al <sub>2</sub> O <sub>3</sub> catalyst. The catalyst was used in LTSR process at 400 °C and S/C of 2.....	146
Figure 5.10	Production of carbon containing gases (CH <sub>4</sub> , CO <sub>2</sub> and CO) at 400 °C and S/C of 2. The arrow line shows the region where average value was taken. ....	149
Figure 6.1	Block diagram of the PEFB conversion to pure CH <sub>4</sub> via pyrolysis-low temperature steam reforming (LTSR) and water scrubbing. ....	153
Figure 6.2	Simplified process simulation flowsheet of biomass pre-treatment.....	156
Figure 6.3	Schematic diagram of single-pass rotary dryer [158]. ....	157
Figure 6.4	Energy consumption for grinding of wood [138] based on work by [162] and [163].....	159
Figure 6.5	Schematic diagram of bio-oil production from biomass via fast pyrolysis [140]. ....	161
Figure 6.6	Discretisation of real PEFB oil DTG curve by weighted individual conversions from thermal decomposition over 6 macro-families. Mass fractions 'zi' as in Table 6.4, 'ai' is conversion of family 'i' [167]. ....	163
Figure 6.7	Simplified process simulation flowsheet of the PEFB fast pyrolysis process. ....	165
Figure 6.8	Simplified process simulation flowsheet of methanation. ....	167
Figure 6.9	Flowsheet of re-modelled of HPWS in Aspen Plus simulation based on literature [142]. ....	169
Figure 6.10	Simplified process simulation flowsheet of HPWS. ....	172

Figure 6.11	Simplified process simulation flowsheet of heat integration for preheating the incoming air by burning bio-char, non-condensable pyrolysis gas and 3.1% of upgraded bio-methane production. ....	175
Figure 6.12	Simplified process simulation flowsheet of heat integration for preheating the incoming air by burning bio-char and 10.6% of upgraded bio-methane production (no burning of non-condensable pyrolyzer gases). ....	177
Figure 6.13	Simplified process simulation flowsheet of heat integration for heating up the water inlet for methanation unit. ....	179
Figure 6.14	Simplified process simulation flowsheet of heat integration for re-vaporizing the bio-oil before entering methanation unit. ....	180
Figure 6.15	Simplified process simulation flowsheet of full heat integration, Process 4 in Table 6.10, methanator feed is bio-oil alone. ....	187
Figure 6.16	Simplified process simulation flowsheet of full heat integration, Process 4 in Table 6.11, methanator feed is combined bio-oil and non-condensable pyrolyzer gases. ....	187
Figure 6.17	Comparison of energy flows in a methanation via pyrolysis-LTSR process for two different of feedstocks in methanation unit. ....	190

## Abbreviations

atm	Atmospheric (pressure)
Bcm	Billion cubic meters
Bio-SNG	Bio-synthetic natural gas
BR	Brassica rapa
Btu	British thermal unit
CEA	Chemical Equilibrium and Application
cm <sup>3</sup>	Cubic centimeters
CMS	Carbon molecular sieves
CNG	Compressed natural gas
DMEA	Di-methyl ethanol amine
EDX	Energy-dispersive X-ray
EFB	Empty fruit bunch
F-T	Fischer-Tropsch
FSU	Former Soviet Union
g	Gram
GC-MS	Gas chromatography-mass spectrometry
GHG	Greenhouse gases
GP	Grape seed
GWh	Gigawatt hours
HHV	Higher heating value
HPWS	High pressure water scrubber
hr	Hour
IEA	International Energy Agency

kg	Kilogram
kJ	Kilojoule
ktoe	Kilotons of oil equivalent
kWh	Kilowatt hours
lb/in <sup>2</sup> g	Pound per square inch (pressure)
LHV	Lower heating value
LNG	Liquefied natural gas
LPG	Liquefied petroleum gas
LTSR	Low temperature steam reforming
MEA	Mono ethanol amine
MF	Mesocarp fiber
m <sup>2</sup>	Square meters
m <sup>3</sup>	Cubic meters
mf	Moisture free
mg	Milligram
min	Minute
MJ	Megajoule
mm	Millimeter
Mtoe	Million tonnes of oil equivalent
MW	Megawatt
NASA	National Aeronautics and Space Administration
NIST	National Institute of Standards and Technology
NPOC	Non-purgeable organic carbon
NRTL	Non-Random-Two-Liquid
PC	Pine cone
PEFB	Palm empty fruit bunch

Peng-Rob	Peng-Robinson
POME	Palm Oil Mill Effluent
PSA	Pressure swing adsorption
psi	Pounds per square inch (pressure)
s	Second (time)
SASOL	South Africa Synthetic Oil Liquid
SEM	Scanning electron microscopy
SE-HTSR	Sorption enhanced-high temperature steam reforming
SE-LTSR	Sorption enhanced-low temperature steam reforming
SESR	Sorption enhanced steam reforming process
SNG	Synthetic natural gas
Syngas	Synthesis gas
TCD	Thermal conductivity detector
Tcm	Trillion cubic meters
TGA	Thermogravimetric analysis
TMP	Thermomechanical pulp
TOC	Total organic carbon
TPO	Temperature programmed oxidation
TREMP	Topsøe's Recycle Energy efficient Methanation Process
UK	United Kingdom
USA	United States of America
XRD	X-ray diffraction
µm	Micrometer

## Nomenclature

Ca:C	Calcium to carbon molar ratio
C:CaO	Carbon to calcium oxide molar ratio
$C_G$	Carbon containing in gases
$C_L$	Carbon present in the condensate
$C_S$	Carbon deposited on the used catalyst
(g)	Vapour state
H	Enthalpy, kJ/mol
$H_2/CO$	Syngas molar ratio
$H_2O:C$	Steam to carbon molar ratio
hp	Assigned Enthalpy and Pressure
$K_H$	Equilibrium constant for the salvation process
(l)	Liquid state
$\dot{m}$	Mass flowrate, kg/s or kg/hr
$\dot{n}$	molar flowrate, mol/s
N/A	Not applicable
P	Pressure, bar or atm
$P_{el}^-$	Process electricity co-generation, kW
$P_{el}^+$	Process electricity demand , kW
$P_x$	Partial pressure of component x
$\dot{Q}^-$	Process excess heat, kW
$\dot{Q}^+$	Process heat demand, kW
R	Gas constant ( $8.3144621 \times 10^{-3}$ kJ/mol.K)

rev	Reverse
(s)	Solid state
S/C	Steam to carbon ratio
$S_{C-i}$	Selectivity to carbon products
$S_{H-i}$	Selectivity to hydrogen products
T	Temperature, °C or K
tp	Assigned Temperature and Pressure
$\dot{V}$	Volumetric flowrate, m <sup>3</sup> /s or m <sup>3</sup> /hr
vol. %	Volume percentage
vs.	Versus
wt. %	Weight percentage
$X_{fuel}$	Fuel conversion to gases
y	Dry gas mole fraction
$Y_{CH_4}$	CH <sub>4</sub> yield, wt. %
$Y_{CH_4,eff}$	CH <sub>4</sub> yield efficiency
$\Delta H$	Enthalpy difference
$\Delta T_{min}$	Minimum temperature difference
$\lambda$	The wavelength of the incident rays
$\eta_{btf}$	Biomass-to-fuel thermal efficiency
$\eta_C$	Carbon conversion efficiency
$\eta_{th}$	Overall thermal efficiency
$\rho$	Density, kg/m <sup>3</sup>
$\theta$	The angle between the incident rays and surface of the plane

**Formulae**

Al	Aluminium
Ar	Argon
C	Carbon or char
Ca	Calcium
CaCO <sub>3</sub>	Calcium carbonate
CaO	Calcium oxide
Ca(OH) <sub>2</sub>	Calcium hydroxide
CH <sub>3</sub> COOH	Acetic acid
CH <sub>4</sub>	Methane
C <sub>2</sub> H <sub>6</sub>	Ethane
Co	Cobalt
CO	Carbon monoxide
CO <sub>2</sub>	Carbon dioxide
Cu	Copper
H	Hydrogen element
H <sub>2</sub>	Hydrogen
H <sub>2</sub> O	Water
H <sub>2</sub> S	Hydrogen sulphide
N	Nitrogen element
N <sub>2</sub>	Nitrogen
N <sub>2</sub> O	Nitrous oxide
Ni	Nickel



Ni/Al <sub>2</sub> O <sub>3</sub>	Nickel supported on alumina catalyst
Ni/Ca-Al <sub>2</sub> O <sub>3</sub>	Nickel supported on calcium aluminate catalyst
NiO	Nickel oxide
NH <sub>3</sub>	Ammonia
NO	Nitrogen oxide
O	Oxygen element
O <sub>2</sub>	Oxygen
Pt	Platinum
S	Sulphur
SO <sub>2</sub>	Sulphur dioxide

## Chapter 1

### Introduction

#### 1.1 Global energy consumption

Energy consumption is increasing faster worldwide than the growth of industries, with approximately 80% of the global energy consumption still depending on fossil fuel feedstock [1]. According to the International Energy Agency, it has been estimated that by the year 2030, there will be a 53% increase in global energy consumption with 70% of the growth demand coming from developing countries. The energy consumption is mainly fossil fuel based (88.1%), which consists of 34.8% crude oil, 29.2% coal and 24.1% natural gas [2].

The increment of global natural gas consumption for different regions in 1965, 1985 and 2003 is shown in the pie charts of Figure 1.1. The size of the pie charts are proportional to the total consumption of natural gas where the statistics are in terms of billion cubic meters (Bcm) and percentage of total share. The natural gas consumption in developing countries, especially in Asia and Pacific regions has increased from 1965 (1%) to 2003 (13%), while North America's share fell more than a half from 73% in 1965 to 30% in 2003. But, it still remains as the main consumer throughout the year.

As one of the developing countries in Asia and Pacific regions, Malaysia is highly dependent on fossil fuels for its energy sector as shown in Table 1.1. The amount of energy supply has increased four-fold from 1990 until 2014, with more than 95% of the energy supply relying on crude oil, petroleum products (such as diesel, kerosene and naphtha), natural gas and coal. Crude oil was the main energy supply in 1990, with 40.9%, but it dropped to 28.9% in 2014 due to its fast depleting supply [3]. Thus, natural gas becomes the main energy supply with 43.4%, followed by crude oil with 28.9%, coal with 16.6% and petroleum products with 7.2% in 2014. On the other hand, biodiesel, solar, biomass and biogas which are specified as 'Others', were not identified as one of the energy supply in Malaysia in 1990, but shares 0.6% of total energy supply in 2014. It is believed that the renewable energy becomes a more attractive resource since it gives more advantages compared to the fossil fuels (crude oils, petroleum products and natural gas) in terms of availability of the resources and environmental impacts.

The composition of natural gas before processing differs with geographic areas, some examples of gas fields in Europe are listed in Table 1.2. From five different gas fields, the total volume of natural gas is composed mainly from methane ( $\text{CH}_4$ ) which represents more than 70%, and the rest is mostly consisting of alkanes (ethane, propane, butane and pentane) with less than 10%. Hydrogen sulphide, carbon dioxide ( $\text{CO}_2$ ) and nitrogen ( $\text{N}_2$ ) gases are also found from trace amounts to larger volume percentages in the natural gas, depending on source location.

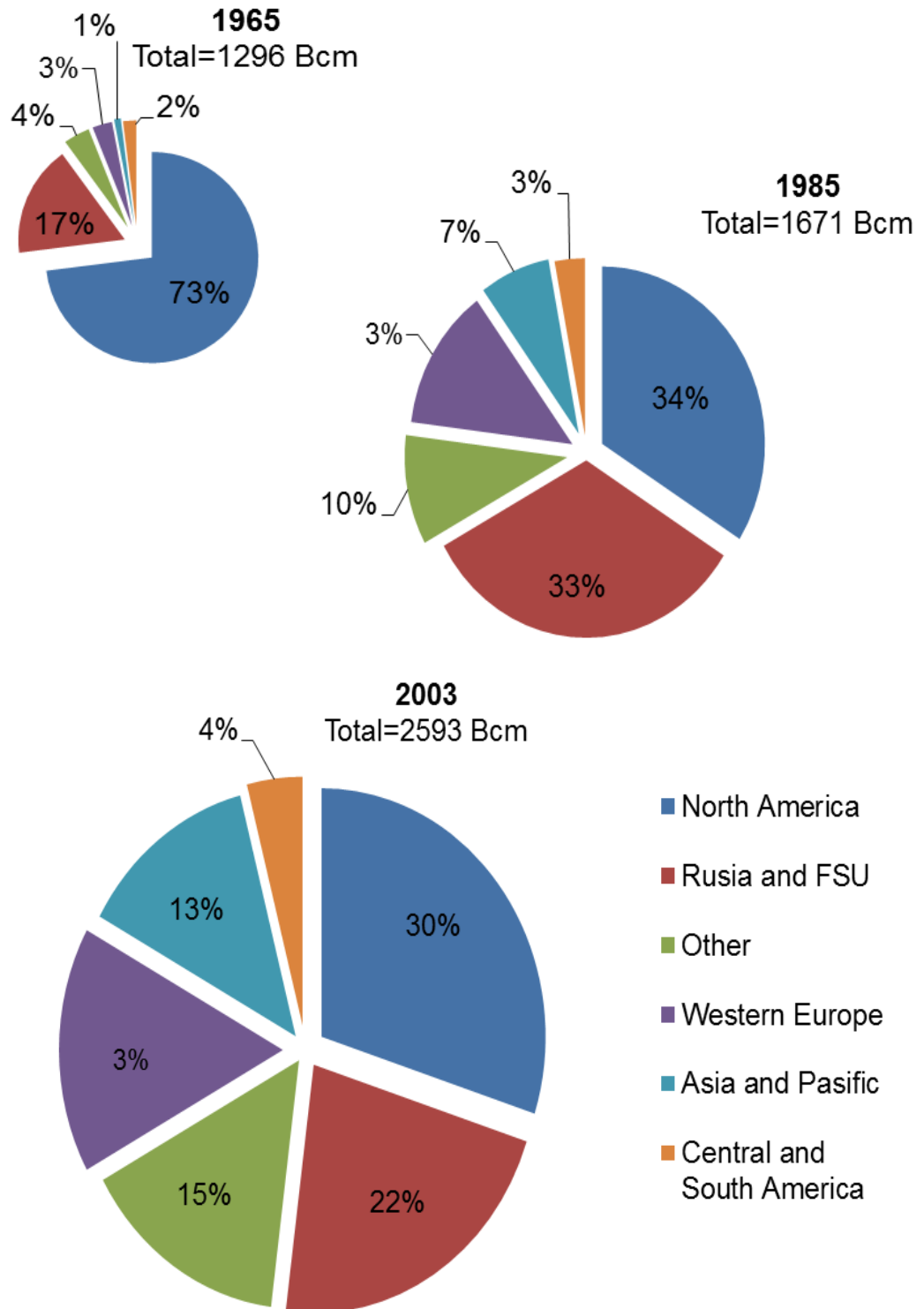


**Figure 1.1** Global natural gas consumption in 1965, 1985 and 2003 [4].  
Source: BP (2004)

**Table 1.1** Primary energy supply share in Malaysia [5]. (ktoe are kilotons of oil equivalent)

	Amount (ktoe)		Share (%)	
	1990	2014	1990	2014
Primary energy supply				
Crude oil	8,783	26,765	40.9	28.9
Petroleum products	3,651	6,699	17.0	7.2
Natural gas	6,801	40,113	31.7	43.4
Coal and coke	1,326	15,357	6.2	16.6
Hydropower	915	3,038	4.2	3.3
Others	-	556	0.0	0.6
Total	21,476	92,528	100	100

**Table 1.2** Natural gas compositions in volume percentage in Europe's gas fields [6].

Constituents	Lacq	Groningen	UK North Sea		Ekofisk
	France	Netherlands	(southern)	(northern)	Norway
Methane	69.52	81.30	95.05	78.08	85.2
Ethane	2.82	2.85	2.86	10.1	8.6
Propane	0.80	0.37	0.49	5.7	2.9
Butanes	0.60	0.14	0.17	2.2	0.9
Pentanes	0.91	0.09	0.05	1.4	0.2
Hydrogen sulphide	15.59	Trace	trace	trace	trace
Carbon dioxide	9.76	0.89	-	1.1	1.7
Nitrogen	-	14.35	1.26	0.7	0.5

As mentioned earlier, natural gas, which consists primarily of methane, has become the main energy supply in Malaysia because of high demand in various sectors, this is shown in Figure 1.2 which includes transport, residential, self-generation, non-energy uses, industrial and power generation. The natural gas consumption has gradually increased from 1990 with 2.4 million tonnes of oil equivalent (Mtoe) to 2014 with 25.2 Mtoe. Power generation is the major sector, consuming half of the total natural gas consumption per annum.

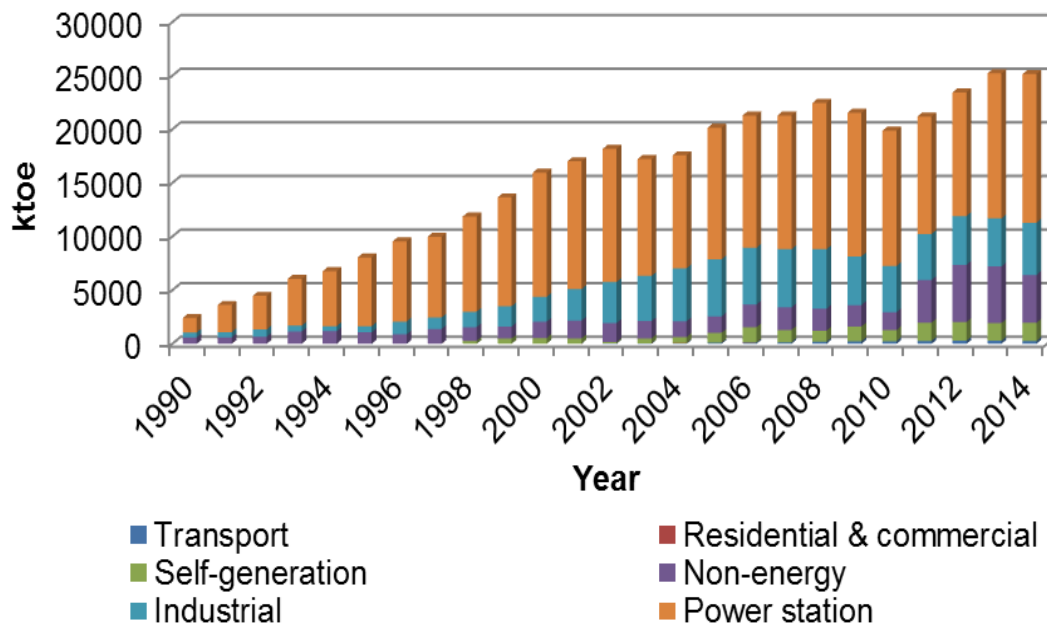


**Figure 1.2** Natural gas consumption by sector in Malaysia from 1990–2014 [7]. Source: PETRONAS, Gas Companies, Power Utilities, IPPs and Self-Generation Plants

However in Italy, residential and commercial became the main sectors as illustrated in Figure 1.3, that consumed more than a half of the total natural gas consumption in year 1995 with 22 billion cubic meters (Bcm) or 19.8 Mtoe, followed by power generation (10.5 Bcm or 9.45 Mtoe) and industry (7.5 Bcm

or 6.75 Mtoe). Although both of countries, Malaysia and Italy showed different values of total gas consumption by sectors, generally, natural gas was consumed as a fuel source.

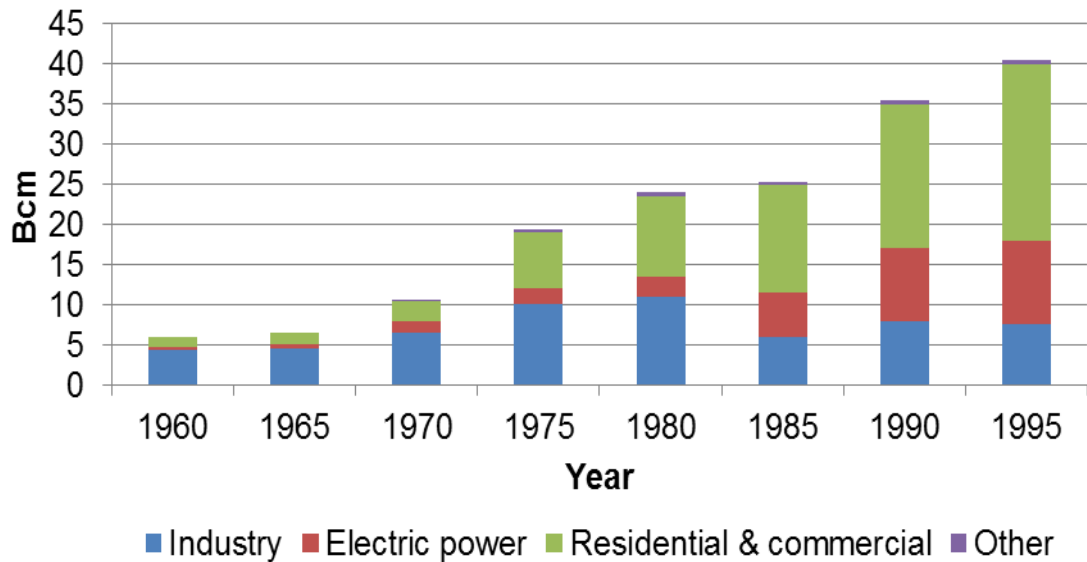


**Figure 1.3** Natural gas consumption by sector in Italy from 1960–1995 [4].  
Source: IEA (2003)

## 1.2 Environmental impact

The increment of fossil fuels consumption in power generating plants have negative impacts on the environment where it has been identified as the main contributor to greenhouse gases (GHG) emissions [8]. Table 1.3 shows the average daily activity of a 2,000 MW power plant by using fossil fuel which include coal, oil and natural gas. Power plants fuelled by natural gas have the lowest of GHG and air pollutant emissions, where less carbon dioxide (CO<sub>2</sub>) is produced with the least emission of sulphur dioxide (SO<sub>2</sub>) and nitrogen oxides

(NO<sub>x</sub>) compared to coal and oil fuel. But, the amount of CO<sub>2</sub> released (21 ktoe) from natural gas power plant still gives a higher level of CO<sub>2</sub> in the atmosphere which is related to global warming.

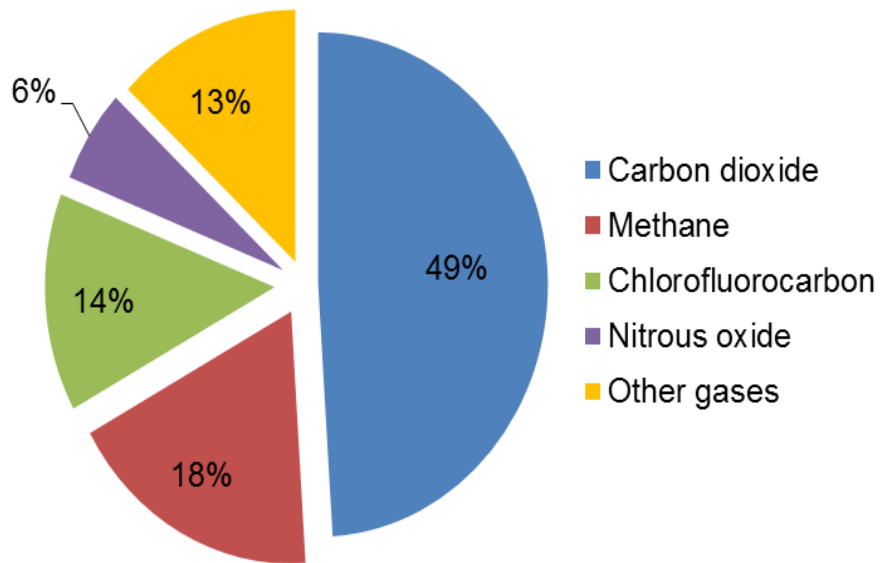
**Table 1.3** The average daily activity of a fossil fuel 2000 MW power plant [6].

Plant type	Coal (1% sulphur)	Fuel oil (3.5% sulphur)	Natural gas
Fuel consumed (tons)	16,500	10,200	7,800
Waste solids (tons)	2,000*	5*	nil
Waste heat (GWh)	76	73	70
SO <sub>2</sub> produced (tons)	350	750	negligible
NO <sub>x</sub> produced (tons)	50–150	40–70	15–75
CO <sub>2</sub> produced (tons)	39,000	33,000	21,000
Net efficiency (%)	38	39	40

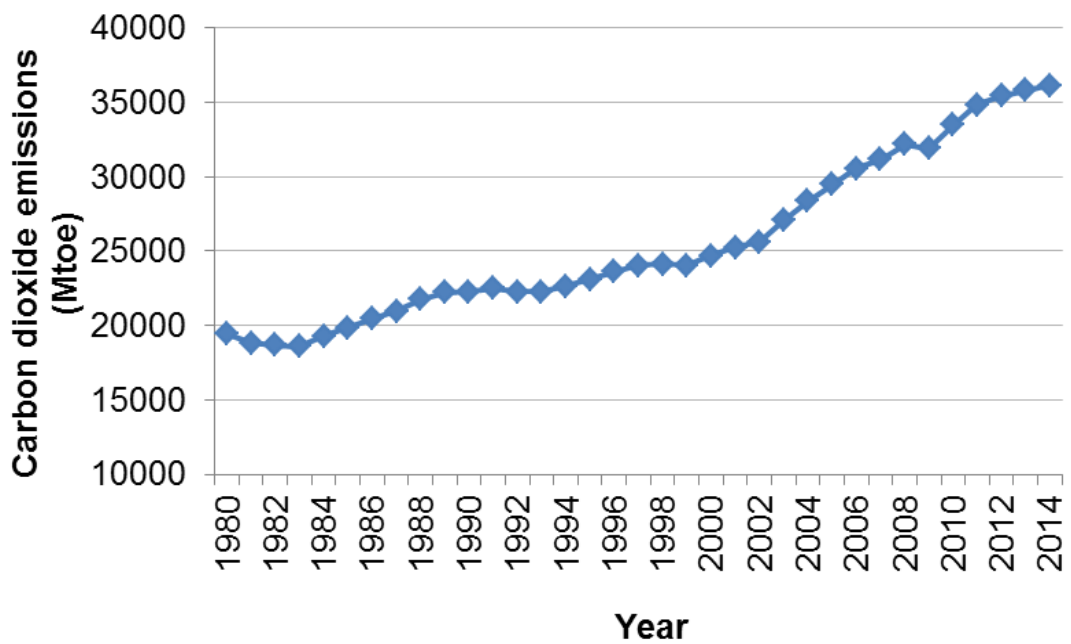
\*Plus sulphur

Figure 1.4 shows various gases of GHG that contribute to global warming, which include carbon dioxide (CO<sub>2</sub>), methane (CH<sub>4</sub>), chlorofluorocarbon and nitrous oxide (N<sub>2</sub>O). CO<sub>2</sub> gas is the major contributor to the global warming affect, which is about half of the total GHG (49%), followed by CH<sub>4</sub> (18%), chlorofluorocarbon (14%) and N<sub>2</sub>O (6%). Moreover, several gases such as nitrous oxide (N<sub>2</sub>O), carbon monoxide (CO), carbon dioxide (CO<sub>2</sub>) and sulfur dioxide (SO<sub>2</sub>) that are produced by combustion of fossil fuel in the industrial sector, contributes to climate forcing, acid rain and smog [3, 9].





**Figure 1.4** Total percentage of Greenhouse Gases (GHG) that contribute to global warming [10].



**Figure 1.5** Worldwide carbon dioxide emissions from 1980–2014 [11].

The National Aeronautics and Space Administration (NASA) has developed a model to determine the relationship between CO<sub>2</sub> emission with global warming, and stated that the temperature increases equivalently with the amount of CO<sub>2</sub> released into the atmosphere [12]. Figure 1.5 shows the worldwide CO<sub>2</sub> emissions from 1980 to 2014 where CO<sub>2</sub> emission increased from 19.4 billion tonnes to 36.1 billion tonnes [11]. It has been estimated up to 2030, CO<sub>2</sub> emission will continuously increase to 40 billion tonnes if no further efforts are made to prevent this issue [13].

### **1.3 Synthetic Natural Gas (SNG) production**

The top 15 countries holders of world natural gas reserves and resources are listed in Table 1.4, where Iran is the leading country in largest gas reserves and resources with 34.0 trillion cubic meters (Tcm). However, the global reserve of crude oil and natural gas is expected to last within 40–60 years [3]. Thus, the global reserve of fossil fuels such as petroleum is limited and caused higher prices, above US\$ 53 per barrel as in January 2017 [14]. However, shale oil and shale gas production have driven a decrease in the natural gas prices from US\$ 8.85 per million Btu in 2008 to US\$ 2.60 per million Btu in 2015 [15] which affected Iran's economy. Because of limited of source as well as negative impact to the environment, government and researchers have been driven to search and find a new replacement of fossil fuel which has long availability with less production cost.

**Table 1.4** The top holders of world conventional natural gas reserves in 2015 [15].

Country	Natural gas reserves (Tcm)	World share (%)
<b>1</b> Iran	34.0	18.2
<b>2</b> Russia	32.3	17.3
<b>3</b> Qatar	24.5	13.1
<b>4</b> Turkmenistan	17.5	9.4
<b>5</b> United States	10.4	5.6
<b>6</b> Saudi Arabia	8.3	4.5
<b>7</b> United Arab Emirates	6.1	3.3
<b>8</b> Venezuela	5.6	3.0
<b>9</b> Nigeria	5.1	2.7
<b>10</b> Algeria	4.5	2.4
<b>11</b> China	3.8	2.1
<b>12</b> Iraq	3.7	2.0
<b>13</b> Australia	3.5	1.9
<b>14</b> Indonesia	2.8	1.5
<b>15</b> Canada	2.0	1.1
Rest of world	22.8	11.9
World Total	186.9	100

The advantage of CH<sub>4</sub> gas is its high energy conversion efficiency and the already existing gas distribution infrastructure, as well end use technologies such as pipelines, power stations, heating and increasing numbers of cars running on compressed natural gas (CNG) in the world [16-19]. For example, the primary energy supply in Malaysia shows that natural gas consumes

53.6% of total natural gas for power generators sector, as shown in Table 1.5. However, commercial and residential in the United Kingdom (UK) are the main consumer of natural gas followed by power generation sector with 48% and 27% respectively. Moreover, Malaysia exports approximately 34.2 Bcm of LNG which brings Malaysia as the third largest exporter of LNG in the world after Qatar (106.4 Bcm) and Australia (39.8 Bcm) in 2015 [15]. Thus, for Malaysia, conversion of biomass to CH<sub>4</sub> is a practical approach to meet the current energy demand in Malaysia as CH<sub>4</sub> has similar composition as natural gas.

**Table 1.5** Share percentage (%) of natural gas consumption by sectors in 2013.

Sector	Malaysia [20]	United Kingdom [21]
Power generators	53.6	26.7
Non-energy	20.9	0.7
Industry	17.8	11.1
Self-generation	6.5	6.5
Commercial and residential	0.1	48.0
Others	1.1	7.0

The advantages of SNG production have motivated several countries including Germany to set a target of replacing imported natural gas per year with SNG in the amount of 6 billion m<sup>3</sup> by the year 2020 [22]. Currently, CH<sub>4</sub> production from biomass are split into two main methods, either biological or thermochemical (combustion, liquefaction, gasification and pyrolysis) processes. In Malaysia, biogas is commonly been produced naturally from

biological anaerobic degradation process such as in municipal landfills and Palm Oil Mill Effluent (POME) anaerobic ponds.

However, some disadvantages of landfilling include limited land and its rising cost for municipal landfills [2], the lack of knowledge and absence of infrastructures availability in palm oil mill industries [23]. Thus, biogas production potential from the palm oil industry is not realised, and  $\text{CH}_4$  escapes into the atmosphere, which contributes to global warming as  $\text{CH}_4$  is 21 times more potent a greenhouse gas than  $\text{CO}_2$  [24]. Moreover, some of oil mill factories failed to meet the standardized discharge where unpleasant odours from anaerobic ponds offend local population [25]. Therefore, POME seems not to fulfill the requirement of Malaysia's National Green Technology Policy (2009) which emphasizes in promoting efficient utilization as well as to conserve and minimize the impact on the environment [2]. For that reason, it is convenient to convert biomass to  $\text{CH}_4$  via thermochemical means in dedicated plants where  $\text{CH}_4$  fugitive emissions can be better controlled.

#### **1.4 Palm oil biomass as a modern fuel**

As the demand for vegetable oils grows worldwide, it causes production of a great volume of biomass, which is recognized as the third main energy resource globally [26]. Figure 1.6 shows a pie chart with the demand in eight different vegetable oils in 2015, including palm, soybean, rapeseed, sunflower, cottonseed, peanut, coconut and olive oil. More than half of the total vegetable

oil demand is overtaken by both palm oil and soya oil with 38% and 28% respectively.

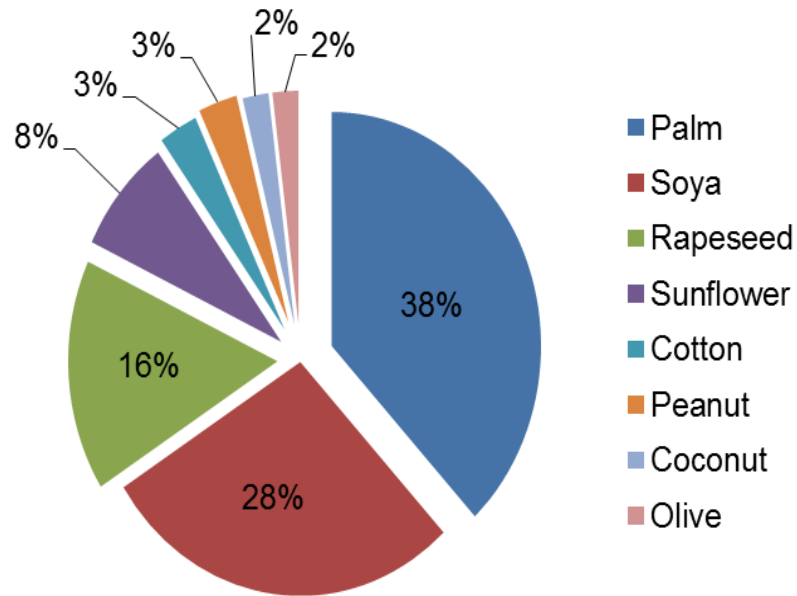


**Figure 1.6** Worldwide vegetable oil demand in 2015 [27].

Palm oil has the highest demand due to several advantages, including higher annual oil yield per hectare [28, 29], and having lower production cost compared to other oilseeds crops [30]. The comparison of oil production per hectare of palm oil plantation compared to soybean, sunflower and rapeseed is shown in Figure 1.7. Palm oil shows a significant difference among the other crops, where it is the highest oil production with the lowest total plantation area. Despite using a minimum land area, palm oil also has the least expensive production cost compared to other major oil crops shown in Table 1.6.

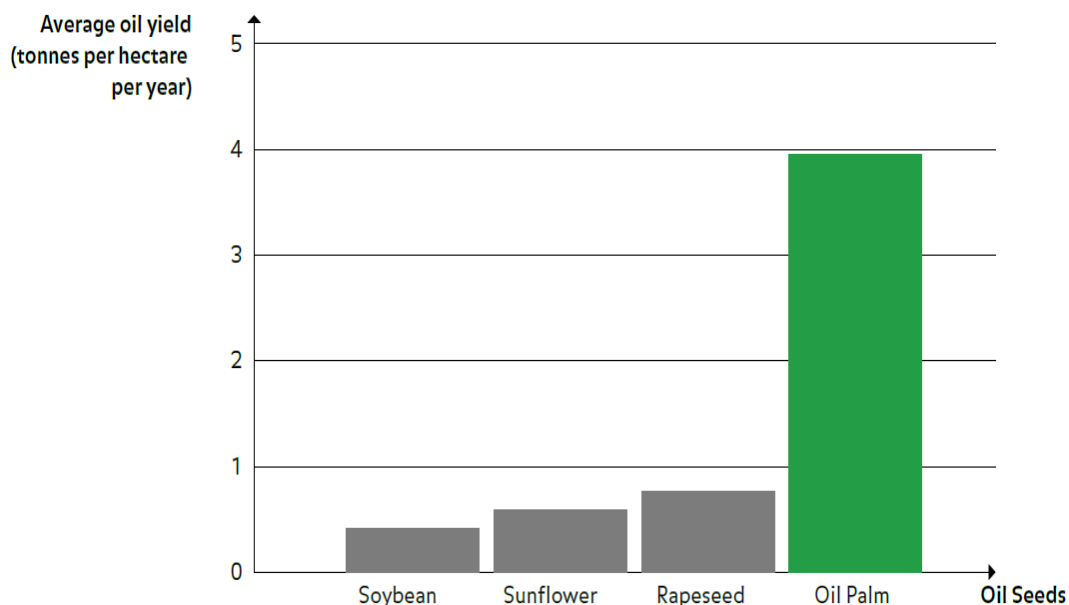


**Figure 1.7** Comparison palm oil efficiency with other major oil crops (soybean, sunflower and rapeseed) [29].  
Source: Oil World 2013.

**Table 1.6** Comparative cost for palm oil compared to soybean and rapeseed in December 2016 [31].

Oil	Cost (USD/tonne)	Country/region
Palm	708	Malaysia
Palm	709	Indonesia
Soybean	861	USA
Soybean	826	Brazil
Rapeseed	918	Dutch
Sunflower	765	Argentina

In 2009, the two largest producers of palm oil were Malaysia and Indonesia, where both countries contributed 86% of the world palm oil production as illustrated in Figure 1.8. The increase of palm oil production generates massive amounts of palm oil derived biomass by-product which includes

empty fruit bunch (EFB), mesocarp fibre, shell, palm kernel, frond and trunk, which are listed in Table 1.7. Empty fruit bunch is the main contributor to the palm oil biomass by-product with 15.5–17.5 million tons per year. Although frond is the second largest of palm oil biomass by-products, it is usually used as erosion control measure as well as soil fertilizer and helps with conservation of the palm oil plantation itself [32]. As for mesocarp fiber and shell, they are typically used as combustion fuel to generate heat and electricity for the palm oil mill [33] rather than using EFB, which contains almost 60% of water [34]. Moreover, most of the palm oil millers do not have the technology for the disposal of EFB [35]. Thus, EFB is typically left outside without any further utilization and becomes an abundant waste, which when left in large piles undergoes anaerobic digestion and generates CH<sub>4</sub> emissions.

**Table 1.7** Palm oil biomass components and quantity produced in Malaysia [36-38].

Biomass component	Quantity/annum (Million tonnes)
Empty fruit bunch (EFB)	15.5–17.5
Frond	12.9
Mesocarp fiber (MF)	9.6–9.7
Trunk	8.2
Shell	4.5–6.0



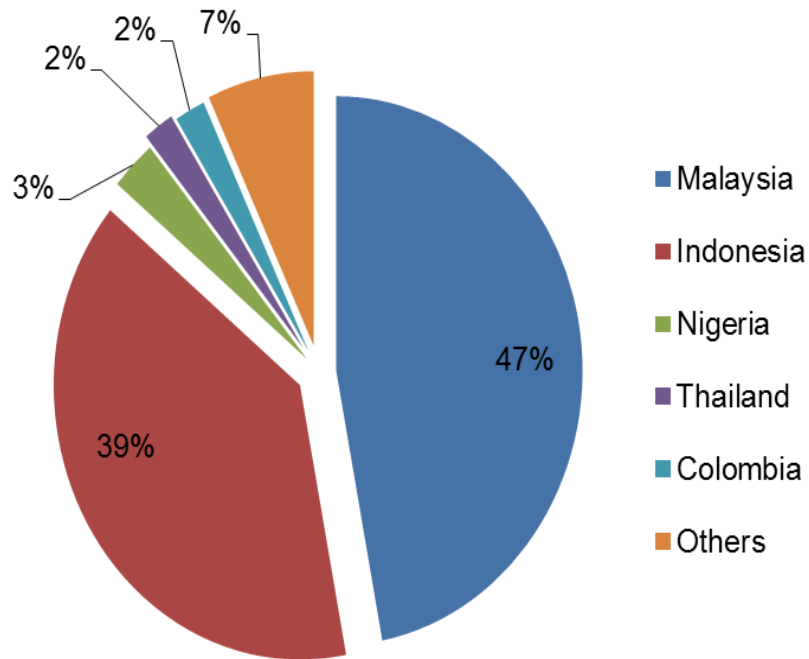


**Figure 1.8** World palm oil production in 2009 [39].

## 1.5 Research aims and objectives

This research is concerned in finding a significant incentive to utilize palm empty fruit bunch (PEFB) as an abundant feedstock for conversion to clean fuels and value added products, via the production of bio-oil from further processing by the fast pyrolysis process. Specifically, the novelty of this research is to investigate and optimize the conversion pyrolysis oil from PEFB to methane via advanced reforming processes. Thus, the aim for this study is to produce a methane-rich gas from PEFB bio-oil.

The objectives for this research are as follows:

1. To perform chemical equilibrium calculations for methanation of palm empty fruit bunch (PEFB) bio-oil feedstock at different values of operating temperatures and steam to carbon ratio (S/C).
2. To define the optimum range of conditions for methane production in steam reforming process, from Objective 1.
3. To investigate the influence of in situ  $\text{CO}_2$  sorption towards methane production by varying carbon to calcium oxide (CaO) ratios (C:CaO), and compare the energy balances of methanation process with the optimum results from Objective 1.
4. To demonstrate feasibility of conversion of acetic acid as surrogate bio-oil compound to methane via direct methanation by low temperature steam reforming process (LTSR) in a packed bed catalytic reactor.
5. To optimize the methane production via LTSR by investigating the effect of operating parameters towards methane production (temperatures and S/C), from Objective 4.
6. To simulate a full process of nearly pure  $\text{CH}_4$  production from biomass (PEFB) conversion via pyrolysis by using Aspen Plus.
7. To demonstrate and identify the possibilities of the process integration between possible streams in the process, from Objective 6 by using Aspen Plus.
8. To evaluate the worth of the proposed process in comparison with the equivalent state of the art technology, which relies on biomass gasification followed by CO and  $\text{CO}_2$  methanation of the produced syngas.

Chapter 2 gives a brief description of the current technologies used for synthetic natural gas (SNG) production and common upgrading techniques used for obtaining high purity of  $\text{CH}_4$  as the final product. Literature reviews which relate to pyrolysis oil production were also included in this chapter since PEFB bio-oil was used in this work as the simulated feedstock for LTSR in the full process plant.

Chapter 3 describes the methodologies used in this study, where this research work was conducted into two parts, experimentation and simulation. The experimental work was carried out in the laboratory of the University of Leeds, UK while the Chemical Equilibrium and Application (CEA) and Aspen Plus programmes were used for simulation work.

In Chapter 4, chemical equilibrium calculations by using CEA were performed, where the aim of this study was to identify the optimum range of conditions for  $\text{CH}_4$  production from of PEFB pyrolysis oil with and without in situ  $\text{CO}_2$  sorption.

Chapter 5 discussed the experimental results of LTSR using acetic acid as model surrogate species for the pyrolysis oil with a nickel catalyst in a packed bed reactor, where the closeness of the outputs were compared with the predicted ideal values and aspects for further research and optimisation were identified.

Chapter 6 illustrated a preliminary study of the process design of a full process of CH<sub>4</sub> production from biomass (PEFB) conversion via pyrolysis by using Aspen Plus. The possibilities of process integration in this process were proposed in order to identify the energy saving opportunities. Comparisons of the modelled plant efficiencies with those of the nearest equivalent state of the art technologies concluded this chapter.

Conclusions and future work recommendations of this work were summarized in Chapter 7.

## Chapter 2

### Literature Review

#### 2.1 Introduction

The increase of global energy demand especially in natural gas consumption has forced researchers to find other solutions since the petroleum fuel production will not last forever. The world is currently discovering and beginning to exploit its shale gas reserves which have been seen to enormously benefit the economy of the USA, which has embraced the technology of shale fracturing for the production of gas and oil. It is expected that in many countries with shale gas reserves, petrol-based transport will gradually be replaced by gas-based transport for economic reasons, bringing about a larger infrastructure based on gas energy. Concurrently, the conversion of biomass as a modern fuel draws a great attention to the world since it is a sustainability energy and helps to reduce environmental problems. The production of synthetic natural gas (SNG) from biomass is to be focused in this study because it can replace the conventional natural gas where it has similar composition, which is mostly methane (CH<sub>4</sub>).

## 2.2 SNG production from coal and fossil fuel

Currently, synthetic natural gas (SNG) in industry is produced from coal or naphtha as the feedstock, by generating synthesis gas (syngas) first. Syngas consists of hydrogen (H<sub>2</sub>) and carbon monoxide (CO) and is produced via a gasification process (steam reforming or partial oxidation). Then, the syngas product will undergo further reactions through methanation processes, which are represented as reactions (R2.1–R2.3) to yield methane (CH<sub>4</sub>). Reaction (R2.1) is taking place if the ratio of syngas (H<sub>2</sub>/CO) is equal or greater than 3:1, which will produce methane (CH<sub>4</sub>) and water (H<sub>2</sub>O), but reaction (R2.2) occurs if the syngas ratio is 1:1, producing carbon dioxide (CO<sub>2</sub>) instead of H<sub>2</sub>O. Reaction (R2.3) shows that the production of CH<sub>4</sub> could occur in a reaction between carbon dioxide (CO<sub>2</sub>) and H<sub>2</sub>.



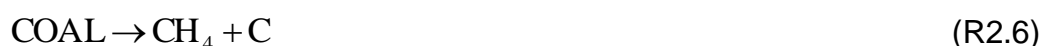
The undesired products which are carbon (C) and higher hydrocarbons such as ethane (C<sub>2</sub>H<sub>6</sub>) may be produced during methanation reactions. Reaction (R2.4) shows a conversion of syngas to ethane, while formation of carbon from CO is shown in reaction (R2.5). Thus, optimizing operating conditions is required to obtain maximum main product, which is CH<sub>4</sub> gas, as well as to reduce the undesired products, since carbon deposition increases with temperature but decreases with pressure and syngas ratio [40].



### 2.2.1 Coal as feedstock

Methanation processes by using coal as the feedstock were usually operated by using fixed bed and fluidized bed reactors, with the temperatures within 250–400 °C and pressures from atmospheric (1 atm) to 1200 psi (81.7 atm) [40]. The flow diagram for general processes of SNG production from coal is shown in Figure 2.1, which involves coal preparation, gasification, shift conversion, gas purification, methanation and dehydration of gas. In the beginning, coal and steam were introduced into the system to produce syngas ( $\text{H}_2$  and  $\text{CO}$ ),  $\text{CH}_4$  and  $\text{CO}_2$  via gasification reactions (i.e. operates within 800–1900 °C [41]), shown by reactions (R2.6–R2.10). Coal is not a homogenous substance, and does not have a fixed chemical formula, therefore, 'COAL' defined in R2.6 can contain from 60 to 90 wt.% of carbon, 3 to 6 wt.% of hydrogen and 1 to 23 wt.% of oxygen [42], depending on coal type (ex. lignite, bituminous, anthracite).

Gasification from coal:





(=rev R2.5)

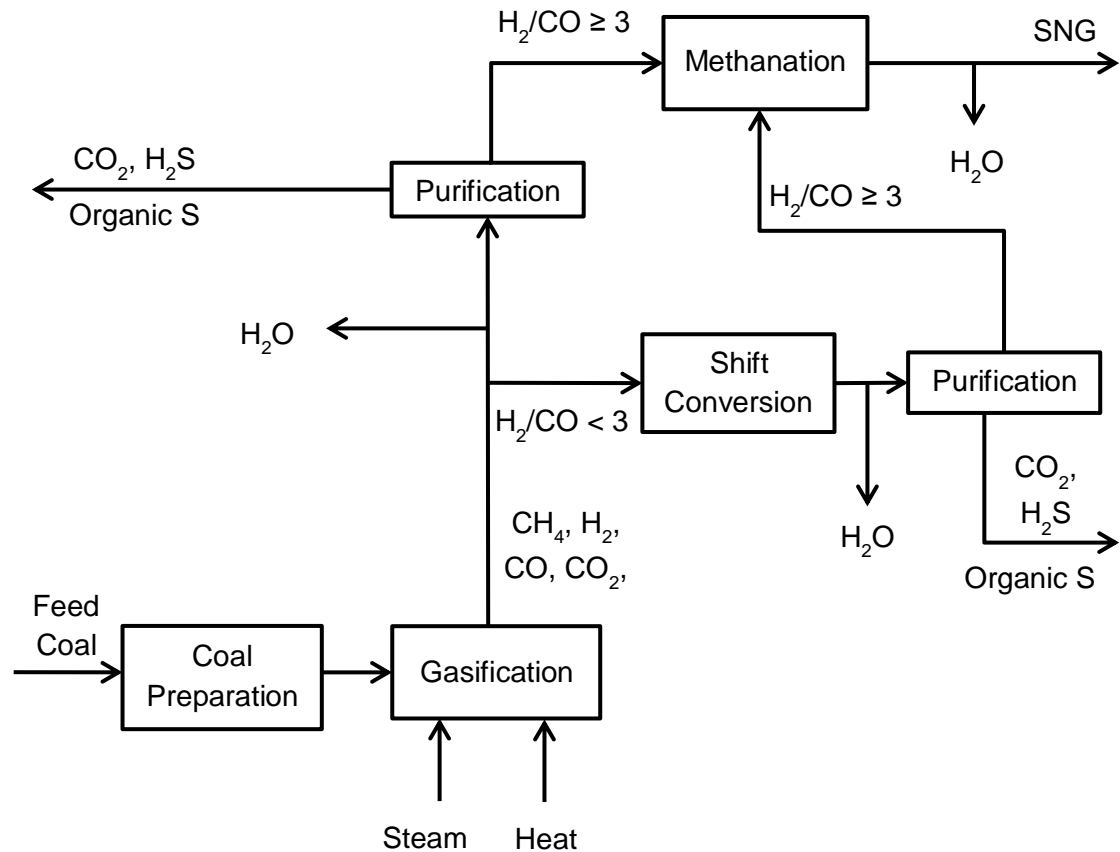


**Figure 2.1** Flow diagram of general processes in SNG production from coal [43].

A  $\text{H}_2:\text{CO}$  ratio in the syngas mixture of 3 or above, as expressed by reaction (R2.1), is required to yield  $\text{CH}_4$  as the final product through the methanation process. But, if the ratio of syngas is less than 3, the gas mixture will undergo water-gas shift reaction, following reaction (R2.10), where  $\text{CO}$  will react with steam to generate additional  $\text{H}_2$  with  $\text{CO}_2$  as co-product which leads to the



methanation process and increases CH<sub>4</sub> production. This shift conversion reaction takes place under the same conditions as the gasification process [41].

However, devolatilization of coal produces several gases, which are listed in Table 2.1, where CO<sub>2</sub> and hydrogen sulphide (H<sub>2</sub>S) productions become impurities in the gas mixtures. CO<sub>2</sub> and H<sub>2</sub>S gases are removed from the system by purification processes including absorption, adsorption, cryogenic condensation and membrane [44], while dehydration is required to eliminate the H<sub>2</sub>O content.

**Table 2.1** Compositions of gas produced in volume percentage (vol.%) from different types of coal.

Coal type	Subbituminous (Rosebud) [45]	Bituminous [46]	Noncaking [47]	Bituminous [48]
Gas				
CO <sub>2</sub>	30.4	6.9	19.5	31.1
CO	15.1	57.7	35.0	48.6
H <sub>2</sub>	41.1	30.0	41.0	18.2
CH <sub>4</sub>	11.2	5.4	3.5	1.7
N <sub>2</sub>	1.2	-	1.0	-
H <sub>2</sub> S	0.5	-	-	0.4
C <sub>2</sub> H <sub>6</sub>	0.5	-	-	-
Type of process	Lurgi (fixed bed)	Wellman-Galusha (fixed bed)	Winkler (fixed bed)	Westinghouse (fluidized bed)

The Lurgi process is one of the example for fixed bed coal gasification process which is widely used in industry, but synthesis gas (syngas) is the main product for mostly operated Lurgi plants, which is listed in Table 2.2. Based on Figure 2.2, oxygen ( $O_2$ ) is fed into the gasifier to provide heat for the gasification process by combustion of char (C). Tar and light oil formations are unwanted by-products of the Lurgi process which can be converted into SNG but, it is not yet been commercialized compared to crude oil as the feedstock [40]. The operating conditions of the Lurgi process will be further discussed in 2.3.1 section.

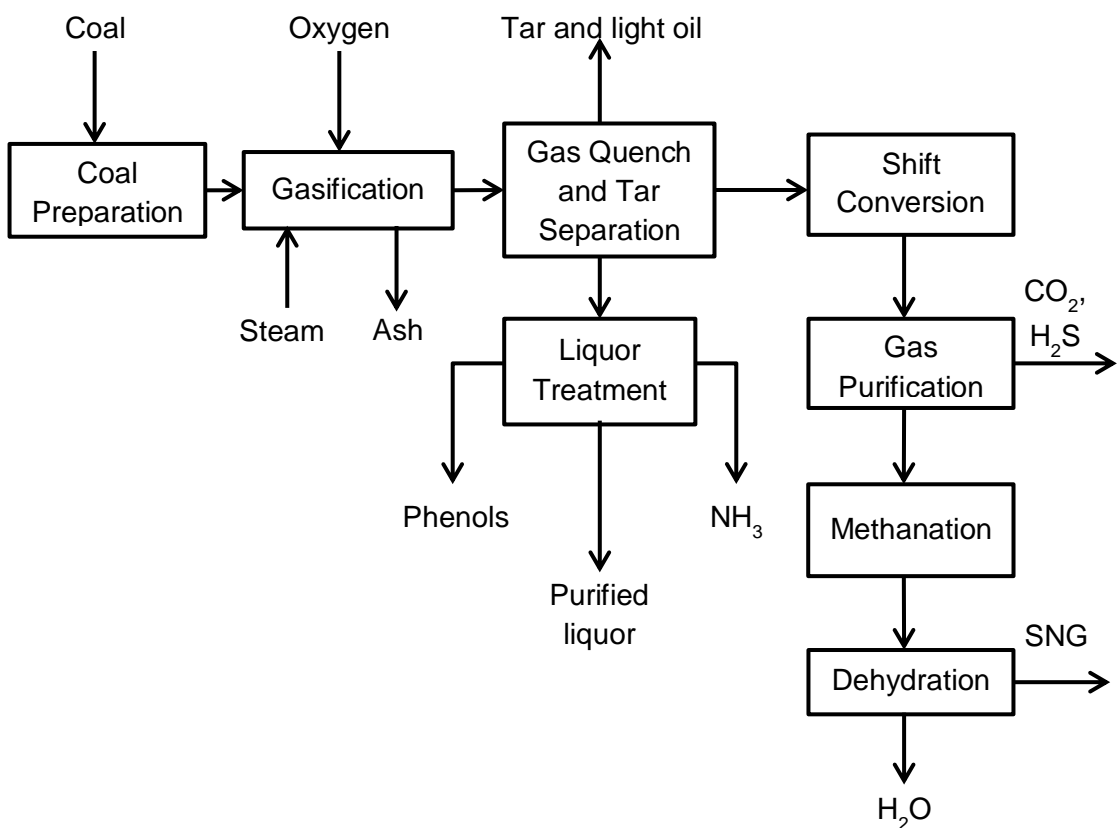


**Figure 2.2** Flow diagram of fixed bed methanation process (Lurgi process) in SNG production from coal [40].

**Table 2.2** Commercial Lurgi plants for coal gasification process [49].

No.	Plant owner	Plant location	Product	Coal type
1	South Africa Coal, Oil and Gas	Sasolburg, South Africa (SASOL-I)  Secunda, South Africa (SASOL-II, SASOL-III)	Syngas for F-T liquids	Subbituminous
2	Pakistan Industrial Development Cooperation	Daud Khel, Pakistan	Syngas	Bituminous
3	Honam Fertilizer	Naju, South Korea	Syngas	Anthracite
4	Great Plains Gasification Associates	Beulah, North Dakota U.S.A	SNG	Lignite
5	China National Technology Import Company	Beijing, China	Syngas for ammonia	Anthracite

## 2.2.2 Fossil fuel as the feedstock

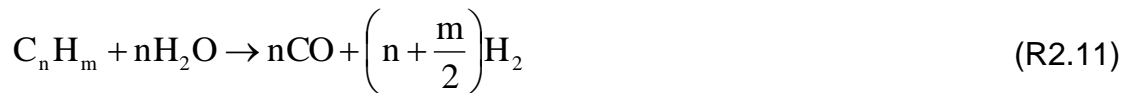
Fossil fuel such as natural gas, liquefied petroleum gas (LPG) and naphtha are extensively used as feedstocks in industrial for synthetic natural gas (SNG) production by hydrogasification and steam reforming processes. Based on Table 2.3, the steam reforming process has carried out with the lowest operating temperature, within 450–550 °C to produce CH<sub>4</sub> gas compared to other processes, including partial oxidation and hydrogasification.

**Table 2.3** The operating temperatures between several type of processes in converting to SNG production from crude [40].

Process type	Temperatures, °C	Main products
Steam reforming		
High temperature	800–900	CO, H <sub>2</sub>
Low temperature	450–500	CH <sub>4</sub>
Hydrogenation/hydrogasification	700–750	CH <sub>4</sub>
Partial oxidation	1250–1300	CO, H <sub>2</sub>

Several reactions occur during the steam reforming process, such as gasification, hydrogenation as expressed by reactions (R2.11–R2.12), water-gas shift conversion and methanation reactions, by equation (R2.10) and (R2.1) respectively. The formula C<sub>n</sub>H<sub>m</sub> represents a fossil fuel feedstock, such as natural gas, LPG and naphtha. Lower temperature steam reforming process is preferable to produce SNG in industry because it less expensive compared to others due to lower number of stages in the methanation process, as well as having the lowest operating temperatures (450–500 °C).

Gasification from fossil fuel:



Hydrogenation or hydrogasification:



## 2.3 Current technologies for synthetic natural gas (SNG) production

Since the methanation (R2.1) is an exothermic reaction, methanation technologies were commonly carried out either in adiabatically with an internal cycle of syngas or cooled fixed beds to maintain at a lower operating temperature, which favours methane production. The most popular industrial methods with several adiabatic stages are Lurgi, TREMP (Haldor Topsøe) and RMP processes while IRMA is an internally cooled reactor for a non-adiabatic process in a methanation plant.

### 2.3.1 Lurgi process

A pilot plant was operated in a Lurgi process in Sasolburg (South Africa) demonstrates the methanation process by using synthesis gas from the Fischer-Tropsch plant (coal gasification plant) [50, 51]. Based on Figure 2.3, the methanation unit includes two adiabatic fixed bed reactors with internal cycle of the product gas. The main objective to recycle the product gas is to

prevent temperature rise in the methanators, where the maximum temperature is 450 °C as shown in Table 2.4.

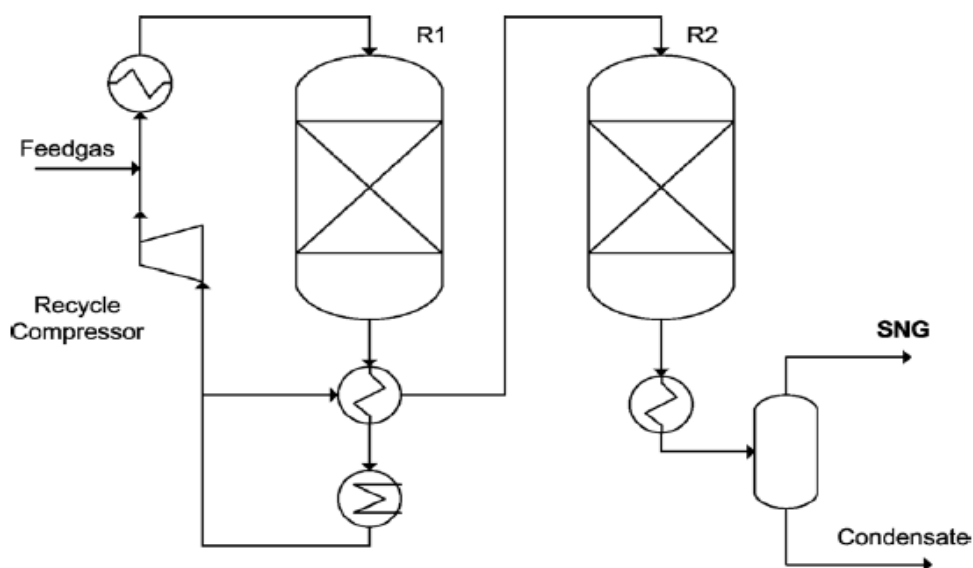


**Figure 2.3** Simplified flow process diagram for the Lurgi process with adiabatic fixed bed methanation reactor [52].

**Table 2.4** Operating parameters and gas compositions in the pilot plant of the Lurgi process at 17.7 bar [51, 53].

	Feed gas	First methanator, R1		Second methanator, R2	
		Inlet	Outlet	Inlet	Outlet
Temperature, °C	270	300	450	260	315
Gas composition					
H <sub>2</sub> (vol.%)	60.1	21.3	7.7	7.7	0.7
CO (vol.%)	15.5	4.3	0.4	0.4	0.05
CO <sub>2</sub> (vol.%)	13.0	19.3	21.5	21.5	21.3
CH <sub>4</sub> (vol.%)	10.3	53.3	68.4	68.4	75.9
C <sub>2</sub> <sup>+</sup> (vol.%)	0.2	0.1	0.05	0.05	0.05
N <sub>2</sub> (vol.%)	0.9	1.7	2.0	2.0	2.0

### 2.3.2 TREMP process of Haldor Topsøe

Topsøe's Recycle Energy efficient Methanation Process (TREMP) is similar to the Lurgi process, but it consists of three adiabatic fixed bed methanation reactors as shown in Figure 2.4. The main purpose of the TREMP process of Haldor Topsøe is to produce high pressure superheated steam in order to provide heat recovery of steam reforming (reverse reaction of R2.1, methanation) at the beginning stage of the process for synthesis gas production. Based on Table 2.5, the operating temperatures in the methanators are higher compared to Lurgi process, where it could reach at the maximum temperature of 604 °C. Moreover, Haldor Topsøe has provided MCR-2X and MCR-4 catalysts that could withstand high temperature methanation of this process [54].

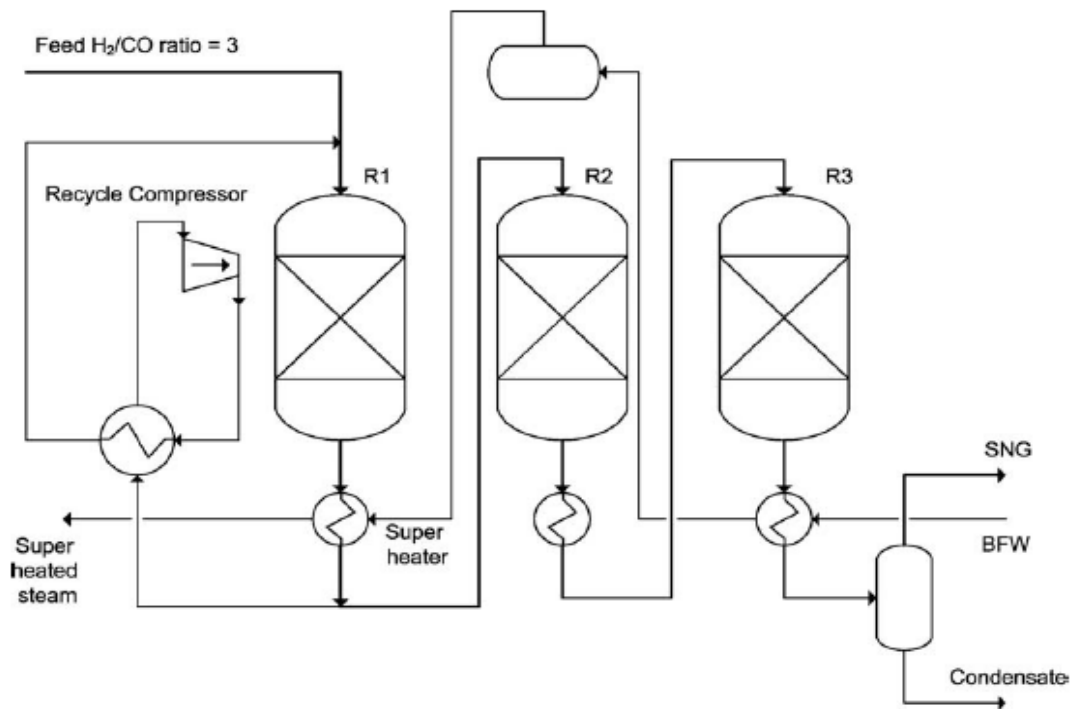


**Figure 2.4** Simplified flow process diagram for the TREMP process of Haldor [55, 56].

**Table 2.5** Operating parameters and gas compositions of the TREMP of Haldor Topsoe process (ADAM and EVA project) [57].

	Feed	R1 Inlet	R1 Exit	R2 Exit	R3 Exit	SNG
Temperature, °C		300	604	451	303	23
Pressure, bar	27.3	27.2	27.1	27.05	27.0	27.0
Gas composition						
H <sub>2</sub> (vol.%)	65.45	36.88	20.96	8.10	1.77	3.11
CO (vol.%)	9.84	4.28	1.17	0.00	0.00	0.00
CO <sub>2</sub> (vol.%)	8.96	6.13	4.46	2.07	0.95	1.67
CH <sub>4</sub> (vol.%)	11.30	28.12	37.44	44.36	47.28	82.95
H <sub>2</sub> O (vol.%)	-	19.19	29.82	38.84	43.06	0.10
N <sub>2</sub> (vol.%)	4.4	5.41	6.15	6.64	6.93	12.16

### 2.3.3 RMP process

On the other hand, a high temperature methanation without product gas recycle was proposed by Ralph M. Parsons Company (United States), which known as RMP process. The methanation process consists of 4–6 adiabatic fixed bed methanation reactors in series with intermediate gas cooling, where the feed syngas could be added in different distribution ratios into the first three reactors and steam was fed into the first reactor as shown in Figure 2.5. Steam was added into the first reactor in order to prevent temperature rise due to the exothermic reaction of methanation, where water gas shift reaction (R2.10) is taking place. Therefore, CO was mainly converted to CO<sub>2</sub> and causing less CH<sub>4</sub> production in the first reactor, shown in Table 2.6.



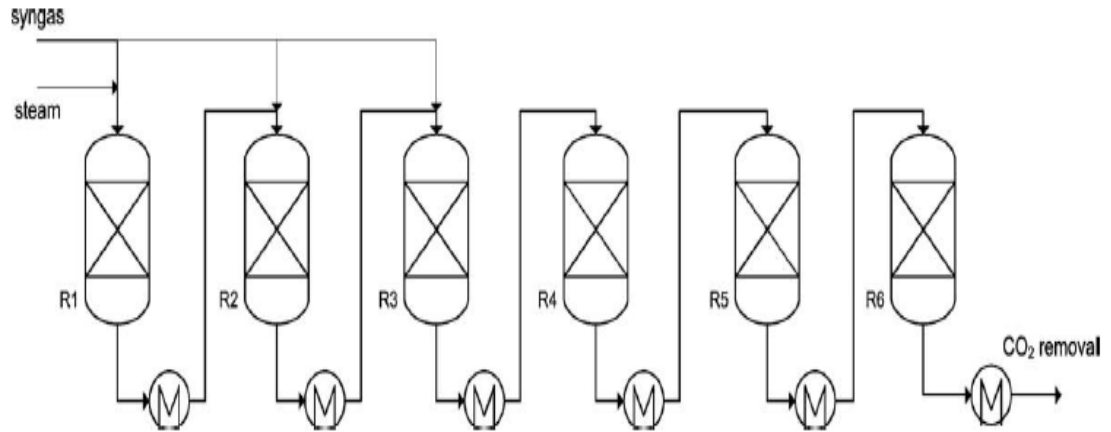


**Figure 2.5** Simplified flow process diagram for the RMP process [58, 59].

**Table 2.6** Operating parameters and gas compositions of the RMP process [58].

	Syngas	R1	R2	R3	R4	R5	R6
Inlet temp., °C	-	482	538	538	538	316	260
Outlet temp., °C	-	773	779	773	717	604	471
Pressure, bar	27.3	26.7	25.6	24.6	23.6	22.6	21.5
Syngas, vol.%	-	40	30	30	-	-	-
Gas composition							
H <sub>2</sub> (vol.%)	49.80	53.53	48.07	43.09	36.90	22.86	9.29
CO (vol.%)	49.80	13.97	18.46	20.63	15.25	5.64	0.87
CO <sub>2</sub> (vol.%)	0.10	25.80	24.04	23.64	29.21	39.90	46.84
CH <sub>4</sub> (vol.%)	0.30	5.70	9.43	12.64	18.64	31.60	43.00

### 2.3.4 Non-adiabatic process (IRMA cooled reactor)

Several stages of the methanation system in adiabatic process could be replaced by a single stage internally cooled reactor-IRMA (Innenbekühter Reaktor einer Methanisierung Anlage), where it contains reaction tubes which are filled with catalyst and externally cooled by water [50]. Based on Figure 2.6, the reaction heat from the reactor was used to raise high-pressure steam, which then to be condensed in the heat exchanger E201. After that, the water is sent back to the outside of the reaction tubes in order to cool down the methanation reactor.

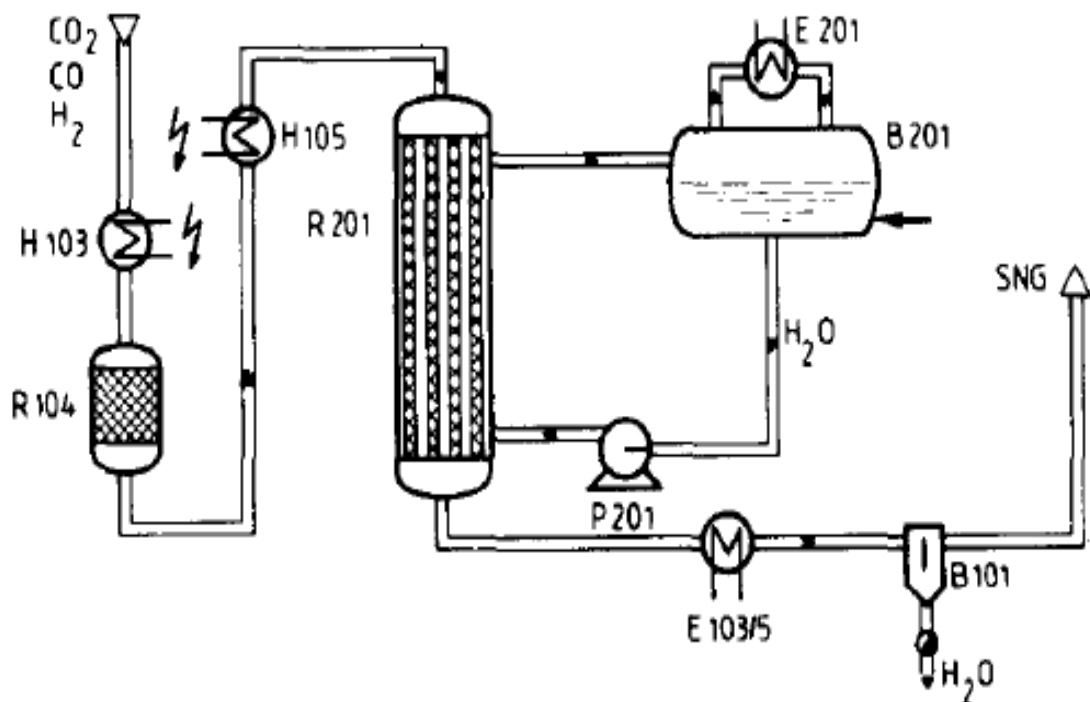


**Figure 2.6** Simplified flow process diagram for non-adiabatic process by using IRMA cooled reactor [60].

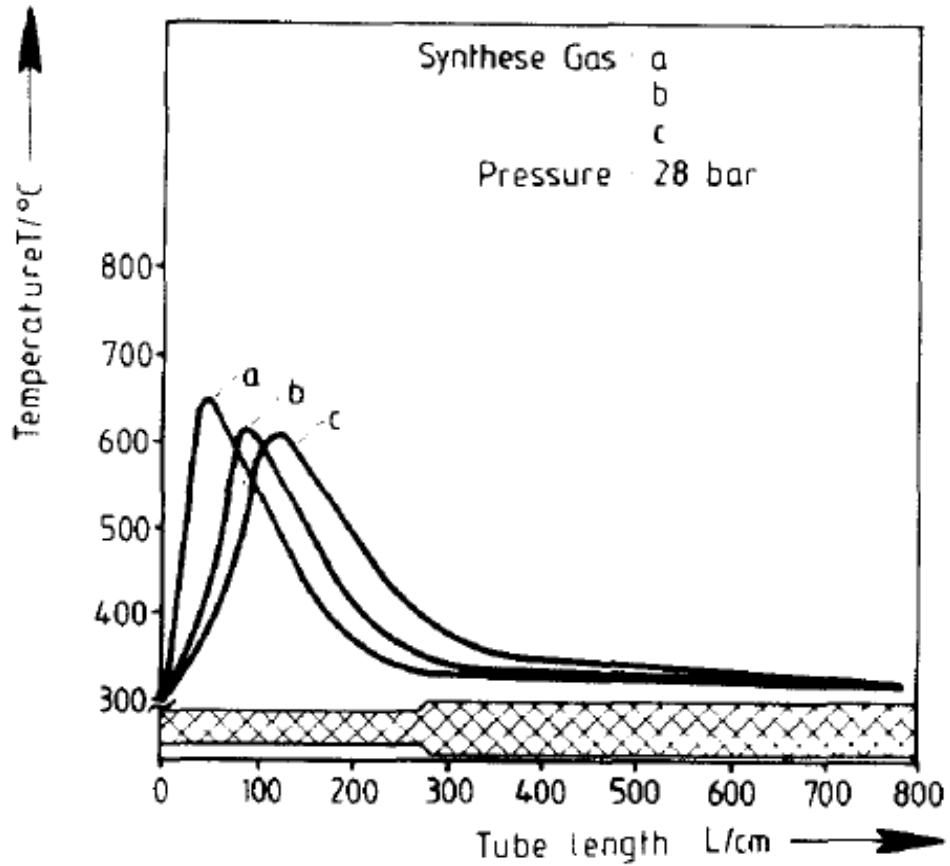


**Figure 2.7** Temperature profiles in the IRMA reactor for three different gas flows of syngas [60].

The operation of IRMA reactor was tested in the pilot plant where the maximum gas temperature was observed less than 650 °C at the inlet of the tube reactor, but then, the temperature was reduced and maintain at 310 °C from 300 cm of the tube length of the reactor, which shown in Figure 2.7. It was reported that about 83 vol.% of CH<sub>4</sub> of the dry gas product was already achieved at 5 m of tube length of the IRMA reactor [60].

Table 2.7 shows the main differences between adiabatic and isothermal reactors for methanation process in terms of working conditions (temperature and pressure) and the benefits for using these types of reactors. The temperature range for adiabatic reactor is higher (240–600 °C) compared to isothermal conditions (around 300 °C) due to the higher exit temperatures for adiabatic conditions. However, an isothermal reactor requires good heat transfer control in maintaining the operating temperature.

Thus, the isothermal reactor has advantages over an adiabatic reactor since it could avoid extremely high exit temperatures from the reactor and prevents sintering of the catalyst [61, 62]. The isothermal condition which is usually operated in a fluidized bed configuration must also have limited gas velocity within the reactor. The gas velocity must not be too low (to assure minimum fluidization conditions) and not too high in order to avoid catalyst elutriation [63].

Although adiabatic reactors feature simple equipment construction and require little maintenance [64], they necessitate more than 2 reactors with intermediate cooling stages in order to achieve high methane production. Therefore, the isothermal concept offers the potential for significant capital cost reductions.

**Table 2.7** Comparison between adiabatic and isothermal reactors for methanation process [61, 63-66].

	Adiabatic methanation	Isothermal methanation
Temperature, °C	240–600	300
Pressure, bar	20–100	1–20
Advantages	Simple construction	Good heat transfer process
Disadvantages	Complex heat transfer	Working material maintenance

Based on the comparison between the adiabatic and isothermal methanation concepts, it is preferable to use isothermal reactor for an average plant size due to the simplicity of the process setup and the opportunity to use waste heat [63]. On the other hand, large scale methanation plants (>100 MW) are well suited for the adiabatic methanation concept (consecutive fixed bed reactors), where highly valuable steam can be produced [67], even though the process setup is relatively complex [68].

## 2.4 Techniques for CH<sub>4</sub> product stream purification

In order to obtain CH<sub>4</sub>-rich as the final product, several commercial technologies are used to remove CO<sub>2</sub> from the gas stream such as physical and chemical absorption, pressure swing adsorption (PSA), membrane separation and cryogenic separation [69], as shown in Figure 2.8. General descriptions of different techniques for CH<sub>4</sub> product stream purification are explained in this section.

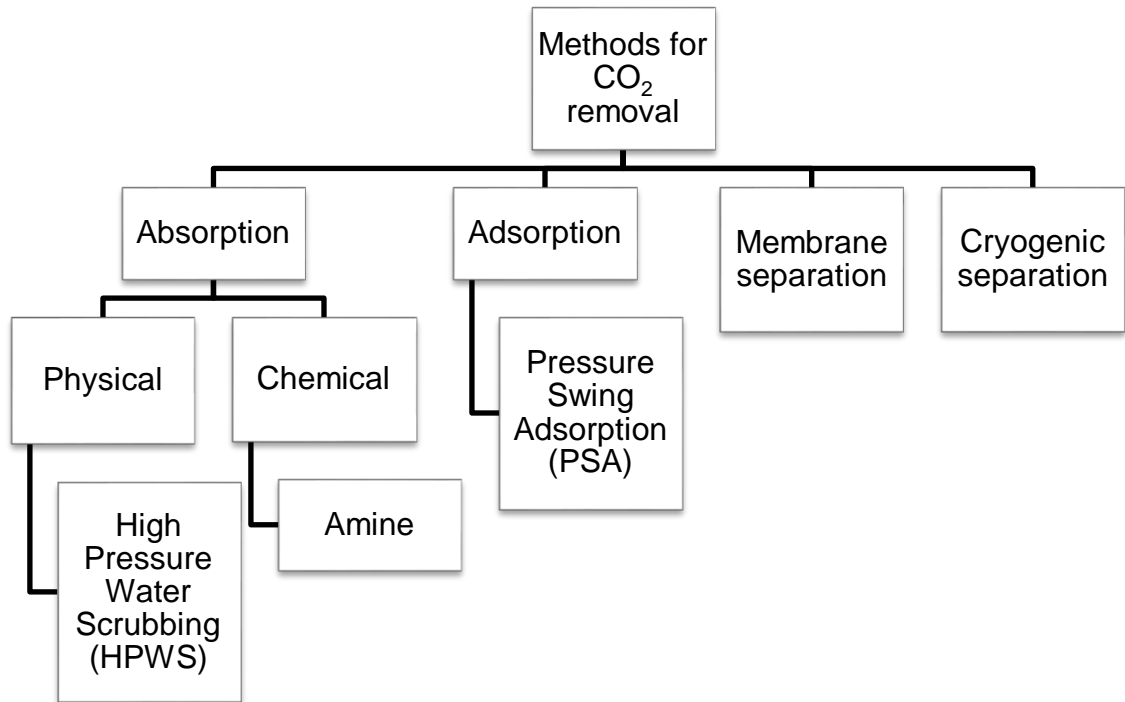


**Figure 2.8** Common techniques used for CO<sub>2</sub> removal.

### 2.4.1 Physical and chemical absorption

Physical absorption is an operation of a non-reactive process in which a gas mixture is contacted with a liquid where one component of the gas mixture is being absorbed into the liquid. The physical absorption of gases in water is explained by Henry's Law (equation 2.1), where gases dissolved in the liquid is determined by the equilibrium constant between undissolved gas and the gas dissolve in the liquid (solvent).

Henry's Law:

$$K_H = \frac{P_x}{C_x} \quad (2.1)$$

where,

$K_H$  = Equilibrium constant for the salvation process;

$P_x$  = Partial pressure of component x;

$C_x$  = Concentration or solubility of component x in liquid solution.

Based on equation (2.1), the amount of gas dissolved is directly proportional to the partial pressure in the gas phase. Moreover, the solubility of gas decreases with increasing of temperature. This is because the relationship between gas solubility with temperature is very similar to the reason that vapour pressure increases with temperature. Increasing of temperature leads to higher kinetic energy causing more motion in molecules which break intermolecular bonds and escape from solution. For that reason, HPWS technique is usually operated at lower temperature (20–30 °C) and higher pressure (8–30 bar) in order to have a better separation of CO<sub>2</sub> from the gas stream.

On the other hand, chemical absorption used a liquid such as amine where CO<sub>2</sub> is not only absorbed into the liquid, but also is chemically bonded with the amine in the liquid. There are two types of amine solutions that commonly used, which are mono ethanol amine (MEA) and di-methyl ethanol amine (DMEA) [70]. In order to recycle the solution, higher energy is required for removing CO<sub>2</sub> from the amine solution (3.2–5.5 MJ per kilogram of recovered CO<sub>2</sub> [71]) since the amine is strongly absorbed and chemically bound with CO<sub>2</sub>.

### **2.4.2 Pressure swing adsorption (PSA)**

Pressure swing adsorption (PSA) purifies gas streams by absorbing the impurities on an adsorbent which is a porous solid with a high surface area. Most of the adsorbents used in the commercial processes are carbon molecular sieves (CMS), activated carbons and zeolites [72]. The adsorption takes place between 4–10 bar [72] and the adsorbent is regenerated through by reducing the pressure to near ambient pressure level (0.13–1 atm) [73]. For an upgrading plant which used PSA technique, four, six or nine vessels are operate in parallel [70]. This is because, when the adsorbent is saturated with CO<sub>2</sub>, the raw gas flow is switched to another vessel while the previous vessel going through a regeneration process.

### **2.4.3 Membrane separation**

For this membrane separation technique, the separation of CH<sub>4</sub> from CO<sub>2</sub> is based on the diffusion of CO<sub>2</sub> through a polymer hollow fibre membrane. The driving force is the partial pressure differences across the membrane for CO<sub>2</sub>, CH<sub>4</sub> and other gas components. CO<sub>2</sub> is the ‘fast’ gas, whereas the CH<sub>4</sub> diffuses at a slower rate, which results in a CH<sub>4</sub>-rich gas at the outlet of the membrane. Therefore, two different streams are obtained by using a membrane separation method which are permeate gas (mainly CO<sub>2</sub>) and the retentate gas (concentrated CH<sub>4</sub>) [72] as shown in Figure 2.9.



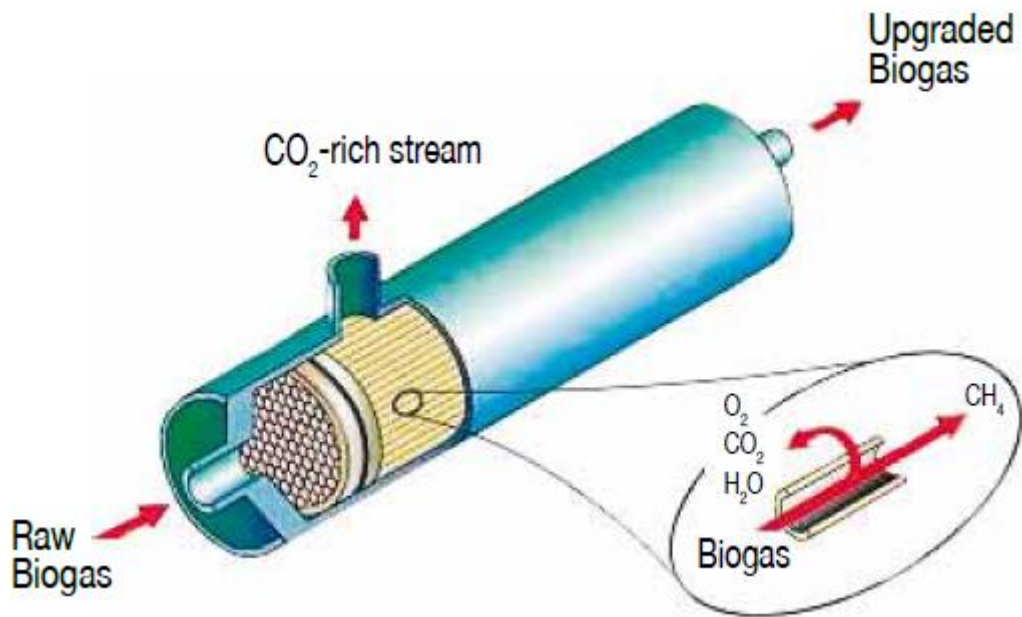


**Figure 2.9** Schematic diagram of membrane separation for biogas upgrading process [74].

#### 2.4.4 Cryogenic separation

CO<sub>2</sub> can be removed by compressing and cooling down in the cryogenic process at 18 bar and -24 °C to liquefied CO<sub>2</sub> [75]. After CO<sub>2</sub> has been removed as a liquid, the remaining CH<sub>4</sub> gas can be cooled further to become a liquid [76]. However, higher energy is required in order to achieve low temperature for cooling down the CO<sub>2</sub> gas.

#### 2.4.5 Comparison between the upgrading techniques

A short comparison of the different upgrading techniques, such as high pressure water scrubber (HPWS), chemical absorption, pressure swing adsorption (PSA), membrane separation and cryogenic separation is listed in Table 2.8. Each of the separation process has its own advantages and

disadvantages in terms of percentage of CH<sub>4</sub> purity, operating and capital expenditure and the level of the difficulties in order to do the maintenance for each of the separation process.

**Table 2.8** Comparison between common CO<sub>2</sub> separation techniques [69, 77, 78]

	HPWS	Chemical absorption	PSA	Membrane separation	Cryogenic separation
Gas pre-cleaning treatment	x	✓	✓	✓	✓
CH <sub>4</sub> loss (%)	1-2	1-2	1-3	0.5-5	0.5-2
CH <sub>4</sub> purity attained (%)	95-98	>99	95-99	>98	99-99.5
Operating cost	Low	Medium	Medium	Low	High
Capital cost	Low	Medium	Medium	Medium	High
Maintenance	Easy	Complex	Easy	Easy	Complex

Although cryogenic separation gives the highest purity of CH<sub>4</sub> as the final product with the lowest of CH<sub>4</sub> lost, but HPWS was found to be the one of the simplest and economical methods compared to chemical absorption, PSA, membrane separation and cryogenic separation [79], which makes it is suitable for a small scale plant [78]. Moreover, HPWS is one of the common technique in biogas plant for removal of CO<sub>2</sub> because of the lower capital and

operational cost, being a reliable and proven technology, as well as the upgrading process is easy to maintain [79-83].

## **2.5 Thermochemical conversion of biomass to SNG production**

There are two main methods to convert biomass into renewable energy which are split into either biological or thermochemical processes. The biological processes are methods that rely on the activity of microorganisms, and many challenges reside in controlling the performance of the microorganisms. This has maintained the attention of researchers in converting biomass via thermochemical processes which are more easily predicted and controlled.

Four different types of thermochemical processes exist for solid biomass conversion. These are combustion, liquefaction, gasification and pyrolysis, as illustrated in Figure 2.10. However, only gasification and pyrolysis processes have the potential to convert biomass to gaseous and vapour fuel, where CH<sub>4</sub> production is the main focus in this research.

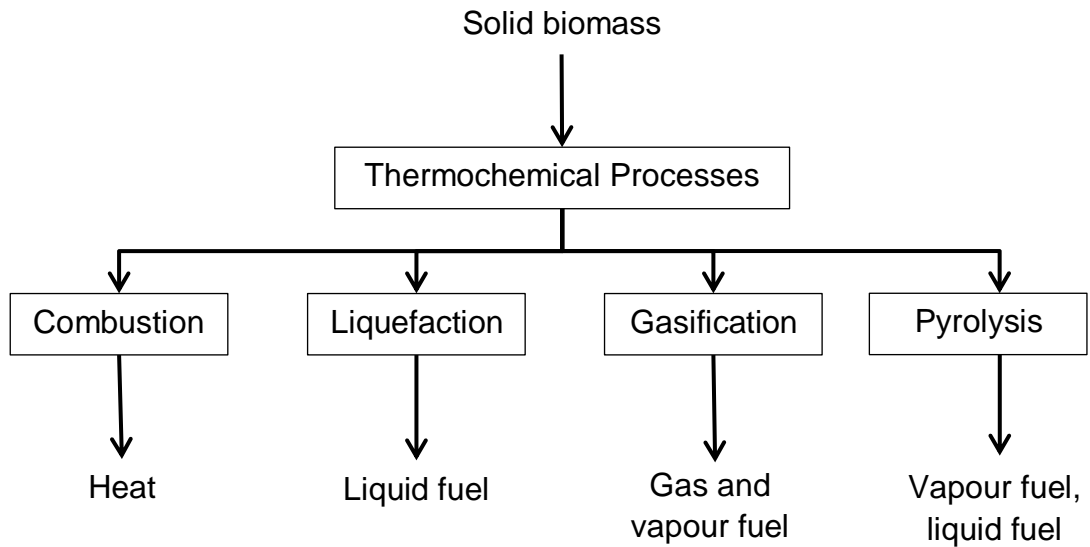
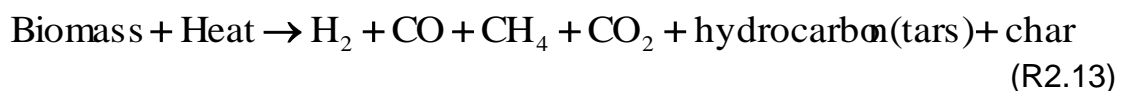


**Figure 2.10** Thermochemical processes of biomass conversion to energy production [39].

The concept of gasification process from biomass is the same as gasification of fossil fuel which was mentioned in the previous section. The biomass feedstock undergoes the gasification reaction, methanation and gas purification accordingly. The conversion process of biomass to SNG production, as reaction (R2.13) requires higher operating temperature (700–1000 °C) to produce syngas, CH<sub>4</sub> and CO<sub>2</sub> gases [84]. Figure 2.11 shows the general gasification process from biomass to SNG production where, syngas is produced from the beginning of the process in the gasifier, which needs to pass through a gas cleaning process due to the tar formation in the gasification process, before the syngas is reacted in the methanation process to produce SNG.



Gasification suffers from poor selectivity to gas products, with typically methane and other alkanes being produced at this stage. It is clear from the reactions (R2.1–R2.3) which represent the methanation stage that the presence of methane in the feed from the gasifier stage would adversely affect their equilibria towards methane consumption. An additional separation stage of the process illustrated in Figure 2.11 and Figure 2.12, where the gas cleaning unit is needed before entering the methanation stage in order to prevent the heavy tar from entering the methanation unit, which might become a threat to the methanation catalysts. The catalytic tar reformer is usually operated at high temperatures in the range of 710–890 °C [85, 86]. Therefore, many researchers have been reviewed on the syngas cleaning process unit for the commercialization of biomass technology regarding to this problem [87].

Moreover, several studies have been working on finding a solution in order to reduce internal reforming tars by providing potassium inside the gasifier [88] which can promote tar cracking reaction [89] and by using suitable bed materials with a moderate tar cracking activity [90]. The general gasification process of conversion of biomass to methane thus appears energetically costly and complex. In addition, the multi stage configuration would represent a safety challenge by providing multiple opportunities for potential leakage of CO (toxic) and H<sub>2</sub> (highly explosive) in addition to the other flammable gases.

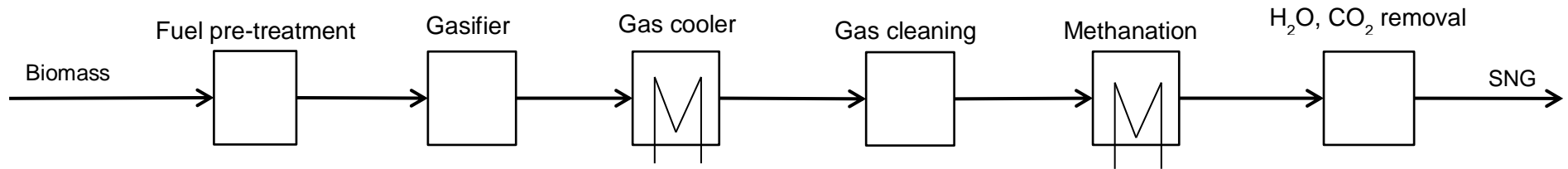


**Figure 2.11** General gasification process of wood to SNG production [91].

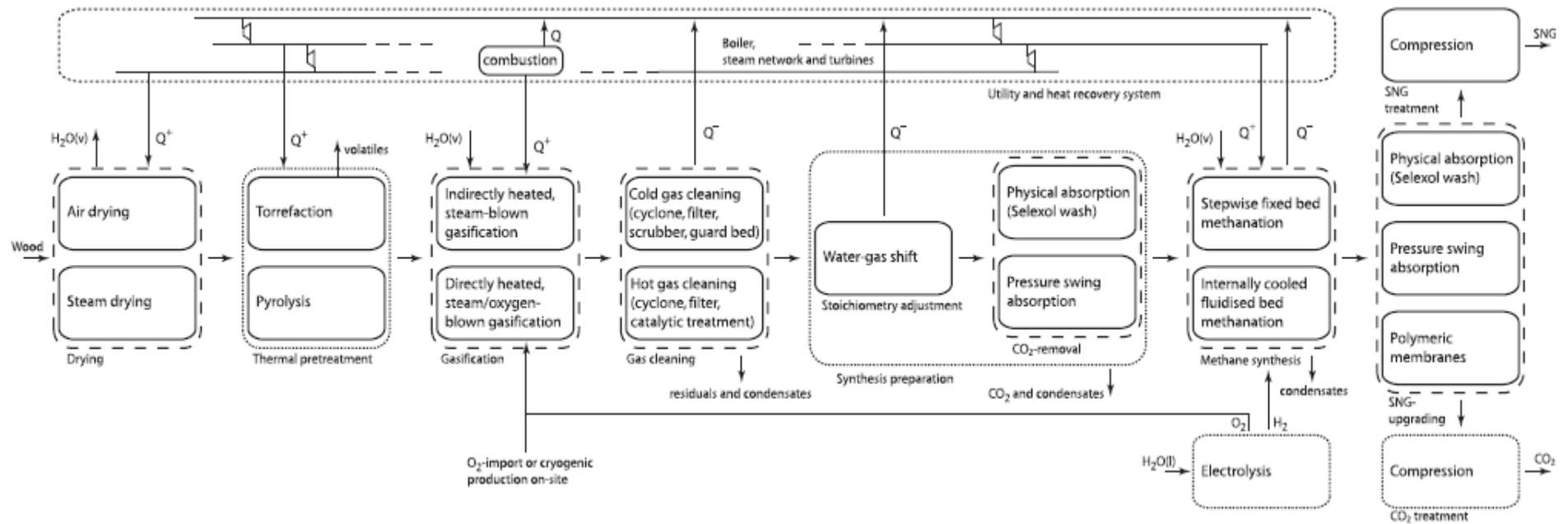


**Figure 2.12** Process flow for production of SNG from lignocellulosic biomass gasification technology [92].

In contrast, the pyrolysis process converts biomass to bio-oil, gas and solid products, as in equation (R2.14) by thermal decomposition of biomass in the absence of oxygen at lower temperature within 350–550 °C [93, 94]. The products are easily separated due to their different phases: solids fall either at the bottom of the pyrolyzer or collected by cyclone at the top, bio-oils are then condensed by cooling, leaving the gases evolve from the condenser separator. Solids can either be upgraded or re-used as fuel for the pyrolysis's energy demand. Gases can join the methanate prior to the final separation stage, leaving the bio-oil as sole feedstock for methanation. Bio-oils are volatiles and therefore would be well suited to catalytic methanation reaction technology, similar to industrial methanation of naphtha.

Furthermore, bio-oils are easier to handle, store and transport [95] than the solid biomass they originate from. For example, an assessment has found that two truckloads of wood chips are equivalent to a single tanker load of bio-oil with the same energy content [96]. Thus, it is convenient to utilize biomass in the form of pyrolysis oil for further reaction to produce SNG.



### **2.5.1 Bio-oil production from pyrolysis**

Bio-oil production via fast pyrolysis is one of the most attractive processes for converting solid biomass into renewable chemicals and higher value fuels [97, 98] due to its feedstock flexibility. This process converts biomass into bio-oil (60–75 wt.%), solid char (15–25 wt.%) and gases (10–20 wt.%), depending on

its feedstock and process parameters [99] by thermal decomposition of biomass in the absence of oxygen in the range of 350–550 °C [93, 94] and reaction time of 0.5–5.0 s [93, 94, 99]. Bio-oil production was also reviewed in 2004 as substitute for fuel oil or diesel for boilers, furnaces, engines and turbines in power plant station [100]. General applications for fast pyrolysis products including gas, bio-oil and charcoal are shown in Figure 2.13.

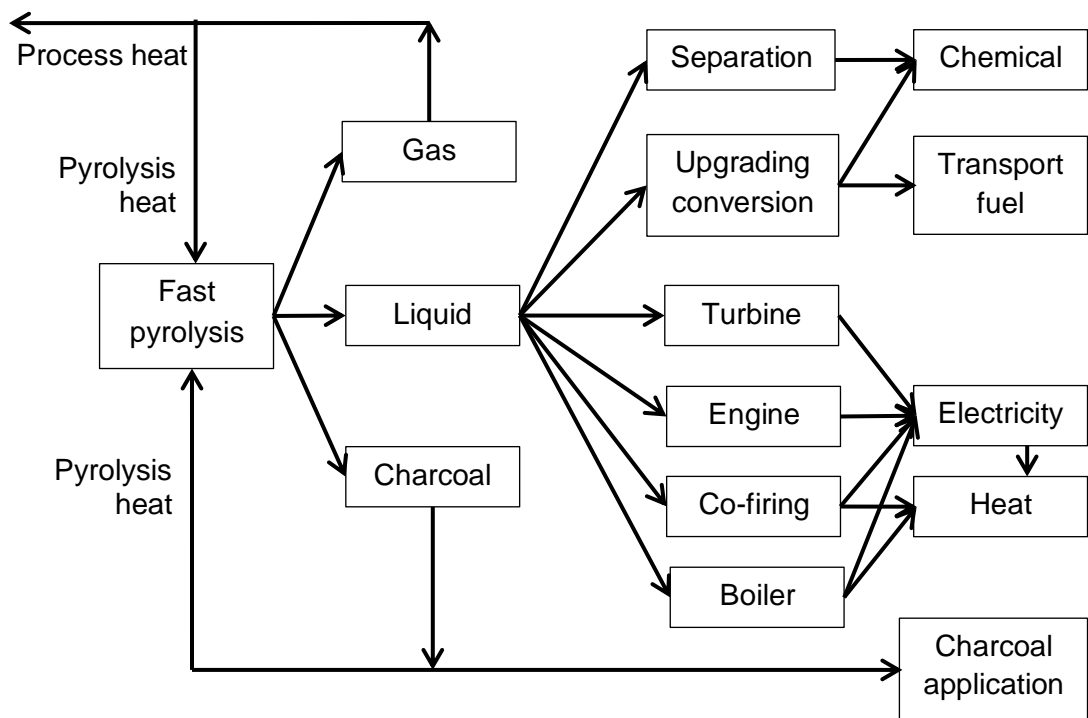


**Figure 2.13** General applications for fast pyrolysis products [93].



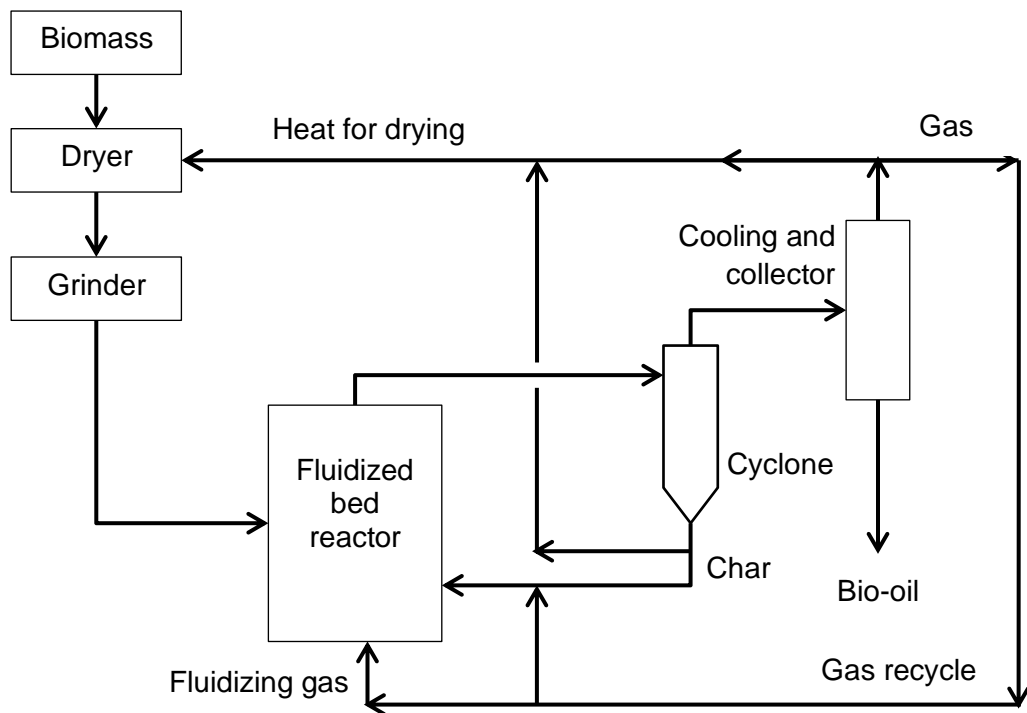


**Figure 2.14** Fast pyrolysis process for fluidized bed [101].

The reactor types recently used for pyrolysis process are fluidized bed, circulating fluid bed and fast fluidized bed [101]. But, most researchers carried out pyrolysis process in fluidized bed since it is easy to operate and gives good results [102]. The fast pyrolysis process for fluidized bed is shown in Figure 2.14, which consists in biomass preparation stage (biomass dryer and grinder), reactor, cyclone (to separate char) and product collector (collection of bio-oil production). Table 2.9 shows several host organizations in 2012 that carried out pyrolysis for bio-oils production from white wood as feedstock and mostly for electricity generation and transport fuel production applications.

**Table 2.9** Pyrolysis for bio-oil production in 2012 from white wood [103].

Host organization	Country	Capacity kg feed/hr	Capacity kg bio-oil/hr	Application	Status
BTG	Netherlands	250	200	Fuel and chemicals	Operational
BTG Bioliquids EMPYRO	Netherlands	6,500	5,000	Fuel	In design phase
Ensyn several	Canada and U.S.A.	3–3,100	2–2,350	Fuel and chemicals	Operational
Mississippi State University	U.S.A.	200	150	Fuel	Construction
National Renewable Energy Laboratory	U.S.A.	12	10	Fuel and chemicals	Operational
RTI International	U.S.A.	40	-	Transportation fuel	Construction
KIT	Germany	1,000	-	Transportation fuel	Operational
UOP	U.S.A.	40	-	Transportation fuel	Operational

### 2.5.2 Properties of bio-oil

Bio-oil is a derivation from lignocellulosic biomass, the latter contains three main components such as cellulose, hemicellulose and lignin. A research was carried out to observe the products distribution from pyrolysis of the components, as listed in Table 2.10. Pyrolysis of cellulose produced the highest yield of bio-oil (81.41 wt.%) with the minimum amount of char

production (6.44 wt.%). This is in contrast to lignin pyrolysis which gives the lowest bio-oil yield (21.77 wt.%) with the highest char production (40.33 wt.%). Bio-oils consist of different compounds for individual biomass feedstock, as listed in Table 2.11.

**Table 2.10** Product of pyrolysis from three main components in biomass [104].

Components	in weight percentage (wt.%)		
	Bio-oil	Gas	Char
Cellulose	81.41	12.15	6.44
Hemicellulose	44.22	36.73	19.05
Lignin	21.77	37.9	40.33

**Table 2.11** Production of several compounds in bio-oil production from biomass pyrolysis [104, 105].

Component	Compound
Cellulose	Levoglucosan
	Anhydro-oligosaccharides
	Altrose
	2,5-Diethoxytetrahydrofuran
Hemicellulose	Acetic acid
	2-Furfural
Lignin	Phenol
	2,6-Dimethoxyphenol
	2,6-Dimethoxy-4-(2-propenyl)phenol

As a result, the bio-oil product from biomass pyrolysis has a complex and variable chemical composition [101, 105]. For example, Table 2.12 shows several identified compounds of bio-oil produced from *Brassica rapa* (BR), pine cone (PC) and grape seed (GP) by using gas chromatography-mass spectrometry (GC-MS). Compounds from guaiacols group were found in higher amounts in three different of bio-oils, followed by phenols and acids. However, the exact amounts of each compound were unknown since GC-MS provides qualitative results.

**Table 2.12** The main compounds of bio-oil from three different type of biomass [106].

Compound	Retention time (min)	Area (%)		
		BR	PC	GS
<b>Acids</b>		<b>2.56</b>	<b>4.19</b>	<b>2.01</b>
Acetic acid	2.89	2.20	3.80	1.92
Propanoic acid	3.673	1.66	0.29	0.09
Butanoic acid	4.929	0.15	0.10	-
Crotonic acid	5.614	0.16	-	-
<b>Aldehyde</b>		<b>2.35</b>	<b>2.20</b>	<b>0.50</b>
Furfural	5.514	2.35	2.20	0.50
<b>Non-aromatic ketones</b>		<b>1.61</b>	<b>1.73</b>	<b>-</b>
<b>Furans</b>		<b>3.45</b>	<b>2.09</b>	<b>3.04</b>
3-Furaldehyde	5.127	0.19	0.13	-
2-Furanmethanol	5.891	2.49	0.32	0.53
1-(2-Furanyl)ethanone	6.871	0.41	0.22	-
5-Methyl-2-furancarboxaldehyde	7.798	0.36	0.93	0.17
2-Pentyl-furan	8.260	-	-	1.33
2-Acetyl-5-methylfuran	9.058	-	0.07	-
7-Menthylbenzofuran	10.151	-	0.22	-

**Table 2.11** (Continued)

Compound	Retention time (min)	Area (%)		
		BR	PC	GS
2- Menthylbenzofuran	10.231	-	0.20	1.01
<b>Phenols</b>		<b>4.16</b>	<b>5.36</b>	<b>9.85</b>
Phenol	8.099	0.77	1.56	2.17
2-Methylphenol	9.328	0.70	0.07	1.78
3-Methylphenol	9.670	1.25	1.94	2.52
2,6-Dimethylphenol	10.189	0.36	0.19	-
2-Ethylphenol	10.677	0.16	0.19	2.24
3,5-Dimethylphenol	11.127	0.43	0.74	-
2,3-Dimethylphenol	11.276	0.26	0.49	0.81
2,3,6-Trimethylphenol	11.684	0.23	0.18	0.33
<b>Guaiacols</b>		<b>5.00</b>	<b>5.64</b>	<b>4.74</b>
Guaiacol	9.920	1.43	1.83	3.69
4-Methylguaiacol	11.525	0.67	1.65	2.07
4-Ethylguaiacol	12.781	0.88	1.04	1.42
Syringol	13.797	1.38	-	0.21
Eugenol	13.871	0.32	0.44	-
Vanillin	14.480	0.32	0.28	-
5-(1-Propenyl)guaiacol	14.546	-	0.40	0.35
<b>Catechols</b>		<b>2.89</b>	<b>3.84</b>	<b>0.25</b>
Catechol	11.588	1.19	1.63	-
3-Methylcatechol	12.508	-	0.45	-
3-Methoxycatechol	12.563	0.90	-	-
Hydroquinone	12.723	-	0.12	-
4-Methylcatechol	12.923	0.42	1.45	-
3,5-Dihydroxytoluene	13.688	0.38	0.19	0.25
<b>Total area (%)</b>		<b>22.02</b>	<b>25.05</b>	<b>20.39</b>

### 2.5.3 Palm empty fruit bunch (PEFB) pyrolysis oil

The higher demand for vegetable oils especially palm oil has caused a massive production of biomass waste. Moreover, palm empty fruit bunch (PEFB) is currently left out without proper utilization compared to other palm oil by-products (frond, mesocarp fiber, trunk and shell). However, the pyrolysis process is an interesting process to convert PEFB, as abundant waste into bio-oil production. Table 2.13 and Table 2.14 shows the functional group composition and main chemical compound which exists in PEFB bio-oil respectively, while Table 2.15 listed the characteristics of PEFB bio-oil.

**Table 2.13** Composition of functional group of PEFB bio-oil [107].

Frequency range (cm <sup>-1</sup> )	Group	Class of compound
3000–2800	C-H stretching	Alkanes
1750–1625	C=O stretching	Aldehydes, carboxylic acids, ketones
1675–1600	C=C stretching	Alkenes
1500–1450	C-H bending	Alkanes
1300–1000	C-O stretching	Alcohols
900–650	O-H bending	Phenolic aromatic compounds

In general, bio-oil consists a significant amount of organic acid, such as acetic acid and propanoic acid, that gives low of pH values (pH 2–3) [108]. Thus, it explained a huge difference values of area percentages (%) of acids with the other compounds in PEFB bio-oil as shown in Table 2.14. But, the amount of

phenols which been detected by GC-MS also gives a significant value that comparable with acids.

**Table 2.14** Main chemical compounds in PEFB bio-oil in area percentage (%).

Compounds	[109]	[110]
<b>Acids</b>	<b>7.68</b>	<b>32.95</b>
Acetic acid	-	32.06
Propanoic acid	-	0.89
Oleic acid	7.68	-
Furantetracarboxylic acid	-	-
<b>Phenols</b>	<b>14.60</b>	<b>21.23</b>
Phenol	14.60	21.23
3-Methylphenol	-	-
4-Methylphenol	-	-
<b>Furans</b>	<b>-</b>	<b>0.28</b>
2,5-Dimethylfuran	-	-
2(5H)-furanone	-	0.28
<b>Guaiacols</b>	<b>7.70</b>	<b>6.97</b>
2-Methoxyphenol (guaiacol)	0.32	1.99
2,6-Dimethoxyphenol (syringol)	7.38	4.60
2-Methoxy-4-methylphenol (methyl guaiacol)	-	0.38
<b>Total area (%)</b>	<b>29.98</b>	<b>61.43</b>

**Table 2.15** Characteristics of PEFB bio-oil [107, 108, 111, 112].

Reactor temperature (°C)	500
Calorific value (MJ/kg)	20.23–21.41
Density (g/cm <sup>3</sup> )	0.90–1.21
pH	2.33–3.00
Total ash (wt.%)	0.65–1.03
Moisture (wt.%)	18.74–21.68
Elemental analysis (wt.%)	
Carbon (C)	41.86–49.80
Hydrogen (H)	7.82–7.98
Oxygen (O)	40.29–50.22
Nitrogen (N)	0.10–1.93

## 2.6 Methanation catalyst

Nickel (Ni) catalyst is widely used in SNG production since it is cheaper than precious metals, but Ni is not the most active catalyst compared to others [113]. Therefore, a study was carried out by combining the Ni catalyst with other elements such as copper (Cu), cobalt (Co), platinum (Pt), etc., as shown in Figure 2.15, in order to observe the possibilities in improving the activity of Ni catalyst [114]. It was found that the promotion of Ni with the elements from periodic group 5–8 give the minimum methanation temperature.



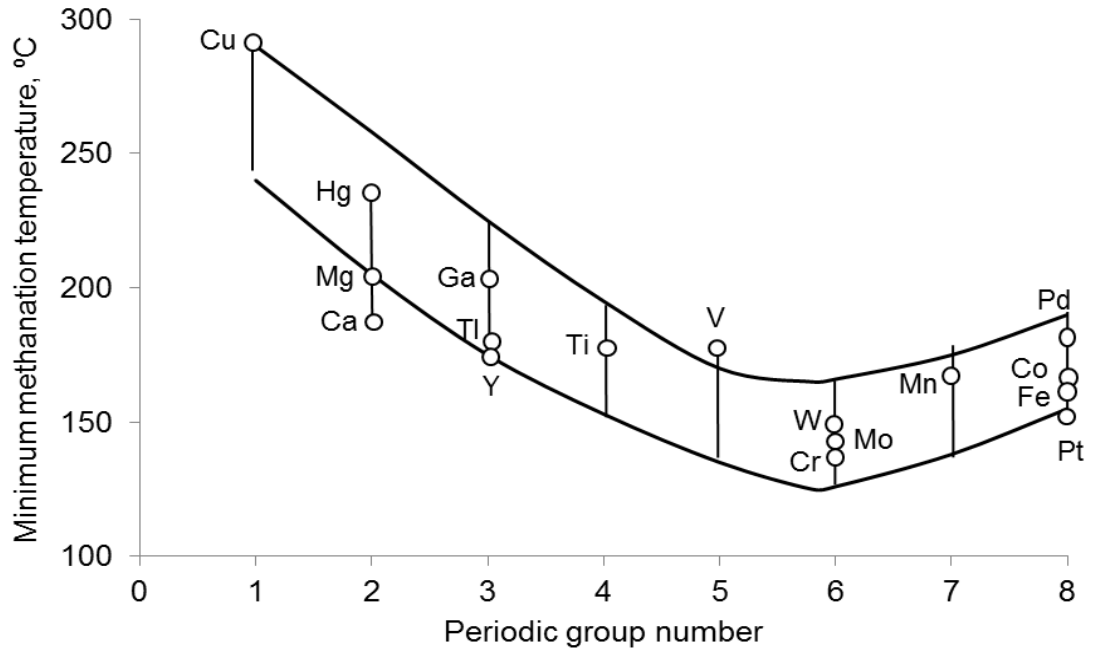


**Figure 2.15** The minimum methanation temperature as a function of elements periodic group number [114].

On the other hand, Figure 2.16 shows the effect of Ni concentration to the surface area of catalyst. The area of catalyst surface is gradually increased with Ni concentration up to approximately 50 wt.%, but then starts to decrease with Ni loading due to the growth in Ni crystallize size [40]. However, the increases in surface area of the catalyst does not always represents a higher catalyst activity, where a study has showed that the activity of Ni for natural gas reforming is increased up to 20–22% of Ni concentration.

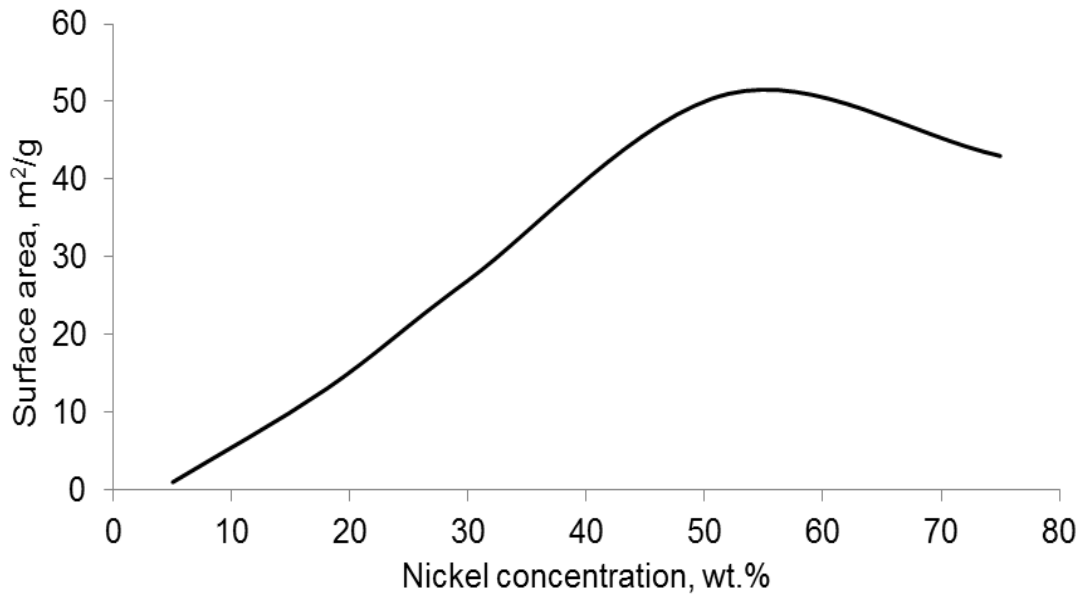


**Figure 2.16** The effect of surface area of catalyst by varying nickel concentration [115].

Several of recent studies have performed methane production from syngas by using mostly Ni as methanation catalyst, these are listed in Table 2.16. Moreover, silica–alumina was preferred to be a better catalyst supporter, since it favours dehydration as the water was produced from methanation process [116]. Nickel supported on alumina catalyst (Ni/Al<sub>2</sub>O<sub>3</sub>) is widely used in most of coal processing plants [117], as well as in the commercial steam reforming of natural gas to produce synthetic natural gas (SNG) [40].

The deactivation the Ni catalyst could lower the catalyst activity due to the carbon deposition, where it encapsulate the Ni particles and loss in carbon-nickel contact [40]. Moreover, sulphur (H<sub>2</sub>S) [40, 117] poisoning could lead to the deactivation of catalyst, as well as thermal sintering [40, 116]. Thus, adsorbents are introduced in the methanation process to remove the impurities [40] which minimize the effect of poisoning on the catalyst [48]. Table 2.17 shows several examples of adsorbents used in gas purification.

**Table 2.16** Current research for using different type of catalyst in methanation process.

Feedstock	Reaction conditions	Catalyst	Reactor type	Reference
Syngas	T=385 °C P=1.5 bar	50 wt.% Ni/Al <sub>2</sub> O <sub>3</sub>	Fluidized bed	[118]
Syngas	T=250–650 °C P=1 atm	Ni/Al <sub>2</sub> O <sub>3</sub>	Fixed bed and fluidized bed	[119]
Syngas	T=300–450 °C P=300 lb/in <sup>2</sup> g (20.7 bar)	Raney nickel-aluminium alloy	Fluidized bed	[120]
Syngas	T=260 °C and 350 °C P=20 bar	20 wt.% Ni/Al <sub>2</sub> O <sub>3</sub>	Fixed bed	[121]

**Table 2.17** Several type of adsorbent used in gas purification [40].

Adsorbent	Impurity removed	Removal efficiency, %
Iron oxide	H <sub>2</sub> S	<99.98 [122]
Molecular sieve	H <sub>2</sub> S and CO <sub>2</sub>	72–100 [123]
Zinc oxide	H <sub>2</sub> S	99.93–99.99 [124]
Dolomite/lime	H <sub>2</sub> S and CO <sub>2</sub>	<90 [125]

Many studies have focussed on sorption enhanced reaction process (SERP) for the past decades in order to enhance steam methane reforming to produce hydrogen (R2.15), where the reforming catalyst is mixed with CO<sub>2</sub> adsorbent together in a single reactor [126-128]. It is also known as calcium looping (CaL) process when a solid CaO-based sorbent (i.e. calcium oxide, CaO) is

used as the CO<sub>2</sub> adsorbent. In this process, the presence of the CaO leads to more hydrogen production by removing CO<sub>2</sub> from the products of the methane steam reforming (R2.15) and water gas shift (R2.16) reactions. By combining the steam methane reforming, water gas shift and carbonation (R2.17) reactions in a single reaction step in a single unit of reactor, the calcium looping and sorption enhanced reforming (CaL-SER) process could reduce the number of process steps by eliminating the shift reactors, as shown in Figure 2.17.

Although the steam methane reforming is a highly exothermic reaction, ( $\Delta H_{298K} = 206.2$  kJ/mol), the combination of heat released from the exothermic water shift and carbonation reactions are thermally balanced and no additional fuel is required in the primary reactor. It was reported that about 20% of potential energy savings of SER process compared to conventional of steam methane reforming [127].

Steam methane reforming:



Water gas shift:



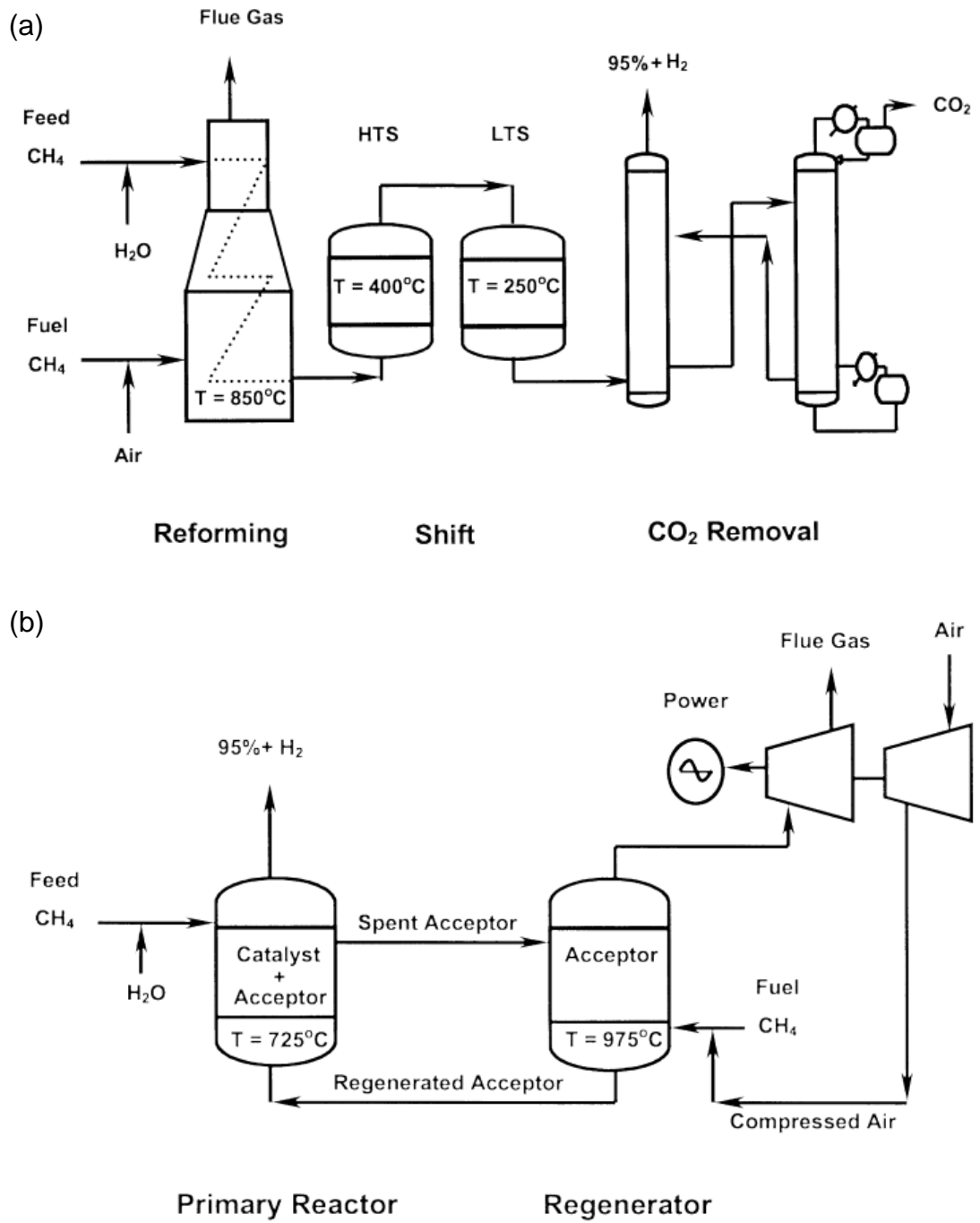


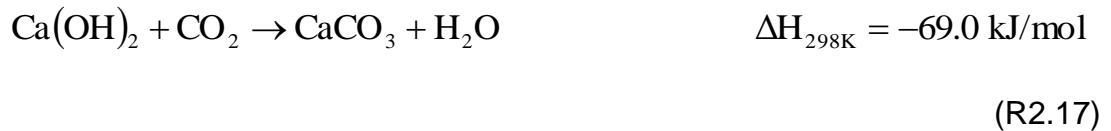
**Figure 2.17** Simplified flow diagram of (a) the conventional and (b) the single step of steam methane reforming processes [128].

Recently, a study has modelled a gasification process from biomass by using calcium oxide (CaO) as sorbents to capture CO<sub>2</sub> in gas production, as expressed in (R2.16) [129]. In the carbonation reaction, production of CO<sub>2</sub> from methanation process reacted with CaO to produce calcium carbonate (CaCO<sub>3</sub>), which resulted higher purity of methane produced. However, the carbonation of Ca(OH)<sub>2</sub> (R2.17) should be accounted since the hydration of CaO into Ca(OH)<sub>2</sub> (R2.18) could readily occur as CaO exposed to humidity in the air.

Carbonation of CaO:



Carbonation of Ca(OH)<sub>2</sub>:



Hydration of CaO:



Moreover, a study [130] shows that Ca(OH)<sub>2</sub> pellet has higher sorption capacity of CO<sub>2</sub> compared to CaO pellet. Based on Table 2.18, Ca(OH)<sub>2</sub> pellet has larger surface area compared to CaO pellet, due to the decomposition of Ca(OH)<sub>2</sub> which release H<sub>2</sub>O and creates much more surface area on the

Ca(OH)<sub>2</sub> pellet that enhanced the CO<sub>2</sub> sorption. Thus, using CaO and Ca(OH)<sub>2</sub> as sorbents for this research, which is the conversion of bio-oil to methane via steam reforming process is potentially to enhance the purity of methane produced, where the results are discussed in Chapter 4.

**Table 2.18** Comparison of surface properties between Ca(OH)<sub>2</sub> and CaO pellets [130].

	Ca(OH) <sub>2</sub> pellet	CaO pellet
BET surface area (m <sup>2</sup> /g)	7.544	2.801
Total pore volume (cm <sup>3</sup> /g)	0.058	0.012
Average pore diameter (Å)	312.29	173.37

## 2.7 Summary

From the review of the literature discussed in this chapter, internally cooled reactor type IRMA (isothermal reactor) is preferable for the sake of the simplicity of the process compared to other common technologies which require more than two adiabatic reactors in the methanation unit for producing  $\text{CH}_4$ . The HPWS for upgrading biogas to bio- $\text{CH}_4$  is suitable for the small scale  $\text{CH}_4$  production due to its lower operational and capital cost. As the biomass gasification to produce  $\text{CH}_4$  is energetically costly and complex, this research attempts to fill the gap by introducing the low temperature steam reforming process (LTSR) of bio-oil for  $\text{CH}_4$  production via fast pyrolysis of biomass, where this process operates at lower temperature than gasification to convert biomass into bio-oil without generation of heavy tars. Therefore, it is convenient to utilise biomass in the form of volatile pyrolysis oil for further catalytic reaction to produce  $\text{CH}_4$ .



## Chapter 3

### Research Materials and Methodology

#### 3.1 Introduction

This chapter describes in detail both the modelling and experimental methodologies that are used in this research. In the modelling approach, NASA's Chemical Equilibrium with Applications (CEA) program was used to obtain chemical equilibrium compositions for assigned thermodynamic states, such as temperature and pressure, or system enthalpy and pressure, while the Aspen Plus (V8.8) process modelling program was used to simulate and develop a full flow process of bio-methane production from biomass via fast pyrolysis and direct methanation of the bio-oil. Experiments of methanation of acetic acid, as single compound surrogate of bio-oil in a packed bed reactor via LTSR were performed in order to observe the feasibility of the process in a real conditions at bench scale. This chapter covers the methods used to run and analyse the outputs of these experiments. The characterization of fresh and used catalysts was carried out and analysed by several techniques which are also discussed in this chapter.

## 3.2 Modelling approach

### 3.2.1 Chemical Equilibrium and Applications (CEA) program

The code Chemical Equilibrium and Applications (CEA) was used in this work to obtain chemical equilibrium compositions for assigned thermodynamic states, such as temperature and pressure, or system enthalpy and pressure. CEA's solution method is based on minimization of Gibbs energy from a chosen set pool of reactants and equilibrium products of known thermodynamic properties, as opposed to from an assumed set of reactions with known equilibrium constants. This offers the advantage that provided the chosen pool of products is comprehensive, no assumptions are made towards which reactions have taken place to reach equilibrium. The simulations of this work are at first mainly focused towards the constant temperature and pressure conditions. Isothermal and isobaric conditions are close to those of a packed bed reactor with negligible pressure drop across the reactive zone where, in the case of an exothermic process like methanation, cooling would be applied throughout the reactor to maintain a controlled, constant temperature.

Additional simulations were performed later with constant enthalpy and pressure, simulating a well insulated reactor whose temperature evolves from a set initial value to a higher one in the case of an exothermic process, or to a lower one for an endothermic process. The equations based on minimization of Gibbs energy presented in CEA [131] are nonlinear in the composition variables and thus CEA relies on an iteration procedure that utilizes a Newton-

Raphson method to solve the corrections to initial estimates of compositions and moles of gaseous species [132]. In addition, the user can expand the thermodynamic data library with new compounds such as bio-oil model chemicals (e.g. phenol, levoglucosan, acetic acid, etc.).

### **3.2.2 Aspen Plus program**

Advanced System for Process Engineering (Aspen) Plus is a commercial software, which is familiar to many users in chemical engineering, and as a common tool used for modelling purposes. This modelling computer software package has proven its capability to model whole plant simulations such as bio-methane production via biomass gasification process modelling [86, 91, 133-135] and fast pyrolysis of biomass for bio-oil production process modelling [136-139] regardless of the system complexity. Aspen Plus software provides a large databank of chemical compounds and a property estimation system for calculating stream properties and chemical reactions, but biomass and pyrolysis products which involve in this study are not included in the databank. Therefore, the corresponding properties must be defined manually by the user, an aspect which is discussed in Chapter 6.

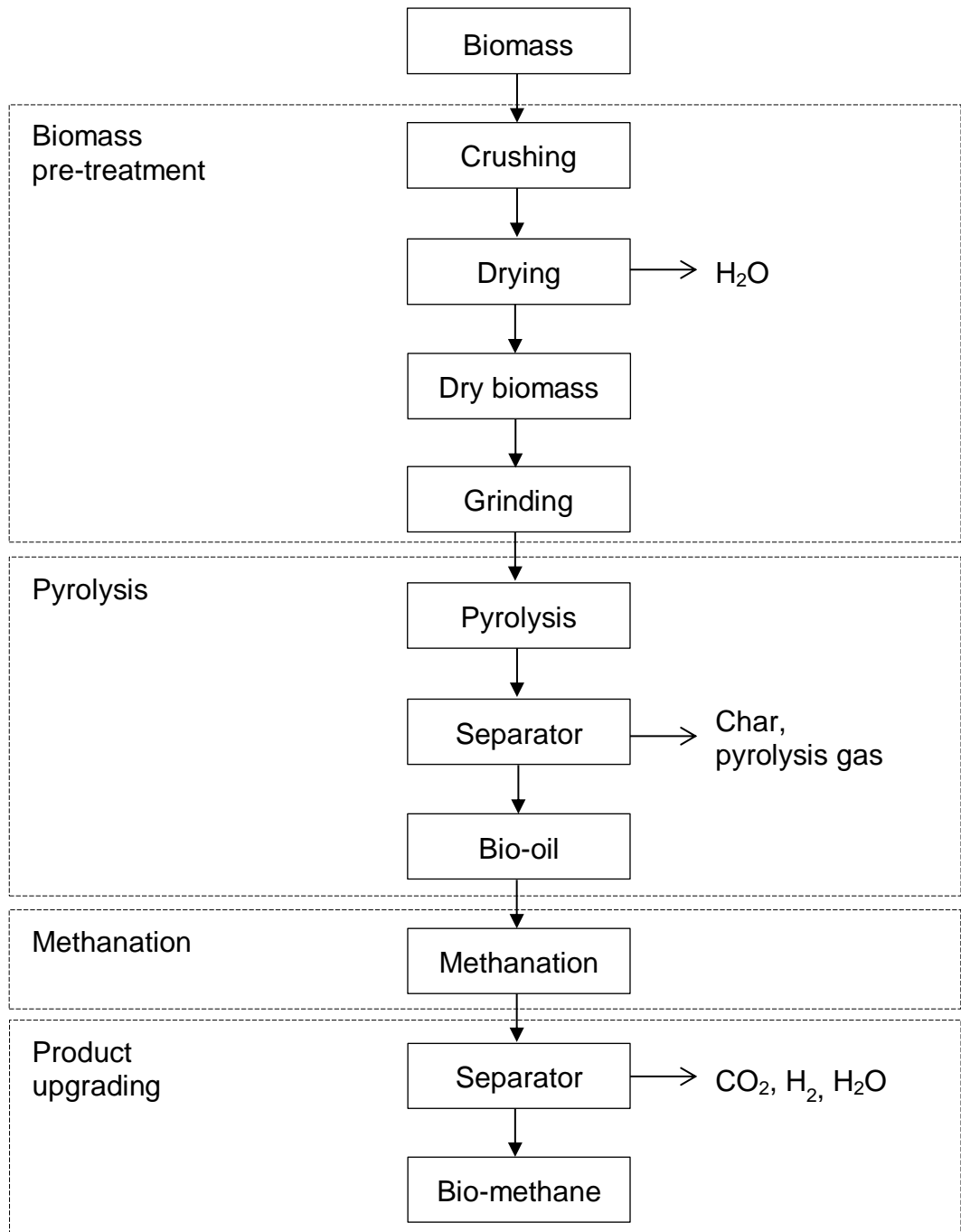


**Figure 3.1** Simplified process flowsheet of bio-methane production from biomass via fast pyrolysis process.

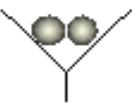





A steady state Aspen Plus V8.8 simulation model has been developed in this study where it provides estimated mass and energy balances for an industrial process of bio-methane production from biomass via fast pyrolysis. The production route consists of four process units, namely biomass pre-treatment, fast pyrolysis, methanation reactor and product upgrading as shown in Figure 3.1. In the first step, biomass, specifically palm empty fruit bunch (PEFB) which is used as the feedstock in this study is chopped and ground into smaller particles (less than 3 mm) and then to be dried, where moisture content in the PEFB is less than 10 wt.% on a dry basis in order to meet the optimal conditions for fast pyrolysis reaction [139, 140]. Next, the dry and smaller size of PEFB is going through a pyrolysis process where the main product is the organic vapour, which is later to be condensed into bio-oil [138]. In the catalytic methanation process, the bio-oil is converted to  $\text{CH}_4$ ,  $\text{CO}_2$ ,  $\text{H}_2$ ,  $\text{CO}$  and water steam products, and continuously flowed into a gas cleaning unit. The by-products which are  $\text{CO}_2$ ,  $\text{H}_2$ ,  $\text{CO}$  and water steam products are removed from the stream to obtain a methane-rich gas, as well as to meet the requirements for injecting the bio-methane into the natural gas grid. The details of modelling approaches taken in each processing unit and its validation for the full process of bio-methane production from PEFB via fast pyrolysis are described in Chapter 6.

In order to develop a simulation model for the bio-methane production from PEFB via fast pyrolysis process, a physical property data set needed to be selected first, which it would later be used to calculate the thermodynamic properties based on the data sources provided in the Aspen Plus software. The Peng-Robinson (Peng-Rob) property method was used in this simulation,



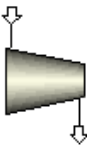
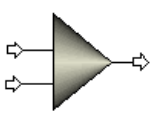
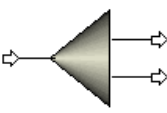

as this model is suitable for nonpolar and mildly polar mixtures, such as those of oxygenated hydrocarbons of bio-oil. This method is also suitable for higher temperature and pressure regions, in which hydrocarbon-processing, gas-processing, refinery and petrochemical applications are usually operated [141]. Moreover, Peng-Rob was used previously to simulate gas processes for the treatment of biomass residues from a paper mill with a thermomechanical pulp (TMP) conversion process into bio-synthetic natural gas (bio-SNG) [90]. For the process unit which involved physical absorption in this thesis' plant model, we chose the Non-Random-Two-Liquid (NRTL) as the property method to describe the behaviour of the dissolved gases in liquid by using Henry's law, which was previously used to simulate a high pressure water scrubber for biogas upgrading [142].

Several unit operation blocks in this thesis' plant model with their own specific process operations (i.e. chopper/grinder, cooler, heater, combustor, cyclone, reactor, pump, etc.) were inserted in the Aspen Plus flowsheet. Table 3.1 shows a general description for different unit operation blocks in the Aspen Plus software that were used in this study. After that, the material streams with specified feed flowrates were introduced on the flowsheet. Creating a link between the selected model blocks and gave a complete process flow diagram. Finally, the simulation needed to be run in order to obtain the results calculated by the Aspen Plus software.

**Table 3.1** Description of unit operation blocks in Aspen Plus software.

Block ID	Unit operation	Role description
 Crusher	Chopper and grinder	To reduce the size of the solid biomass where the energy requirement for both chopper and grinder are based on literature data.
 Heater	Cooler and heater	To cool down or heat up the feed stream to a specified temperature.
 Sep	Separator	To separate components based on specified flows or split fractions in a specified operating temperature.
 Flash	Flash drum and evaporator	To separate components based on the phase difference in a specified operating temperature and pressure.
 Cyclone	Cyclone	To separate solid (char) from volatiles and gases.
 RYield	Pyrolyzer	A nonstoichiometric reactor based on known yield distribution, which is taken from literature data. RYield block used as pyrolyzer converts biomass into a specified composition of bio-oil, non-condensable gases and char that are produced during the pyrolysis process.

**Table 3.1** (Continued)

Block ID	Unit operation	Role description
 RGibbs	Combustor	An equilibrium reactor, the combustor which burns bio-char in the presence of air into combustion products based on the principle of minimizing Gibbs energy during the oxidation process.
	Methanator	An equilibrium reactor, the methanator converts bio-oil and non-condensable gases into a CH <sub>4</sub> -rich gas via the LTSR process, based on the principle of minimizing Gibbs energy.
 Pump	Pump	To increase the pressure of the inlet of the liquid stream to a specified pressure.
 Compr	Compressor	To increase the pressure of the inlet of the gas stream to a specified pressure.
 Mixer	Mixer	As a stream mixer, where two or more input streams can be mixed into a single output stream.
 FSplit	Splitter	As a stream splitter, where the input stream can be divided into two or more streams based on the specified flows or split fractions in each of the outlet stream.
 Radfrac	Water scrubber	A simple distillation column based on Henry's Law, which describes the physical absorption of gases with high solubility in water in order to obtain higher purity of the CH <sub>4</sub> gas product.



As the mass and energy balances for all of the processing units are carried out at the beginning of the simulation work, a proposed of heat integration process modelling is then developed by using these energy balances. Therefore, several of heat exchanger network between possible streams are simulated with the aim to minimize energy consumption and to achieve higher performance of bio-methane production from the PEFB conversion process. Figure 3.2 shows the unit operation block for heat exchanger which is provided in the Aspen Plus software, where two input streams that need to be cooled (hot stream) or heated (cold stream) are determined at first before running the simulation. Based on the heat content or enthalpy (H) of the stream, the hot stream will cool down by transferring some of the heat to the cold stream where a minimum temperature difference,  $\Delta T_{\min}$  of 20 °C was used to ensure the driving force for the heat exchanger network [143]. More detail of discussion regarding to the implementation of heat exchangers in the process are further discussed in Chapter 6. This process modelling with heat integration is then to be compared with the conventional gasification-methanation of syngas using similar feedstock to PEFB (e.g. wood) in terms of energy efficiency, where the results are fully discussed in Chapter 6.

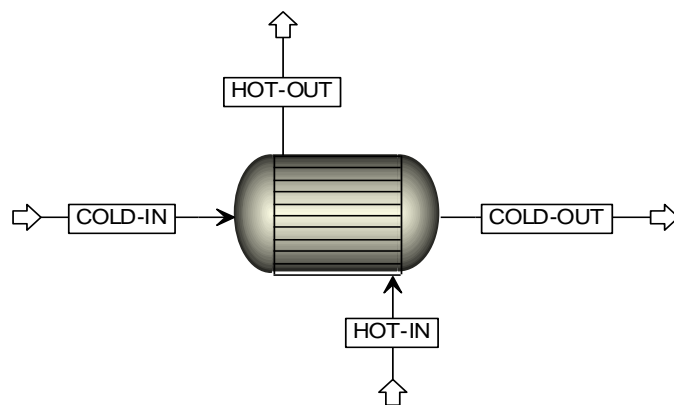


**Figure 3.2** Unit operation block of a heat exchanger in Aspen Plus software.

### **3.3 Experimental approach**

#### **3.3.1 Research materials**

In this section, the chemical compositions of palm empty fruit bunch (PEFB) bio-oil, together with the commercial catalyst (Ni/Ca-Al<sub>2</sub>O<sub>3</sub>) used for the methanation of bio-oil in a packed bed reactor via LTSR experiments are discussed.

##### **3.3.1.1 Chemical compositions of PEFB bio-oil**

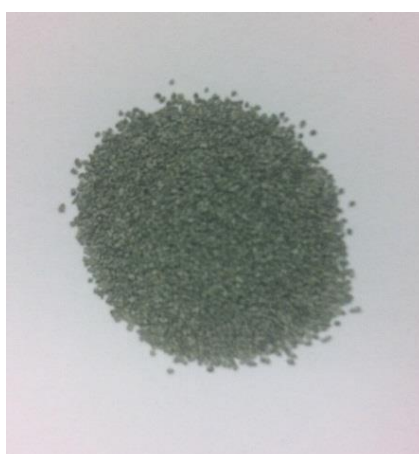
PEFB contains a great range of carboxylic acids, phenols, ketones, alcohols and aldehydes, in which acetic acid was found as the main compounds of PEFB bio-oil, in addition to many other oxygenated organics [107, 108, 110]. For this study, acetic acid was used as bio-oil surrogate for low-temperature steam reforming (LTSR) process in a packed bed catalytic reactor, and therefore could form the basis for evaluating optimum conditions before the utilization of the complex bio-oils. However, sensitivity analysis was also being conducted to demonstrate that the results at chemical equilibrium using CEA for different PEFB bio-oil compositions are not sensitive to a precise bio-oil composition, provided the elemental composition is preserved, which are discussed in Chapter 4.

### 3.3.1.2 Catalyst

The commercial catalyst, nickel supported on calcium aluminate ( $\text{Ni}/\text{Ca-Al}_2\text{O}_3$ ) supplied by Twigg Scientific and Technical Ltd (TST Ltd) was used in this research. The catalyst was provided in the form of raschig ring pellets as shown in Figure 3.3(a). However, the catalyst was then crushed and sieved within 250–355  $\mu\text{m}$  of particle size shown in Figure 3.3(b) for the packed bed experiments.



(a)



(b)

**Figure 3.3**  $\text{Ni}/\text{Ca-Al}_2\text{O}_3$  catalyst from TST Ltd in form of (a) as-received pellet and (b) after crushing and sieving (250–355  $\mu\text{m}$  of particle size).

### **3.3.2 Experimental set-up**

The methodologies used for the methanation of acetic acid in a packed bed reactor via low-temperature steam reforming (LTSR) carried out in this research are discussed. The experimental rig was designed by a former PhD student of Dr. Valerie Dupont and formerly used for hydrogen production from acetic acid.

#### **3.3.2.1 Operation description of LTSR in a packed bed reactor**

A packed bed reactor as shown in Figure 3.4 and Figure 3.5 was used in this study for the investigation of acetic acid conversion into methane, CH<sub>4</sub> production via LTSR. The feedstocks (fuel and water) were pumped into the reactor using programmable syringe pumps, but it was vaporised at first by setting the water vaporiser at 130 °C and fuel vaporiser at 150 °C. Both of the vaporisers were insulated with super wool insulation material to prevent the heat loss from the preheating coils. Then, the N<sub>2</sub>, (carrier gas), which was controlled by MKS Instruments, UK mass flow controller was mixed with the hot vapours from the vaporisers. The heating tape was provided around the pipe connecting the vaporisers to the reformer in order to maintain the temperature. The mixture of the fuel vapour, steam and N<sub>2</sub> passed through a reactor were maintained at the desired temperature, where a type K thermocouple was placed under the catalyst bed to monitor the reaction temperature.

The gaseous products from the reactor were carried by N<sub>2</sub> into the condenser system and underwent separation between volatile and non volatile into the liquid condensate and gas product mixtures. A mixture of ethylene glycol and water with the volume ratio of 1:1 was used as a coolant that circulated between the condenser and a chiller (Fisher Scientific 3016S), which was set at 0 °C to maintain the condenser at a low temperature. The liquid product (condensate) was collected after finishing the experiment for further analysis, in particular closure of the carbon balance. The product gases, which were mainly CH<sub>4</sub>, CO<sub>2</sub>, CO, H<sub>2</sub> and N<sub>2</sub> continuously flowed into a silica gel trap to remove any moisture left in the products. Finally, the dry gaseous production was analysed by micro-GC (Varian) for composition analysis.

A series of steam reforming experiments were conducted with different of reactor temperatures and water flow rates were performed, which are discussed in Chapter 4.

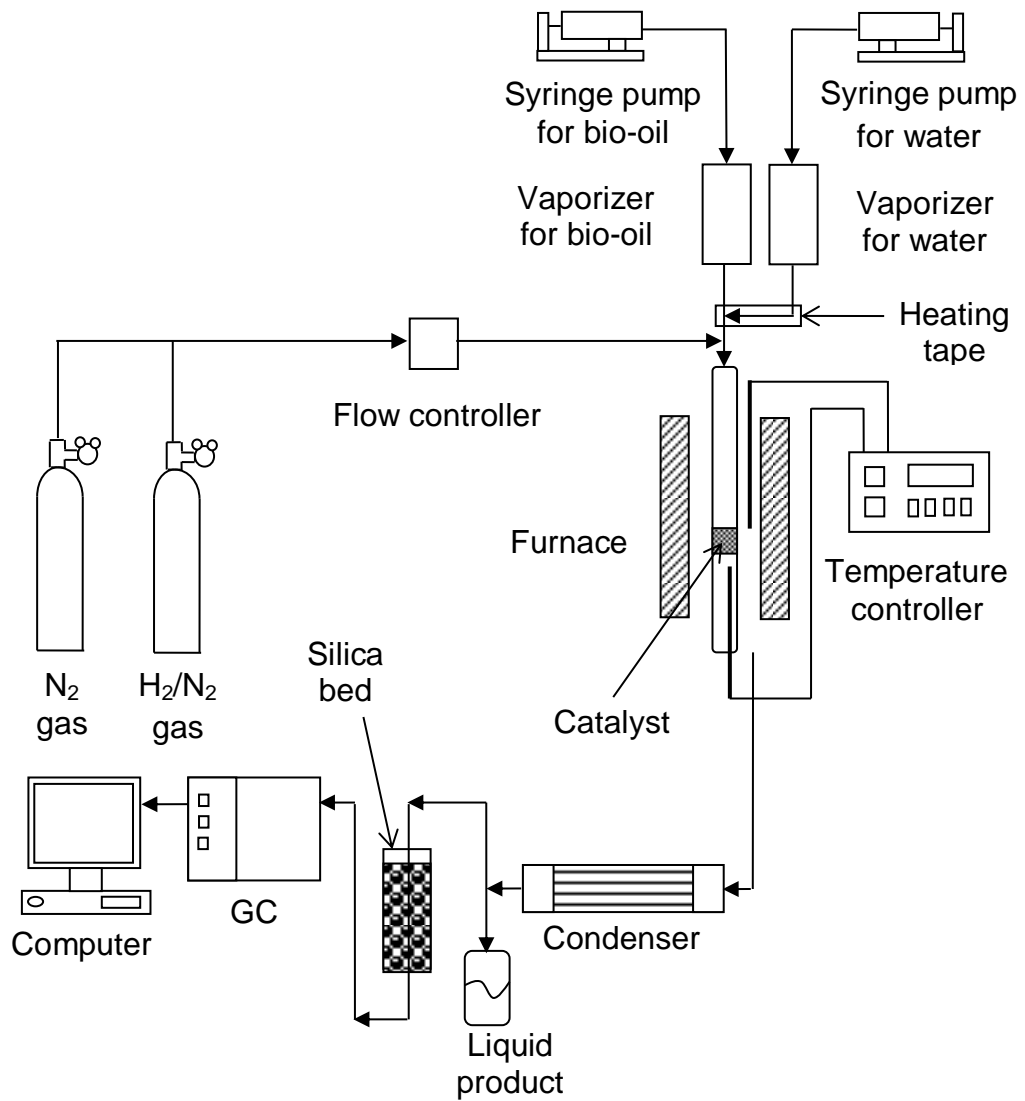


**Figure 3.4** Schematic diagram of experimental set-up for bio-oil conversion into  $\text{CH}_4$  production via LTSR.

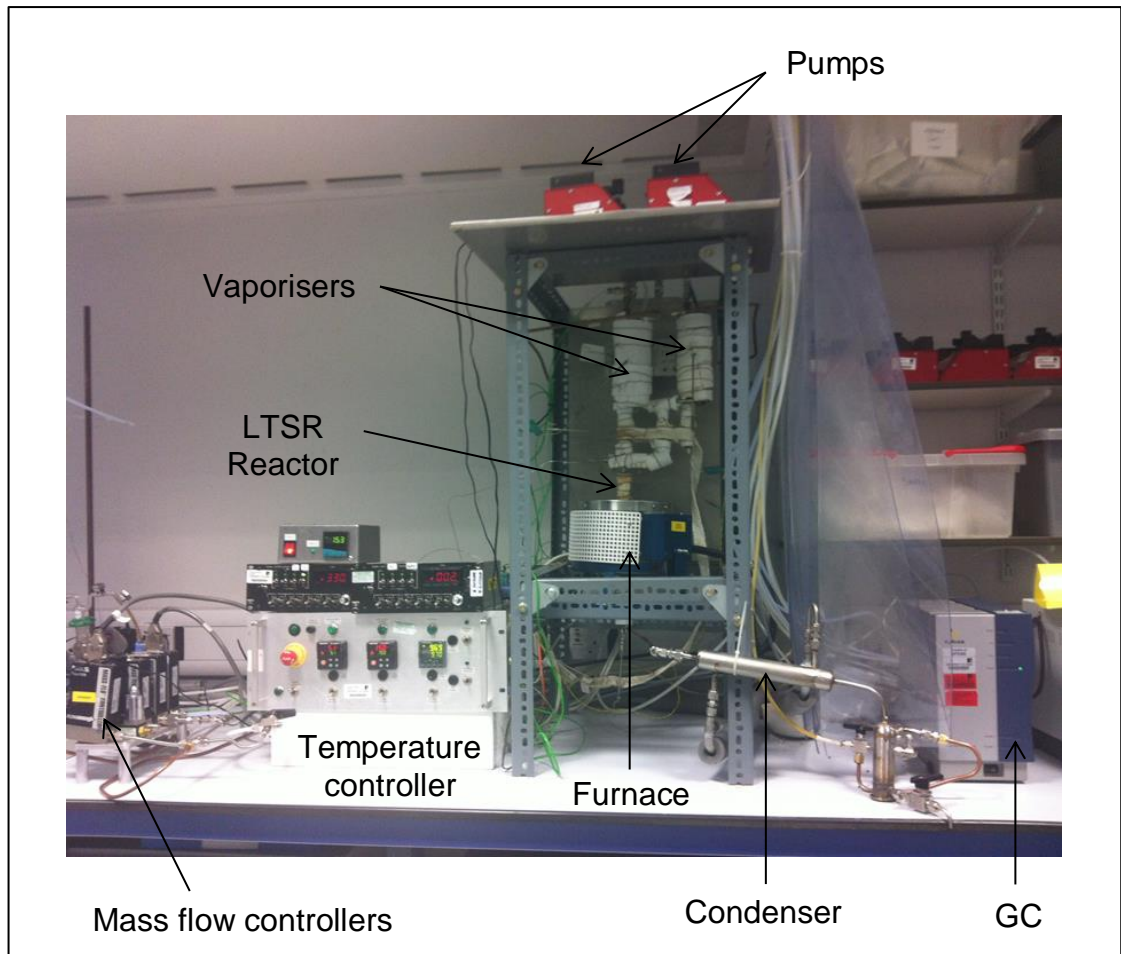


**Figure 3.5** Photograph of experiment rig for bio-oil conversion into  $\text{CH}_4$  production via LTSR.

### 3.3.2.2 Gas chromatograph (GC)

The micro-GC (CP 4900) supplied by Varian Instruments, UK was used to analyse dry gas production as shown in Figure 3.6. There were two thermal conductivity detectors (TCD) and two different of columns which provided in the GC for the analysis. The first column, a molecular sieve 5A was used for the analysis of  $\text{H}_2$ ,  $\text{O}_2$ ,  $\text{CH}_4$ ,  $\text{CO}$ , and  $\text{N}_2$  whereas the Pora Plot Q (Column 2) was used to analyse  $\text{CO}_2$ ,  $\text{C}_2\text{H}_4$ ,  $\text{C}_2\text{H}_6$ ,  $\text{C}_3\text{H}_6$  and  $\text{C}_3\text{H}_8$ . Column 2 could also detect  $\text{CH}_4$ . Moreover, both of the columns used argon as a carrier gas.



**Figure 3.6** Photograph of micro-GC (CP 4900).

In Column 1, the presence of CO<sub>2</sub> could disrupt the stability of the column operation, where it enters the pores of molecular sieve column and affecting the column performance. This may poison the column and it needs to be regenerated by heating to 180 °C, which requires a long time because of the limitation of the oven temperature. Therefore, column 1 was operated with a back flush option, which prevented CO<sub>2</sub> from entering the column. However, the columns were conditioned after finishing every experiment by selecting the column conditioning method, where they heat up to 180 °C to get rid of the moisture, which might enter the columns. The Galaxie Chromatography Data System software was provided by the manufacturer to set the column conditions as well as other essential parameters for the instrument.



### 3.3.3 Solids and liquids characterization

In this section, the analytical techniques such as powder x-ray diffraction (XRD), thermogravimetric analysis (TGA), scanning electron microscopy coupled with energy dispersive X-ray analysis (SEM-EDX), elemental (CHNS) analysis and total organic carbon (TOC) analysis were used to determine the characteristics of the fresh and used catalysts are discussed.

#### 3.3.3.1 X-ray diffraction (XRD)

The catalyst powder was analysed by using X-ray diffraction (XRD) analysis, which is based on Bragg's law principle, as given in equation 3.1.

$$n\lambda = 2d \sin\theta \quad (3.1)$$

where:

$n$  = positive integer;

$\lambda$  = the wavelength of the incident rays;

$d$  = the interplanar distance;

$\theta$  = the angle between the incident rays and surface of the plane.

The Brucker D-8 diffractometer was used to record the XRD patterns of the catalysts by using a Cu-K $\alpha$  radiation X-ray source. The scanning range was set at 10–90° with the step size of 0.025° and a speed of 2.5 second/step. The crystallographic of phase of the fresh and used catalysts in this research were obtained by searching and comparing with a standard reference diffraction

patterns in International Centre for Diffraction Data (ICDD) database by using the X'Pert High Score Plus software.

### **3.3.3.2 Thermogravimetric analysis (TGA)**

Thermogravimetric analysis (TGA) measures weight changes of a sample as a function of temperature or time under a specific gas at atmosphere pressure. The mass loss of a sample could be observed if the volatile compound is lost or a solid-gas chemical reaction, such as combustion occurred. In this study, the temperature programmed oxidation (TPO) analysis was carried out by using a thermogravimetric analyser (Stanton Redcroft TGA1000) to determine the amount and type of carbon present on the catalyst surface. Approximately 150 mg of used catalyst was placed on the TGA crucible (as shown in Figure 3.7) and was heated from ambient temperature to 900 °C at the rate of 10 °C/min in 50 cm<sup>3</sup>/min of air at atmospheric pressure. A plotted graph of the weight of the catalyst against temperature was used to illustrate a weight loss within a specific range of temperature, indicating that the combustion of carbon present in the catalyst was taking place.

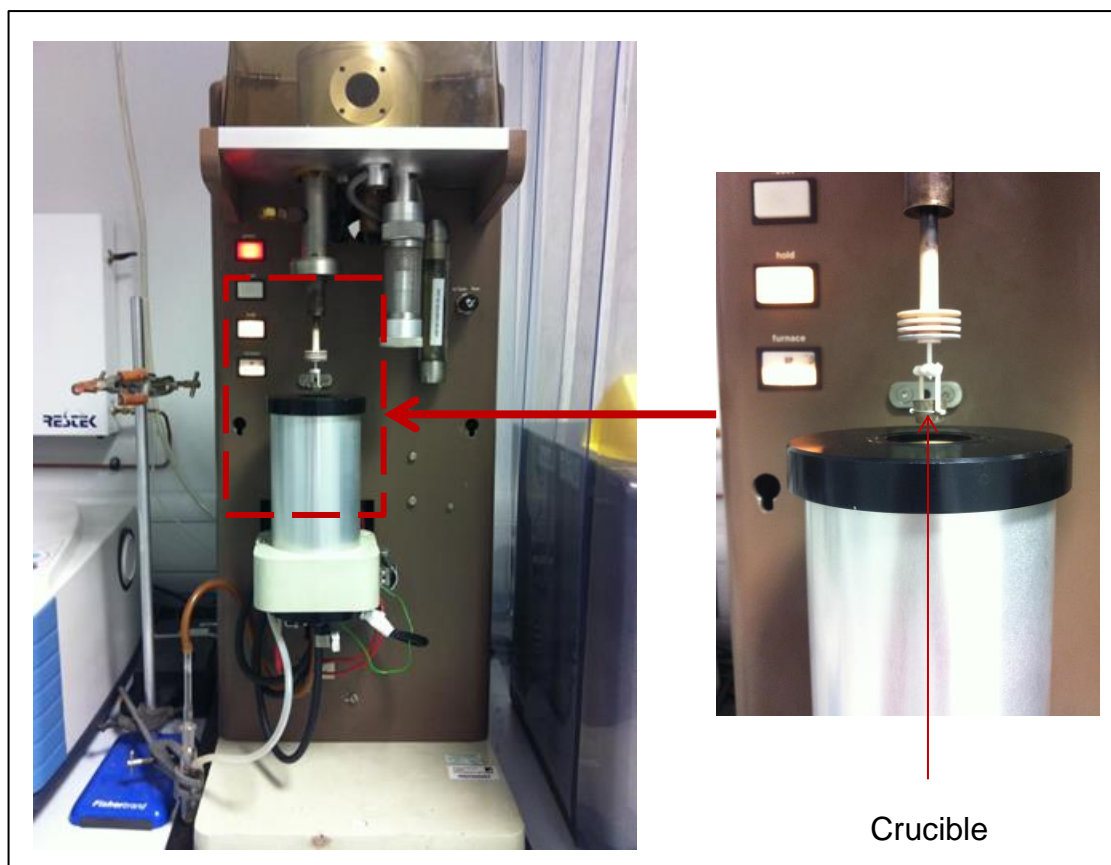


**Figure 3.7** Photograph of TGA (Stanton Redcroft TGA1000) for TPO analysis.

### 3.3.3.3 Scanning electron microscopy and energy dispersive X-ray analysis (SEM-EDX)

Scanning electron microscopy (SEM) provides high resolution images of the sample by scanning the surface sample using a high-energy beam of electrons. These various signals which are produced from the sample surface are picked up by the detector, revealing the sample surface images, thus it also can be used to study the sample topography. On the other hand, the energy-dispersive X-ray (EDX) is used to provide the elemental identification of the sample, where this technique relies on an interaction of the X-rays emitted by excited atoms and the sample. The fresh and used catalysts in this

study were analysed using a scanning electron microscopy (Carl Zeiss EVO MA15) coupled with an energy-dispersive X-ray (Oxford Instruments AZtecEnergy) system. The SEM-EDX (as shown in Figure 3.8) was performed on fresh and used catalysts in order to study the morphology of the catalyst surface before and after the experiment. Moreover, this technique was used to observe the elemental dispersion (Al, O, Ni and Ca) and carbon formation on the catalyst surface.



**Figure 3.8** Photograph of SEM (Carl Zeiss EVO MA15) coupled with EDX (Oxford Instruments AZtecEnergy).

In order to prepare the sample for SEM-EDX analysis, the sample particles were first placed on a sticky pad of a SEM stem, and then were coated with an iridium layer of 10 nm. The chemical characterisation of all the samples was analysed by using Aztec software supplied by Oxford Instruments.

#### 3.3.3.4 Elemental (CHNS) and Total Organic Carbon (TOC) analysis

CHNS elemental analysis was used to measure the elemental compositions of the catalyst samples as well as in the condensates, in terms of the mass fractions of carbon, hydrogen, nitrogen and sulphur. Therefore, the amount of carbon deposited on the catalyst surface was determined by using an elemental analyser, Thermo Flash EA 112 series CE instrument. The sample (approximately 10 mg) was placed in the tin capsule, where it was then folded properly to remove any air trapped in it. The folded sample was placed in the auto-sampler of the analyser, where it was fully combusted with an excess oxygen at 1800 °C. The amount of combustion products, carbon dioxide, CO<sub>2</sub> and water, H<sub>2</sub>O were measured by a thermal conductivity detector (TCD) of this equipment, where it gives the mass percentages of carbon and hydrogen of the sample. For each analysis, the sample was duplicate in order to ensure the result was precise.

The amount of the organic carbon in the condensate samples collected from the packed bed experiments were analysed by using a Hach-Lange IL550 analyser. The total organic carbon (TOC) of the sample was measured based on the non-purgeable organic carbon (NPOC) method, where at first, the sample was acidified by using hydrofluoric acid and flushing with a carbon-free gas to remove inorganic carbon. Then, the sample was going through for a combustion process, where the organic carbon reacts with oxygen to produce CO<sub>2</sub>. Before performing the analysis, the condensate samples were diluted with deionised water by 10 times due to the sensitivity to the TOC measurement.

## Chapter 4

### Thermodynamic Equilibrium Analysis using Chemical Equilibrium and Applications (CEA) Program

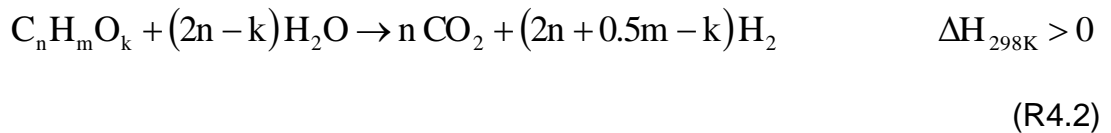
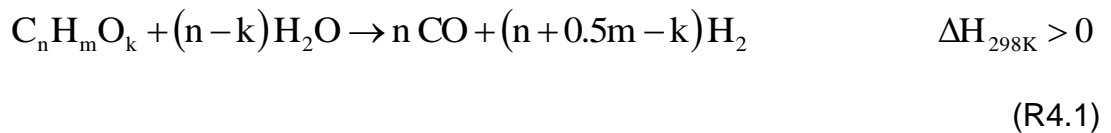
#### 4.1 Introduction

Thermodynamic equilibrium analysis for conversion of palm empty fruit bunch (PEFB) bio-oil to methane using low-temperature steam reforming (LTSR) process was conducted by assuming either isothermal or adiabatic condition, with and without sorption enhancement (SE-LTSR), with  $\text{CaO}_{(s)}$  or  $\text{Ca(OH)}_{2(s)}$  as  $\text{CO}_2$  sorbent. The present work relies on chemical equilibrium calculations by using Chemical Equilibrium and Application (CEA) programme, where it is aimed to identify the optimum range of conditions for methane production from bio-oil feedstock in LTSR process. In addition, LTSR with in situ  $\text{CO}_2$  sorption using  $\text{CaO}_{(s)}$  or  $\text{Ca(OH)}_{2(s)}$  is investigated for a PEFB bio-oil feedstock model in terms of  $\text{CH}_4$  purity, yield and energy balances, and these processes are named 'sorption-enhanced LTSR' or SE-LTSR. Comparisons between LTSR and SE-LTSR are then performed with respect to their energy demand according to reforming temperature, molar steam to carbon ratio (S/C) and molar calcium to carbon ratio (Ca:C).

## 4.2 Methane production from bio-oil via steam reforming process

Several global reactions occur in producing CH<sub>4</sub> gas from bio-oil feedstock, where initially steam reforming reactions take place (R4.1–R4.2), followed by water-gas shift reaction (R4.3) and methane synthesis (R4.4–R4.5). Reaction R4.6 collectively represents all the consecutive global reactions resulting in methane synthesis. By using matrices solution (Cramer's Rule), there are two main reactions for methane production from bio-oil which can be derived based on reactions (R4.3–R4.6) which are expressed as reactions (R4.7) and (R4.8).

Steam reforming:



Water-gas shift:

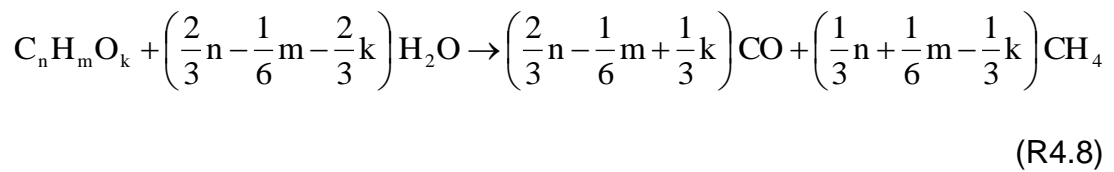
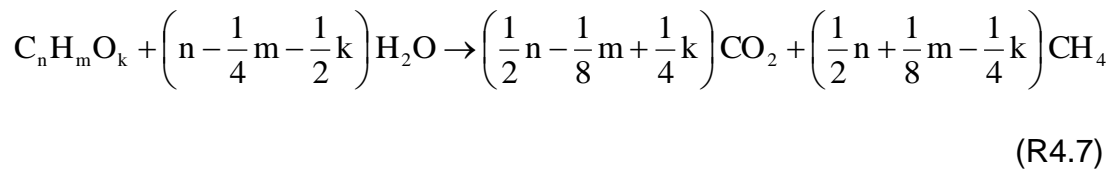


Methane synthesis:





Rearranging and combining (R4.1–R4.6), the global reactions of methane production from bio-oil become:



Recently, a study has modelled a gasification process from biomass by using calcium oxide, CaO as sorbent to capture carbon dioxide, CO<sub>2</sub> in gas production [129]. This work has used biomass (straw) as feedstock for CH<sub>4</sub> production where the gasification system is simulated within 600–700 °C in the presence of CO<sub>2</sub> sorbent, at atmospheric pressure followed by a separate methanation stage (R4.4 & R4.6), for which temperature and pressure are kept constant at 300 °C and 10 bar. This is in contrast with our research, where bio-oil is used as direct methanation feedstock due to its higher calorific value than the biomass source. In addition, the process of low temperature steam reforming does not requires multiple stages to produce CH<sub>4</sub>. The novelty of our work is also in considering a CO<sub>2</sub> sorbent present during the combined steam reforming/methanation reaction environment, and not just steam gasification. Thus the effects of in situ CO<sub>2</sub> capture can be gauged on



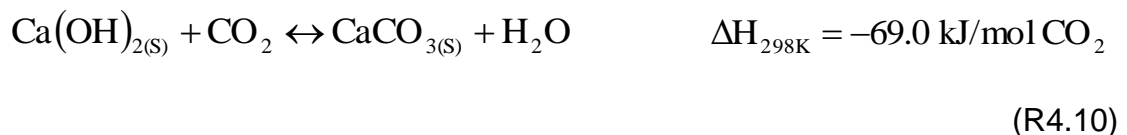
the methane production mechanism rather than just the syngas production stage.

In the carbonation reaction (R4.9), CO<sub>2</sub> production from methanation synthesis (R4.5) reacts with CaO to produce calcium carbonate (CaCO<sub>3</sub>), which results in higher purity of CH<sub>4</sub>. Thus, CaO sorbent is expected to enhance the purity and also potentially the yield of CH<sub>4</sub> production from bio-oil via LTSR, which is investigated throughout this study. The following reactions are involved in the process featuring CO<sub>2</sub> sorption with CaO<sub>(s)</sub> and Ca(OH)<sub>2(s)</sub> sorbents:

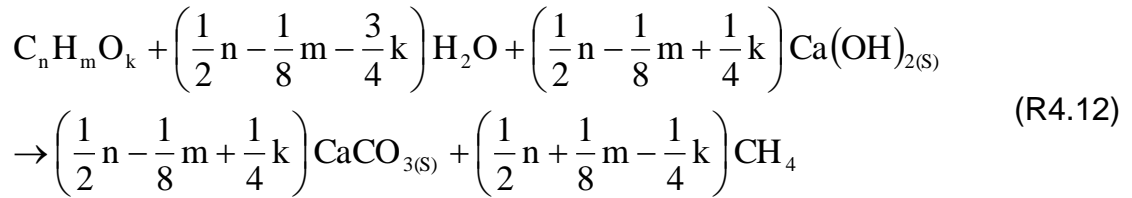
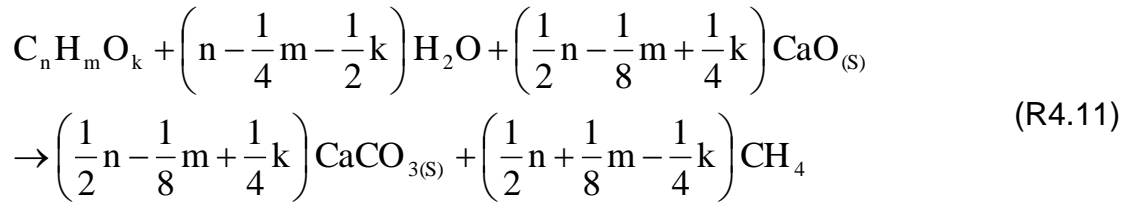
Carbonation of CaO<sub>(s)</sub>:



Carbonation of Ca(OH)<sub>2(s)</sub>:



By combining the results of R4.7 and R4.9 in the global reaction of LTSR with the in situ CO<sub>2</sub> sorption via CaO sorbent (R4.11), as well as via the Ca(OH)<sub>2(s)</sub> sorbent (R4.12), both approaches can achieve a reformat consisting of pure CH<sub>4</sub>:



### 4.3 Thermodynamic equilibrium calculations for CH<sub>4</sub> production from PEFB bio-oil

The CEA programme presents results in terms of mole fractions in the equilibrium mixture. In order to easily determine the total molar output at equilibrium, argon (Ar) was used in the initial reactant mixture with 0.01 mole fraction so that an Ar balance would provide directly the total molar output at equilibrium, as expressed by equation (4.1). As the amount of Ar chosen is relatively small, it is assumed that the equilibrium mixture is not affected by the presence of Ar.

Number of moles produced for species "i":

$$n_i = y_{i,out} \times n_{total,out} \tag{4.1}$$

where:

$y_{i,out}$  = mole fraction for species  $i$  produced, output of CEA;

$n_{total,out}$  = total number of moles produced,  $n_{Ar,in}/y_{Ar,out}$ .

The overall enthalpy balance ( $\Delta H_{Tot}$ ), i.e. the heat demand for methane production is the sum of the enthalpy change terms for each reactant (PEFB bio-oil  $\Delta H$  and  $H_2O$   $\Delta H$ ) and reaction enthalpies. The reactant enthalpy terms consist in bringing the feed species bio-oil and water from ambient temperature (298 K, 1 atm) in their natural phases to the chosen reformer temperature ( $T$ ), and reaction enthalpies are the enthalpy change between equilibrium mixture and feed at  $T$ , as well as sorbent related reactions. We assume here that if the process operates with excess steam (by way of S/C or  $Ca(OH)_{2(s)}$ ), the unreacted steam is then recycled to the reformer, and only the net amount of  $H_2O$  feed requires heating from ambient temperature, liquid phase to vapour phase at  $T$ . In addition, when simulating the sorption-enhanced LTSR with in situ  $CO_2$  capture (SE-LTSR), it is assumed that the carbonate is subsequently calcined to  $CaO_{(s)}$  at  $T$ .

In the case of  $CaO_{(s)}$  as the  $CO_2$  sorbent, it is then returned straight to the reformer at  $T$ . When using  $Ca(OH)_{2(s)}$  as the sorbent, the enthalpy change of rehydrating  $CaO_{(s)}$  to  $Ca(OH)_{2(s)}$  with the net amount of water is taken into account in the overall enthalpy balance. Rehydration of  $CaO_{(s)}$  at  $T$  takes place first with excess water vapour also at  $T$ , and then, the remainder of  $CaO_{(s)}$  at  $T$  is hydrated with net liquid water at ambient temperature. These assumptions reflect ideal conditions of heat integration by ignoring the thermal efficiencies of the recycling processes (water, sorbent) and the practicalities of

calcination. The latter would require higher temperature (typically 1170 K for Ca-sorbents), followed by heat recuperation measures. Nevertheless, these ideal conditions allow closer comparisons between LTSR and SE-LTSR processes without going into more comprehensive process modelling where auxiliary units would have to be depicted together with their heat losses (fluid and solids movers, piping and valves, heat exchangers). The data of enthalpy in standard conditions (298 K and 1 atm) were obtained from the National Institute of Standards and Technology (NIST) and also from the thermodynamic properties database file 'thermo.inp' in the CEA programme.

Individual enthalpy change calculations were carried out using the enthalpy of individual species (i.e. CH<sub>4</sub>, CO<sub>2</sub>, CO, H<sub>2</sub>, C(gr), H<sub>2</sub>O, phenol and acetic acid). Equation (4.2) was used when using NIST data where equation (4.3) was used for the data taken from the CEA programme.

$$H^{\circ} = (At) + \left(\frac{Bt^2}{2}\right) + \left(\frac{Ct^3}{3}\right) + \left(\frac{Dt^4}{4}\right) + \left(\frac{E}{t}\right) + F - H \quad (4.2)$$

$$\frac{H^{\circ}}{RT} = (-a_1T^{-2}) + (a_2T^{-1}\ln T) + a_3 + \left(\frac{a_4T}{2}\right) + \left(\frac{a_5T^2}{3}\right) + \left(\frac{a_6T^3}{4}\right) + \left(\frac{a_7T^4}{5}\right) + \left(\frac{b_1}{T}\right) \quad (4.3)$$

where:

H<sup>0</sup> = standard enthalpy of formation (kJ/mol);

t = reaction temperature (K)/1000;

T = reaction temperature (K);

R = gas constant (8.3144621×10<sup>-3</sup> kJ/mol.K).

The calculations for reactant enthalpy changes of PEFB bio-oil  $\Delta H$ ,  $H_2O$   $\Delta H$ , and the enthalpy of reaction expressed by equations (4.4–4.7) were used to determine the energy required or released for the overall reactions in producing one mole of  $CH_4$  from PEFB bio-oil feedstock. Enthalpy change of decarbonation of  $CaCO_3$  back to  $CaO$  is represented by equation (4.8).

$\Delta H$  reactants (kJ/mol  $CH_4$  produced):

$$\text{PEFB bio oil } \Delta H = \frac{n_{\text{oil,in}} \times (H_{\text{oil,T}} - H_{\text{oil,298K}})}{n_{\text{CH}_4,\text{out}}} \quad (4.4)$$

$$H_2O \Delta H = \frac{n_{H_2O,\text{net}} \times (H_{H_2O,T} - H_{H_2O,298K})}{n_{\text{CH}_4,\text{out}}} \quad (4.5)$$

where  $n_{H_2O,\text{net}} = n_{H_2O,\text{in}} - n_{H_2O,\text{out}}$ .

Summing up all reactant enthalpies:

$$\text{Reactants } \Delta H = \text{PEFB bio oil } \Delta H + H_2O \Delta H \quad (4.6)$$

$\Delta H$  of reaction (kJ/mol  $CH_4$  produced):

$$\text{Reaction } \Delta H = \left( \sum H_{\text{products,T}} - \sum H_{\text{reactants,T}} \right) / n_{\text{CH}_4,\text{out}} \quad (4.7)$$

$\Delta H$  of decarbonation (kJ/mol  $CH_4$  produced):

$$\text{Decarb } \Delta H = \frac{n_{\text{CaCO}_3,\text{out}} \times (H_{\text{CaO,T}} + H_{\text{CO}_2,\text{T}} - H_{\text{CaCO}_3,\text{T}})}{n_{\text{CH}_4,\text{out}}} \quad (4.8)$$

When using  $CaO_{(s)}$  as the sorbent,  $Ca(OH)_{2(s)}$  formed in the reformer and not carbonated due to excess Ca compared to  $CO_2$  product will require dehydration (calcination) before recycling:

$$\text{DeHy } \Delta H = n_{\text{Ca(OH)}_{2(\text{s}),\text{out}}} \times \left( H_{\text{CaO}_{(\text{s}),\text{T}}} + H_{\text{H}_2\text{O},\text{T}} - H_{\text{Ca(OH)}_{2(\text{s}),\text{T}}} \right) \quad (4.9)$$

However, when using  $\text{Ca(OH)}_{2(\text{s})}$  as the sorbent, this term is zero as excess  $\text{Ca(OH)}_{2(\text{s})}$  is directly recycled to the reformer.

Rehydration with excess water, when  $n_{\text{H}_2\text{O},\text{out}} > n_{\text{CaCO}_{3(\text{s}),\text{out}}}$ :

$$\text{ReHy1 } \Delta H = n_{\text{H}_2\text{O},\text{out}} \times \left( H_{\text{CaO}_{(\text{s}),\text{T}}} + H_{\text{H}_2\text{O},\text{T}} - H_{\text{CaCO}_{3(\text{s}),\text{T}}} \right) \quad (4.10a)$$

Rehydration with net water:

$$\text{ReHy2 } \Delta H = \left( n_{\text{CaCO}_{3(\text{s}),\text{out}}} - n_{\text{H}_2\text{O},\text{out}} \right) \times \left( H_{\text{CaO}_{(\text{s}),\text{T}}} + H_{\text{H}_2\text{O}(\text{liq}),298\text{K}} - H_{\text{CaCO}_{3(\text{s}),\text{T}}} \right) \quad (4.10b)$$

where:

$n_{\text{oil},\text{in}}$  = number of moles of PEFB bio-oil feed;

$n_{\text{CH}_4,\text{out}}$  = number of moles of  $\text{CH}_4$  produced;

$n_{\text{H}_2\text{O},\text{in}}$  = number of moles of water feed;

$n_{\text{CaCO}_3,\text{out}}$  = number of moles of  $\text{CaCO}_3$  produced;

H = enthalpy in kJ/mol;

T = reformer temperature (K).

Finally, total enthalpy process:

$$\Delta H_{\text{Tot}} = \text{Reactants } \Delta H + \text{Reaction } \Delta H + \text{Decarb } \Delta H + \text{DeHy } \Delta H + \text{ReHy1 } \Delta H + \text{ReHy2 } \Delta H \quad (4.11)$$

#### 4.4 PEFB bio-oil composition and choice of model bio-oil

In this research, bio-oil from the fast pyrolysis of palm empty fruit bunch (PEFB) was modelled as the feedstock for CH<sub>4</sub> production. PEFB bio-oil contains a great range of carboxylic acids, phenols, ketones, alcohols and aldehydes, in which acetic acid and phenol were found as the main compounds of PEFB bio-oil, in addition to many other oxygenated organics [107, 108, 110]. Since the exact composition of PEFB bio-oil is unknown, sensitivity analysis was first conducted to demonstrate that the results at chemical equilibrium for different PEFB bio-oil/H<sub>2</sub>O systems are not sensitive to a precise bio-oil composition, provided the elemental content of PEFB bio-oil is well known. Table 4.1 shows the characteristics of PEFB bio-oil compositions with and without water content, where C<sub>0.3238</sub>H<sub>0.4957</sub>O<sub>0.1798</sub>N<sub>0.0007</sub> of moisture free (mf) elemental formula was used as the basis for this study [107, 111].

The bio-oil mixture is represented in C<sub>n</sub>H<sub>m</sub>O<sub>k</sub> elemental format since the bio-oil composition is too complex to determine the precise amount of different compounds in the bio-oil. A sensitivity analysis for bio-oil composition was conducted using C<sub>0.3238</sub>H<sub>0.4957</sub>O<sub>0.1798</sub>N<sub>0.0007</sub> from reference [111] as the basis for elemental content of PEFB bio-oil approximated by different values of mole fractions of acetic acid, phenol and levoglucosan.

**Table 4.1** Characteristics of PEFB bio-oil [107, 111].

Water content, wt. %	21.68	-
Elemental analysis, wt. %		
Carbon	41.86	53.45
Hydrogen	7.82	6.88
Oxygen	50.22	39.54
Nitrogen	0.1	0.13
Molar formula	$C_{0.3821}H_{0.0060}O_{0.6108}N_{0.0011}$	$C_{0.3238}H_{0.4957}O_{0.1798}N_{0.0007}$

Therefore, CEA programme was used in order to predict CH<sub>4</sub> production using the same value of total feed of 3000 moles of carbon for all the conditions tested and in the temperature range of 300–800 K at 1 atm. Three different PEFB model bio-oil mixtures consisting of acetic acid, phenol and levoglucosan were used to simulate the target bio-oil elemental composition  $C_{0.3238}H_{0.4957}O_{0.1798}N_{0.0007}$ , which are listed in Table 4.2. These were then tested for a range of temperatures and S/C in equilibrium LTSR at atmospheric pressure to assess the sensitivity of CH<sub>4</sub> yield to the model mixture make up (Figure 4.1). CEA allows the inclusion of condensed species (liquids and solids), therefore solid CO<sub>2</sub> sorbents like CaO<sub>(s)</sub>, Ca(OH)<sub>2(s)</sub> and CaCO<sub>3(s)</sub> are able to be considered in the systems studied, which are discussed in the next section.

Based on CH<sub>4</sub> production from bio-oil reaction (R4.7), the predicted equilibrium CH<sub>4</sub> yield was calculated using equation (4.12), whereas the percentage error was calculated via equation (4.13).



$$\text{CH}_4 \text{ yield} = 100 \times \left[ \frac{M_{\text{CH}_4} \times n_{\text{CH}_4, \text{out}}}{(M_{\text{C}} \times n_{\text{C}, \text{in}}) + (M_{\text{H}} \times n_{\text{H}, \text{in}}) + (M_{\text{O}} \times n_{\text{O}, \text{in}})} \right] \quad (4.12)$$

Percentage error for bio-oil of composition between the target and the model bio-oil is:

$$\text{Error (\%)} = 100 \times \left[ 1 - \left| \frac{\text{max CH}_4 \text{ yield for model bio - oil}}{\text{max CH}_4 \text{ yield for target bio - oil}} \right| \right] \quad (4.13)$$

where:

$M_{\text{CH}_4}$  = molar mass of  $\text{CH}_4$ ;

$M_{\text{C}}$  = molar mass of carbon element in bio-oil;

$M_{\text{H}}$  = molar mass of hydrogen element in bio-oil;

$M_{\text{O}}$  = molar mass of oxygen element in bio-oil;

and the maximum  $\text{CH}_4$  yield is that obtained from complete reaction R4.7 using LTSR or complete reactions R4.11 or R4.12 using SE-LTSR for a given bio-oil.

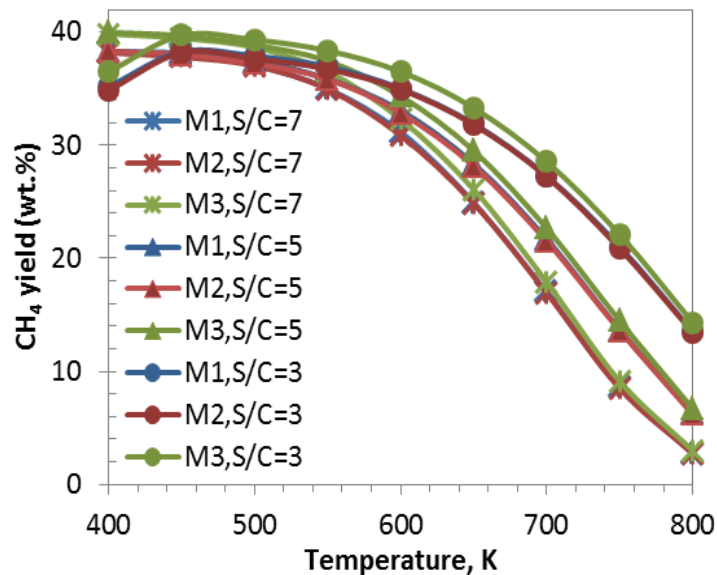
Table 4.2 lists three very distinct mixtures of the model compounds (acetic acid, phenol and levoglucosan) that are known to feature significantly in PEFB bio-oil composition from experiments [110]. Each mixture (M1, M2 and M3) was modelled in order to achieve an elemental formula closest to that of the target material  $\text{C}_{0.3238}\text{H}_{0.4957}\text{O}_{0.1798}\text{N}_{0.0007}$  as in Table 4.1. It can be seen that despite significant differences in the amount of acetic acid, phenol and levoglucosan, each mixture results in a theoretical maximum  $\text{CH}_4$  yield of less than 3% error with the target material. Figure 4.1 shows that the equilibrium

CH<sub>4</sub> yields calculated using equation (4.12) for the temperature range (400–800 K) and the three model mixtures (M1–M3) defined in Table 4.2 were very similar for a given S/C and temperature. Note the intended mixture elemental formula had a theoretical maximum CH<sub>4</sub> yield of 39.5 wt. % of C<sub>n</sub>H<sub>m</sub>O<sub>k</sub> feed. Thus, the LTSR process does not appear to be sensitive to an exact composition of bio-oil feedstock as long as its elemental content remains the same. However, the differences in boiling point between the model mixtures (M1–M3) are too significant, where M2 had the highest boiling point, 340 °C (less volatile) while M3 had the lowest value, 160 °C (more volatile) among the three mixtures. This is because the major component in M2 is levoglucosan, with the highest boiling point (385 °C) compared to acetic acid (118 °C) and phenol (182 °C). It also explained why the M3 model mixture had lower boiling point value (160 °C) due to the acetic acid being the main component in the mixture, M3. As the difference of compounds in the mixture affected the boiling point values, Chapter 6 will be using the real components (qualitative and quantitative) of the bio-oil for process plant modelling. But, this chapter is focusing into maximum of CH<sub>4</sub> yield despite of having difference values of the mixture's volatility.

Subsequently, mixture M3, which contains only acetic acid and phenol, was chosen in this investigation to represent the LTSR and SE-LTSR of PEFB bio-oil since it gave the smallest percentage error in the theoretical maximum CH<sub>4</sub> yield (1.13%) compared to the target bio-oil.

**Table 4.2** Estimation for three different PEFB bio-oil compositions based on the intended elemental formula  $C_{0.3238}H_{0.4957}O_{0.1798}N_{0.0007}$ .

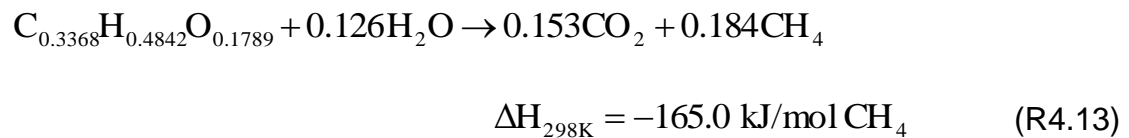
Mixture	M1	M2	M3
Mole fraction:			
Acetic acid	0.55	-	0.7
Phenol	0.3	0.41	0.3
Levoglucosan	0.15	0.59	-
Molar formula	$C_{0.3319}H_{0.4803}O_{0.1878}$	$C_{0.3386}H_{0.4718}O_{0.1896}$	$C_{0.3368}H_{0.4842}O_{0.1789}$
CH <sub>4</sub> yield, wt.% (Eq.4.12)	38.44	38.31	39.97
Error, % (Eq.4.13)	2.7	3	1.1
Boiling point, °C	300	340	160

**Figure 4.1** CH<sub>4</sub> yield (wt. %) for three different PEFB bio-oil mixture compositions listed in Table 4.2 for S/C from 3 to 7 and 1 atm.

## 4.5 Thermodynamic equilibrium analysis of direct CH<sub>4</sub> production from PEFB bio-oil by LTSR with and without in situ CO<sub>2</sub> sorption

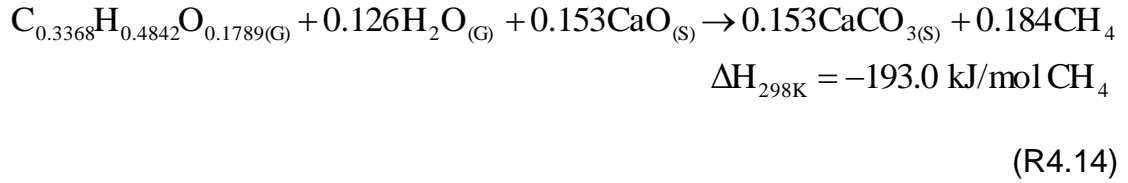
### 4.5.1 Expected outputs from stoichiometry of LTSR and SE-LTSR reactions and relevance to LTSR process design

The mixture M3 (Table 4.2) with the elemental formula C<sub>0.3368</sub>H<sub>0.4842</sub>O<sub>0.1789</sub> was chosen as the model mixture for PEFB bio-oil, and the generic global reaction of CH<sub>4</sub> production from bio-oil (in vapour state) with CO<sub>2</sub> as a co-product (R4.7), can be expressed by reaction (R4.13) using M3 as the feedstock:

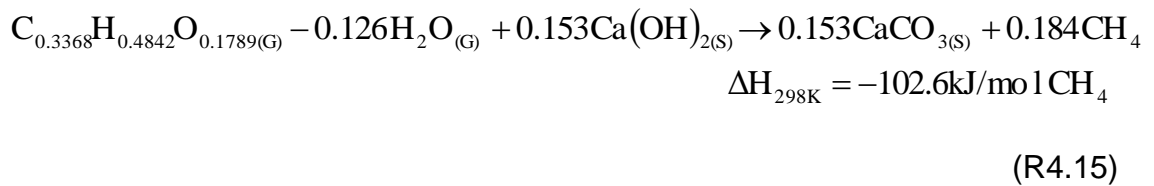


Thus, LTSR of M3 as expressed by (R4.13) is significantly exothermic and therefore, there may be a potential for heat recovery to bring the reactants to reformer temperature and achieve a near-autothermal process. The stoichiometric molar steam to carbon ratio (S/C) was at a low value of 0.375 (= 0.1263/0.3368), corresponding to a maximum CH<sub>4</sub> yield of 40.0 wt.% of M3, and associated with an ideal CH<sub>4</sub> purity of 54.7 mol% in the CH<sub>4</sub>-CO<sub>2</sub> reformat mixture. By comparison, the S/C required for H<sub>2</sub> and CO<sub>2</sub> production through high-temperature steam reforming (HTSR) of M3 (S/C = 1.47) was significantly higher and would produce a maximum of H<sub>2</sub> yield of 20.1 wt.% of M3.

When using  $\text{CaO}_{(s)}$  as the  $\text{CO}_2$  sorbent and combining the results of (R4.13) and (R4.9) in (R4.14), the SE-LTSR of M3 model PEFB bio-oil is:



Furthermore, when using  $\text{Ca}(\text{OH})_{2(\text{S})}$  as the in situ  $\text{CO}_2$  sorbent and combining the results of (R4.13) and (R4.10) in (R4.15), this potentially generates pure  $\text{CH}_4$  reformat:



High-temperature steam reforming (HTSR) for  $\text{H}_2$  and  $\text{CO}_2$  generation also has a stoichiometric Ca:C of 1 when coupled with in situ Ca-based  $\text{CO}_2$  sorption. Thus, temperature and S/C variations in a reformer are expected to change rapidly from conditions favourable to SE-LTSR to those advantages for sorption enhanced-HTSR or 'SE-HTSR', where  $\text{H}_2$  product is preferred over  $\text{CH}_4$ . In addition to improving reformat purity in  $\text{H}_2$ , in situ  $\text{CO}_2$  capture has other benefits that have been identified in SE-HTSR: lower S/C for threshold of carbon formation, higher  $\text{H}_2$  yields from equilibrium shifts in steam reforming and water gas shift reactions, lower overall energy demand from operating at lower S/C and T, a wider range of temperatures of maximum yield, collectively known as enhancement effects of sorption-enhanced steam

reforming process (SESR) [110, 144]. The present study aims to assess for the first time whether similar benefits can be observed for SE-LTSR in equilibrium production of pure methane reformat.

Unlike SE-HTSR, which always requires H<sub>2</sub>O co-reactant whether CaO<sub>(s)</sub> or Ca(OH)<sub>2(s)</sub> is used as the sorbent, SE-LTSR theoretically does not need H<sub>2</sub>O feed when using Ca(OH)<sub>2(s)</sub> because its stoichiometric S/C for reaction R4.15 is negative (i.e. -0.026). The stoichiometric S/C of R4.14 and R4.15 differ greatly due to the sorbent in R4.15 being already hydrated, which is represented in the considerably exothermic reaction R4.16.

Hydration of CaO<sub>(s)</sub>:



When operating at temperatures approximately below 400 °C, CaO<sub>(s)</sub> readily hydrates to Ca(OH)<sub>2(s)</sub>, whereas above this temperature, Ca(OH)<sub>2(s)</sub> dehydration is favoured. Calcination of Ca-based CO<sub>2</sub> sorbents at around 900 °C via the reverse of (R4.9) enables the release of captured CO<sub>2</sub> from CaCO<sub>3(s)</sub>, thereby regenerating the Ca-based sorbent for another carbonation cycle. Without such regeneration step, the sorbent would eventually reach full capacity for CO<sub>2</sub> intake and cease to be active for sorption-enhanced H<sub>2</sub> or CH<sub>4</sub> production.

Ca-based sorbents are, however, well known to deactivate significantly, principally via sintering through repeated cycles of calcination [145]. Many studies of sorption-enhanced reforming have investigated hydration of Ca-based sorbents as a means to counteract the deactivation caused by calcination-induced sintering. It has been found that direct hydration, i.e. direct use of hydrated Ca-sorbent for high-temperature CO<sub>2</sub> sorption is more effective than indirect hydration, whereby calcination in an inert atmosphere is employed between hydration and subsequent carbonation [146].

Such investigations are, however, dedicated to higher temperature processes than LTSR, such as syngas production or post-combustion CO<sub>2</sub> capture. Particular concerns for SE-LTSR will be the sensitivity of CH<sub>4</sub> yield to fluctuations in the operating S/C and to temperature, exacerbated by the exothermicity of R4.14 and R4.15. In adiabatic process conditions, the use of CaO<sub>(s)</sub> with LTSR will see the hydration reaction R4.16 take place first, which will lower H<sub>2</sub>O partial pressures, followed by R4.15. The heat release of R4.16 and R4.15 would raise the system temperature in two stages, potentially creating inhomogeneity in local S/C, with risks of carbon deposition where S/C would dip too low, or hydrogen production to the detriment of methane via SE-HTSR where S/C would rise too high.

In contrast, the adiabatic SE-LTSR process using Ca(OH)<sub>2(s)</sub> would provide a one-step temperature rise with a steady supply of excess steam as an intermediate product, as R4.15 exhibits a negative stoichiometric S/C, in addition to the fact that no exothermic CaO<sub>(s)</sub> hydration will take place in the reformer. Thus, Ca(OH)<sub>2(s)</sub> offers advantages over CaO<sub>(s)</sub> as the preferred

sorbent to enter the adiabatic low-temperature steam reformer: controlled reactivation after calcination of the sorbent and a one-step exothermic process in the reformer. Nevertheless, whether  $\text{CaO}_{(s)}$  or  $\text{Ca(OH)}_{2(s)}$  is used, with both R4.14 and R4.15 being significantly exothermic, there is a risk that the adiabatic reformer temperature may reach the unwanted sorbent calcination mode through exotherms, thus switching off the in situ  $\text{CO}_2$  capture. In comparison, in the isothermal (controlled cooled) LTSR process using  $\text{Ca(OH)}_{2(s)}$ , the heat released during SE-LTSR would ensure operating at set temperatures is favourable for carbonation, but maintaining a constant temperature inside the reformer housing hot solid carbonate would add complexity to process control and design.

As mentioned in Chapter 3, under CEA method,  $\text{CH}_4$  production was predicted using two different types of problems in the CEA code, which were the 'Assigned Temperature and Pressure' (tp), i.e. the isothermal reactor, and the 'Assigned Enthalpy and Pressure' (hp), i.e. the adiabatic reactor. The results for 'tp' are presented first, and the 'hp' results are compared and discussed at the end of this section, as they are both relevant to practical issues as discussed above.

Table 4.3 lists the molar inputs corresponding to the bio-oil mixture model used in equilibrium calculations. Other reactants in the system feed (e.g.  $\text{H}_2\text{O}$ , Ca sorbents, negligible Ar) are then defined by the molar ratios of Ca:C and  $\text{H}_2\text{O}$ :C used, and the latter is also termed S/C for steam to carbon ratio when no sorbent is used, as previously.



**Table 4.3** Molar inputs of reactants in mixture M3 based on 3000 of total moles of carbon input.

Compound	Input moles	C (moles)	H (moles)	O (moles)
Acetic acid (CH <sub>3</sub> COOH)	656.25	1312.5	2625	1312.5
Phenol (C <sub>6</sub> H <sub>5</sub> OH)	281.25	1687.5	1687.5	281.25
Total	937.5	3000	4312.5	1593.75

The theoretical maximum CH<sub>4</sub> production for the M3 model bio-oil mixture molar inputs of Table 4.3 would therefore be 1641 moles, and this would be accompanied by 1359 moles of CO<sub>2</sub> via R4.13, or 1359 moles of CaCO<sub>3(s)</sub> via R4.14 or R4.15, which would then require calcination of the Ca-sorbent, releasing the same moles in the form of CO<sub>2</sub>.

#### 4.5.2 Temperature and S/C effects on the equilibria of isothermal LTSR and SE-LTSR of PEFB bio-oil model

In this section, the effects of changing temperature between 400 and 800 K and S/C from 0.5 to 7.0 at atmospheric pressure were investigated on the equilibrium system in order to determine the optimum conditions for PEFB bio-oil conversion to CH<sub>4</sub> via LTSR. Isothermal process (as opposed to adiabatic process) is considered. The conditions of optimum CH<sub>4</sub> yield for LTSR were then compared to the process outputs, which introduced Ca(OH)<sub>2(s)</sub> as the CO<sub>2</sub> sorbent in the feed mixture, simulating isothermal SE-LTSR.

Figure 4.2(a) shows that values close to the theoretical maximum of 1641 moles of  $\text{CH}_4$  can be produced by LTSR without sorbent for  $\text{S/C} \geq 2$  and temperatures  $\leq 550$  K. This threshold minimum  $\text{S/C}$  is itself much higher than the stoichiometric  $\text{S/C}$  of 0.375 from the intended reaction R4.13. The reason for this discrepancy in  $\text{S/C}$  for maximum  $\text{CH}_4$  yield can be found in Figure 4.3(a), which shows carbon graphite as the main equilibrium carbon-containing product at low temperatures and  $\text{S/C}$  below 2.

For temperatures below 650 K and all  $\text{S/C}$ , negligible CO was produced, as seen in Figure 4.3(b), with the only other carbon-containing co-products of methane being carbon graphite and  $\text{CO}_2$  (Figure 4.3(c)). At temperatures above 650 K,  $\text{H}_2$  becomes the dominant hydrogen-containing product, as seen in Figure 4.3(d), and it increased with  $\text{S/C}$  as per HTSR process, accompanied by CO and  $\text{CO}_2$ .

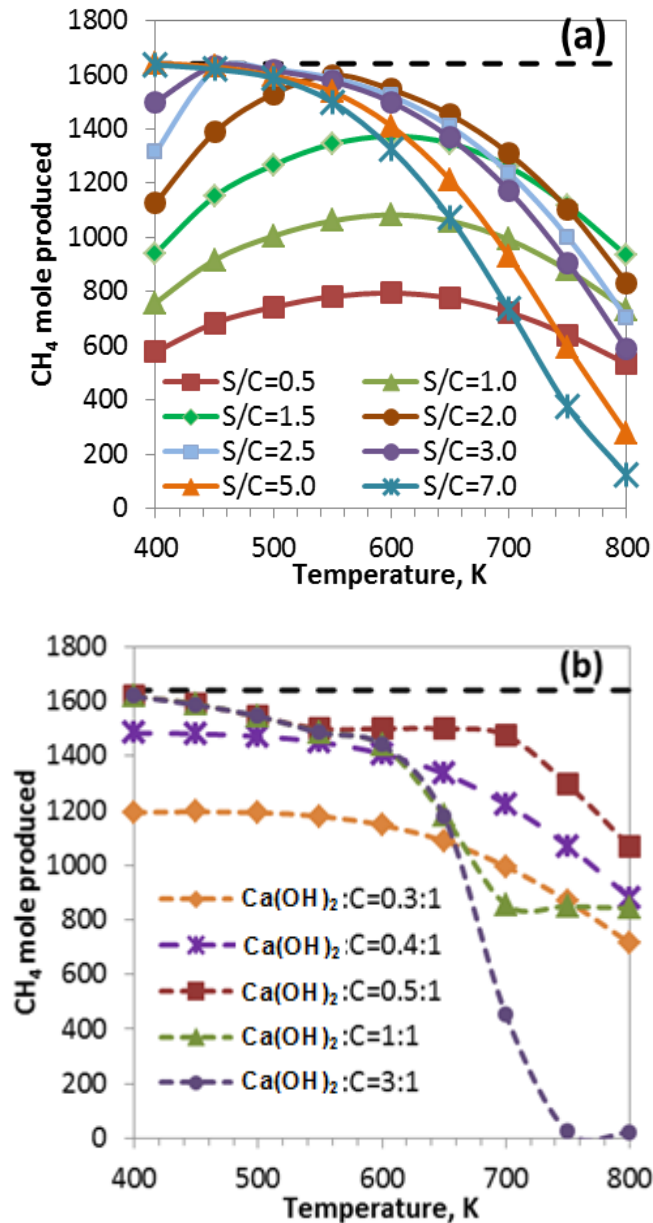


**Figure 4.2** CH<sub>4</sub> production vs. temperature from M3 mixture (Table 4.3) without (a) and with Ca(OH)<sub>2</sub>(s) (b) at 1 atm. The top horizontal line is the theoretical maximum production via (R4.13).

The dominance of solid carbon at low temperatures, low S/C and hydrogen at higher temperatures results in a dome-shaped profile of methane yield with temperature (Figure 4.2(a)), whose top flattened and shifted towards lower temperatures as S/C increased. In order to avoid too high sensitivity of methane yield to fluctuations in either temperature or S/C in a practical isothermal LTSR process of PEFB bio-oil, given that it will be overall

exothermic in the reformer and thus highly dependent on good cooling controls, it is thus recommended to operate the isothermal LTSR of PEFB bio-oil in the S/C range of 2.5 to 3, and between 450 and 550 K, where CH<sub>4</sub> yield plateaus.

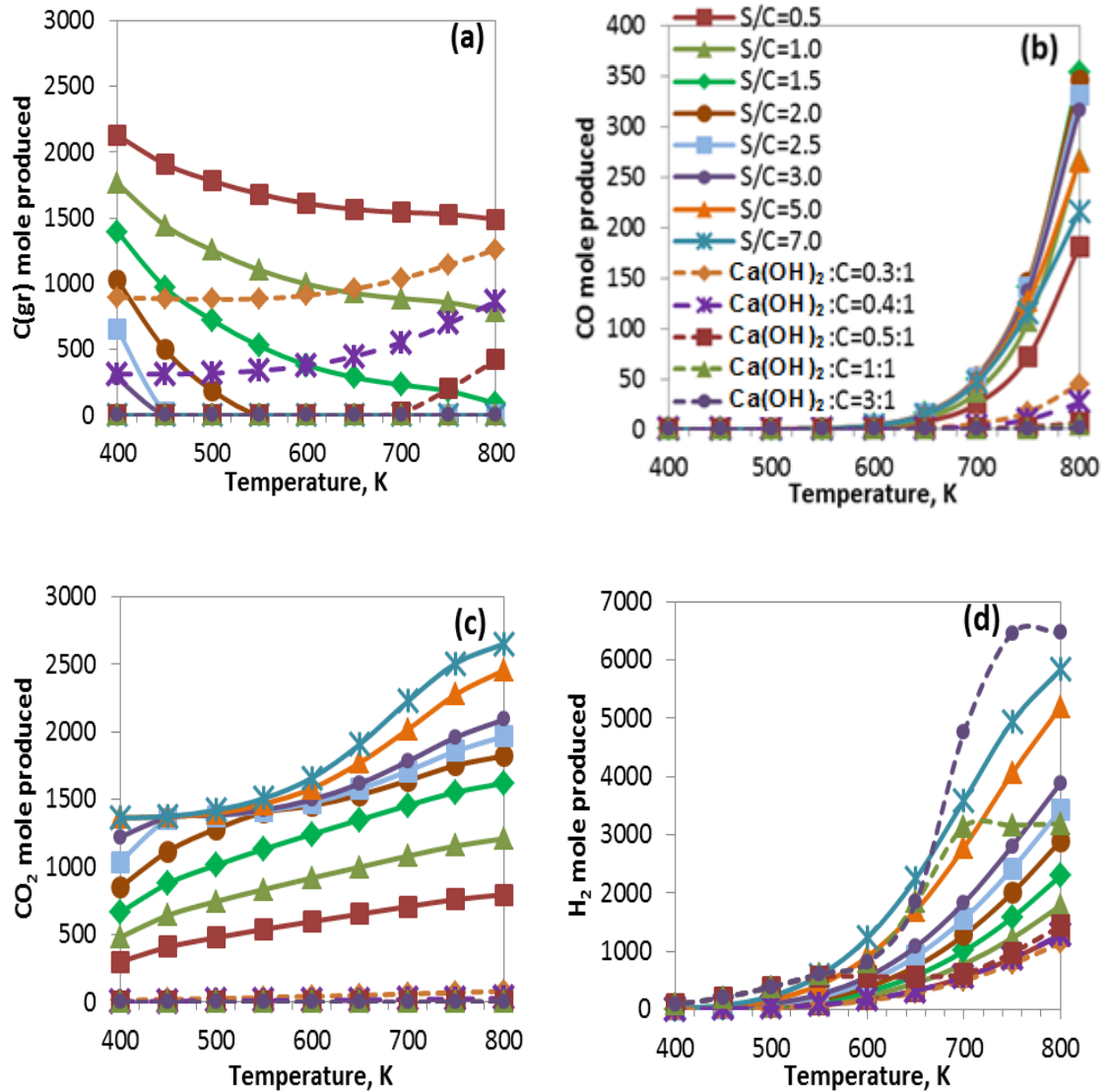


**Figure 4.3** Production of (a) carbon graphite, (b) CO, (c) CO<sub>2</sub> and (d) H<sub>2</sub> between 400 and 800 K at 1 atm for LTSR (solid lines) and SE-LTSR (dashed lines) processes.

In the presence of  $\text{Ca(OH)}_{2(s)}$ , the maximum  $\text{CH}_4$  production reached the theoretical maximum at  $\text{Ca:C} = 0.5$ , i.e. close to the stoichiometric  $\text{Ca:C}$  of 0.45 as determined from the intended reaction R4.15 (Figure 4.2(b)). This condition used comparatively much less steam than the sorbent-free system to achieve close to the theoretical maximum yield of  $\text{CH}_4$ . The SE-LTSR equilibrium process thus behaves very closely to the intended reaction R4.15. As in LTSR,  $\text{CH}_4$  yield in the isothermal SE-LTSR process decreased at high temperatures due to the rise in hydrogen co-product (Figure 4.3(d)). In sharp contrast with LTSR, SE-LTSR has no solid carbon predicted at equilibrium. This is true except for the conditions of sub-stoichiometric  $\text{Ca:C}$  ( $< 0.453$ ), which results in a lack of steam generation via R4.10 (see Figure 4.3(a)) and thus prevents carbon oxidation. SE-LTSR also features a lack of both CO and  $\text{CO}_2$  as long as the  $\text{Ca:C}$  is at or above stoichiometry of R4.15 (Figure 4.3 (b,c)). Thus, prevention of equilibrium solid carbon is a sorption-enhancement effect that SE-LTSR shares with SE-HTSR. The only impediment to reach the theoretical maximum of  $\text{CH}_4$  production is that even at low temperatures (400–500 K), concurrent  $\text{H}_2$  production occurs, though in a limited way. Surprisingly, this results in a medium temperature region where  $\text{CH}_4$  production via LTSR exceeds slightly that of SE-LTSR in isothermal conditions.

In theory, the use of a much lower S/C of SE-LTSR may result in energy cost savings by avoiding having to raise excess steam compared to LSTR. This issue will be explored in a later section (4.5.4). An immediate benefit of operating in SE-LTSR, however, is that the  $\text{CH}_4$  in the dry reformat increased from 45 vol. % with LTSR (S/C = 3) to 88 vol. % with SE-LTSR ( $\text{Ca:C} = 0.5$ ), when both at 450 K, i.e. at maximum  $\text{CH}_4$  yield. This high level of purity in the

reformer may or may not remove the need for a CH<sub>4</sub> separation step downstream of SE-LTSR process, depending on the intended use for the CH<sub>4</sub> produced. However, the absence of a downstream CH<sub>4</sub> separation step may itself be mitigated by having to introduce a sorbent regeneration measure, also downstream of the reformer. Incidentally, the sorption enhancement effect on HTSR can be seen in the high temperature range (> 650 K) by the decrease in CO and increase in H<sub>2</sub> production due to the more favourable equilibrium in the water gas shift reaction (R4.3) caused by the removal of CO<sub>2</sub> from the products via carbonation. The latter was observed experimentally, as well as equilibrium modelling in [110].

As discussed earlier in Section 4.5.1, there are a number of advantages in potentially rating Ca(OH)<sub>2(s)</sub> above CaO<sub>(s)</sub> as the active sorbent in the isothermal SE-LTSR process. These are relevant to the stability of both temperature and S/C in the cooled reformer by eliminating CaO<sub>(s)</sub> hydration through reaction R4.16. Inhomogeneity in temperature and S/C caused by the heat released by R4.16 and water demand may result in either local carbon formation or too high H<sub>2</sub> co-product. When replacing Ca(OH)<sub>2(s)</sub> with CaO<sub>(s)</sub> in the system and adding the required equivalent H<sub>2</sub>O co-reactant separately, the same production profiles of CH<sub>4</sub>, CO, C and H<sub>2</sub> for Ca(OH)<sub>2(s)</sub> based SE-LTSR were obtained, and thus the results for CaO<sub>(s)</sub> based SE-LTSR are not shown here. This is because in isothermal conditions below 700 K, i.e. LTSR conditions, the hydration reaction R4.16 is complete in excess of steam conditions.

### 4.5.3 Pressure effects in the equilibria of isothermal LTSR and SE-LTSR of PEFB bio-oil model

Methane synthesis exothermic reactions (R4.4–R4.6) involve the production of less moles of gas products than the initial moles of reactant. According to Le Chatelier's principle, an increase in pressure will imbalance the reactants more than the products and the system equilibrium will counteract this change by increasing conversion. This effect can be seen in Figure 4.4, where increasing the system pressure from 1 to 30 atm at S/C of 3 brings the profile of CH<sub>4</sub> product closer to the theoretical maximum. An industrial process of LTSR of PEFB would therefore benefit in terms of CH<sub>4</sub> yield from operating at higher pressures than atmospheric, with pressure of just 5 atm significantly expanding the temperature zone of maximum CH<sub>4</sub> yield compared to 1 atm by approximately 60 K, and compared to 30 atm by 150 K from its starting point of optimum temperature. This could be advantageous in the industrial process where the kinetics of methanation catalyst may be very sensitive to temperature in the range of maximum equilibrium CH<sub>4</sub> yield, and activity at 550 K could be significantly lower than at 610 K (5 atm) or 700 K (30 atm). The drawback of operating at higher pressures would be in the increased boiling point of the reactants, the resulting surge in energy demand for vaporisation of liquid water feed.

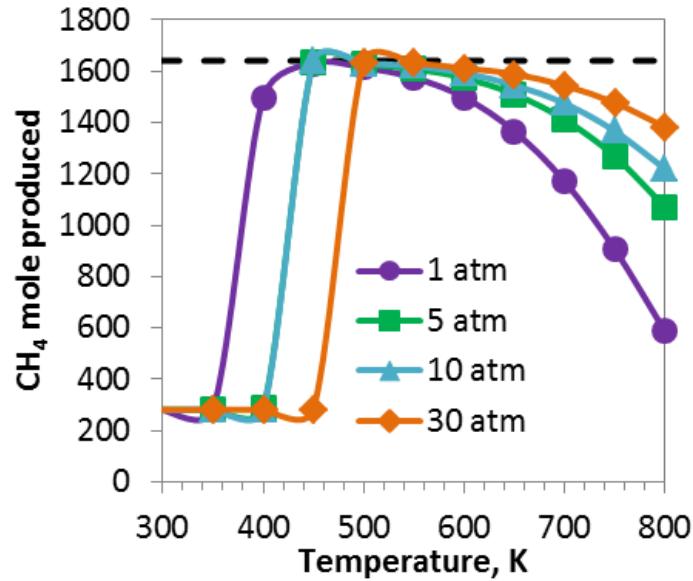


**Figure 4.4** CH<sub>4</sub> production within 300–800 K at S/C = 3.0 for total pressures between 1 and 30 atm. The top horizontal line is the theoretical maximum production via (R4.13).

#### 4.5.4 Enthalpy balances for the equilibria of isothermal LTSR and SE-LTSR of PEFB bio-oil model

The main global reactions that are related to the LTSR process for CH<sub>4</sub> production from the M3 model bio-oil mixture, such as several CH<sub>4</sub> synthesis reactions (R4.4–R4.6, R4.13–R4.15), water-gas shift, hydration of CaO, and carbonation of both CaO and Ca(OH)<sub>2</sub>, are listed in Table 4.4 with their standard enthalpies of reaction. The overall process for isothermal CH<sub>4</sub> production via LTSR is expected to be exothermic in the reformer since all of the reactions involved exhibit negative value of reaction enthalpy. In the process start-up, using reactants at ambient temperature and natural phases will introduce a significant heat demand to first, vaporise volatile reactants in condensed phases (net liquid water, liquid acetic acid and crystalline phenol) and secondly, bringing all the reactants in the vapour phase to reformer temperature. Beyond start-up conditions, however, the process will operate



cyclically, where solids will be regenerated from carbonate state to oxide and excess water will be used either to rehydrate CaO or used as a reforming co-reactant. In order to represent ideal processes where heat recuperation has 100% efficiency, we will assume that decarbonation occurs at reformer temperature (in practice, temperature in excess of 900 °C is typically required), and thus solids and water recycling will not incur sensible enthalpy changes, but only reaction enthalpy changes. This section looks at the total heat demand of LTSR compared to SE-LTSR.

**Table 4.4** Reaction of enthalpy ( $\Delta H_R$ ) for main global reactions that are related to LTSR for methane production at 298 K (M3 =  $C_{0.3368}H_{0.482}O_{0.1789(G)}$ ).

R	Reaction	Stoichiometry (mol)	$\Delta H_{298 K}$ (kJ)
4.3	Water gas-shift	$CO + H_2O_{(G)} \leftrightarrow CO_2 + H_2$	-41.2/mol CO
4.4	Methanation of CO	$CO + 3H_2 \leftrightarrow CH_4 + H_2O_{(G)}$	-206.2/mol CH <sub>4</sub>
4.5	As above	$2CO + 2H_2 \leftrightarrow CH_4 + CO_2$	-247.3/mol CH <sub>4</sub>
4.6	Methanation of CO <sub>2</sub>	$CO_2 + 4H_2 \leftrightarrow CH_4 + 2H_2O_{(G)}$	-165.0/mol CH <sub>4</sub>
4.9	Carbonation of CaO	$CaO_{(S)} + CO_2 \leftrightarrow CaCO_{3(S)}$	-178.2/mol CO <sub>2</sub>
4.12	Carbonation of Ca(OH) <sub>2</sub>	$Ca(OH)_{2(S)} + CO_2 \leftrightarrow CaCO_{3(S)} + H_2O$	-69.0/mol CO <sub>2</sub>
4.13	LTSR of M3 bio-oil	$M3 + 0.126 H_2O \rightarrow 0.153CO_2 + 0.184 CH_4$	-45.4/mol CH <sub>4</sub>
4.14	SE-LTSR, CaO <sub>(S)</sub>	$M3 + 0.126H_2O + 0.153CaO_{(S)} \rightarrow 0.153CaCO_{3(S)} + 0.184CH_4$	-193.0/mol CH <sub>4</sub>
4.15	SE-LTSR, Ca(OH) <sub>2(S)</sub>	$M3 - 0.026H_2O + 0.153Ca(OH)_{2(S)} \rightarrow \text{as (R4.14)}$	-102.6/mol CH <sub>4</sub>
4.16	Hydration of CaO	$CaO_{(S)} + H_2O_{(G)} \leftrightarrow Ca(OH)_2$	-109.2/mol H <sub>2</sub> O

Figure 4.5 plots  $\Delta H_{\text{Tot}}$  derived from equation (4.11) for the isothermal LTSR and SE-LTSR cases at atmospheric pressure. We remind that  $\Delta H_{\text{Tot}}$  is the sum of enthalpy changes of raising bio-oil and net water reactants from their natural phases from 298 K to vapour state at reforming temperature  $T$  and the reaction enthalpy change at  $T$ , as well as calcination enthalpy change at  $T$ , if carbonate was present in the products, with rehydration of  $\text{CaO}_{(s)}$  product in the case of the calcium hydroxide sorbent used as the reactant, and dehydration in the case of  $\text{Ca}(\text{OH})_{2(s)}$  product and calcium oxide used as the reactant. From previous thermodynamic equilibrium calculations, SE-LTSR with  $\text{Ca}:\text{C} = 0.5:1$  and LTSR with  $\text{S}:\text{C} = 3.0$  were identified as the optimum conditions for maximum  $\text{CH}_4$  production, with their maxima reached within the temperature interval of 400–600 K. In this section, the two processes are further compared in terms of individual energy terms for reforming temperature at 450 K (see Table 4.5) in order to determine the conditions that could potentially provide more energy savings for  $\text{CH}_4$  production.

From Figure 4.5, for LTSR and SE-LTSR, the total  $\Delta H$  for producing one mole of  $\text{CH}_4$  increased with temperature. This was caused by an increase in the reactants  $\Delta H$  calculated using equation (4.6), as well as an increase in  $\Delta H$  of reaction, which evolved from very exothermic due to carbon graphite co-product to very endothermic due to  $\text{H}_2$  co-product. In the maximum methane production region for LTSR ( $\text{S}:\text{C} = 3$ ,  $T = 450$  K),  $\Delta H_{\text{Tot}}$  was 31.3 kJ/mol  $\text{CH}_4$ , resulting from 75.2 kJ/mol  $\text{CH}_4$  produced which attributed to reactants heating demand, and -44 kJ/mol  $\text{CH}_4$  of exothermic reaction in the reformer (Table 4.5). By comparison, at the maximum methane production for SE-LTSR ( $\text{Ca}(\text{OH})_2:\text{C} = 0.5:1$ , 450 K), the total  $\Delta H_{\text{Tot}}$  of 37.2 kJ/mol of  $\text{CH}_4$  produced

was the result of a very exothermic reaction  $\Delta H$  of  $-104$  kJ/mol  $\text{CH}_4$ , overwhelmed later by a strongly endothermic decarbonation of the sorbent ( $+157.1$  kJ/mol  $\text{CH}_4$ ), with the other terms (reactants heating  $\Delta H > 0$ , rehydration of  $\text{CaO}_{(s)} < 0$ ) roughly cancelling each other.

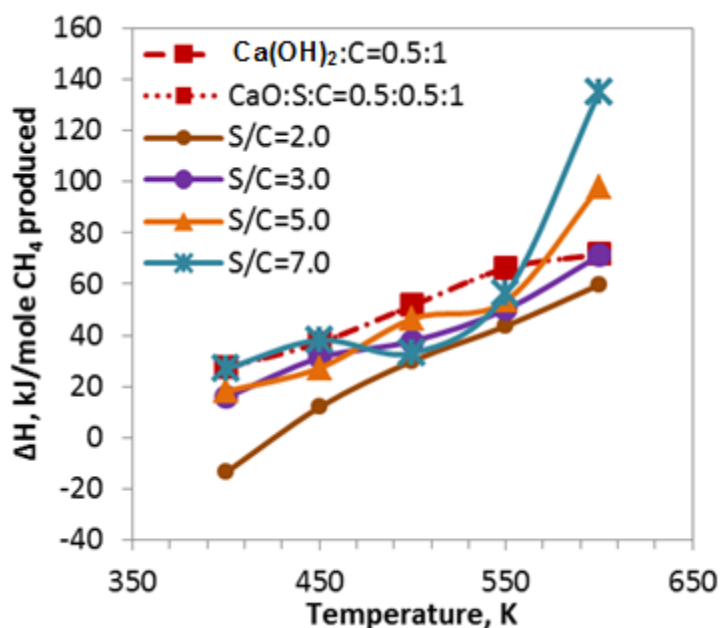


**Figure 4.5** Total enthalpy ( $\Delta H_{\text{Tot}}$ ) for producing 1 mole of  $\text{CH}_4$  from bio-oil steam reforming for LTSR in the range of  $S/C = 2-7$ , SE-LTSR using  $\text{Ca}(\text{OH})_2:C = 0.5:1$  (no inlet steam) and  $\text{CaO}:S:C = 0.5:0.5:1$  for reformer temperatures of 400–600 K at 1 atm. (S = steam)

The results shown in Figure 4.5 and Table 4.5 assume ideal heat recuperation conditions when recycling water and regenerated sorbent to the reformer and therefore, there are no great differences in  $\Delta H_{\text{Tot}}$  for a given reforming temperature when  $S/C$  varies from 2 to 7. In practice, the  $\Delta H_{\text{Tot}}$  of LTSR would significantly increase with  $S/C$  had more realistic recycling and heat recuperation conditions been considered. This is now illustrated in the worst case scenario of LTSR without recycling or heat recuperation of water, for which the calculated  $\Delta H_{\text{Tot}}$  at  $S/C$  of 2 was 202 kJ per mol  $\text{CH}_4$  produced,

rising to 268 and 639 kJ/mol CH<sub>4</sub> at S/C of 3 and 7, respectively, for similar reforming temperature of 450 K (results are not shown in figure or table). Similarly, SE-LTSR's heat demand would also increase significantly as decarbonation above 1170 K (calcination by oxy-combustion, for example) followed by non-ideal cooling of CaO<sub>(s)</sub>, and subsequently by its rehydration and recycling that would introduce heat and material losses. Again, in the worst case scenario of SE-LTSR where decarbonation is conducted at 1170 K, and neither the sorbent nor the water or their heat is recycled, the  $\Delta H_{\text{Tot}}$  of SE-LTSR with CaO<sub>(s)</sub> as the sorbent would be 381 kJ per mol CH<sub>4</sub> produced.

Table 4.5 lists the  $\Delta H_{\text{Tot}}$  of LTSR and SE-LTSR at atmospheric pressure, but similar calculations were performed at 30 atm (not shown). It was found that the  $\Delta H_{\text{Tot}}$  of isothermal LTSR and SE-LTSR in ideal conditions of recycle and heat recuperation was approximately 28–29 kJ per mol of CH<sub>4</sub> produced, with the differences of 1 atm found mainly in the 'reaction  $\Delta H$ ' term for LTSR and 'decarbonation  $\Delta H$ ' for SE-LTSR, indicating modest pressure effect on the enthalpy balance. More significant benefits of lower energy costs were observed when operating at higher temperatures (up to 600 K) when comparing 30 atm with 1 atm conditions due to the higher maximum CH<sub>4</sub> yield at 30 atm (as seen in Figure 4.4).

**Table 4.5** Enthalpy change terms for 1 mole of CH<sub>4</sub> produced by isothermal LTSR at S/C of 3 and isothermal SE-LTSR with Ca:C of 0.5:1 (with CaO and Ca(OH)<sub>2</sub> as sorbents) at 1 atm. All calculations were done at 450 K and  $\Delta H$  terms were given in kJ/mol of CH<sub>4</sub>.

Eq.	Enthalpy change term	Initial state → Final state	LTSR S/C = 3	CaO-LTSR 0.5:0.5:1	Ca(OH) <sub>2</sub> (s)- LTSR 0.5:1
4.4	Acetic acid $\Delta H$	298 K (l) → (g) 450 K	25.3	25.9	25.9
4.4	Phenol $\Delta H$	298 K (s) → (g) 450 K	15.2	15.6	15.6
4.5	H <sub>2</sub> O $\Delta H$	298 K (l) → (g) 450 K	34.7	38.0	N/A
4.7	Reaction $\Delta H$	450 K (g) → (g) 450 K	-43.9	-205.4	-104.4
4.8	Decarb $\Delta H$	450 K (s) → (s) 450 K	0.0	157.1	157.1
4.9	DeHy $\Delta H$	450 K (s) → (s) 450 K	N/A	6.0	N/A
4.10a	ReHy1 $\Delta H$	450 K (l,s) → 450 K (s)	N/A	N/A	-12.3
4.10b	ReHy2 $\Delta H$	(s) 450K & (l) 298 K → (s) 450 K	N/A	N/A	-44.6
4.11	$\Delta H_{Tot}$	298K (l,s) → (g,s) 450 K	31.3	37.2	37.2

Given the difficulties in recycling solid sorbent streams that becomes worse at high pressure (blockages at valves, risks of compromised seals) and for efficiently recuperating their heat, and also due to the fact that the reformat product of SE-LTSR may still require further purification post-processing stage to remove H<sub>2</sub> impurities and uncaptured CO<sub>2</sub>, there seem to be no clear advantages of SE-LTSR over LTSR in isothermal conditions, where both are expected to produce maximum CH<sub>4</sub> amounts.

The recommendation thus remains that for the isothermal process, LTSR at S/C of 3 (in order to clearly avoid equilibrium solid carbon product) and temperatures between 450 and 500 K, be utilised in combination with each other, as they provide more energy efficient and high methane yield conditions. Operating at higher pressures than atmospheric would bring about higher yields but also higher costs associated with fluid movers and reactor vessel specifications. These conditions will then require moderate heating in order to maintain the desired temperature.

#### **4.5.5 Comparison between isothermal and adiabatic LTSR processes for CH<sub>4</sub> production from PEFB bio-oil model**

As mentioned earlier, the 'hp' problem (i.e. constant enthalpy, constant pressure) was also conducted in the CEA programme to simulate the adiabatic LTSR and SE-LTSR processes (i.e. without heat losses, representing a well-insulated reformer without internal cooling). Figure 4.6 shows CH<sub>4</sub> production at varying S/C and temperatures for the adiabatic LTSR process at 1 atm. CH<sub>4</sub> production was favoured at lower initial temperatures (400–550 K) than the isothermal process, and the optimum conditions for CH<sub>4</sub> production were obtained at and above S/C = 2. This was caused by the significant increase in the equilibrium temperature of the adiabatic process (Figure 4.7) at low initial temperatures compared to the isothermal process, thus avoiding carbon graphite and CO by-products for S/C above 2 (C and CO not shown).

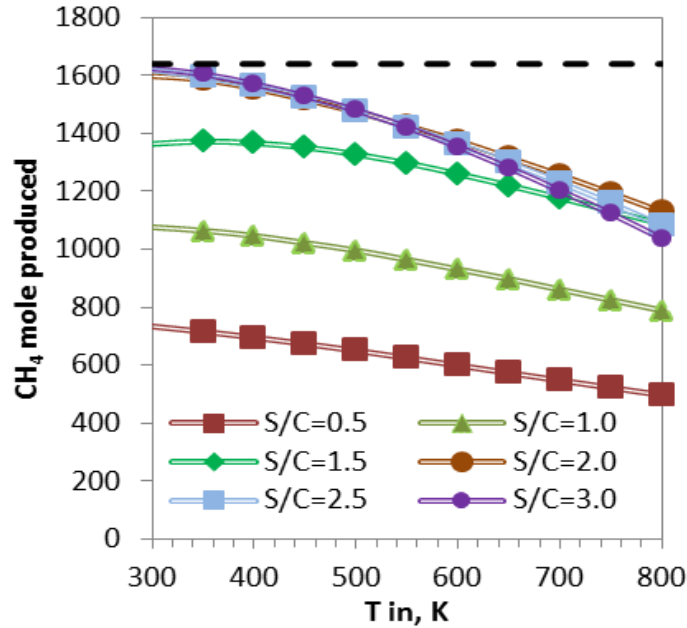


**Figure 4.6** CH<sub>4</sub> production for adiabatic LTSR within 300–800 K at 1 atm. This figure is to be compared to Figure 4.1(a) of the isothermal case.

If operating LTSR in adiabatic conditions from low initial temperature is possible in practice, higher yield of CH<sub>4</sub> than in the isothermal case would be obtained, as the dome-shaped methane production with temperature shifted to the left due to the heat released in the reformer hampering the carbon graphite by-product as long as there is sufficient steam co-reactant. In reality, as inlet temperatures fall towards ambient conditions (where the theoretical benefits on adiabatic equilibrium CH<sub>4</sub> yield have been found compared to the isothermal case), the bio-oil mixture will risk entering the reformer in liquid form, thus most likely deactivating the catalyst. In addition, kinetic rates of the catalytic reactions at low input temperatures will fall drastically and the exotherms on which the process relies may not occur. Thus, operating the adiabatic reactor would still require significant input temperatures in the reformer to guarantee adequate vapour phase of bio-oil components and significant catalytic activity.

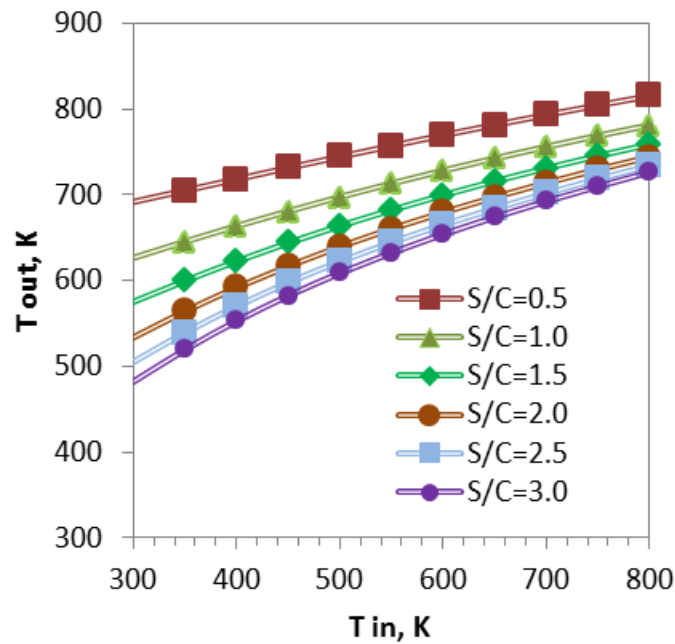


**Figure 4.7** Temperature output of the process for different values of S/C ratio (1–3) within 300–800 K of input temperature at 1 atm.

To conclude our comparison between isothermal and adiabatic LTSR processes without CO<sub>2</sub> sorbent, the reality will most likely reflect a hybrid case; not fully adiabatic, hence, close to isothermal. Therefore, the recommended operating conditions of LTSR in order to ensure reactants in vapour phase are in contact with the active catalyst in the reformer are an adiabatic reactor with downstream heat and water recuperation from the reformat of S/C of 3 and inlet temperature of ca. 450 K (177 °C) whether at 1 atm or higher. This will help to meet the overall moderate energy costs dominated by heating up the reactants whilst the reformer temperature may rise to 582 K (309 °C) as a result of exothermic reforming.



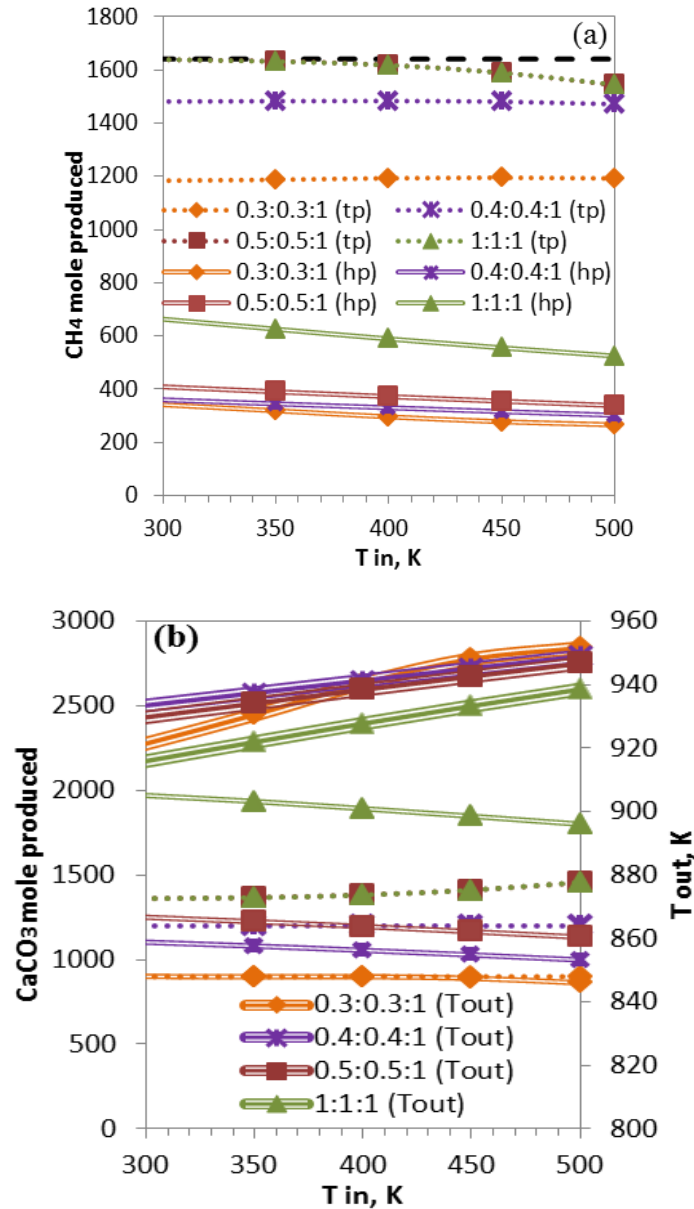


**Figure 4.8** CH<sub>4</sub> production (a) and CaCO<sub>3</sub> production and equilibrium temperature (b) in the isothermal (tp) and adiabatic (hp) cases for SE-LTSR using CaO as CO<sub>2</sub> sorbent within 300–800 K at 1 atm. The top line in (a) is the theoretical maximum. The format of molar ratio is presented in CaO:H<sub>2</sub>O:C. (S = steam)

Based on Figure 4.8, CH<sub>4</sub> production with CaO<sub>(s)</sub> in the SE-LTSR process in adiabatic and isobaric conditions (hp) was far below both the theoretical maximum and equilibrium CH<sub>4</sub> produced in the isothermal-isobaric (tp) case. This is due to the predicted equilibrium temperatures (output temperatures) being much higher than the initial temperatures (above 900 K, Figure 4.8(b)),

which, despite being favourable for CO<sub>2</sub>-capture by very exothermic carbonation, as evidenced by the significant carbonate product profiles in Figure 4.8(b), moved the process in SE-HTSR regime, benefitting H<sub>2</sub> to the detriment of CH<sub>4</sub> production.

Consequently, adiabatic SE-LTSR would not be achievable in practice, as the large temperature increase caused by carbonation would only allow for SE-HTSR, with minimal methane production. Given the large heat released for both CaO<sub>(s)</sub> and Ca(OH)<sub>2(s)</sub> SE-LTSR per mole of CH<sub>4</sub> produced, in practice, isothermal SE-LTSR would introduce major reactor design complexities from having to internally cool down the reformer, in which solid sorbents are the main source of heat due to carbonation. The only advantage of isothermal SE-LTSR over adiabatic LTSR would be the production of reformat with high methane concentration from the reactor, although small amounts of H<sub>2</sub> would still be present. This benefit is here considered insufficient to countermand the challenges posed by process solid flow recycling and heat recuperation. The final recommendation is therefore to operate at close to adiabatic LTSR with S/C of 3 and inlet temperature of ca. 450 K to achieve CH<sub>4</sub> yield of 38.3 wt. %, i.e. near the theoretical maximum of 40 wt. %, with a reformat dry composition of 44.5 vol. % CH<sub>4</sub>, 42.7 vol. % CO<sub>2</sub> and 12.7 vol. % H<sub>2</sub>. This process would then lend itself to post-process CO<sub>2</sub> capture via CH<sub>4</sub> purification, and this may influence the choice of pressure for the reformer. The moderate heat demand of the LTSR process in bringing the reactants to vapour phase may be partly met if an on-site pyrolysis/LTSR process is designed, where the volatiles from the PEFB pyrolysis stage are directed with

little heat loss to a nearby LTSR stage, and only the vapour co-reactant would require heating/vaporising with excess steam being recycled.

## 4.6 Conclusion

PEFB bio-oil has the potential to be converted into  $\text{CH}_4$  via the low-temperature steam reforming (LTSR) process.  $\text{CH}_4$  production was favoured in the 400–600 K range at atmospheric pressure with and without  $\text{CO}_2$  sorption. The large exothermicity of SE-LTSR precluded this process to be recommended, as the adiabatic reactor produced more  $\text{H}_2$  than  $\text{CH}_4$ . Furthermore, isothermal SE-LTSR would require costly internal cooling capability, as well as solids and heat recuperation design features for the small benefit of producing a reformat with high  $\text{CH}_4$  concentration. Therefore, the optimum conditions of  $\text{CH}_4$  production can be achieved by operating LTSR at around molar steam to carbon ratio of 3, with inlet temperature of ca. 450 K (or lower, if allowed by the catalyst activity and vapour state of the reactants), with efficient water recycle and heat recuperation from wet reformat. Pressures higher than atmospheric would contribute to reaching close to maximum  $\text{CH}_4$  yields at higher temperatures. These conditions would have a moderate overall heat demand, whilst producing near the theoretical maximum  $\text{CH}_4$ , albeit with a purity of ca. 45 vol. %.

Moreover, the isothermal sorption enhanced-low temperature steam reforming (SE-LTSR) would introduce major reactor design complexities from having to internally cool down the reformer, in which the solid sorbent becomes the main source of the large heat released due to carbonation. Although thermodynamically the maximum  $\text{CH}_4$  production can be achieved at 450 K (177 °C), the catalytic activity with Ni catalysts is limited at this temperature. Therefore, most of the industrial processes operate methanation in the range of 250–300 °C and 27–29 bar. It may therefore be preferable to operate an isothermal reactor (internally cooled reactor type IRMA) in the methanation process due to the simplicity of the process compared to the adiabatic reactor (where a series of fixed bed methanation reactors need to be implemented). For that reason, the operating conditions for isothermal methanator at 300 °C and 27 bar was chosen for simulating in the Aspen Plus program for the small scale bio-methane production from PEFB for this study.

## Chapter 5

### Experimental Results on Methanation of Acetic Acid as Bio-oil Surrogate in a Packed Bed Reactor

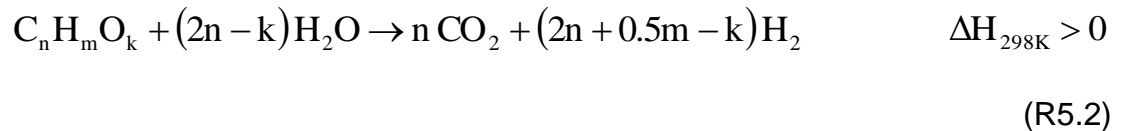
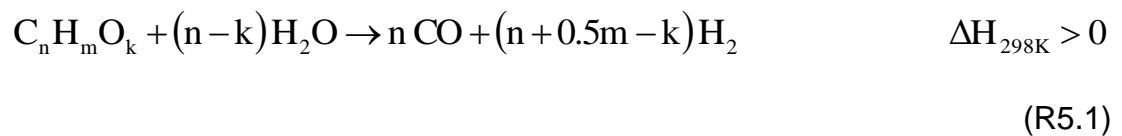
#### 5.1 Introduction

In this chapter, the feasibility of methane ( $\text{CH}_4$ ) production from acetic acid as bio-oil surrogate via low-temperature steam reforming (LTSR) has been investigated. Based on the thermodynamic equilibrium analysis of  $\text{CH}_4$  production from model bio-oil discussed in the previous chapter (Chapter 4),  $\text{CH}_4$  production was favoured at 130–330 °C and 2–3 of molar steam to carbon ratio (S/C) at atmospheric pressure. Recall that increases in pressure above atmospheric would present more thermodynamically favourable conditions for methane yield and purity in the gas product mixture, therefore conducting laboratory experiments at atmospheric pressure represent non ideal conditions compared to an industrial application conducted at higher pressures. By using these conditions as a basis for determining optimal conditions of acetic acid steam reforming at atmospheric pressure, the performance of the commercial catalyst, nickel-calcium aluminate ( $\text{Ni/Ca-Al}_2\text{O}_3$ ) towards  $\text{CH}_4$  production was carried out. The characteristics of the carbon deposited on the used catalyst ( $C_S$ ) and carbon present in the condensate ( $C_L$ ) were also reported in this chapter.

## 5.2 CH<sub>4</sub> production from acetic acid by LTSR

The bio-oil product from biomass pyrolysis has a complex and variable composition [23, 147], where acetic acid is prominent in biomass pyrolysis oils. Here, acetic acid was used as bio-oil surrogate in this study for LTSR process in a packed bed catalytic reactor, and therefore could form the basis for evaluating optimum conditions before the utilization of the complex bio-oils. As mentioned from the previous chapter (Chapter 4), various reactions such as steam reforming (R5.1–R5.2), water-gas shift (R5.3) and methane synthesis (R5.4–R5.6) are involved in producing CH<sub>4</sub> from bio-oil feedstock (R5.7). Some reactions listed here are repeated from previous sections, but for clarity's sake they have been renumbered for this chapter. In the case of acetic acid (CH<sub>3</sub>COOH), the values of n, m and k in the molar feedstock formula C<sub>n</sub>H<sub>m</sub>O<sub>k</sub> are 2, 4 and 2 respectively.

Steam reforming:



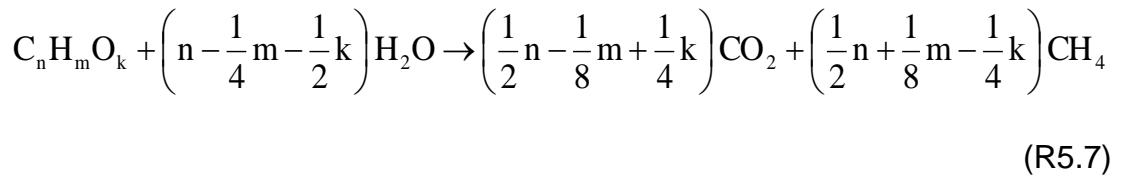
Water-gas shift:



Methane synthesis:

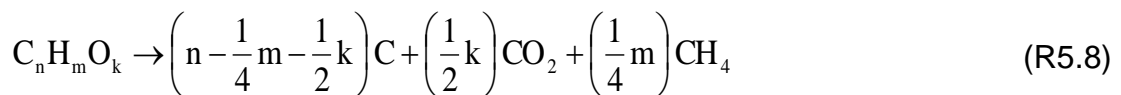


Methane production from bio-oil:



However, the undesirable carbon formation from thermal decomposition of oxygenated hydrocarbons (R5.8) and  $\text{CH}_4$  decomposition (R5.9) may take place during methanation.

Bio-oil decomposition:



Methane decomposition:



In the above reactions (R5.1–R5.9),  $C_nH_mO_k$  is a moisture free molar formula where n, m, and k are represented as molar numbers of carbon, hydrogen and oxygen atom in the bio-oil.

Several studies on methanation of syngas [119, 148-150] and methanation of carbon dioxide ( $CO_2$ ) [151-153] over nickel-based catalyst have found higher selectivity to  $CH_4$  product in the temperature range of 300–400 °C because the catalytic activity was limited at a lower temperatures. Due to that circumstance, methanation reaction R5.6 may compete with the steam reforming reaction (via the reverse of R5.6) since the steam reforming reaction is dominant at higher temperatures which consumes  $CH_4$ , thus affecting  $CH_4$  yield. Therefore, the influence of process conditions (reaction temperature and S/C) were conducted in this study in order to observe the performance of the Ni/Ca- $Al_2O_3$  catalyst and to determine the optimum conditions for  $CH_4$  production from direct acetic acid conversion via LTSR.

### 5.3 Experimental procedure

The catalytic tests for acetic acid conversion via LTSR were conducted in a continuous flow process using a stainless steel tube in a packed bed reactor at atmospheric pressure. For each experiment runs, approximately 4 grams of Ni/Ca- $Al_2O_3$  catalyst (250–355  $\mu m$  of particle size) were loaded between two quartz wool plugs in a stainless steel tubular reactor. A type K thermocouple was placed under the catalyst bed to monitor the reaction temperature. As part



of the procedure of catalyst activation by reduction, the fresh catalyst was first heated to 600 °C under nitrogen (N<sub>2</sub>) flow (200 cm<sup>3</sup>/min, 20 °C, 1 atm) and started to reduce at this temperature by switching the N<sub>2</sub> flow to one of 5 vol.% of hydrogen (H<sub>2</sub>) in N<sub>2</sub> flow (200 cm<sup>3</sup>/min of total flow) for 2 hours. The completion of the catalyst reduction was determined when the micro-gas chromatograph (GC) showed a return to a steady state of H<sub>2</sub> concentration of 5% of H<sub>2</sub>. Then, the reactor was purged and cooled using a high N<sub>2</sub> flowrate and until the temperature matched that chosen for the LTSR experiment (set point between 350 and 450 °C). Both vaporizers of fuel (acetic acid) and water were switched on during the cooling of the reactor. Once the vaporizers and reactor temperatures reached the set point, the heating tape around the pipe connecting the vaporizers to the reformer was then to be turned on. The methanation experiment over Ni/Ca-Al<sub>2</sub>O<sub>3</sub> catalyst was conducted at the range of 350–450 °C and S/C of 1–3 under 18 cm<sup>3</sup>/min of N<sub>2</sub> flow. In this experiment, fuel and water were pumped into the reactor using programmable syringe pumps, where the fuel flowrate was set to 0.978 cm<sup>3</sup>/hr (20 °C, 1 atm), which gave a carbon input flow rate of  $9.5 \times 10^{-6}$  mol/s. However, the liquid water flowrate varied from 0.616 to 1.849 cm<sup>3</sup>/hr to obtain desired S/C of 1 and 3 respectively. The products flowed through the condenser and underwent separation between volatile and non volatile into the liquid condensate and gas product mixtures, where the condensate was collected for further analysis. Then, the moist gas products continuously flowed into the silica bed to trap any moisture left in products. Finally, the dry gaseous production was analysed by micro-GC (Varian) according to experimental method described in Chapter 3.

## 5.4 Calculations of process outputs

The process performance of acetic acid conversion by LTSR was presented in terms of fuel conversion to gases ( $X_{\text{fuel}}$ ), CH<sub>4</sub> yield ( $Y_{\text{CH}_4}$ ), CH<sub>4</sub> yield efficiency ( $Y_{\text{CH}_4,\text{eff}}$ ), selectivity to carbon products ( $S_{\text{C-i}}$ ) and selectivity to hydrogen products ( $S_{\text{H-i}}$ ) by using equations (5.1–5.12). In these equations,  $\dot{n}$  and  $y$  represent the molar flowrate and dry gas mole fraction of a product species respectively. Since the composition of gas products from the GC analysis gives results in volume fraction (or %), analog to mole fractions, the chemically inert N<sub>2</sub> flow was used via a nitrogen balance to determine the total output of the molar flowrate for each experimental run. Accordingly, the dry gas molar flowrate ( $\dot{n}_{\text{out,dry}}$ ) is calculated via equation 5.1 where  $j$  is the elemental N of the fuel. For acetic acid,  $j$  is zero, but bio-oils are expected to have a non negligible  $j$  value. The subscript 'fuel' represents the organic feedstock.

$$(j \times \dot{n}_{\text{fuel,in}}) + (2 \times \dot{n}_{\text{N}_2,\text{in}}) = \dot{n}_{\text{out,dry}} \times (2 \times \dot{n}_{\text{N}_2,\text{out}}) + (j \times \dot{n}_{\text{fuel,out}}) \quad (5.1)$$

By rearranging equation 5.1, the total molar flowrate of dry gas,  $\dot{n}_{\text{out,dry}}$  can be expressed as,

$$\dot{n}_{\text{out,dry}} = \frac{\dot{n}_{\text{N}_2,\text{in}}}{y_{\text{N}_2,\text{out}}} \quad (5.2)$$

On the other hand, the molar flowrate of the reactants which are fuel (acetic acid) and water are calculated using equation 5.3 and 5.4 respectively.

$$\dot{n}_{\text{fuel, in}} = \frac{\dot{m}_{\text{fuel, in}}}{M_{\text{fuel}}} = \frac{\rho_{\text{fuel, in}} \times \dot{V}_{\text{fuel, in}}}{M_{\text{fuel}}} \quad (5.3)$$

$$\dot{n}_{\text{H}_2\text{O, in}} = \frac{\dot{m}_{\text{H}_2\text{O, in}}}{M_{\text{H}_2\text{O}}} = \frac{\rho_{\text{H}_2\text{O, in}} \times \dot{V}_{\text{H}_2\text{O, in}}}{M_{\text{H}_2\text{O}}} \quad (5.4)$$

where:

$\dot{n}_{\text{fuel, in}}$  or  $\dot{n}_{\text{H}_2\text{O, in}}$  = inlet molar flowrate of fuel or water (mol/s);

$\dot{m}_{\text{fuel, in}}$  or  $\dot{m}_{\text{H}_2\text{O, in}}$  = inlet mass flowrate of fuel or water (kg/s);

$M_{\text{fuel}}$  or  $M_{\text{H}_2\text{O}}$  = molar mass of fuel or water (kg/mol);

$\rho_{\text{fuel, in}}$  or  $\rho_{\text{H}_2\text{O, in}}$  = density of fuel or water (kg/m<sup>3</sup>);

$\dot{V}_{\text{fuel, in}}$  or  $\dot{V}_{\text{H}_2\text{O, in}}$  = inlet volumetric flowrate of fuel or water (m<sup>3</sup>/s).

Thus,  $X_{\text{fuel}}$  which is interpreted as ‘fuel conversion to CH<sub>4</sub>, CO<sub>2</sub>, CO, C<sub>2</sub>H<sub>4</sub>, C<sub>2</sub>H<sub>6</sub>, C<sub>3</sub>H<sub>6</sub> and C<sub>3</sub>H<sub>8</sub> gases’ can be determined by using equation 5.5.

$$X_{\text{fuel}} = \left[ \frac{\dot{n}_{\text{out, dry}} \left( y_{\text{CH}_4} + y_{\text{CO}_2} + y_{\text{CO}} + 2 \times y_{\text{C}_2\text{H}_4} + 2 \times y_{\text{C}_2\text{H}_6} + 3 \times y_{\text{C}_3\text{H}_6} + 3 \times y_{\text{C}_3\text{H}_8} \right)}{n \times \dot{n}_{\text{fuel, in}}} \right] \times 100 \quad (5.5)$$

Recall for acetic acid, ‘n’ used at the denominator is 2 for the ‘fuel C<sub>n</sub>H<sub>m</sub>O<sub>k</sub>N<sub>j</sub>’ acetic acid C<sub>2</sub>H<sub>4</sub>O<sub>2</sub>. The CH<sub>4</sub> yield was calculated using equation 5.6.

$$Y_{\text{CH}_4} (\text{wt}\%) = \left( \frac{M_{\text{CH}_4} \times y_{\text{CH}_4} \times \dot{n}_{\text{out, dry}}}{M_{\text{fuel}} \times \dot{n}_{\text{fuel, in}}} \right) \times 100 \quad (5.6)$$

In equation 5.6,  $M_{\text{CH}_4} / M_{\text{fuel}} = 16.04 \text{ g mol}^{-1} / 60.06 \text{ g mol}^{-1} = 0.2671$ .

CH<sub>4</sub> yield efficiency is here defined as the percent ratio of CH<sub>4</sub> yield obtained during the experiment to that predicted by chemical equilibrium using the same initial conditions of P, T, and flow composition. Because the experiment uses a rather small reactor and rigorous adiabatic conditions are too hard to implement, and heat losses would have been significant, the equilibrium calculations were made by choosing the isothermal and isobaric option with the code in the Chemical Equilibrium and Applications (CEA) programme. CEA's solution method is based on the minimization of Gibbs energy from a chosen set pool of reactants and equilibrium products of known thermodynamic properties, as opposed to an assumed set of reactions with known equilibrium constants. This offers an advantage to this work, provided that the chosen pool of products is comprehensive, no assumptions are made towards which reactions have taken place to reach equilibrium.

$$Y_{\text{CH}_4,\text{eff}}(\%) = \left( \frac{Y_{\text{CH}_4,\text{exp}}}{Y_{\text{CH}_4,\text{eq}}} \right) \times 100 \quad (5.7)$$

Selectivity of carbon containing gases to CH<sub>4</sub> ( $S_{\text{C-CH}_4}$ ), CO<sub>2</sub> ( $S_{\text{C-CO}_2}$ ) and CO ( $S_{\text{C-CO}}$ ) were determined using the following equations (5.8–5.10).

$$S_{\text{C-CH}_4}(\%) = \left( \frac{y_{\text{CH}_4}}{y_{\text{CH}_4} + y_{\text{CO}_2} + y_{\text{CO}} + 2 \times y_{\text{C}_2\text{H}_4} + 2 \times y_{\text{C}_2\text{H}_6} + 3 \times y_{\text{C}_3\text{H}_6} + 3 \times y_{\text{C}_3\text{H}_8}} \right) \times 100 \quad (5.8)$$

$$S_{\text{C-CO}_2}(\%) = \left( \frac{y_{\text{CO}_2}}{y_{\text{CH}_4} + y_{\text{CO}_2} + y_{\text{CO}} + 2 \times y_{\text{C}_2\text{H}_4} + 2 \times y_{\text{C}_2\text{H}_6} + 3 \times y_{\text{C}_3\text{H}_6} + 3 \times y_{\text{C}_3\text{H}_8}} \right) \times 100 \quad (5.9)$$

$$S_{C-CO}(\%) = \left( \frac{y_{CO}}{y_{CH_4} + y_{CO_2} + y_{CO} + 2 \times y_{C_2H_4} + 2 \times y_{C_2H_6} + 3 \times y_{C_3H_6} + 3 \times y_{C_3H_8}} \right) \times 100 \quad (5.10)$$

Selectivity to CH<sub>4</sub> ( $S_{H-CH_4}$ ) and H<sub>2</sub> ( $S_{H-H_2}$ ) with respect to hydrogen containing gases were calculated using equations 5.11 and 5.12 respectively.

$$S_{H-CH_4}(\%) = \left( \frac{4 \times y_{CH_4}}{4 \times y_{CH_4} + 2 \times y_{H_2} + 4 \times y_{C_2H_4} + 6 \times y_{C_2H_6} + 6 \times y_{C_3H_6} + 8 \times y_{C_3H_8}} \right) \times 100 \quad (5.11)$$

$$S_{H-H_2}(\%) = \left( \frac{2 \times y_{H_2}}{4 \times y_{CH_4} + 2 \times y_{H_2} + 4 \times y_{C_2H_4} + 6 \times y_{C_2H_6} + 6 \times y_{C_3H_6} + 8 \times y_{C_3H_8}} \right) \times 100 \quad (5.12)$$

On the other hand, the carbon in the condensate and the carbon formed on the catalyst surface were measured separately by other techniques which are elemental (CHNS) and total organic compounds (TOC) analysis as described in Chapter 3.

## 5.5 Influence of process parameters on CH<sub>4</sub> production from acetic acid by LTSR

As previous research found that higher selectivity of CH<sub>4</sub> production occurs in the range 300–400 °C [119], the experiments for acetic acid conversion via LTSR over Ni/Ca-Al<sub>2</sub>O<sub>3</sub> catalyst were conducted in the temperature range of 350–450 °C. Based on the results from the CEA program (Chapter 4), S/C of 2–3 were used in this study in order to determine the optimum conditions for

CH<sub>4</sub> productions. Thus, the effects of reaction temperature and S/C towards CH<sub>4</sub> productions are discussed in this section.

### 5.5.1 Temperature effect

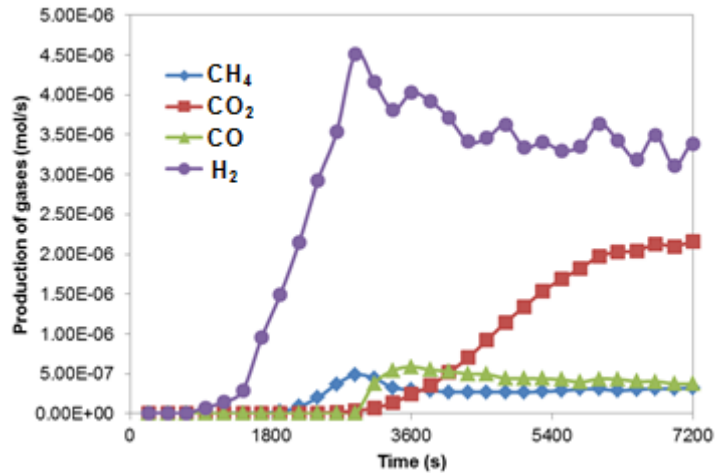
The methanation performance outputs of Ni/Ca-Al<sub>2</sub>O<sub>3</sub> catalyst in the temperature range of 350–450 °C are listed in Table 5.1. At 350 °C, only 29.4% of the acetic acid feedstock was converted into gaseous products, but this increased drastically to 81.9% at 400 °C. The feedstock conversion at 450 °C was comparatively close to that at 400 °C, which was 78.6%. This finding is consistent with CO and CO<sub>2</sub> methanation catalytic activity with Ni catalysts having been found to be limited at 350 °C, whilst temperatures above 350 °C is required to obtain higher fuel conversion using Ni based catalyst [150, 151, 153]. Although both reaction temperatures at 400 °C and 450 °C achieved higher acetic acid conversion, higher CH<sub>4</sub> selectivity was obtained at 400 °C compared to 450 °C. This is because the steam reforming reaction (via the reverse of R5.6) became increasingly favourable at higher temperature, which favours H<sub>2</sub> production. From Table 5.1, the highest value of CH<sub>4</sub> yield was obtained at 400 °C with 15.7 wt.%.

Moreover, it was observed that the yield efficiency in Table 5.1 increases with temperature. As the temperature increases the kinetics, it brings closer to equilibrium faster. Therefore, for a same residence time in the reactor, the highest temperature is expected closer to equilibrium. Thus, the experimental results in Table 5.1 showed the yield efficiency at 350 °C was far from equilibrium, close at 400 °C, but closer at 450 °C.

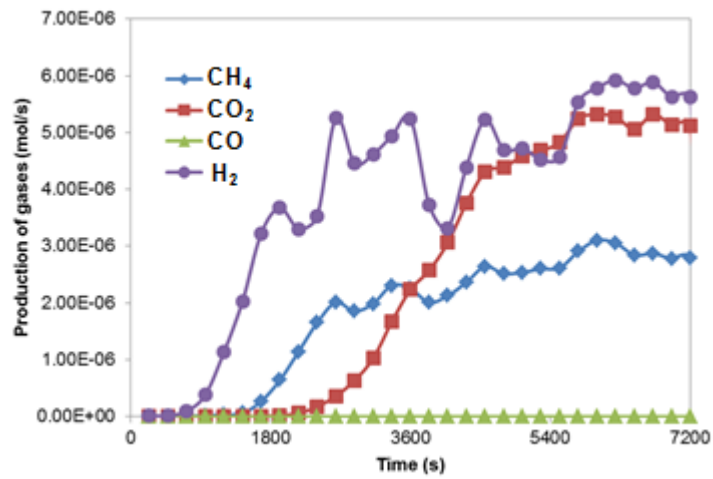
**Table 5.1** The effect of reaction temperature towards CH<sub>4</sub> production at constant S/C of 2 using 4 grams of Ni/Ca-Al<sub>2</sub>O<sub>3</sub> catalyst.

Temperature, °C	350	400	450
Fuel conversion to gases, %	29.4	81.9	78.6
CH <sub>4</sub> yield, wt.% (Experimental)	1.7	15.7	14.6
CH <sub>4</sub> yield, wt.% (Equilibrium)	23.6	21.0	17.2
CH <sub>4</sub> yield efficiency (Exp./Equil.)	7.3	74.8	86.1
<b>% Selectivity to C-products in the gas</b>			
i. CH <sub>4</sub>	11.0	35.8	35.2
ii. CO <sub>2</sub>	74.8	64.2	64.8
iii. CO	14.2	0.0	0.0
<b>% Selectivity to H-products in the gas</b>			
i. CH <sub>4</sub>	8.5	34.4	31.5
ii. H <sub>2</sub>	91.5	65.6	68.5

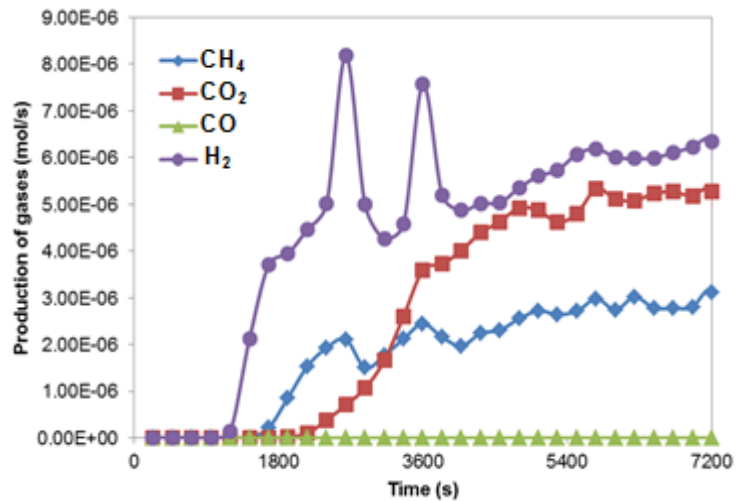
Furthermore, Figure 5.1 clearly showed that the increment of reaction temperature has reduced the time for all of the gaseous products (CH<sub>4</sub>, CO<sub>2</sub>, CO and H<sub>2</sub>) in achieving to their steady state. Approximately 6240 s was required for the carbon containing gases (CH<sub>4</sub>, CO<sub>2</sub> and CO) to reach at the maximum production and continues to maintain their stability at 350 °C (Figure 5.1a). However, less time was needed for the production of CH<sub>4</sub>, CO<sub>2</sub> and CO at 400 °C (Figure 5.1b) and 450 °C (Figure 5.1c), which are approximately at 4800 s and 3840 s. It was suggested that the formation of carbon was taking place at the beginning of the reaction. Further investigation of carbon deposition on the catalyst is discussed in the next section.



(a)



(b)



(c)

**Figure 5.1** Production of gases ( $\text{CH}_4$ ,  $\text{CO}_2$ ,  $\text{CO}$  and  $\text{H}_2$ ) at (a) 350 °C, (b) 400 °C and (c) 450 °C. The value of steam to carbon ratio of 2 was used at atmospheric pressure.

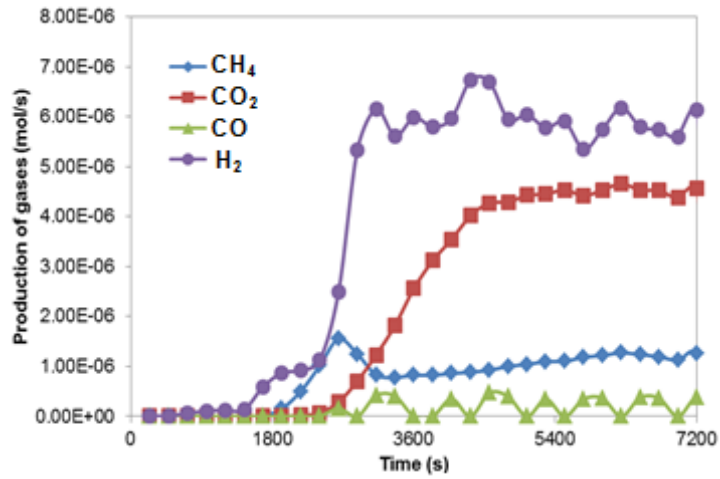


### 5.5.2 Steam to carbon ratio (S/C) effect

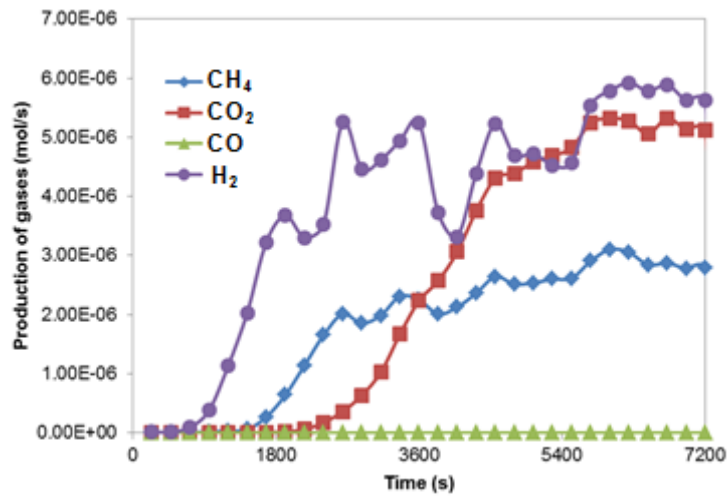
Table 5.2 illustrates the catalytic performance of Ni/Ca-Al<sub>2</sub>O<sub>3</sub> catalyst with different of S/C (1–3) at 400 °C. It shows that S/C of 2 is the best condition in terms of CH<sub>4</sub> yield and CH<sub>4</sub> selectivity, with 15.7 wt.% and 35.8% respectively. Apparently, lower CH<sub>4</sub> yield was obtained at S/C of 1 due to the lack of water in the methanation reaction. However, excessive water in the process at S/C of 3 was observed to have a higher selectivity towards H<sub>2</sub> and CO<sub>2</sub> production, causing lower of CH<sub>4</sub> yield. This is because the water as an excess reactant favours the water-gas shift reaction (R5.3).

**Table 5.2** The effect of steam to carbon ratio towards CH<sub>4</sub> production at constant 400 °C using 4 grams of Ni/Ca-Al<sub>2</sub>O<sub>3</sub> catalyst.

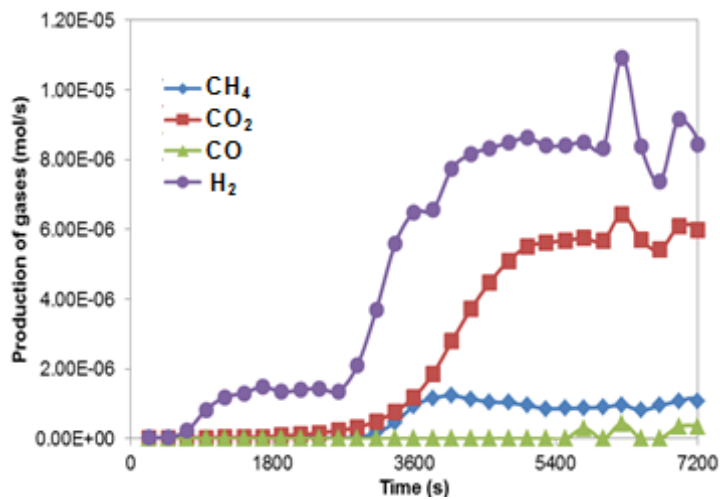
Steam to carbon ratio, S/C	1.0	2.0	3.0
Fuel conversion to gases, %	61.8	81.9	72.2
CH <sub>4</sub> yield, wt.% (Experimental)	6.5	15.7	5.3
CH <sub>4</sub> yield, wt.% (Equilibrium)	19.0	21.0	19.2
CH <sub>4</sub> yield efficiency (Exp./Equil.)	34.2	74.8	27.4
<b>Selectivity to carbon (%):</b>			
i. CH <sub>4</sub>	19.7	35.8	13.6
ii. CO <sub>2</sub>	76.5	64.2	84.5
iii. CO	3.9	0.0	1.9
<b>Selectivity to hydrogen (%):</b>			
i. CH <sub>4</sub>	16.5	34.4	9.8
ii. H <sub>2</sub>	83.5	65.6	90.2



(a)



(b)



(c)

**Figure 5.2** Production of gases ( $\text{CH}_4$ ,  $\text{CO}_2$ ,  $\text{CO}$  and  $\text{H}_2$ ) at S/C of (a) 1, (b) 2 and (c) 3. The operating temperature was set at 400 °C atmospheric pressure.

Similar times were observed for all of the production gases to achieve their steady state with different of S/C values (Figure 5.2), where 4800 s for S/C of 1 and 2 and 5040 s for S/C of 3. However, excessive water, which is at S/C of 3 leads to have a slower of CH<sub>4</sub> production as shown in Figure 5.2(c). It clearly shows that the water-gas shift reaction (R5.3) has taken place at first when an excessive of water was introduced in the process, which resulted in higher H<sub>2</sub> production compared to CH<sub>4</sub> production.

Based on the results of catalytic activity at different temperatures and S/C values, it can be concluded that the optimum conditions for methanation of acetic acid over a Ni/Ca-Al<sub>2</sub>O<sub>3</sub> catalyst at atmospheric pressure was achieved at 400 °C and S/C of 2.

## 5.6 Catalyst characterization

In order to have a better understanding of catalyst's activity, the used catalyst was characterized after each experimental run using powder x-ray diffraction (XRD), thermogravimetric analysis (TGA), elemental (CHNS) analysis, scanning electron microscopy and energy dispersive X-ray analysis (SEM-EDX).

### 5.6.1 Catalyst phases and crystallite size with X-ray diffraction (XRD)

The XRD patterns of fresh and used Ni/Ca-Al<sub>2</sub>O<sub>3</sub> catalysts are shown in Figure 5.3. It can be seen that the main peaks on fresh catalyst at 25.6° and 43.5° correspond to pure phase of  $\alpha$ -Al<sub>2</sub>O<sub>3</sub> support, and this remains so after catalytic testing (used catalyst). The peaks assigned to cubic NiO were found at 37.4°, 43.4°, 62.9°, 75.6° and 79.7° on the fresh catalyst. However, the diffraction peaks of NiO species were no longer observed on used catalyst, indicating that NiO in fresh catalyst were fully reduced to metallic Ni which were observed in the XRD pattern of used catalyst at 44.8°, 52.6° and 77.0°. In addition, one of the peaks (43.4°) indicating to cubic NiO was assumed overlapped with a diffraction peak of  $\alpha$ -Al<sub>2</sub>O<sub>3</sub>. Therefore, it was clearly observed that the diffraction intensity decreased at 43.4° on used catalyst due to the reduction of NiO. Meanwhile, the intensity of graphitic carbon on used catalyst at 27.6° was very small and could hardly be distinguished from the background noise. This is possibly because of a small amount of carbon present on the catalyst bulk, thus less sensitive towards XRD analysis. The peaks corresponding to CaO were also found at 32.6°, 37.8° and 68.2° in both the fresh and used catalysts, but diffraction peaks for Ca(OH)<sub>2</sub> were only observed on fresh catalyst at 18.3°, 29.0° and 63.3°. This is due to the exposure of the catalyst to humidity in the air when hydration of CaO into Ca(OH)<sub>2</sub> readily occurred.

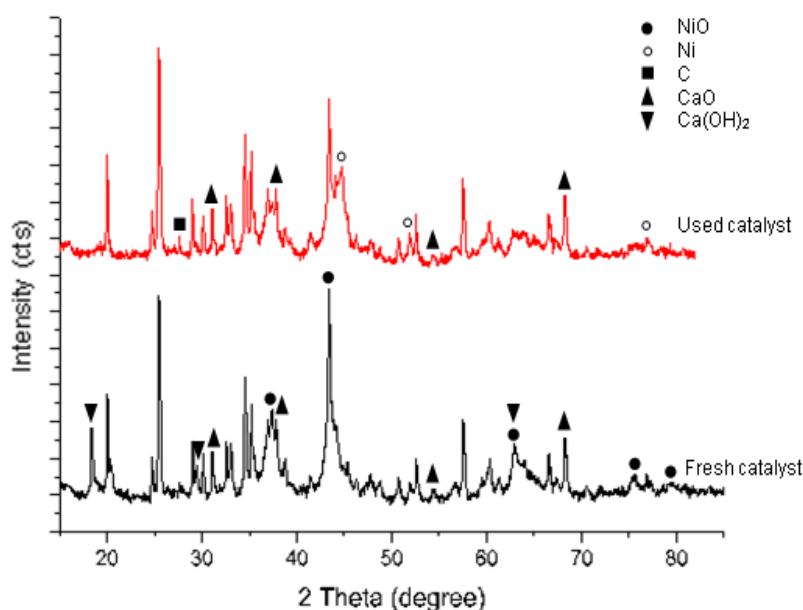


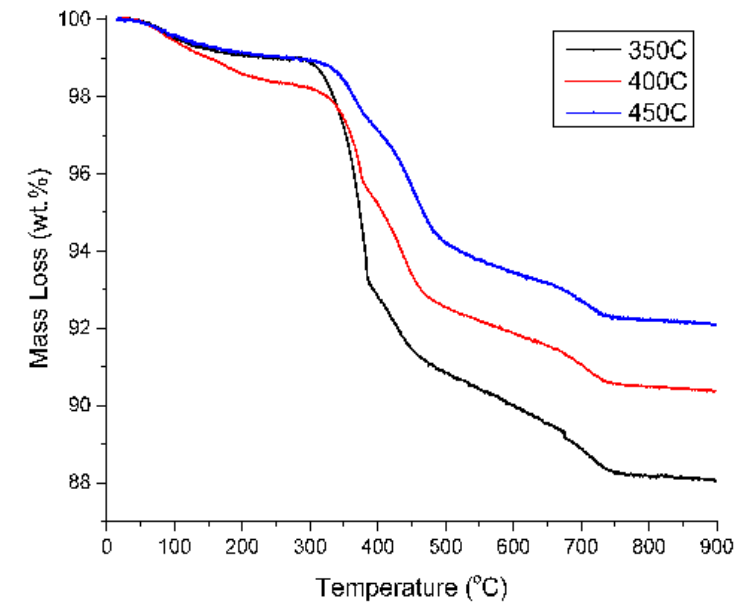
**Figure 5.3** XRD patterns of fresh and used Ni/Ca-Al<sub>2</sub>O<sub>3</sub> catalysts.

### 5.6.2 Carbon in the catalyst by TGA and elemental analysis

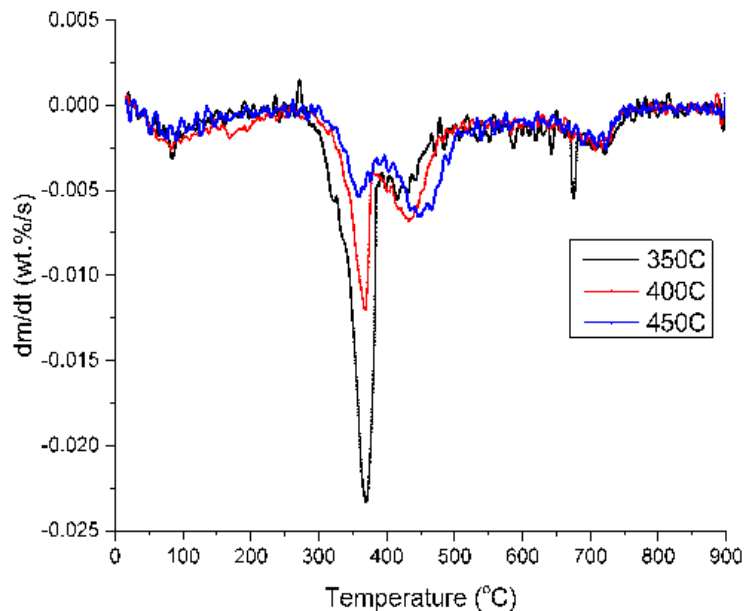
In order to estimate the total amount of carbon deposition on the Ni/Ca-Al<sub>2</sub>O<sub>3</sub> catalyst, TGA-TPO (temperature programmed oxidation) and elemental analysis were carried out, as described in Chapter 3. From these analyses, the effects of reaction temperature (Figure 5.4 and Table 5.3) and S/C (Figure 5.5 and Table 5.4) towards the carbon formation on the catalyst surface were also being investigated.

From Figure 5.4, TG analysis in air flow (TPO) clearly showed that the total weight loss of the used catalysts decreased with the reaction temperatures. The weight loss for 350 °C, 400 °C and 450 °C were 11.7%, 9.4% and 7.7% respectively, indicating that the combustion of carbon present in the catalyst was less. However, an insignificant difference of total weight loss for S/C was

found out, as shown in Figure 5.5. Therefore, the reaction temperature for methanation has revealed to have an important role in mitigating carbon formation, which can causes deactivation of the catalyst.

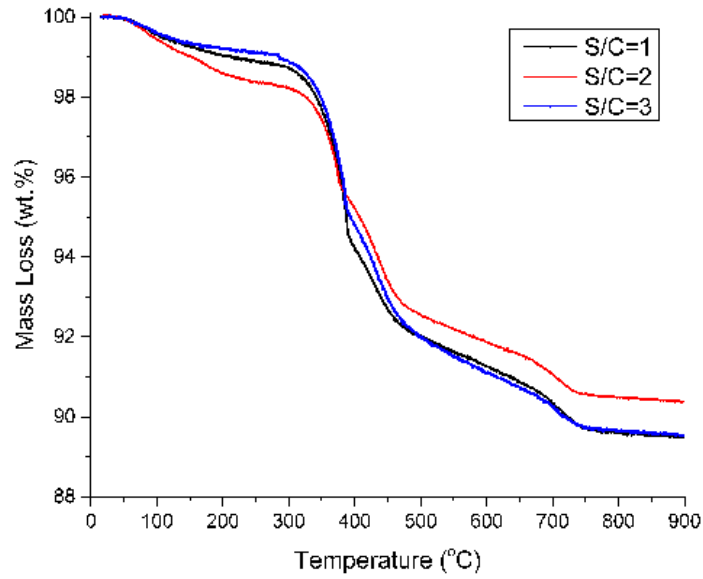


(a)

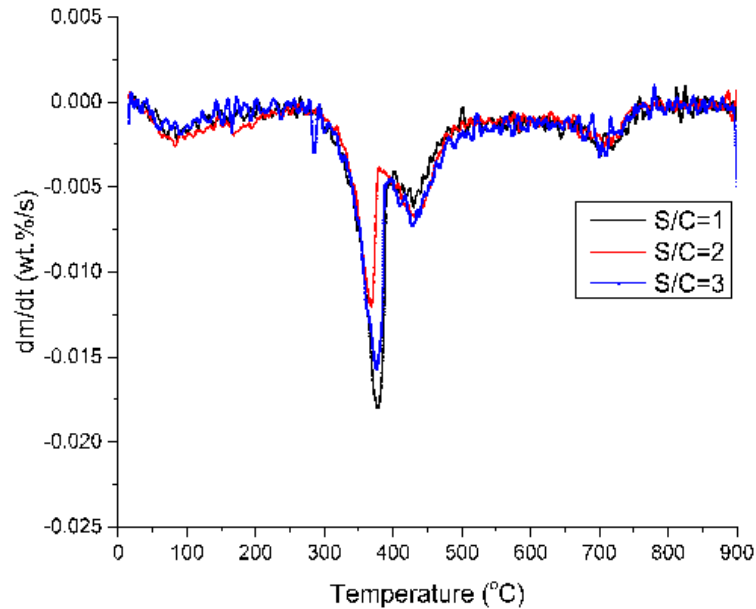


(b)

**Figure 5.4** TPO results of the used catalysts (Ni/Ca-Al<sub>2</sub>O<sub>3</sub>) (a) TGA-TPO and (b) DTG-TPO for different reaction temperatures under air flow (50 ml/min) at a heating rate of 10 °C/min. The catalysts were used in LTSR process at constant S/C of 2.



(a)



(b)

**Figure 5.5** TPO results of the used catalysts ( $\text{Ni}/\text{Ca}-\text{Al}_2\text{O}_3$ ) (a) TGA-TPO and (b) DTG-TPO for different steam to carbon ratio (S/C) under air flow (50 ml/min) at a heating rate of 10 °C/min. The catalysts were used in LTSR process at constant 400 °C.

Based on the weight loss in Figure 5.4 and Figure 5.5, more than 75% of the amount of carbon deposition could be burned below 500 °C. As reported in oxidation of carbons in Ni catalyst, there are two types of carbon species exist

on the catalyst which are, easily oxidized carbon (110–400 °C), and deactivating carbon (400–800 °C) [149, 154], in agreement with our results.

According to the weight percentage of carbon determined by elemental analysis shown in Table 5.3, the results from TPO exhibited a similar trend, where the amount of carbons on the surface of used catalyst decreases with the increasing of reaction temperature. Moreover, similar amount of carbon was detected from CHNS analysis with different of S/C, as listed in Table 5.4, which also correlates from the previous results in TGA analysis.

**Table 5.3** Comparison of components (C, H, N and S) of used catalysts (Ni/Ca-Al<sub>2</sub>O<sub>3</sub>) for different reaction temperature. The catalysts were used in LTSR process at constant S/C of 2.

Temperature, °C	C, wt.%	H, wt.%	N, S wt.%
350	6.73	0.82	0.00
400	5.49	0.56	0.00
450	4.82	0.75	0.00

**Table 5.4** Comparison of components (C, H, N and S) of used catalysts (Ni/Ca-Al<sub>2</sub>O<sub>3</sub>) for different steam to carbon ratio (S/C). The catalysts were used in LTSR process at constant 400 °C.

S/C	C, wt.%	H, wt.%	N, S wt.%
1	6.93	0.65	0.00
2	5.49	0.56	0.00
3	6.10	0.58	0.00



### 5.6.3 Morphology and elemental composition of catalyst with SEM-EDX

SEM image of the fresh catalyst is shown in Figure 5.6 with magnification of 10,000 $\times$ , and Figure 5.7 corresponds to the EDX mapping for the spatial distribution of different elements (Al, O, Ca and Ni) on the fresh catalyst. It was found that the fresh Ni/Ca-Al<sub>2</sub>O<sub>3</sub> catalyst had a rough surface morphology with uneven structure, but Ca and Ni species were dispersed uniformly on the surface of Al<sub>2</sub>O<sub>3</sub> as illustrated in Figure 5.7(c) and (d).

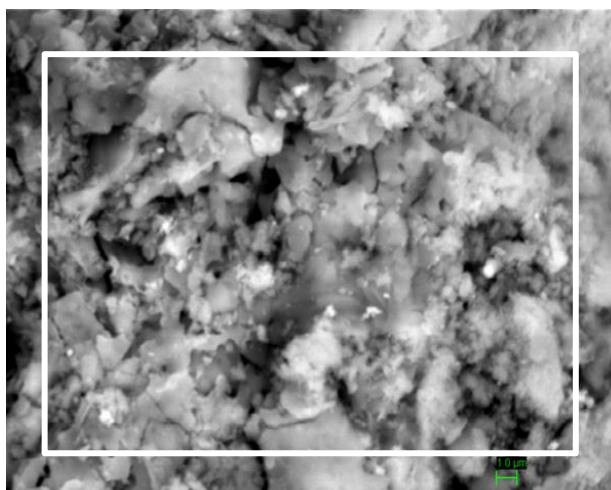
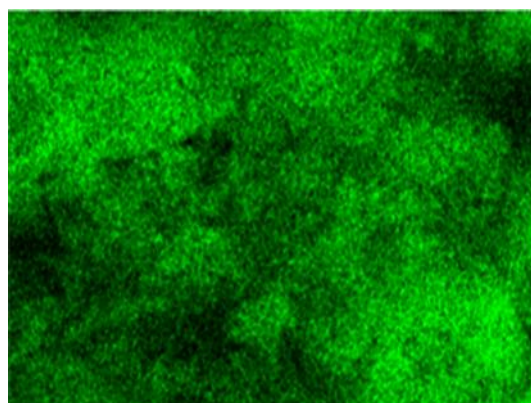
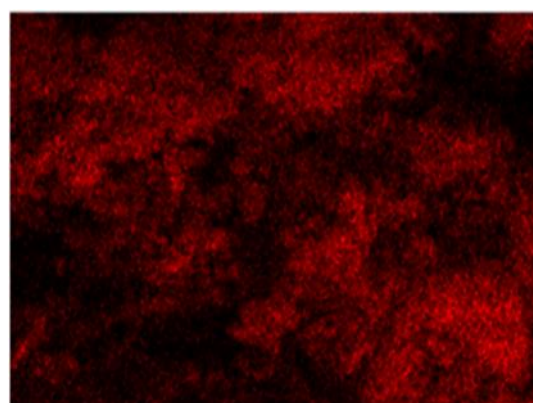


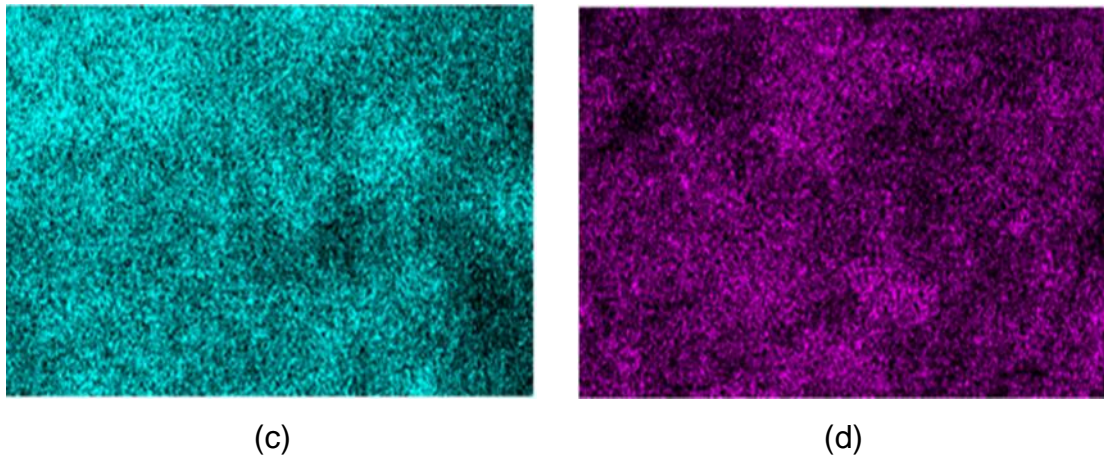
**Figure 5.6** SEM image of fresh Ni/Ca-Al<sub>2</sub>O<sub>3</sub> catalyst at 10.00 K mag.



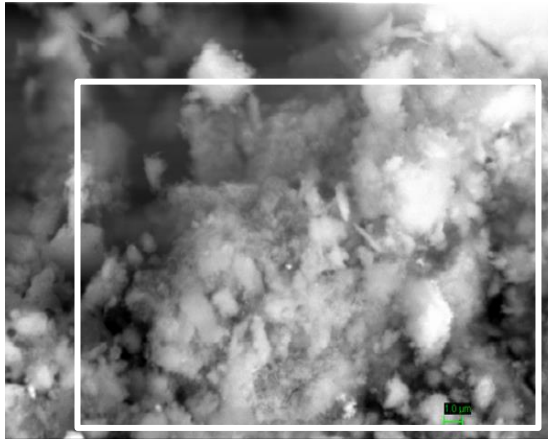
(a)



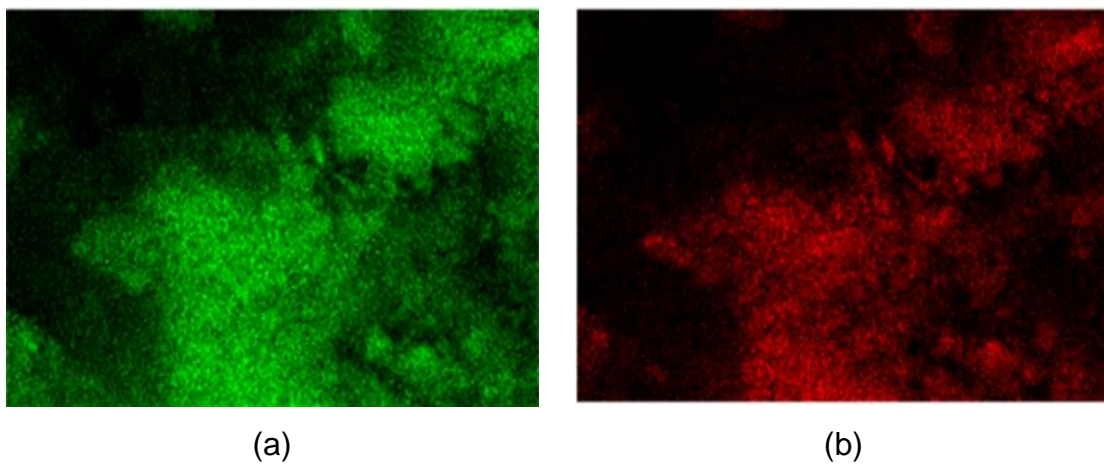
(b)



**Figure 5.7** EDX mapping for elemental distribution (a) Al, (b) O, (c) Ca and (d) Ni elements of fresh Ni/Ca- $\text{Al}_2\text{O}_3$  catalyst.



**Figure 5.8** SEM image of used Ni/Ca- $\text{Al}_2\text{O}_3$  catalyst at 10.00 K mag. The catalyst was used in LTSR process at 400 °C and S/C of 2.



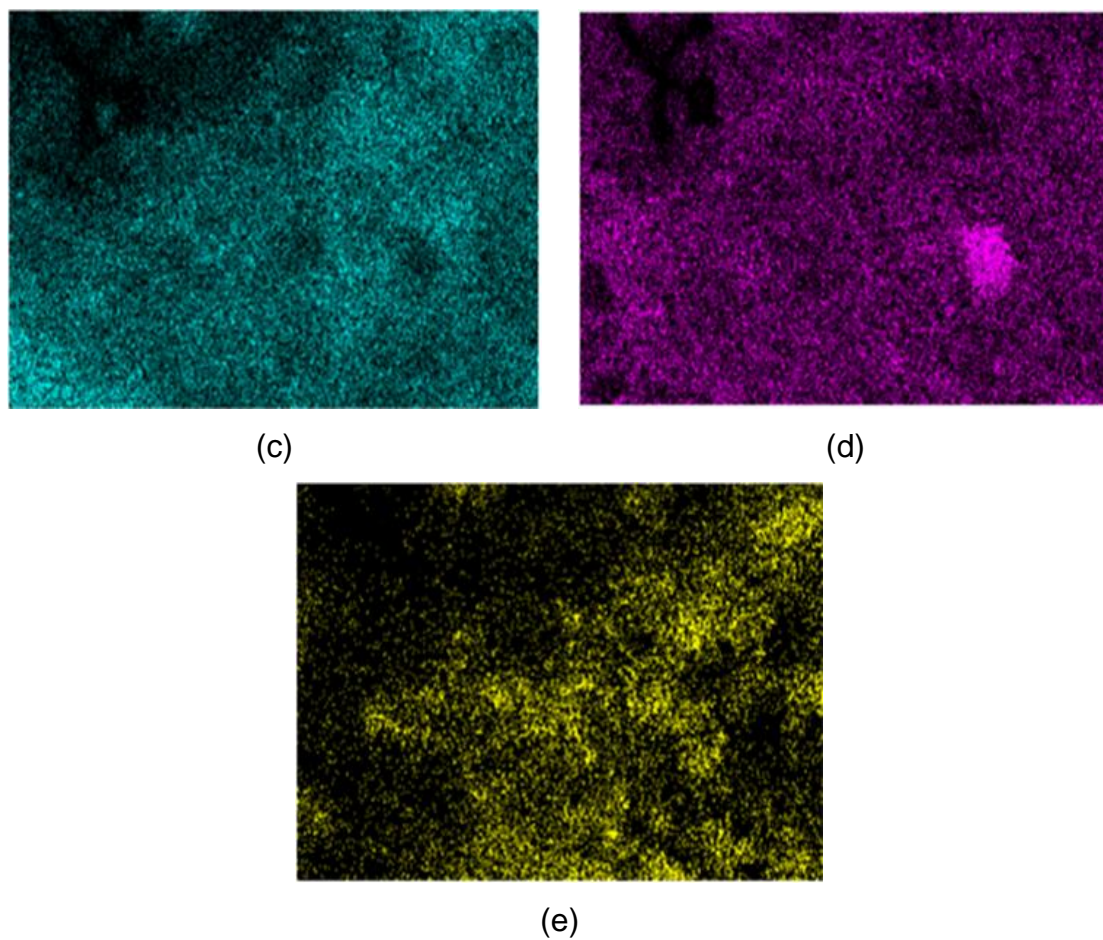


**Figure 5.9** EDX mapping for elemental distribution (a) Al, (b) O, (c) Ca and (d) Ni elements of used Ni/Ca- $\text{Al}_2\text{O}_3$  catalyst. The catalyst was used in LTSR process at 400 °C and S/C of 2.

Figure 5.8 shows the SEM image of the catalyst used at 400 °C and S/C of 2, with the corresponding EDX mapping shown in Figure 5.9. The formation of agglomerated of Ni species in Figure 5.9(d) was clearly observed, in conjunction with a regional lack of Ca species as in Figure 5.9(c). It is suggested that the existence of Ni clusters was due to the sintering process during a long run of the experiment, causing the growth of Ni crystallite size and accelerate the carbon formation on the catalyst [149]. Thus, carbon deposition was observed in Figure 5.9(e), which covering unevenly on the surface of used catalyst.

## 5.7 Product distributions of acetic acid conversion via LTSR

The effect of reaction temperatures (350–450 °C) and of S/C (1–3) on the product distributions are presented in Table 5.5 and Table 5.6 respectively. Insignificant carbon content was detected in the liquid condensate in all of the conditions except for 350 °C and S/C of 1. This is due to a limitation of the catalytic activity at 350 °C that reveals higher percentage of carbon in the condensate. Moreover, acetic acid became an excess reagent at S/C of 1 which resulted in a significant amount of carbon in the condensate as measured in the TOC analysis.

**Table 5.5** Total carbon balance of LTSR experiments using Ni/Ca-Al<sub>2</sub>O<sub>3</sub> catalyst with different of reaction temperatures. The value of steam to carbon ratio of 2 was used at atmospheric pressure.

Temp.	C in gas, C <sub>G</sub>		C in condensate, C <sub>L</sub>		C on catalyst, C <sub>S</sub>	
	mol	%	mol	%	mol	%
350	2.01×10 <sup>-3</sup>	30.9	2.09×10 <sup>-2</sup>	32.1	2.40×10 <sup>-2</sup>	37.2
400	5.60×10 <sup>-2</sup>	74.3	4.72×10 <sup>-5</sup>	0.1	1.93×10 <sup>-2</sup>	25.7
450	5.38×10 <sup>-2</sup>	76.1	4.24×10 <sup>-5</sup>	0.1	1.69×10 <sup>-2</sup>	23.9

**Table 5.6** Total carbon balance of LTSR experiments using Ni/Ca-Al<sub>2</sub>O<sub>3</sub> catalyst with different of steam to carbon ratio, S/C. The operating temperature was set at 400 °C and atmospheric pressure.

S/C	C in gas, C <sub>G</sub>		C in condensate, C <sub>L</sub>		C on catalyst, C <sub>S</sub>	
	mol	%	mol	%	mol	%
1	4.23×10 <sup>-2</sup>	59.7	3.77×10 <sup>-3</sup>	5.3	2.48×10 <sup>-2</sup>	35.0
2	5.60×10 <sup>-2</sup>	74.3	4.72×10 <sup>-5</sup>	0.1	1.93×10 <sup>-2</sup>	25.7
3	4.94×10 <sup>-2</sup>	69.3	1.49×10 <sup>-4</sup>	0.4	2.16×10 <sup>-2</sup>	30.2

From carbon element distribution at temperatures 400 and 450 °C and S/C 2–3, the results suggest that the conversion of acetic acid consisted in gases production and char deposition on catalyst only. However, the carbon content on catalyst ( $C_S$ ) was measured for 2 hours of experiment. Meanwhile, carbon containing in gases ( $C_G$ ) was taken as an average value of the gas production ( $CH_4$ ,  $CO_2$  and  $CO$ ) at their stability state, which was achieved over an 1 hour after conducting the experiment, as shown in Figure 5.10. It seems that the decomposition of acetic acid (R5.8) may occur in the early stage of the process, followed by methanation of acetic acid steam reforming (R5.10), which was a relatively slow process. Therefore, the carbon element distribution was re-calculated in order to determine the amount of carbon formation on catalyst within the region where the methanation reaction was predominant (steady state).

Based on R5.7, the methane production from acetic acid as bio-surrogate is expressed as,



Based on the gas compositions produced at 400 °C and S/C of 2 in Figure 5.10, it was observed that all of the carbon containing in gases ( $CH_4$ ,  $CO_2$  and  $CO$ ), especially  $CH_4$  production achieved their stability at 4800 s onwards. As we believed that the measurement for gas production are correct, therefore, the amount of carbon formation on the catalyst was re-calculated by carbon balance after taking an account of the total carbon production in gases within stability region, as listed in Table 5.7 and Table 5.8.

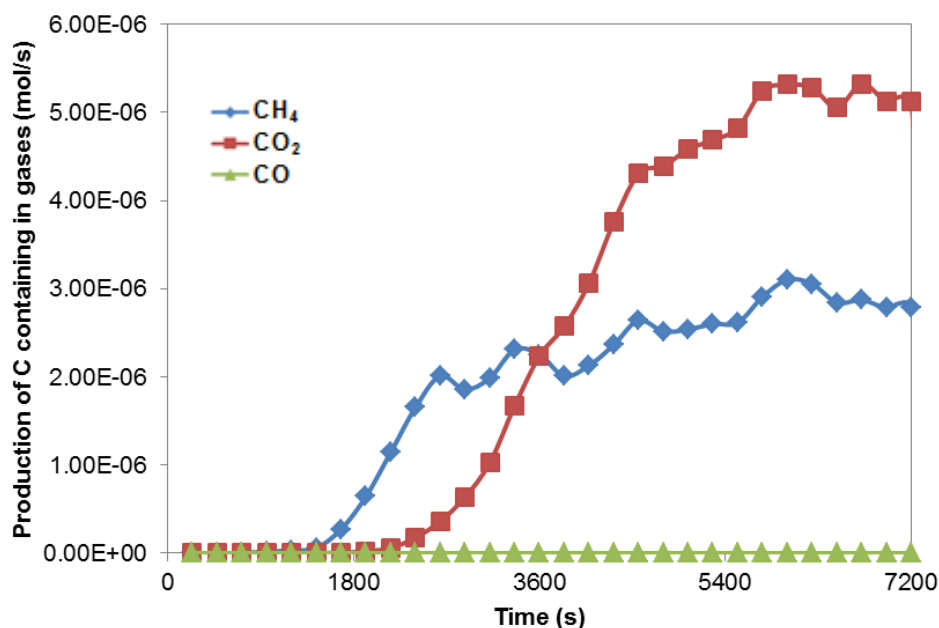


**Figure 5.10** Production of carbon containing gases ( $\text{CH}_4$ ,  $\text{CO}_2$  and  $\text{CO}$ ) at  $400\text{ }^\circ\text{C}$  and S/C of 2. The arrow line shows the region where average value was taken.

**Table 5.7** Re-calculated C in gas and on catalyst from carbon balance of LTSR experiments using  $\text{Ni}/\text{Ca-Al}_2\text{O}_3$  catalyst with different of reaction temperatures. The value of steam to carbon ratio of 2 was used at atmospheric pressure.

Temperature $^\circ\text{C}$	C in gas, $C_G$		C on catalyst, $C_S$	
	mol	%	mol	%
400	$1.87 \times 10^{-2}$	81.9	$4.12 \times 10^{-3}$	18.1
450	$2.51 \times 10^{-2}$	78.6	$6.82 \times 10^{-3}$	21.4

**Table 5.8** Re-calculate the total carbon balance of LTSR experiments using  $\text{Ni}/\text{Ca-Al}_2\text{O}_3$  catalyst with different of steam to carbon ratio, S/C. The operating temperature was set at  $400\text{ }^\circ\text{C}$  and atmospheric pressure.

S/C	C in gas, $C_G$		C on catalyst, $C_S$	
	mol	%	mol	%
2	$1.87 \times 10^{-2}$	81.9	$4.12 \times 10^{-3}$	18.1
3	$1.48 \times 10^{-2}$	72.2	$5.70 \times 10^{-3}$	27.8

As mentioned in the previous discussion, we have stated that most of the carbon was formed on the catalyst at the beginning of the reaction, where decomposition of acetic acid reaction (R5.8) was taking place at first. Therefore, the amount of carbon deposited on the catalyst in the early stage of 2 hours of experiment can be estimated by determining the difference between the total amount of carbon from CHNS analysis with the amount of carbon within the stability region, which shown in Table 5.9. It clearly shows that at the higher temperature of 450 °C less amount of carbon formation on the catalyst occurred in the early stage of the process compared to the lower reaction temperature (400 °C). However, the amount of carbon formation was slightly different at S/C of 2 and 3, which proves that reaction temperature is the main operating parameter affecting carbon accumulation.

**Table 5.9** The amount of carbon deposition on the catalyst at the beginning of the reaction in 2 hours of experiment.

Temp., °C	S/C	The amount of C <sub>S</sub> at the beginning of the reaction, mol
400	2	$1.52 \times 10^{-2}$
450	2	$1.00 \times 10^{-2}$
400	3	$1.59 \times 10^{-2}$

From the experimental results, it is suggested to operate methanation of acetic acid as bio-oil surrogate via LTSR at high temperature at first, until all of the gaseous products become stable to avoid carbon deposition on the catalyst at the early stage of the reaction. Then, the reaction temperature can be lowered in order to have a higher selectivity of CH<sub>4</sub> production without significant carbon accumulation. As the methanation process commonly operated at

higher pressure (20–30 bar) in industry [16, 60], where higher of CH<sub>4</sub> production is thermodynamically favoured, less carbon formation on the catalyst can be obtained.

## 5.8 Conclusion

This study investigates the conversion of acetic acid as surrogate bio-oil compound towards CH<sub>4</sub> production on the Ni/Ca-Al<sub>2</sub>O<sub>3</sub> catalyst surface via direct methanation by LTSR process. In our flow conditions, the optimum CH<sub>4</sub> production was 15.67 wt.% of the acetic acid feed and obtained at 400 °C and S/C of 2 at atmospheric pressure. As undesirable carbon formation on the catalyst was observed during the experiments, it is suggested to operate at higher pressure (20–30 bar), which is commonly used in the CO and CO<sub>2</sub> methanation industrial processes due to higher of CH<sub>4</sub> production being thermodynamically favoured and less carbon formation on the catalyst can be obtained.



## Chapter 6

### **Plant Modelling for Bio-methane Production from Palm Empty Fruit Bunch (PEFB) Bio-oil**

#### **6.1 Introduction**

A simulation model (Aspen Plus V8.8) has been developed in this study where it provides estimated mass and energy balances for an industrial process of bio-methane production from biomass, specifically palm empty fruit bunch (PEFB) via fast pyrolysis followed by low temperature steam reforming, which is direct catalytic methanation of the pyrolysis bio-oil. The objective of this work is to perform a preliminary study of the process design in order to find its optimal operating parameters. Then, the possibilities of process integration are proposed where energy saving opportunities are identified. This work also presents process performance indicators of the process in terms of thermal conversion efficiency and energy consumption of PEFB conversion into methane production and compares them with equivalent data from similar biomass to biogas gasification plants taken from the literature.

## 6.2 Process description

The production route consists of four process units, which are: wet biomass pre-treatment, fast pyrolysis of the dried biomass particles, methanation of the bio-oil pyrolysis product and upgrading of the reformat to high purity methane gas. Figure 6.1 shows a summary block diagram with conditions and flows to the main units. The modelling of the bio-methane production from PEFB process was based on a 3000 kg/hr of PEFB feedstock with an as-received a 50 wt. % moisture content. In the biomass pre-treatment facility, PEFB was assumed to have an initial size of 25 mm [137, 138] that needed to be crushed into the smaller particle size of 1 mm and dried around 8–10 wt. % of moisture content [137-139], which is optimal for further pyrolysis reactions in fluidized bed conditions [139] under fast pyrolysis conditions.

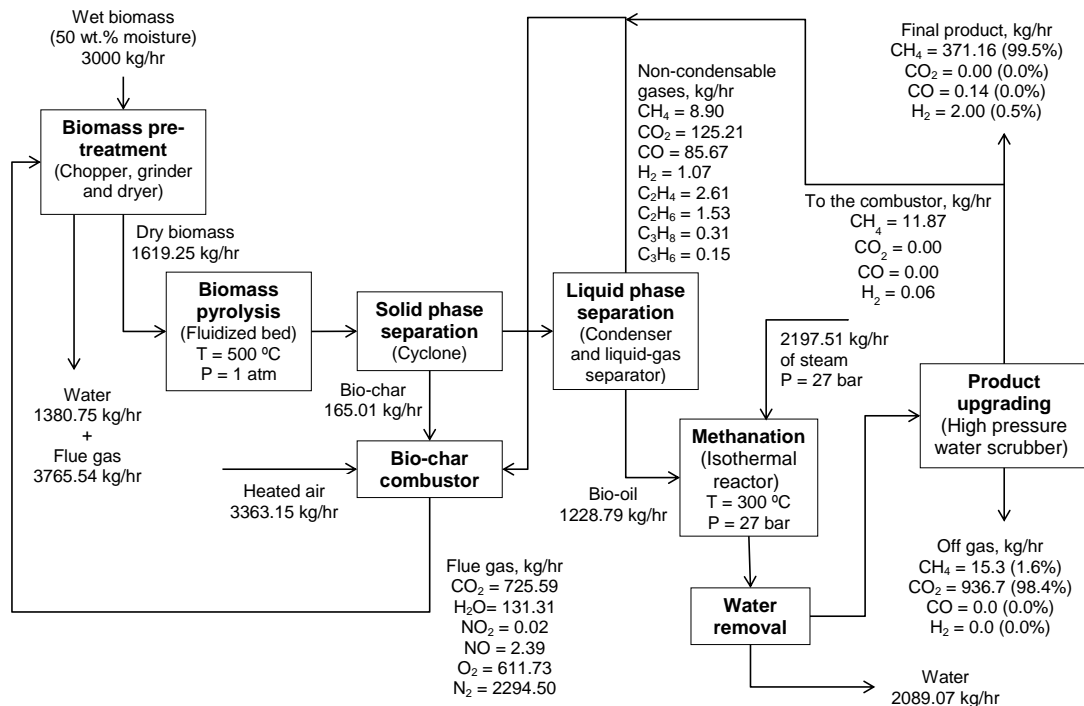


**Figure 6.1** Block diagram of the PEFB conversion to pure CH<sub>4</sub> via pyrolysis-low temperature steam reforming (LTSR) and water scrubbing.

In the isothermal methanation process (investigated in Chapter 4 and published in [155]), the bio-oil is converted to  $\text{CH}_4$ ,  $\text{CO}_2$ ,  $\text{H}_2$ ,  $\text{CO}$  and water products, where water was removed at first and the dry gas continuously flowed into a gas cleaning unit. The by-products  $\text{CO}_2$ ,  $\text{H}_2$  and  $\text{CO}$  were removed from the stream by high pressure water scrubbing (HPWS) to obtain a methane-rich gas [142].

### **6.3 Biomass pre-treatment and characterisation in the model**

Biomass, which is PEFB, used in this study is not included in the databank of chemical compounds in the Aspen Plus program. Therefore, PEFB is specified as a non-conventional component in Aspen Plus, where they are specified by empirical factors representing their elemental composition. The only properties calculated for non-conventional component in Aspen Plus are the enthalpy and density by using empirical correlations. Thus, PEFB properties are defined in the simulation model by using the ultimate and proximate analysis as listed in Table 6.1. Moisture was fed into the process separately as a conventional component [138], where typically 50 wt. % of moisture content was determined in fresh PEFB [90, 156].

**Table 6.1** Proximate and ultimate analyses (mf wt.%) of PEFB [107] which is defined in Aspen Plus.

Proximate analysis (mf wt.%)	
Moisture	7.95
Fixed carbon	10.78
Volatile matter	83.86
Ash	5.36
Ultimate analysis (mf wt.%)	
Carbon	49.12
Hydrogen	6.49
Nitrogen	0.70
Oxygen	38.33
Ash	5.36

In the biomass pre-treatment facility, PEFB was assumed to have an initial size of 25 mm [137, 138], to be subsequently crushed into 5 mm of length fibre. Since there is a limited study of PEFB crushing process, it was assumed that the power requirement for crushing 3000 kg/hr of PEFB from 25 mm into 5 mm of particle size is approximately 90 kW as per reference [157]. After crushing, the output fibre was passed through a dryer for removing the water content around 8 wt. % in order to minimize the water in the product liquid oil during pyrolysis process. Then, the dried PEFB was fine-crushed into the final particle size of 1 mm, which is ideal for feeding the fluidized bed fast pyrolysis reactor [139].

As we assumed the water content in as received PEFB is 50 wt.%, the input in the 'WET-BIO' stream (as shown in Figure 6.2) was defined as 1500 kg/hr of dry PEFB and 1500 kg/hr of water. However, only 1381 kg/hr of water is identified as a conventional component, whereas 119 kg/hr of water, which corresponds 7.95 mf wt.% of moisture content [107] is defined as non-conventional component. It means that 7.95 mf wt.% of moisture content is listed in proximate analysis as properties of PEFB in Aspen Plus program. Further explanation for categorizing the water into two different components (conventional and non-conventional) is discussed in the next paragraph.

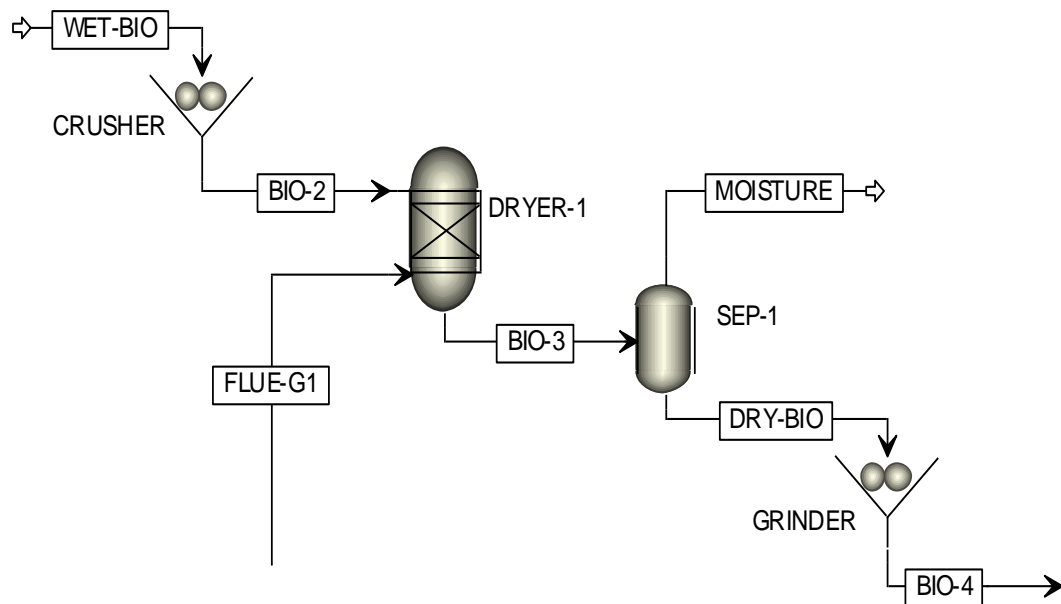


**Figure 6.2** Simplified process simulation flowsheet of biomass pre-treatment.

A directly heated single-pass rotary dryer was selected for drying the PEFB in this process because it is the most common type of dryer used for biomass [158]. Based on Figure 6.3, the wet biomass and hot flue gas flows co-currently through the dryer, where the hottest gases are contacted with the

wettest material inside a rotating drum. The rotation of the drum promotes better heat and mass transfer because it lifts the solids in the dryer and tumble through the hot gas. However, most dryers are not designed to completely dry the biomass in order to avoid over-drying of biomass, which might ignite and causing of fire hazards [158, 159]. Therefore, moisture content in the PEFB pyrolyzer feed should be less than 10 wt.% [137, 138]. For that reason, 7.95 mf wt. % of moisture content [107] was listed earlier as non-conventional component, indicating a 'dry' PEFB, while the remaining of water (1380.75 kg/hr) was specified as conventional components. Thus, the energy required for drying up the wet PEFB was calculated by using Aspen Plus without considering the moisture content in 'dry' PEFB which as non-conventional component, did not participate in any phase or chemical equilibrium calculations in the drying process.

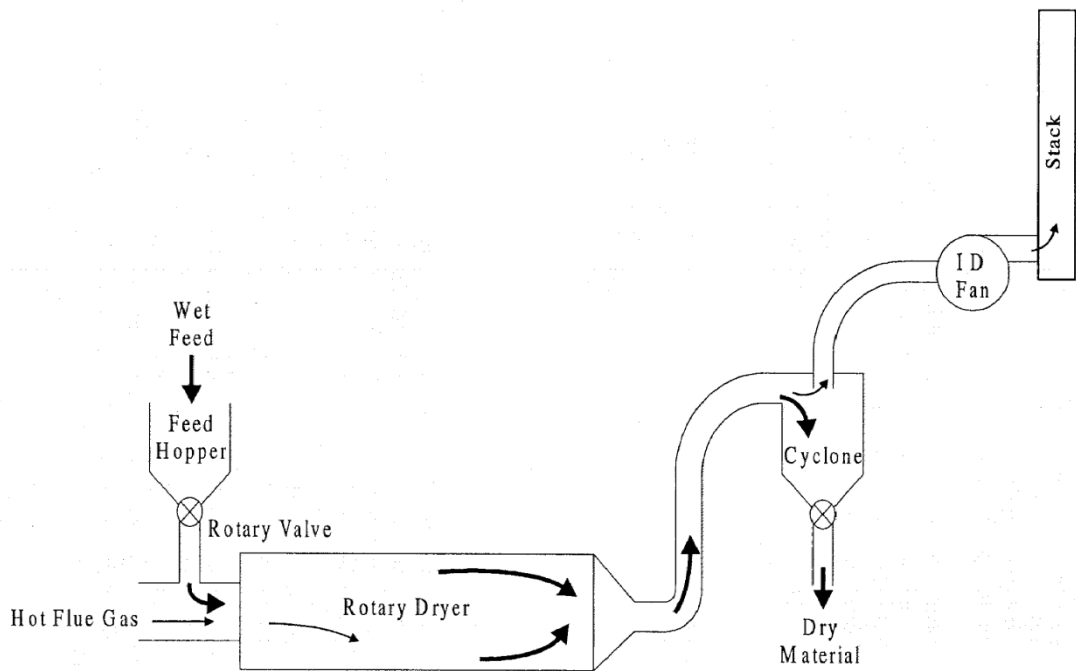


**Figure 6.3** Schematic diagram of single-pass rotary dryer [158].

Flue gases from the combustion of the bio-char pyrolysis by-product was used in this study as the medium for drying the wet PEFB. It was reported that the outlet temperature from rotary dryers can vary from 71 to 110 °C [158]. Thus, the amount of energy needed for the PEFB drying process by using flue gases from the bio-char combustion was determined by maintaining the outlet temperature of the dryer at 110 °C.

This drying process was modelled in Aspen Plus using a RYIELD block while a separator block was used to separate the water from the dry PEFB by phase solid/vapour separation. Then, the dry PEFB was finely crushed into the particle size of 1 mm for fast pyrolysis. Since there is a limited study of PEFB crushing process, it was assumed that the power requirement for crushing PEFB is the same as that for wood. This is because the power requirements for crushing in both of wood and PEFB into the same size (10–30 mm) with the same feedstock capacity (3–5 tonne of biomass per hour) are the same, i.e. 45 kW according to [160, 161]. Therefore, it was believed that the power demand for PEFB finely crushed into 1 mm is the same as wood, resulting in 140 kWh/t on dry basis, as shown in Figure 6.4. Thus, approximately 227 kW was consumed for grinding 1619.25 kg/hr of dry PEFB into 1 mm of particle size.

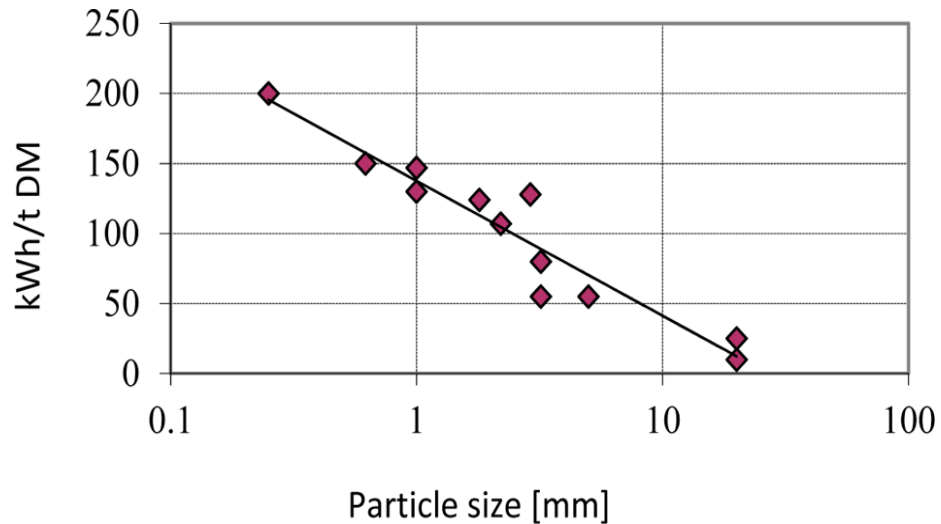


**Figure 6.4** Energy consumption for grinding of wood [138] based on work by [162] and [163].

## 6.4 Bio-oil production modelling

Fast pyrolysis of biomass is defined as a direct thermal decomposition at moderate temperatures where biomass is repeatedly heated in the absence of oxygen [100] to produce a mixture of liquid bio-oil (60–75 wt. %), solid char (15–25 wt. %) and gases (10–20 wt. %), depending on its feedstock and process parameters [99]. In this study, the pre-treated biomass (dry PEFB) was fed to a fluidized bed pyrolyzer at operating temperature of 500 °C and atmospheric pressure to maximise the bio-oil yield [139]. Due to lack of reaction mechanism data or kinetic data for this process, a RYIELD block was used to simulate the pyrolyzer according to the specifications of the product yields during biomass pyrolysis which based on literature data. For modelling this fluidized bed reactor in pyrolysis process, the overall product yield [111], non-condensable gases [111], char [164] and composition of bio-oil [165] were



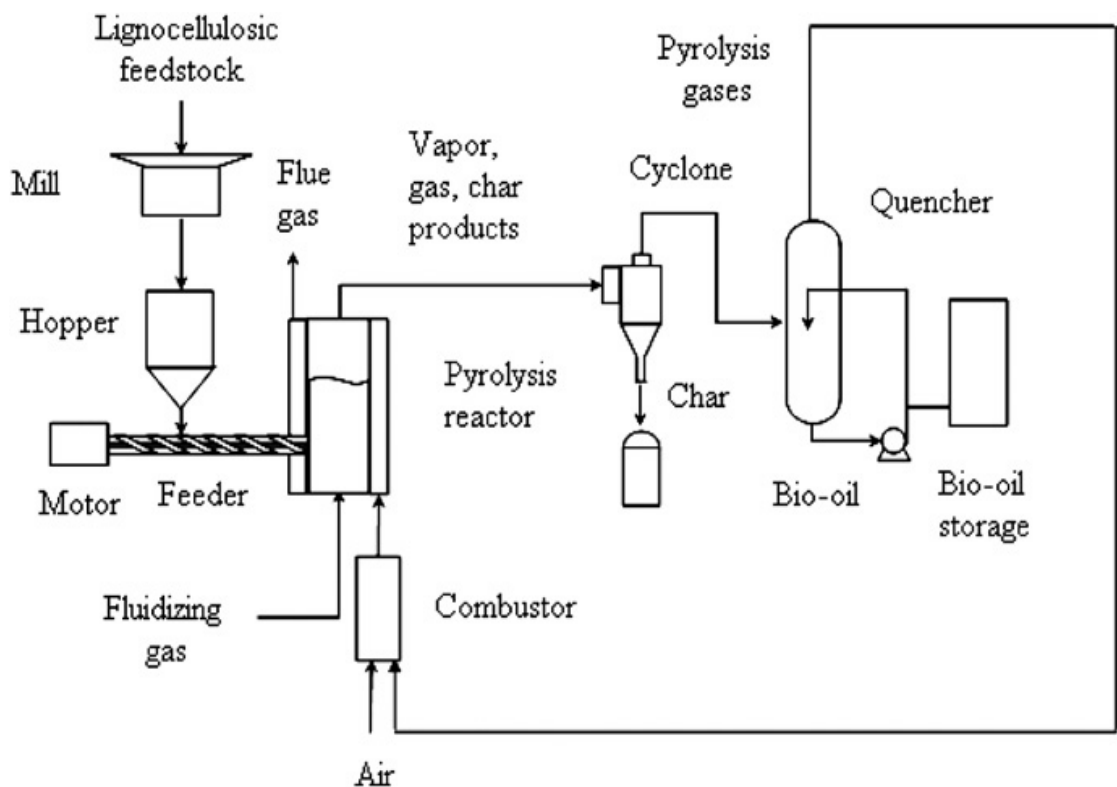
taken from literature data as listed in Table 6.2, Table 6.3, and Table 6.4 respectively.

**Table 6.2** Product distributions for pyrolysis process.

Product distributions	Yields, mf wt.%	Yields, wt.% [our work]
	[111]	
Char	11.00	10.19
Gas	15.03	13.92
Total liquid	73.97	75.89
Gas	Yields, mf wt.%	Yields, wt.% [our work]
	[111]	
Methane, CH <sub>4</sub>	0.58	0.55
Carbon dioxide, CO <sub>2</sub>	8.17	7.73
Carbon monoxide, CO	5.59	5.29
Hydrogen, H <sub>2</sub>	0.07	0.07
Ethylene, C <sub>2</sub> H <sub>4</sub>	0.17	0.16
Ethane, C <sub>2</sub> H <sub>6</sub>	0.1	0.09
Propane, C <sub>3</sub> H <sub>8</sub>	0.02	0.02
Propylene, C <sub>3</sub> H <sub>6</sub>	0.01	0.01

**Table 6.3** Ultimate analysis of bio-char from the pyrolysis of PEFB [164].

Components	wt. %
Carbon	65.32
Hydrogen	4.56
Nitrogen	1.43
Oxygen	28.69

**Figure 6.5** Schematic diagram of bio-oil production from biomass via fast pyrolysis [140].

Commonly, bio-oil production from biomass via fast pyrolysis used its own pyrolysis gas mixture (non-condensable gases Table 6.2) as fluidizing gas, where it needs to be sent back to the pyrolyzer [136, 140, 166], as shown in Figure 6.5. Therefore, the fluidizing gas, which is taken from the pyrolyzers' own gas output in the initial transient stages and then fully recycled at steady state, thus not affecting the net gas output of the pyrolyzer.

**Table 6.4** Model mixture of bio-compounds for PEFB bio-oil based on DTG analysis Figure 6.6 with ultimate analysis [167].

PEFB bio-oil	C	H	O
Ultimate analysis , mol frac. [165]	0.286	0.491	0.223
Model mixture, mol frac.	0.268	0.519	0.213
Percentage of error, %	6.2	5.8	4.8
<hr/>			
Water, wt.% [165]		24.3	
Model water, wt.%		24.0	
Percentage of error, %		1.2	
<hr/>			
Model compounds	Mass frac.	Family	Family wt.%
Formaldehyde, CH <sub>2</sub> O	0.08	1	
Acetaldehyde, C <sub>2</sub> H <sub>4</sub> O	0.01	1	F1=10%
1-hydroxy-2-butanone, C <sub>4</sub> H <sub>8</sub> O <sub>2</sub>	0.01	1	
<hr/>			
Acetic acid, C <sub>2</sub> H <sub>4</sub> O <sub>2</sub>	0.07	2	F2=30%
Water, H <sub>2</sub> O	0.23	2	
<hr/>			
Furfural, C <sub>5</sub> H <sub>4</sub> O <sub>2</sub>	0.13	3	
Phenol, C <sub>6</sub> H <sub>6</sub> O	0.01	3	F3=15%
Water, H <sub>2</sub> O	0.01	3	
<hr/>			
Creosol, C <sub>8</sub> H <sub>10</sub> O <sub>2</sub>	0.14	4	F4=15%
Guaiacol, C <sub>7</sub> H <sub>8</sub> O <sub>2</sub>	0.01	4	
<hr/>			
Catechol, C <sub>6</sub> H <sub>6</sub> O <sub>2</sub>	0.24	5	
Palmitic acid, C <sub>16</sub> H <sub>32</sub> O <sub>2</sub>	0.01	6	F5+F6=30%
Levoglocusan, C <sub>6</sub> H <sub>10</sub> O <sub>5</sub>	0.05	6	

A particular consideration of the study was the desire to represent accurately the PEFB bio-oil produced by the pyrolysis reactor and subsequently used for methanation, and its thermal decomposition behaviour, with the aim of improving the methanator's model using a RGibbs reactor block (chemical equilibrium via minimisation of Gibbs energy) to a more realistic dynamic model, such as non-ideal plug flow hybrid homogeneous/catalytic reactor. Therefore, a real PEFB bio-oil mixture that this group had studied previously for H<sub>2</sub> production [165] was simulated in Aspen Plus using 6 macro-families of model compounds (as listed in Table 6.4 and Figure 6.6) using curve-fitting procedures, where molar mass distribution curves were quantified from DTG and compounds identified from GC-MS [168].

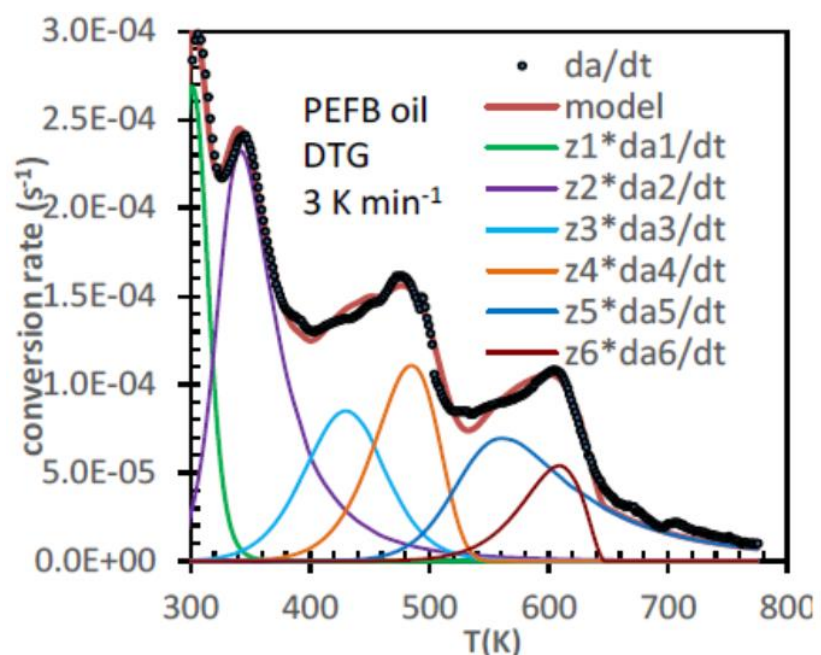


**Figure 6.6** Discretisation of real PEFB oil DTG curve by weighted individual conversions from thermal decomposition over 6 macro-families. Mass fractions 'z<sub>i</sub>' as in Table 6.4, 'a<sub>i</sub>' is conversion of family 'i' [167].

Bio-char from the pyrolyzer was separated by a cyclone from the condensable vapours and non-condensable gases and subsequently combusted to provide heat to the pyrolyzer, as shown in Figure 6.7. A RYIELD block was used for decomposing the biochar into volatile matter such as carbon, hydrogen ( $H_2$ ), oxygen ( $O_2$ ) and nitrogen ( $N_2$ ) [134] based on the bio-char's ultimate analysis (as listed in Table 6.3). The bio-char needed to be combusted under excess of air to prevent incomplete combustion of the fuel, which would have caused lower combustion efficiency and increased air pollution by emitting the unburned components to the atmosphere. Thus 20 % of excess air was selected in this study for combustion of bio-char, where 1.10–1.30 % is the range of excess air of combustion plant for coal powder and gas burner [169]. The decomposed bio-char with 20% of excess air entered the RGibbs combustor and converted into combustion products such as  $CO_2$ ,  $H_2O$ ,  $CO$  and  $NO$ . Then, the flue gas from the combustion process was used for drying the as received, wet PEFB.

Pre-heated combustion air is commonly used in order to improve the efficiency and productivity for fuel-fired industrial heating processes [170]. It is a common practice for the industry to pre-heat the air by using the flue gas from the combustion process [86], a process called 'recuperative incineration'. Although the main purpose of burning the bio-char was to provide heat for the pyrolyzer unit, it was found that it was not sufficient for the energy demand of the pyrolyzer and the PEFB drying and air pre-heating requirements. Thus, the combustion bio-char fuel needed to be supplemented up with all of the non-condensable gases from the pyrolysis process as well as 3.1% of methane-

rich product of the plant. Further details will be discussed in 'Heat Integration' section.

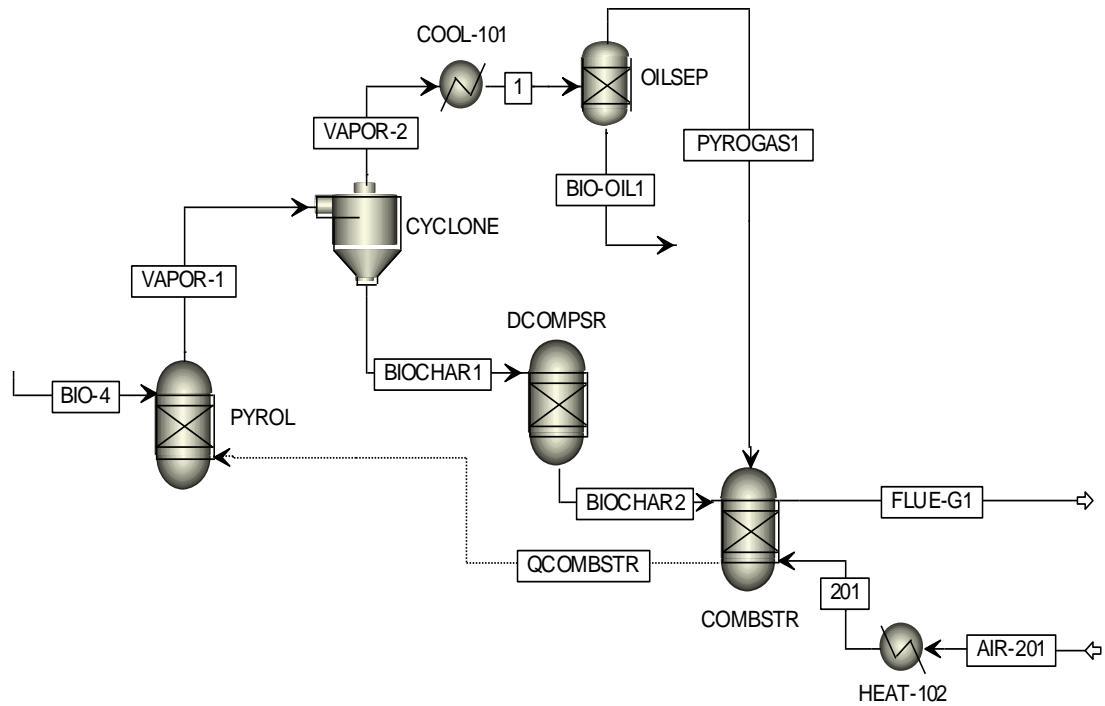


**Figure 6.7** Simplified process simulation flowsheet of the PEFB fast pyrolysis process.

Downstream of the cyclone unit, the hot vapours after char separation were cooled down to the temperature around 35 °C [138], which condensed the bio-oil into liquid feed for the methanator unit, whereas the non-condensable gases were being burned as described above.

## 6.5 Methanation reactor modelling

There are several methanation processes which have been widely applied in the industrial scale, such as Lurgi, TREMP, RMP and IRMA [16, 60, 171]. As described in the literature review, IRMA is the only methanation process which operates isothermally, while the rest (Lurgi, TREMP and RMP) operate in adiabatic conditions with intercooling stages. Since the methanation reaction process is highly exothermic, at least two adiabatic reactors need to be implemented in the methanation process to ensure the feed gas could fully convert into methane production. It is because low production of methane is obtained in the first methanator, where higher output temperature is obtained due to the exothermic reaction of methanation process (i.e. not favourable for methane production with increasing temperature). In methanation processes which operate in adiabatic conditions, a series of fixed bed methanation reactors with intermediate gas cooling is usually being implemented in order to ensure a higher amount of methane production.

For the sake of the simplicity of the process, it is preferable to operate an isothermal reactor (internally cooled reactor type IRMA) in the methanation process for the small scale bio-methane production from PEFB for this study as found in [155] and Chapter 4. The operating conditions for isothermal methanator at 300 °C and 27 bar was chosen for simulating in the Aspen Plus program, which is in the range of the industrial conditions (250–300 °C and 27–29 bar) of syngas conversion to methane. As prior to feeding the fixed bed catalytic LTSR, the bio-oil from the pyrolysis process was pumped to 27 bar and then vapourised before entering the methanator (modelled as 'RGibbs')

block as shown in Figure 6.8). Minimisation of the Gibbs free energy was used to model the ideal equilibria methane yields for model bio-oil mixture feedstock where it considers all the possibilities species without specifying any of the reactions. Thus, the optimum condition in achieving higher methane production was observed within 2–3 of steam to carbon ratio, S/C, resulting 2198 kg/hr of water inlet need to be consumed in this methanation step, which corresponds to S/C of 3.

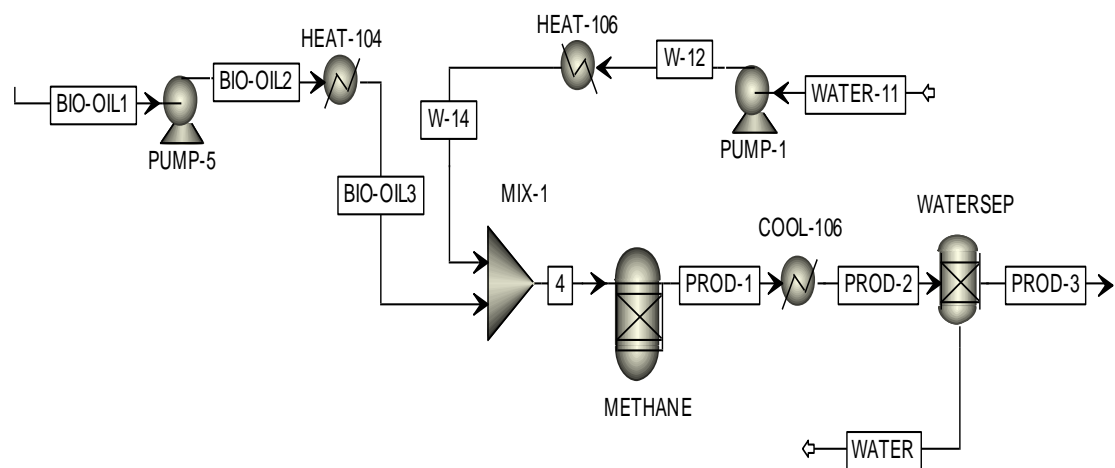


**Figure 6.8** Simplified process simulation flowsheet of methanation.

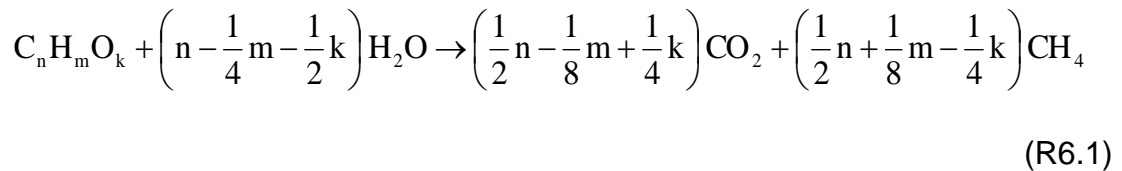
The gas output from the methanator (listed in Table 6.5) is naturally rich in  $\text{CO}_2$  (45.1 mf mol%) as expressed in R6.1. Therefore, purification was achieved by removing the water at first by cooling down the stream to 25 °C. Then, the dry gas continuously flowed into a gas cleaning unit, which is a high pressure water scrubbing (HPWS) unit at 25 bar.



**Table 6.5** Dry gas products from methanation process.

Dry gas products	Mol flowrate, kmol/hr	mf mol %
Methane, CH <sub>4</sub>	24.8	52.5
Carbon dioxide, CO <sub>2</sub>	21.3	45.1
Carbon monoxide, CO	0.0	0.0
Hydrogen, H <sub>2</sub>	1.1	2.4
Total	47.2	100.0

Methane production from bio-oil:



## 6.6 CH<sub>4</sub> stream purification modelling

A model for simulating high pressure water scrubber (HPWS) for biogas production from anaerobic process [142] was used as a reference in this study as a gas cleaning unit for upgrading CH<sub>4</sub> in the stream. The input for their HPWS model [142] was based on data taken from the existing commercial plant. By re-modelled the HPWS for biogas production from anaerobic process (as shown in Figure 6.9) using the same operating conditions, the results of the final products from their work were been compared with our simulation. From Table 6.6, the results from the literature was compared with our results

obtained through our simulation where it shows less than 5% of error. Then, the operating conditions of the HPWS was modified which fit accordingly to our process.

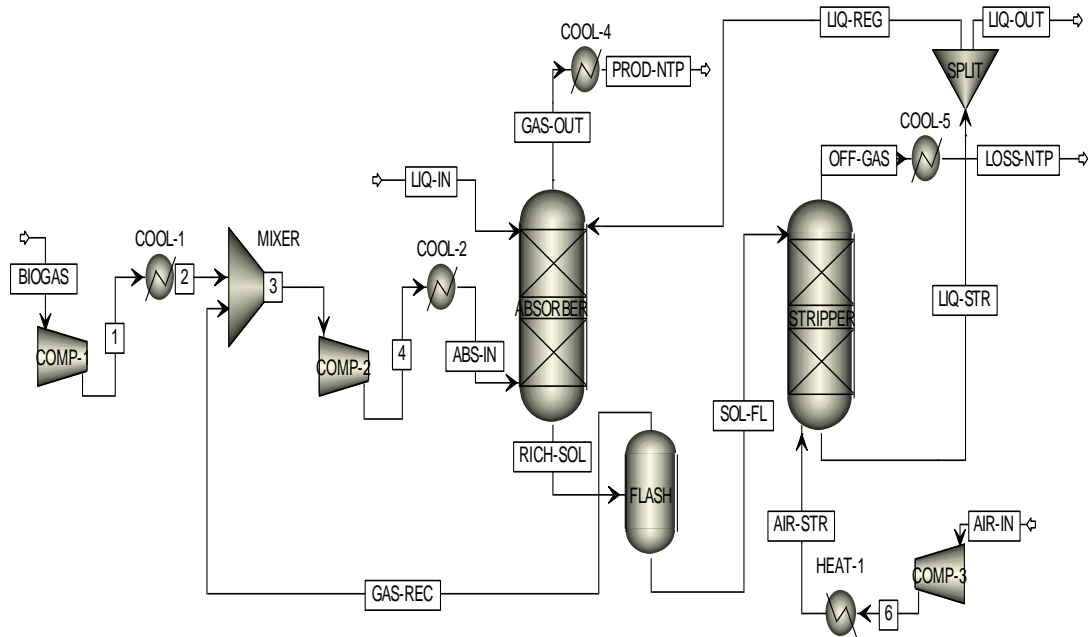


**Figure 6.9** Flowsheet of re-modelled of HPWS in Aspen Plus simulation based on literature [142].

For operation of the absorber column in HPWS at 20 °C and 10 bar (as listed in Table 6.6), it was found that the solubility of CO<sub>2</sub> in water is 0.45 kg of CO<sub>2</sub>/100 kg of water [172]. Therefore, approximately 84,400 kg/hr of total water was needed in order to absorb 380 kg/hr of CO<sub>2</sub> in the crude biogas from anaerobic process. However, it was assumed 2.4% of the total water flow is lost due to the evaporation [142]. Thus, at least 2000 kg/hr of water needs to be replaced (water top-up) whereas 82,465 kg/hr of water was assumed to be recycled continuously in a closed loop (water pump around).

**Table 6.6** Parameters values for HPWS simulation for biogas production from anaerobic process [142] and comparison of the results between literature and our simulations results.

Parameters	Units	Parameters values based on literature data [142]	
CH <sub>4</sub> /CO <sub>2</sub>	vol. %	60/38.97	
H <sub>2</sub> S	vol. %	0.03	
N <sub>2</sub> /O <sub>2</sub>	vol. %	0.5/0.5	
P <sub>absorber</sub>	bar	10	
P <sub>stripper</sub>	bar	1	
T <sub>absorber</sub>	°C	20	
T <sub>stripper</sub>	°C	20	
Biogas flow rate	m <sup>3</sup> /hr	500	
Water top-up	m <sup>3</sup> /hr	2	
Air flow rate	m <sup>3</sup> /hr	1000	
Water-pump around	m <sup>3</sup> /hr	82.5	
P <sub>flash</sub>	bar	3	
Number of theoretical stages		7	
Upgraded biogas		Results from literature [142]	Results from our simulation
CO <sub>2</sub>		2.8 (0.009)	2.7 (0.009)
CH <sub>4</sub>		299.2 (0.967)	287.6 (0.963)
H <sub>2</sub> S	m <sup>3</sup> /hr	0.3 (0.001)	0.0 (0.00)
N <sub>2</sub>	(fraction of vol. flowrate)	3.4 (0.011)	4.5 (0.015)
O <sub>2</sub>		3.1 (0.010)	3.2 (0.011)
H <sub>2</sub> O		0.6 (0.002)	0.6 (0.002)
Treated flow rate	m <sup>3</sup> /hr	309.4	298.6

Based on our work, almost 935 kg/hr of CO<sub>2</sub> was produced from bio-oil conversion in methanation process. By referring the operating conditions of the absorber column used in biogas production to those of an anaerobic digestion process (i.e. 20 °C and 10 bar), 187,000 kg of total water was required in HPWS unit, which corresponds approximately 0.50 kg of CO<sub>2</sub>/100 kg of water of CO<sub>2</sub> [172], where at least 4488 kg/hr of water (i.e. 2.4% of the total water flow rate) was needed to replace the water lost due to the evaporation.

Since the stream from the methanation unit was already at 27 bar, a pressure of 25 bar was selected to operate the absorber column of the HPWS unit. Moreover, it is an advantage to operate HPWS unit at higher pressure where, according to Henry's law, CO<sub>2</sub> dissolves in higher amounts in water at higher partial pressures. Some of the CH<sub>4</sub> product unfortunately also dissolves in the water flow alongside with CO<sub>2</sub>. Separation of this gas-laden water was then carried out in a flash drum at 3 bar, where a desorbed mixture of CH<sub>4</sub> and CO<sub>2</sub> gas was recycled with the fresh bio-methane after re-compression to 27 bar. The CO<sub>2</sub>-laden water collected from the flash drum was then sent to the stripper for separate CO<sub>2</sub> and recycle water. Figure 6.10 shows the flowsheet of HPWS which used as a gas cleaning unit in this study.

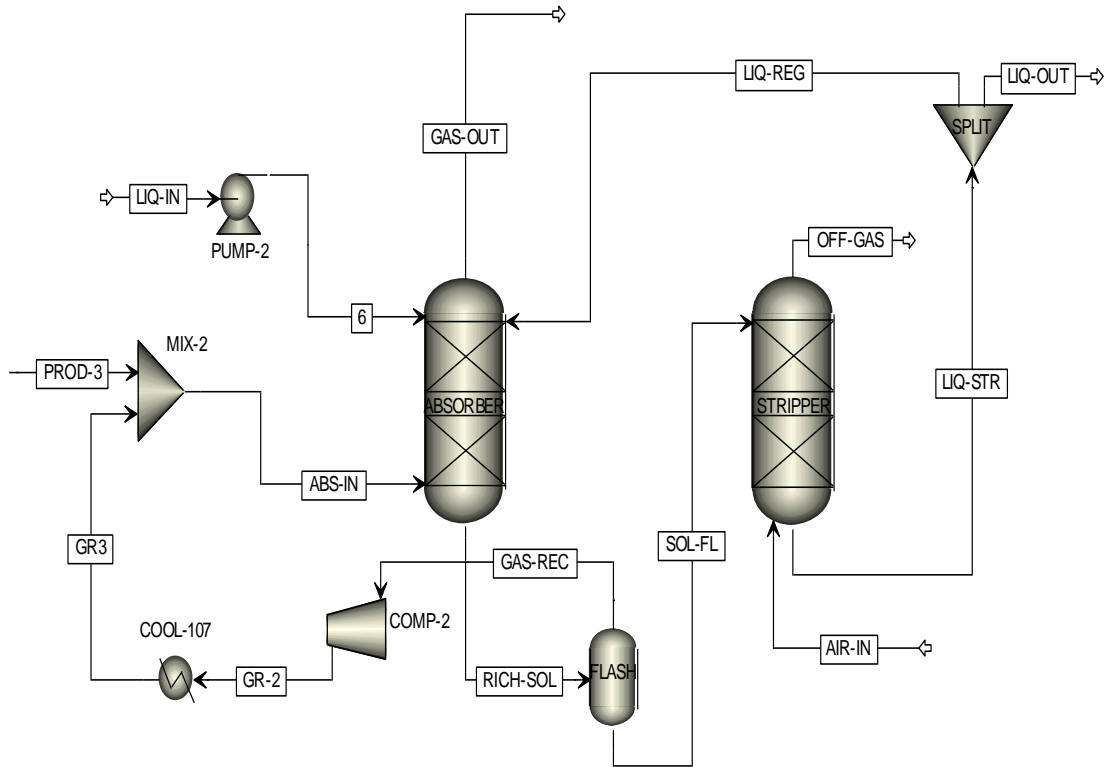


**Figure 6.10** Simplified process simulation flowsheet of HPWS.

The operating conditions of the HPWS unit which was used in this study and the compositions of upgraded gas products is listed in Table 6.7. It was found that almost all of the  $\text{CO}_2$  was being removed from the stream by using the HPWS unit, effectively carrying out bio-CCS, and resulted in a gas product of 99.5 wt.% of  $\text{CH}_4$  and 0.5 wt.% of  $\text{H}_2$  (corresponding to vol.% of 95.9 and 4.1 respectively) and less than 3% of methane loss.

**Table 6.7** Parameters values for HPWS simulation and compositions of the upgraded bio-methane production from PEFB bio-oil.

Parameters	Units	Parameters values
CH <sub>4</sub>	kg/hr	397.9
CO <sub>2</sub>	kg/hr	937.9
CO	kg/hr	0.1
H <sub>2</sub>	kg/hr	2.3
P <sub>absorber</sub>	bar	25
P <sub>stripper</sub>	bar	1.0
T <sub>absorber</sub>	°C	25
T <sub>stripper</sub>	°C	25
Flowrate of gas feed (from methanator)	kg/hr	1337.2
Water top-up	kg/hr	4488
Air flow rate	kg/hr	2859
Water-pump around	kg/hr	182512
P <sub>flash</sub>	bar	3
Number of theoretical stages		10
Upgraded bio-methane		
CH <sub>4</sub>	kg/hr	383.0 (0.994)
CO <sub>2</sub>	(fraction of	0.0 (0.00)
CO	mass	0.1 (0.00)
H <sub>2</sub>	flowrate)	2.1 (0.006)
Treated flow rate	kg/hr	385.4

## 6.7 Heat integration

It is important to minimize energy consumption in order to achieve higher performance of the methane production from the wet PEFB conversion process. Therefore, several process integration stages were proposed in this study to model the heat exchanger network between possible streams in the process. The heat load for each process unit in this methane production from biomass via pyrolysis process was calculated in Aspen Plus, which were then matched with the heat exchanger network between possible streams in the process. A minimum temperature difference,  $\Delta T_{\min}$  of 20 °C was used to ensure the driving force for the heat exchanger network [143]. There are four possibilities of process integrations which were taken in consideration.

### 6.7.1 Process 1 (air-preheater integration)

The main process steps of bio-methane production from biomass are the pyrolysis and the methanation process. The production of bio-oil from fast pyrolysis of PEFB is an endothermic process. As mentioned earlier, the purpose of combusting the bio-char and non-condensable gases from pyrolysis process combustion was to provide the heat to the pyrolyzer unit, while the flue gas from combustor was used to dry up the wet PEFB. The incoming air is usually being pre-heated at first by the energy from flue gas of the combustor, by placing a heat exchanger between flue gas stream and incoming air to the combustor [169]. Unfortunately, it was found that the energy from burning the bio-char and non-condensable pyrolyzer gases was not sufficient for pre-heating the air as well as drying the wet PEFB. Therefore,

it was observed that only 3.1% of methane production needed to be burned together with the bio-char and non-condensable gases for this purpose, as shown in Figure 6.11. The compositions of the upgraded bio-methane production is listed in Table 6.8.

**Table 6.8** Gas compositions of the upgraded bio-methane production before and after splitting 3.1% of upgraded bio-methane production.

Compounds	After gas purification		Final upgraded bio-methane	
	kg/hr (wt.%)	kmol/hr (mol%)	kg/hr (wt.%)	kmol/hr (mol%)
CH <sub>4</sub>	383.0 (99.4)	23.9 (96.0)	371.2 (99.5)	23.1 (95.9)
CO <sub>2</sub>	0.0 (0.0)	0.0 (0.0)	0.0 (0.0)	0.0 (0.0)
CO	0.1 (0.0)	0.0 (0.0)	0.1 (0.0)	0.0 (0.0)
H <sub>2</sub>	2.1 (0.6)	1.0 (4.0)	2.0 (0.5)	1.0 (4.1)
Total flowrate	385.2	24.9	373.3	24.1

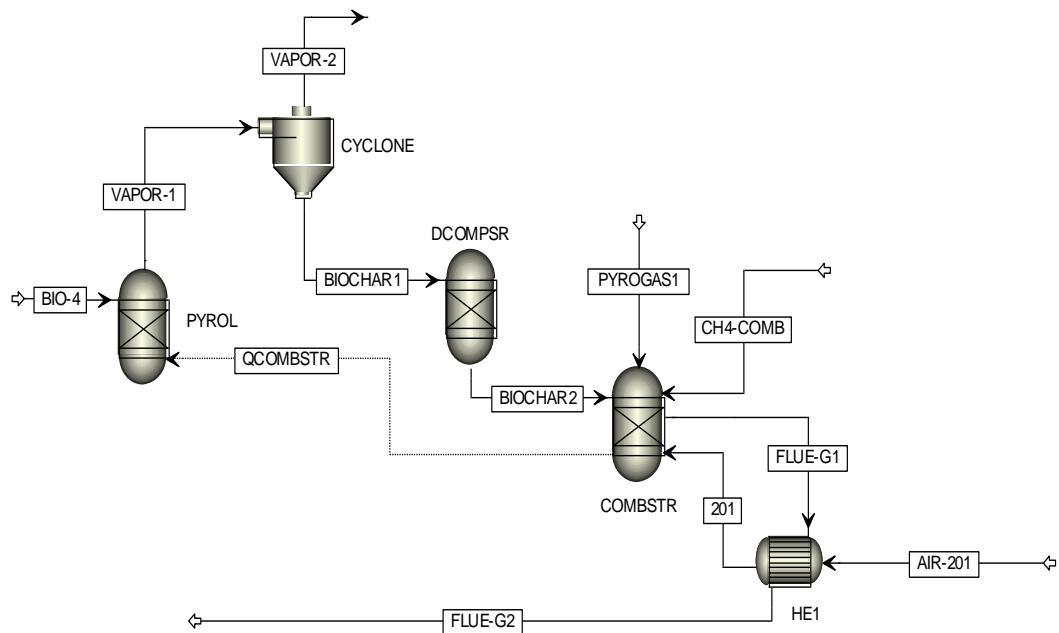


**Figure 6.11** Simplified process simulation flowsheet of heat integration for preheating the incoming air by burning bio-char, non-condensable pyrolysis gas and 3.1% of upgraded bio-methane production.



As a part of the upgraded bio-methane production was determined to be necessary as a heat source for the process demand, it is deemed worth to study the effect of the process performance (further discussion in the 'Process performance' section) when burning the bio-char and the upgraded bio-methane production only, without the non-condensable gases. The non-condensable gases from pyrolysis stage, together with the bio-oil could then be used as combined feedstock for the methanation process. Based on the simulation results, it was found that higher amount of upgraded bio-methane production (10.6%) would need to be burned together with the bio-char compared to the process that burned bio-char, non-condensable gases and 3.1% of the upgraded bio-methane product. The simulation flowsheet in Aspen Plus (as shown in Figure 6.12) for this process integration (i.e. combustion of 10.6% of upgraded bio-methane production and bio-char) and its compositions of the final upgraded bio-methane production is listed in Table 6.9.

Although the bio-oil and pyrolysis gas were used as feedstock for methanation unit, which contributes of higher amount of bio-methane production, it was found that the amount of the final upgraded bio-methane production was less compared to the process which used only bio-oil as feedstock in methanation process. This is because 10.6% of bio-methane production had to burn in order to provide sufficient heat to the pyrolyzer, air pre-heater and drying process of the wet PEFB.

**Table 6.9** Gas compositions of the upgraded bio-methane production before and after splitting 10.6% of upgraded bio-methane production.

Compounds	After gas purification		Final upgraded bio-methane	
	kg/hr (wt.%)	kmol/hr (mol%)	kg/hr (wt.%)	kmol/hr (mol%)
CH <sub>4</sub>	412.0 (99.4)	25.7 (95.9)	368.3 (99.4)	22.9 (95.8)
CO <sub>2</sub>	0.0 (0.0)	0.0 (0.0)	0.0 (0.0)	0.0 (0.0)
CO	0.2 (0.0)	0.0 (0.0)	0.1 (0.0)	0.0 (0.0)
H <sub>2</sub>	2.3 (0.6)	1.1 (4.1)	2.1 (0.6)	1.0 (4.2)
Total flowrate	414.5	26.8	370.5	23.9

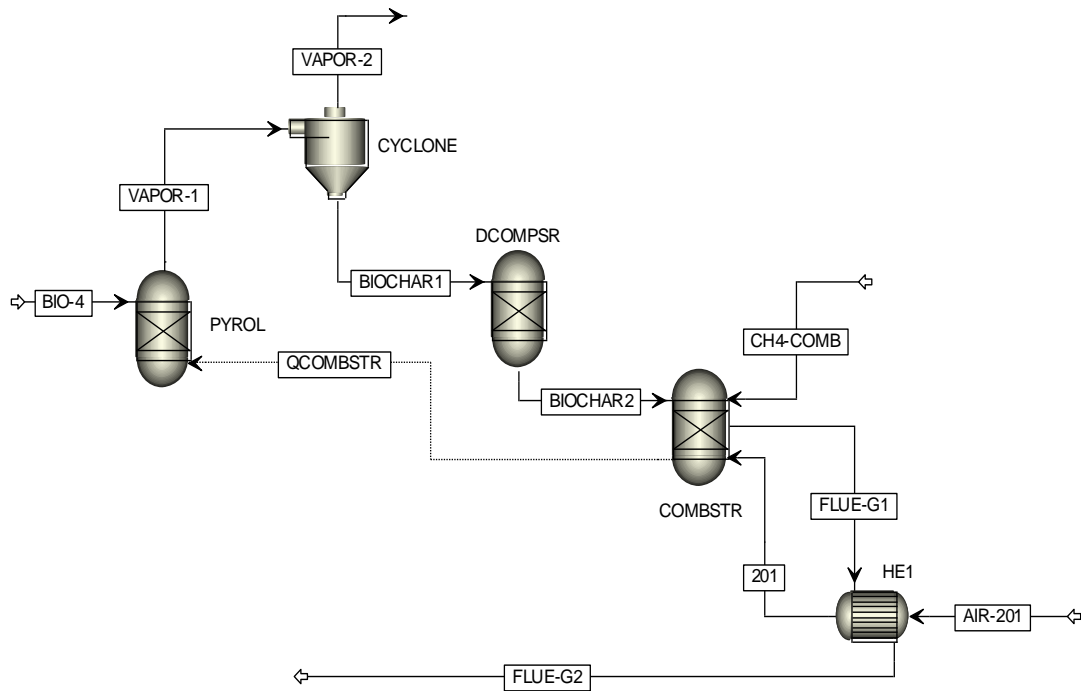


**Figure 6.12** Simplified process simulation flowsheet of heat integration for preheating the incoming air by burning bio-char and 10.6% of upgraded bio-methane production (no burning of non-condensable pyrolyzer gases).

### 6.7.2 Process 2 (steam integration)

The methanation reactions are highly exothermic, where it is possible to cool down the methanator by heat pipes that transport the heat to a pressurized boiler. Moreover, the water fed to the boiler can firstly be preheated by the gaseous products leaving from the methanator [135]. Based on the minimum temperature difference of  $\Delta T_{\min}$  of 20 °C, the exchanger which was placed between the water inlet stream to a boiler and raw product gas stream from the methanation unit (as shown in Figure 6.13) shows only 454 kW from gas products stream (PROD-1) that can be transferred for heating up the water inlet stream (W-12). An additional cooler needs to be placed on 'PROD-1' stream in order to achieve 25 °C. On the other hand, 743 kW of energy transfer was still needed to heat up the water inlet for the methanation unit since the heat transfer from the methanator to the pressurized boiler was still insufficient. Up to 1055 kW could be saved from these heat integration steps, which corresponds to approximately 60% of energy saving for heating up the water.

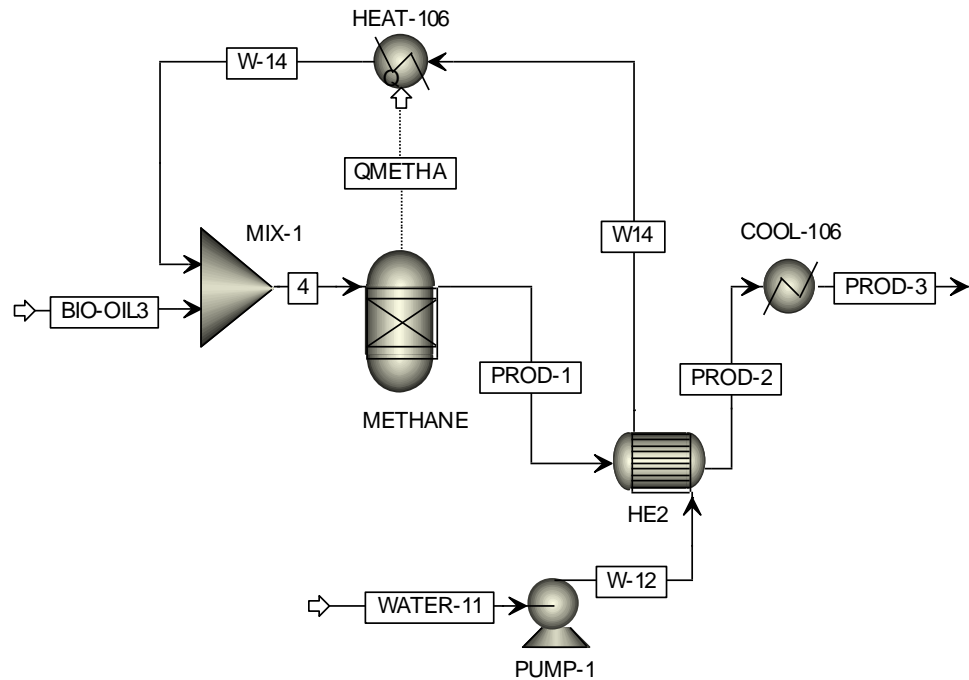


**Figure 6.13** Simplified process simulation flowsheet of heat integration for heating up the water inlet for methanation unit.

### 6.7.3 Process 3 (vaporized bio-oil integration)

From the simulation results, it was found that a significant amount of energy, at least 510 kW of energy, were required to vaporize the bio-oil before entering the methanation unit. Therefore, the only option as a heat source to re-vaporize the bio-oil stream (BIO-OIL2) is by implementing a heat exchanger on the stream where pyrolysis products had to cool down to 35 °C (VAPOR-2), as shown in Figure 6.14. However, additional heater and cooler in both streams were still needed, where 274 kW of energy were required to vaporize the bio-oil and 405 kW to cool down the pyrolysis products.

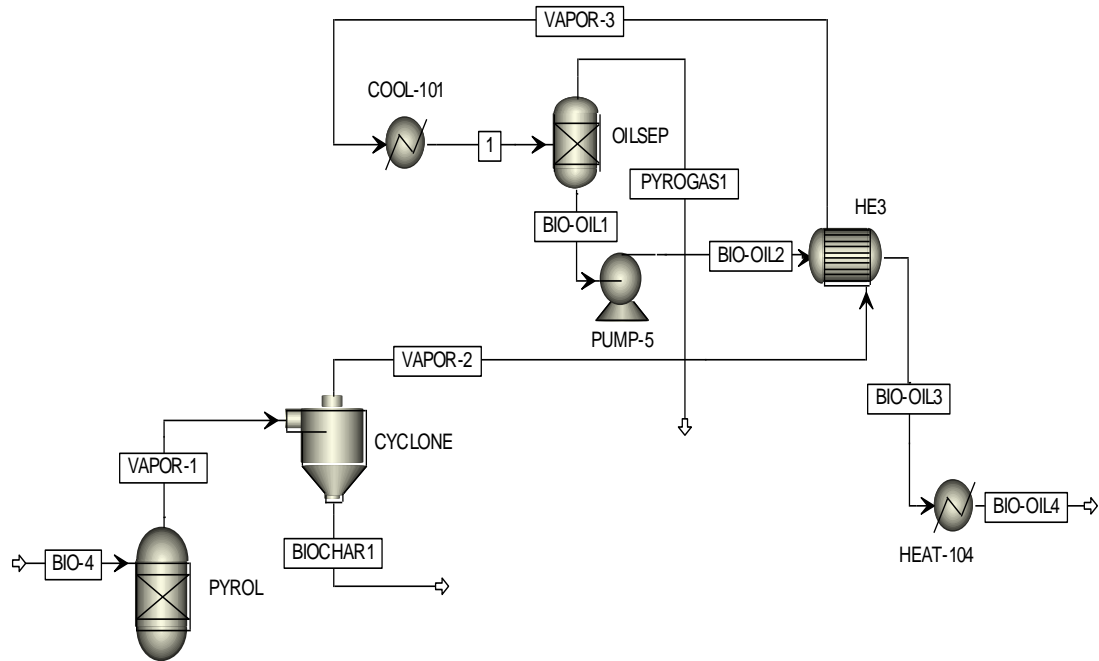


**Figure 6.14** Simplified process simulation flowsheet of heat integration for re-vaporizing the bio-oil before entering methanation unit.

#### 6.7.4 Process 4 (air-preheater, steam and re-vaporized bio-oil integration)

The fully integrated system is the combination of the three options of the heat integrations discussed in the previous sections, which are air-preheat, steam and bio-oil vaporization integration. Further details regarding the energy demand and the final upgraded product gas compositions for different process integration are discussed in the next section.

## 6.8 Process performance

In order to evaluate the process performance, different indicators such as energy conversion efficiency and energy consumption for bio-methane production are defined. The biomass-to-fuel thermal efficiency ( $\eta_{\text{btf}}$ ), as expressed in equation 6.1 is commonly used to give a general idea of the total amount biomass energy that is conserved in the final product. However, equation 6.2 is used to describe the overall thermal efficiency ( $\eta_{\text{th}}$ ) of the process taking into account contributions of the electricity and heat net flows [173]. The energy or thermal efficiency of the process from fresh PEFB to bio-methane production are based on lower heating values (LHV). This is because the final product of this process, which is methane, is intended mainly for engine combustion, power generation and for cooking purposes, and therefore does not account for the potential recuperation of heat via condensation of the water product.

$$\text{Biomass to fuel energy efficiency, } \eta_{\text{btf}} = \frac{\dot{m}_{\text{methane}} \times \text{LHV}_{\text{methane}}}{\dot{m}_{\text{biomass}} \times \text{LHV}_{\text{biomass}}} \quad (6.1)$$

where:

$\dot{m}_{\text{methane}}$  = mass flowrate of methane (kg/s);

$\dot{m}_{\text{biomass}}$  = mass flowrate of biomass (kg/s);

$\text{LHV}_{\text{methane}}$  = higher heating value of methane (kJ/kg);

$\text{LHV}_{\text{biomass}}$  = higher heating value of biomass (kJ/kg).

$$\text{Thermal efficiency, } \eta_{\text{th}} = \frac{\dot{m}_{\text{methane}} \times \text{LHV}_{\text{methane}} + (\dot{Q}^- - \dot{Q}^+)}{\dot{m}_{\text{biomass}} \times \text{LHV}_{\text{biomass}} + (P_{\text{el}}^+ - P_{\text{el}}^-)} \quad (6.2)$$

where:

$\dot{m}_{\text{methane}}$  = mass flowrate of methane (kg/hr);

$\dot{m}_{\text{biomass}}$  = mass flowrate of biomass (kg/hr);

$\text{LHV}_{\text{methane}}$  = higher heating value of methane (kW.hr/kg);

$\text{LHV}_{\text{biomass}}$  = higher heating value of biomass (kW.hr/kg);

$P_{\text{el}}^-$  = process electricity co-generation (kW); here assumed 0.

$P_{\text{el}}^+$  = process electricity demand (kW);

$\dot{Q}^-$  = process excess heat (kW);

$\dot{Q}^+$  = process heat demand (kW).

In equation (6.2) giving the thermal efficiency, we taking into account that the process excess heat rate exceeds heat demand rate (term  $\dot{Q}^- - \dot{Q}^+$  is positive) and that the power consumption exceeds power generated (term  $P_{\text{el}}^+ - P_{\text{el}}^-$  is positive), therefore net heat rate appears as an output of the process (numerator term) and net power as an input (denominator term), according to [173]. This is later confirmed by Aspen calculations of positive net excess heat and positive net power consumption.

Higher heating value (HHV) of a dry biomass was estimated by using Channiwala and Parikh's correlation equation 6.3 [174] while equation 6.4 [173] was used to calculate lower heating value (LHV) for a dry biomass. Since 50 wt.% of moisture of raw PEFB was used in this study, the LHV on a wet basis ( $LHV_{\text{biomass,wet}}$ ) was used for calculating the thermal efficiency and energy consumption for methane production by using equation 6.5 [173].

$HHV_{\text{biomass,dry}}$  (Channiwala & Parikh)

$$= 0.3491C_C + 1.1783C_H + 0.1005C_S - 0.1034C_O - 0.0151C_N - 0.0211C_A \quad (6.3)$$

where:

$C_C$  = wt.% of carbon in dry biomass;

$C_H$  = wt.% of hydrogen in dry biomass;

$C_S$  = wt.% of sulphur in dry biomass;

$C_O$  = wt.% of oxygen in dry biomass;

$C_N$  = wt.% of nitrogen in dry biomass;

$C_A$  = wt.% of ash in dry biomass.

On dry biomass basis,

$$LHV_{\text{biomass,dry}} (\text{Lind}) = HHV_{\text{biomass,dry}} - H_{\text{evap}} \left( w_H \times \frac{M_{\text{water}}}{M_H} + \frac{f_M}{1 - f_M} \right) \quad (6.4)$$

On wet biomass basis,

$$LHV_{\text{biomass,wet}} (\text{Lind}) = LHV_{\text{biomass,dry}} \times \left( \frac{m_{\text{dry}}}{m_{\text{wet}}} \right) = LHV_{\text{biomass,dry}} \times (1 - f_M) \quad (6.5)$$



where:

$LHV_{\text{biomass,dry}}$  = lower heating value on dry basis;

$LHV_{\text{biomass,wet}}$  = lower heating value on wet basis;

$H_{\text{evap}}$  = latent heat of vaporization water at 25 °C (2440 kJ/kg);

$w_{\text{H}}$  = mass fraction of hydrogen in the dry biomass;

$M_{\text{water}}$  = Molar mass of water (0.018 kg/mol);

$M_{\text{H}}$  = Molar mass of hydrogen (0.002 kg/mol);

$f_{\text{M}}$  = moisture fraction ( $\text{kg}_{\text{water}} / \text{kg}_{\text{wet biomass}}$ );

$m_{\text{water}}$  = mass of water (kg);

$m_{\text{dry}}$  = mass of dry biomass (kg);

$m_{\text{wet}}$  = mass of wet biomass (kg).

There are two possible types of feedstock for the methanation process, either the bio-oil on its own, or the combined feed of bio-oil and non-condensable gases from the pyrolysis of the dried PEFB. These two cases were compared in terms of energy demand as shown in Table 6.10 and Table 6.11. Generally, the non heat-integrated process which uses both the bio-oil and non-condensable pyrolysis gas results in a higher total energy demand compared to using bio-oil alone as feedstock in the methanation unit. This is due to the additional power consumption for compressing the non-condensable gases to 27 bar before entering the methanation unit, as well as the insufficient energy for pre-heating the incoming air to the combustion unit.

**Table 6.10** Comparison of heat and power demand for different levels of process integration (Feedstock for methanation process = Bio-oil).

Energy demand, kW	Non-integrated process	Process 1	Process 2	Process 3	Process 4
Crushing			90		
Grinding			227		
Pump – Liquid bio-oil			3		
Pump – Water feed in methanation unit			5		
HPWS power consumption			529		
Power consumption ( $P_{el}^+$ )			854		
Power generation ( $P_{el}^-$ )			0		
<b>Net power consumption (<math>P_{el}^+ - P_{el}^-</math>)</b>			<b>854</b>		
Cooling – After re-compression in HPWS unit	-317	-317	-317	-317	-317
Heating – Air for combustion	+180	-	+180	+180	-
Cooling – After pyrolyzer	-641	-641	-641	-405	-405
Heating – Vaporized bio-oil	+510	+510	+510	+274	+274
Heating – Vaporized water for methanation	+1798	+1798	+743	+1798	+743
Methanation	-601	-601	-	-601	-
Cooling – After methanator	-1914	-1914	-1460	-1914	-1460
$\Sigma$ of all excess heat rates ( $\dot{Q}^-$ )	3473	3473	2418	3237	2182
$\Sigma$ of all heating demand rates ( $\dot{Q}^+$ )	2488	2308	1433	2252	1017
<b>Net excess heat rate (<math>\dot{Q}^- - \dot{Q}^+</math>)</b>	<b>985</b>	<b>1165</b>	<b>985</b>	<b>985</b>	<b>1165</b>

**Table 6.11** Comparison of heat and power demand for different levels of process integration (Feedstock for methanation process = Bio-oil and non-condensable pyrolysis gas).

Energy demand, kW	Non-integrated process	Process 1	Process 2	Process 3	Process 4
Crushing			90		
Grinding			227		
Pump – Liquid bio-oil			3		
Pump – Water feed in methanation unit			6		
Compressor – Non-condensable pyrolysis gas			35		
HPWS power consumption			704		
Power consumption ( $P_{el}^+$ )			1065		
Power generation ( $P_{el}^-$ )			0		
<b>Net power consumption (<math>P_{el}^+ - P_{el}^-</math>)</b>			<b>1065</b>		
Cooling – After re-compression in HPWS unit	-435	-435	-435	-435	-435
Heating – Air for combustion	+97	-	+97	+97	-
Heating – Drying wet PEFB	+489	-	+489	+489	-
Cooling – After pyrolyzer	-643	-643	-643	-406	-406
Heating – Vaporized bio-oil	+547	+547	+547	+274	+274
Heating – Vaporized water for methanation	+2097	+2097	+879	+2097	+879
Methanation	-689	-689	-	-689	-
Cooling – After methanator	-2222	-2222	-1693	-2222	-1693
$\Sigma$ of all excess heat rates ( $\dot{Q}^-$ )	3989	3989	2771	3752	2534
$\Sigma$ of all heating demand rates ( $\dot{Q}^+$ )	3230	2644	2012	2957	1153
<b>Net excess heat rate (<math>\dot{Q}^- - \dot{Q}^+</math>)</b>	<b>759</b>	<b>1345</b>	<b>759</b>	<b>795</b>	<b>1381</b>

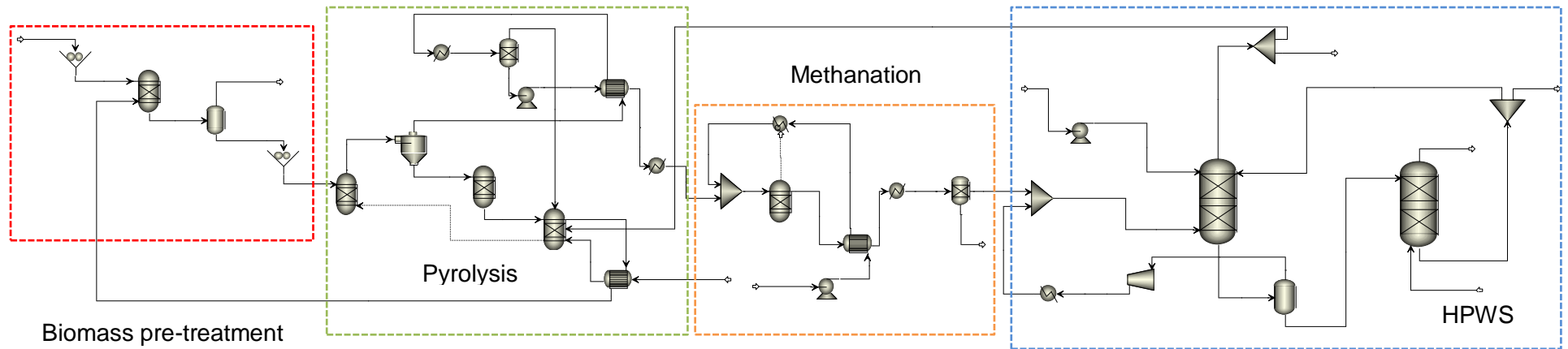


**Figure 6.15** Simplified process simulation flowsheet of full heat integration, Process 4 in Table 6.10, methanator feed is bio-oil alone.

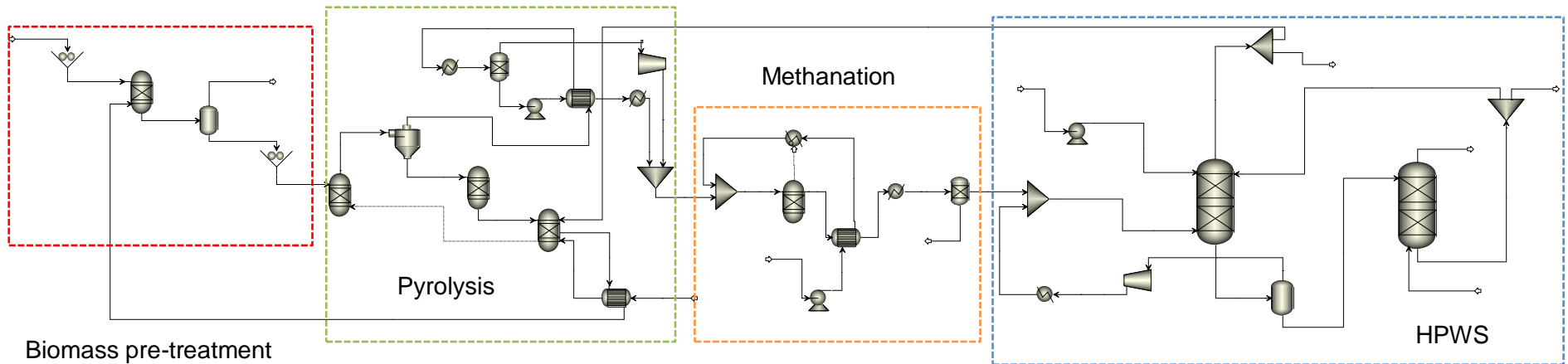


**Figure 6.16** Simplified process simulation flowsheet of full heat integration, Process 4 in Table 6.11, methanator feed is combined bio-oil and non-condensable pyrolyzer gases.

**Table 6.12** Comparison of the process performance between the two different feedstocks options in the methanation process.

Parameters	Bio-oil as feed in methanation unit	Bio-oil and non-condensable pyrolysis gas as feed in methanation unit
$LHV_{PEFB(wet)}$ , MJ/kg	8.42	8.42
$LHV_{methane}$ , MJ/kg	49.9	49.9
Mass flow rate of raw PEFB, kg/s	0.833	0.833
Mass flow rate of pure CH <sub>4</sub> production, kg/s	0.103	0.102
$\eta_{btf}$ , % (MJ of CH <sub>4</sub> / MJ of biomass)	73.4	72.8

**Table 6.13** Comparison of the process performance between the two different feedstocks options which includes heat and power demand in the methanation process.

Parameters	Bio-oil as feed in methanation unit	Bio-oil and non-condensable pyrolysis gas as feed in methanation unit
$LHV_{PEFB(wet)}$ , kW.hr/kg	2.34	2.34
$LHV_{methane}$ , kW.hr/kg	13.9	13.9
Mass flow rate of raw PEFB, kg/hr	3000	3000
Mass flow rate of pure CH <sub>4</sub> production, kg/hr	371.3	368.3
Net power consumption ( $P_{el}^+ - P_{el}^-$ ), kW	854	1065
Net excess heat ( $\dot{Q}^- - \dot{Q}^+$ ), kW	1165	1381
$\eta_{th}$ , % (kW of CH <sub>4</sub> / kW of biomass)	80.3	80.3

Moreover, it was observed that the power consumption in the HPWS unit also contributed to this higher amount of energy demand in this process. As higher amount of feedstock was used for the methanation, larger CO<sub>2</sub> production was expected. This increased the amount of water usage in the HPWS unit compared to the process which only used bio-oil as feed for the methanation process in order to achieve high purity of methane product. This situation led to a higher amount of energy consumption to the pump recirculating liquid in the HPWS unit.

By comparing the individual contribution terms to the total energy demand of the heat integrated processes in both cases (i.e. using bio-oil only or using both bio-oil and non-condensable pyrolysis gas as feedstock in the methanation unit), most of the reduction in energy consumption was achieved by implementing the integration of raising steam. Figure 6.15 and Figure 6.16 show a fully integrated process, termed Process 4 (listed in both of Table 6.10 and Table 6.11). The process performance for both cases (i.e. using bio-oil or using both of bio-oil and non-condensable pyrolysis gas as feedstock in the methanation unit) was then compared in terms of thermal conversion efficiency which based on LHV value, as shown in Table 6.12 and Table 6.13. Figure 6.17 shows the overall energy balance for fully integrated processes for both cases. Based on Table 6.12, the thermal efficiency when using bio-oil alone as the feedstock in the methanation unit (73.4%) is slightly higher compared to that using both bio-oil and non-condensable gases as feedstock (72.8%). This is due to the higher energy demand especially in HPWS unit and vaporising the steam for methanation but less amount of the final methane production was achieved compared to using bio-oil alone as the

feedstock in the methanation unit. For the overall thermal efficiency, which includes heat and power demand in the complete plant (Table 6.13), both cases resulted in the same value, 80.3%.

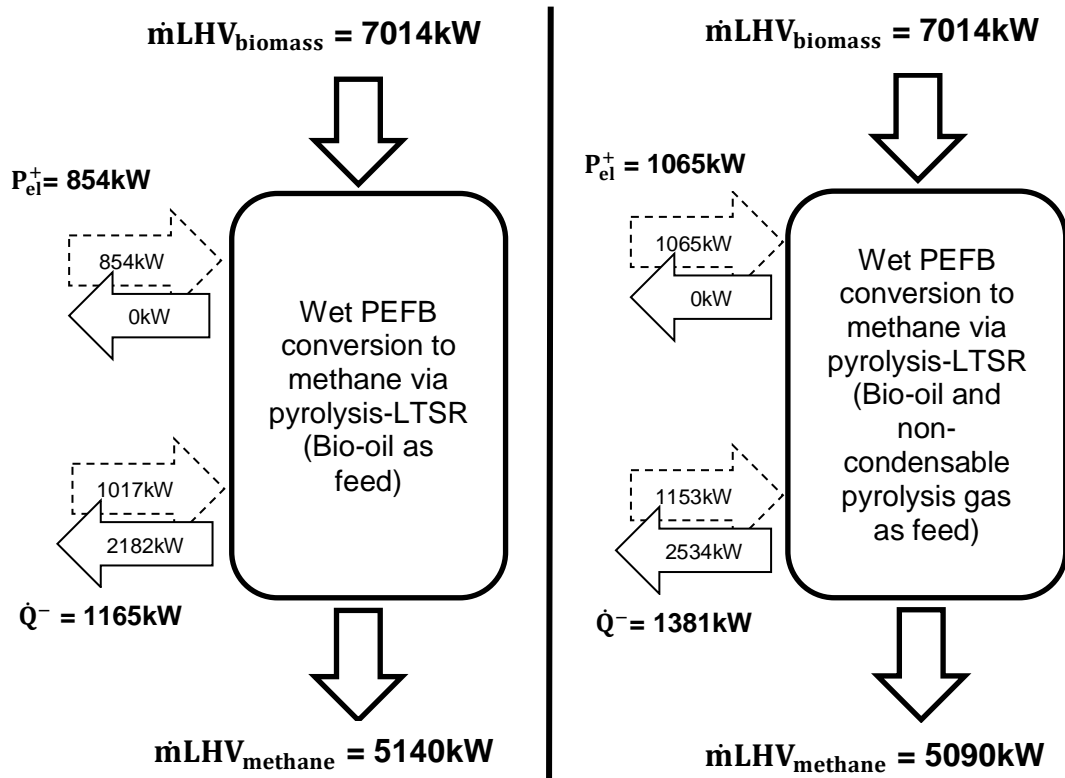


**Figure 6.17** Comparison of energy flows in a methanation via pyrolysis-LTSR process for two different of feedstocks in methanation unit.

Several works have modelled allothermal biomass gasification systems to SNG production where it was found that 73.7% [135] and 70.3% [91] of thermal efficiencies (the power and heat demand of the system was not included, using equation 6.1) which were based on LHV. However, 62.5% of thermal efficiency was achieved for biomass gasification by using fluidized bed technology [86] and 73.8% for biomass gasification modelled via circulating fluidized bed gasifier [92]. Only 58.0% of thermal efficiency (Eq. 6.1) was obtained for using indirectly heated fluidized bed gasifier to methane

production [175]. On the other hand, 71.2% and 91.0% of the overall thermal efficiency (i.e. power and heat demand are included) were reported by [86] and [135] respectively for allothermal biomass gasification system. Thus, the methane production from PEFB conversion via fast pyrolysis followed by LTSR process from our work is comparable with the biomass gasification route, since it gives similar value of the thermal efficiencies of 74.3%, when the power and heat flows are not included in the process, and 81.1%, when the power and heat flows are included in the process.

A more detailed discussion of the comparison between efficiencies obtained in the present study and those found in the literature for similar biomass to biogas systems is presented below, and is based on data listed Table 6.14. In this table, we introduce another performance indicator, which is the percent efficiency of methane yield, defined the ratio of the process-derived methane yield to that of the maximum stoichiometric methane yield achievable by complete conversion of the source biomass to methane, according to reaction (R6.1). This indicator allows comparing different gasification plants performance despite their operation on diverse biomass feedstocks.



**Table 6.14** Comparison of the process performance of our work with other biomass gasification systems to CH<sub>4</sub> production.

	Our work (a) before and (b) after splitting 3.1% CH <sub>4</sub> production		Fendt [86]	Tremel [135]	Meijden [91]	Gassner [92]	Duret [175]
Biomass	(a) PEFB	(b) PEFB	Beech wood	Spruce wood	Wood	Wood	Wood
Moisture, wt.%	50	50	20	25	15	50	0
Elemental analysis, mf wt.%							
i. C	49.07	49.07	47.97	49.80	50.19	50.60	47.42
ii. H	6.48	6.48	5.78	6.30	6.04	5.70	6.25
iii. O	38.29	38.29	45.39	43.20	42.37	42.50	46.33
iv. N	0.70	0.70	0.22	0.13	0.30	0.20	0
v. S	0.10	0.10	0.03	0	0.06	0	0
vi. Cl	0	0	0	0	0.05	0	0
vii. Ash	5.36	5.36	0.61	0.57	1.00	1.00	0
C <sub>n</sub> H <sub>m</sub> O <sub>k</sub>	CH <sub>1.57</sub> O <sub>0.59</sub>	CH <sub>1.57</sub> O <sub>0.59</sub>	CH <sub>1.43</sub> O <sub>0.71</sub>	CH <sub>1.50</sub> O <sub>0.65</sub>	CH <sub>1.43</sub> O <sub>0.63</sub>	CH <sub>1.34</sub> O <sub>0.63</sub>	CH <sub>1.57</sub> O <sub>0.73</sub>
LHV <sub>biomass,wet</sub>	8.42	8.42	13.23	14.55	15.98	9.30	18.20
CH <sub>4</sub> yield wt.% of dry biomass (Aspen plus model)	25.5	24.7	20.5	28.2	n/a	27.4	21.2
Maximum theoretical CH <sub>4</sub> yield, wt.% of dry biomass	36.1	36.1	32.2	35.0	34.9	34.5	32.5
% efficiency of CH <sub>4</sub> (produced, Aspen plus model max theor. CH <sub>4</sub> , wt.%/wt.%)	70.8	68.7	63.6	80.6	n/a	79.5	65.1
Biomass to fuel energy efficiency (using Eq. 6.1)							
η <sub>btf</sub> , % (MJ of max theor. CH <sub>4</sub> / MJ of biomass)	106.9	106.9	97.0	89.9	n/a	92.5	89.1
η <sub>btf</sub> , % (MJ of CH <sub>4</sub> /MJ of biomass, Aspen Plus model)	75.7	73.4	61.8	72.5	n/a	73.5	58.0
η <sub>btf</sub> , % (MJ of bio-SNG/MJ of biomass, Aspen Plus model)	76.7	74.3	62.5	73.7	70.3	73.8	n/a
Thermal efficiency (using Eq. 6.2)							
η <sub>th</sub> , % (MW of bio-SNG/MW of biomass)	81.0	81.1	71.2	91.0	n/a	n/a	n/a
Carbon conversion efficiency (using Eq. 6.6)							
η <sub>C</sub> , % (kmol.s <sup>-1</sup> of CH <sub>4</sub> produced/kmol.s <sup>-1</sup> of inlet carbon)	39.1	37.8	32.0	42.5	n/a	40.6	33.5

Based on Table 6.14, and the stoichiometry of the methanation of biomass reaction (R6.1) the maximum theoretical  $\text{CH}_4$  yield when using PEFB feed was slightly higher (36.1 wt.%) compared to that when using wood (32.2–35.0 wt.%) as the feedstock for  $\text{CH}_4$  production. This is because of the higher amount of hydrogen and lower amount of oxygen contained in the PEFB compared to wood, where 1.57 of H/C ratio and 0.59 of O/C ratio were obtained in the PEFB. 73.4% was calculated for the thermal efficiency of PEFB conversion to  $\text{CH}_4$  production (using Eq. 6.1), which was found to close to the highest thermal efficiency (73.5%) among the wood gasification processes. However, the efficiency of  $\text{CH}_4$  production compared to the maximum of theoretical  $\text{CH}_4$  production for PEFB was 68.7%, which was within the range of the wood gasification process (63.6–80.6%). Although the sacrifice of 3.1% of the upgraded bio-methane production to the furnace resulted in a lower thermal efficiency (using Eq. 6.1) of 74.3% compared to the plant without this top-up  $\text{CH}_4$  (76.7%), it was still preferable to burn 3.1% of the bio-methane product due to the resulting slightly higher thermal efficiency (using Eq. 6.2) of 81.1% compared with 81.0%. At the same time, the overall carbon conversion efficiency, 37.8% (using Eq. 6.6) for the case 'after splitting 3.1% of  $\text{CH}_4$  production' was slightly lower compared to 39.1% (before splitting the  $\text{CH}_4$  production) due to the sacrifice of 3.1% of the upgraded bio-methane production. The thermal efficiency of 81.1% (using Eq. 6.2) by using PEFB was comparable with those of the wood gasification processes reviewed from the literature to date, which were within 71.2–91.0%.

Overall carbon conversion efficiency [175],

$$\eta_C = \frac{\dot{n}_{C,out}}{\dot{n}_{C,in}} \quad (6.6)$$

where:

$\dot{n}_{C,in}$  = molar flowrate of inlet carbon of biomass, kmol/hr;

$\dot{n}_{C,out}$  = molar flowrate of the final upgraded CH<sub>4</sub> production, kmol/hr.

The biomass to fuel efficiency values and the thermal efficiency values are extremely dependent on the choice of LHV for their calculations. Below we review the LHV values of the dry wood which were used in [86, 91, 92, 135, 175] and compared them with the LHV values calculated using equations 6.3–6.5. LHV values from the literature sources and their equivalent calculated LHV based on elemental composition stated in the same sources are listed in Table 6.15. It was found that the LHV values for wood on a dry basis, which were reported in [86, 91, 92, 135, 175] were close to the LHV values calculated using equations 6.3–6.5. The LHV value for PEFB reported in the literature is within 17.02–20.34 MJ/kg [164, 176-180], revealing a large discrepancy between the minimum and maximum of LHV values. Thus we decided to use the calculated value of 16.83 MJ/kg on a dry basis of the LHV value for the PEFB used in this work, determined using equations 6.3–6.5 and the elemental composition of the PEFB feed used in the plant model.

By using bio-oil as feedstock in the methanation process, Table 6.16 shows the gas compositions and operating conditions for different unit processes while Table 6.17 lists the thermal efficiency of the plant based on the ratio of lower heating values of the CH<sub>4</sub> product as recovered chemical energy and of the wet PEFB biomass as input chemical energy. Based on Table 6.17, the methanation and purification stages, idealised by the assumed equilibrium conditions, have a high efficiency, compared to that of the fast pyrolysis stage, which inevitably results in char product.

**Table 6.15** Comparison of heating values (HHV and LHV) by using Channawala and Parikh (Eq. 6.3) and Lind (Eq. 6.4–6.5) for different of biomass.

	Our work	Fendt (2012) [86]	Tremel (2013) [135]	Meijden (2010) [91]	Gassner (2009) [92]	Duret (2005) [175]
Biomass	PEFB	Beech wood	Spruce wood	Wood	Wood	Wood
Moisture, wt. %	50	20	25	15	50	0
Elemental analysis, mf wt. %						
i. C	49.07	47.97	49.80	50.19	50.60	47.42
ii. H	6.48	5.78	6.30	6.04	5.70	6.25
iii. O	38.29	45.39	43.20	42.37	42.50	46.33
iv. N	0.70	0.22	0.13	0.30	0.20	0
v. S	0.10	0.03	0	0.06	0	0
vi. Cl	0	0	0	0.05	0	0
vii. Ash	5.36	0.61	0.57	1.00	1.00	0
Heating values, MJ/kg						
HHV <sub>biomass, dry</sub> (Channawala & Parikh)	20.69	18.85	20.33	20.24	19.96	19.13
LHV dry biomass (Lind + Channiwala & Parikh)	16.83	16.97	18.13	18.48	16.27	17.75
LHV dry biomass (journal+Lind)	17.02- 20.34	16.53	19.40	18.80	18.60	18.20

**Table 6.16** Gas compositions, pressures, temperatures and flow rates of the process streams based on 3000 kg/hr of raw PEFB.

	Pyrolysis	Methanation	Gas purification
CH <sub>4</sub> , wt. %	0.6	11.6	99.5
CO <sub>2</sub> , wt. %	7.7	27.4	0.0
CO, wt. %	5.3	0.0	0.0
H <sub>2</sub> , wt. %	0.1	0.1	0.5
C <sub>2</sub> H <sub>4</sub> , wt. %	0.1	0.0	0.0
C <sub>2</sub> H <sub>6</sub> , wt. %	0.1	0.0	0.0
H <sub>2</sub> O, wt. %	n/a	60.9	0.0
Wet bio-oil, wt. %	75.9	0.0	0.0
Char, wt. %	10.2	0.0	0.0
P, bar	1	27	25
T, °C	500	300	25
Flow rate, kg/hr	1619	3426	373

**Table 6.17** Efficiencies at the two main conversion stages, and overall efficiency of PEFB to pure CH<sub>4</sub> process.

Efficiency based on chemical energy output/input, PEFB feedstock	%
Pyrolysis, Wet PEFB → Bio-oil	89.5
Methanation, Bio-oil → Pure Methane	81.9
Full process, wet PEFB → Pure Methane	73.3

## 6.9 Conclusion

This study has presented a process design for bio-methane production from PEFB via fast pyrolysis. From the simulation results, only 3.1% of the upgraded bio-methane production needs to be burned in the combustor in order to supply extra heat for pre-heating the incoming air to the combustor and to dry up the wet PEFB, as the combustion of both bio-char supplemented by the non-condensable gases from the pyrolysis process was not sufficient. The estimated thermal efficiencies were 74.3% (when net power and heat demand are not included in the process) and 81.1% (when net power and heat demand are included in the process). These efficiencies are comparable with the state of art biomass gasification route to methane production via syngas followed by CO and CO<sub>2</sub> methanation.

Despite the fact that an economic assessment has not been conducted in the present study (future work), it is therefore expected that capital and operational expenditures of the gasification-CO methanation plants would be significantly larger than those of the pyrolysis-direct methanation of bio-oil plant, when operating on a same feedstock. Thus eliminating carbon accumulation on the direct methanation of bio-oil catalyst is paramount to attain the high efficiency values predicted in this plant modelling study and realise the advantages of the pyrolysis-direct methanation of bio-oil route.

## Chapter 7

### Conclusions and Recommendations for Future Work

#### 7.1 Introduction

The aim of this research work was to investigate the feasibility of producing a CH<sub>4</sub>-rich gas from palm empty fruit bunch (PEFB) via fast pyrolysis followed by direct catalytic methanation of the pyrolytic oil using a low temperature steam reforming (LTSR) process. As CO<sub>2</sub> is a co-product of the LTSR process, a thermodynamic equilibrium analysis was conducted initially using NASA's Chemical Equilibrium with Application (CEA) software to observe the effect of the introduction of CaO<sub>(s)</sub> or Ca(OH)<sub>2(s)</sub> as CO<sub>2</sub> sorbent towards the potential enhancement of the CH<sub>4</sub> production by in-situ CO<sub>2</sub> capture. The CH<sub>4</sub> yield and purity predicted for the equilibrium process in the presence of, or free of CO<sub>2</sub> sorbent were also studied for adiabatic and isothermal conditions, where temperatures of 300–800 K, molar steam to carbon (S/C) ratios of 0.3–7.0, pressures of 1–30 atm and molar calcium to carbon ratios (Ca:C) of 0.3–1.0 were simulated. Using the optimum conditions observed from the thermodynamic equilibrium calculations, the experimental feasibility of CH<sub>4</sub> production from acetic acid as single compound bio-oil surrogate via LTSR was performed at bench scale by using a catalyst typical of steam reforming commercial formulation, nickel-calcium aluminate (Ni/Ca-Al<sub>2</sub>O<sub>3</sub>) in a packed bed reactor at 350–450 °C and S/C in the range of 1–3. The characteristics of



the carbon deposited on the used catalyst ( $C_S$ ) and carbon present in the condensate ( $C_L$ ) were also reported in this work. Then, a preliminary process design for an industrial scale process of  $CH_4$  production from PEFB wet biomass via fast pyrolysis followed by direct catalytic methanation of the pyrolysis bio-oil using LTSR was carried out using Aspen Plus V8.8 software. The heat integration between possible streams in the plant was also modelled to determine the opportunities for energy savings in the plant, where it gives the process performance of the process in terms of thermal conversion efficiency and energy consumption of PEFB conversion into  $CH_4$  production.

## 7.2 Conclusions

Based on thermodynamic analysis, it can be concluded that PEFB bio-oil has the potential to be converted into  $CH_4$  via LTSR process, where it was favoured in the 400–600 K range and at around molar steam to carbon ratio of 3 at atmospheric pressure resulting in a reformat consisting of 44.5 vol.%  $CH_4$ , 42.7 vol.%  $CO_2$  and 12.7 vol.%  $H_2$ . This investigations have met both of the Objectives 1 and 2 of this study.

The influence of in situ  $CaO_{(s)}$  or  $Ca(OH)_{2(s)}$  as  $CO_2$  sorbents towards  $CH_4$  production, as described in Research Objective 3 found that the  $CH_4$  production in the adiabatic condition was far below both the theoretical stoichiometric maximum and the equilibrium  $CH_4$  produced in the isothermal condition. This was because of the predicted equilibrium temperatures being

much higher for the adiabatic condition than the initial temperatures due to the exothermic carbonation, where it moved the process in sorption enhanced-high temperature steam reforming (SE-HTSR) regime, favouring H<sub>2</sub> production and minimal CH<sub>4</sub> production.

As the research work was carried using both experimental and modelling approaches, conclusions were divided into two different parts which are experimental results and modelling results.

### **7.2.1 Conclusion of experimental results**

As mentioned in Research Objective 4, the conversion of acetic acid as surrogate bio-oil compound has proven that it is possible to produce CH<sub>4</sub> on the Ni/Ca-Al<sub>2</sub>O<sub>3</sub> catalyst surface via LTSR in a packed bed catalytic reactor. From the experimental results, Research Objective 5 has been achieved with the investigation of the optimum conditions for CH<sub>4</sub> production which was obtained at 400 °C and S/C of 2 with a CH<sub>4</sub> yield of 15.7 wt.% of the acetic acid feed at atmospheric pressure. This compared favourably to 21.0 wt.% as the predicted equilibrium value in the same conditions. As undesirable carbon formation on the catalyst was observed during the experiments, it is recommended to operate at higher pressures (20–30 bar), which are commonly used in the CO and CO<sub>2</sub> methanation industrial processes because higher of CH<sub>4</sub> production is thermodynamically favoured and less carbon formation on the catalyst can be achieved.

### 7.2.2 Conclusion of plant scale modelling results

According to Research Objective 6, a process design for CH<sub>4</sub> production from PEFB via fast pyrolysis followed by LTSR was modelled by using Aspen Plus software and consisted of four process units, namely, wet biomass pre-treatment, fast pyrolysis of the dried biomass particles, direct methanation of the bio-oil pyrolysis product and upgrading of the reformat to high purity methane gas. Based on the simulation results, a final gas product with composition of 99.5 wt.% CH<sub>4</sub> and 0.5 wt.% H<sub>2</sub> (corresponding to vol.% 95.9 and 4.1 respectively) was obtained with less than 3% of methane loss.

Minimization of energy consumption was required in order to achieve higher performance of the CH<sub>4</sub> production from the wet PEFB conversion process. Therefore, the possibilities of the process integration between possible streams in the process consisting of (i) air-preheat for bio-char combustion in the biomass pre-treatment unit (including by burning 3.1% of methane production together with the bio-char and non-condensable gases for this purpose), (ii) vaporizing the water to steam in the methanation unit, (iii) bio-oil vaporization in the pyrolysis unit and (iv) biomass drying by the furnace flue gases, were simulated using the Aspen Plus software. Research Objective 7 was achieved where the fully integrated system for this process (the combination of those four process integrations), yielded the estimated thermal efficiencies of 74.3%, when net power and heat flows were not included in the process, compared to 81.1%, when net power and heat flows were included in the process.

Research Objective 8 was also met in this investigation, where 81.1% of the efficiency (that includes the net power and heat flows) of our proposed process was found to be comparable with the biomass gasification route to methane production quoted in the literature for wood conversion to biomethane, which was within 71.2–91.0%.

### **7.2.3 Final conclusions**

Finally, it can be concluded that the main objectives of this research have been achieved, where this research work has proven the feasibility of the CH<sub>4</sub> production from acetic acid as bio-oil surrogate via direct catalytic methanation using LTSR, giving the optimum results of CH<sub>4</sub> yield 15.7 wt.% of the acetic acid feed at 400 °C and S/C of 2 at atmospheric pressure, i.e. close to 21.0 wt.% the equilibrium optimum in the same conditions. Moreover, the simulation work of plant scale of CH<sub>4</sub> production from PEFB via fast pyrolysis followed by LTSR and purification of the biogas gives comparable thermal efficiency (81.1%) with the common technologies based on wood gasification followed by CO and CO<sub>2</sub> methanation. The final gas product from PEFB pyrolysis-LTSR-HPWS had a composition of 99.5 wt.% of CH<sub>4</sub> and 0.5 wt.% of H<sub>2</sub> (corresponding to vol.% of 95.9 and 4.1 respectively), with the advantage of avoidance of heavy tar formation normally associated with the direct biomass gasification processes into syngas which are then followed by methanation of the syngas product. Thus the proposed process could offer less maintenance issues related to tar handling and clean up as well as a simpler plant layout, and cheaper reactor materials, provided the issue of carbon deposition on the catalyst can be addressed.

### 7.3 Recommendations for future work

As the carbon formation on the catalyst affecting the conversion of bio-oil to  $\text{CH}_4$  production, a study of catalyst optimisation to increase conversion to gases and avoid solid carbon accumulation on the catalyst is recommended for the future work. Although a significant amount of carbon was found deposited on the catalyst surface, it could be improved by operating at higher pressure because it is more thermodynamically favourable conditions for methane yield and purity in the gas product mixture, which is commonly used in the CO and  $\text{CO}_2$  methanation industrial processes. In addition, a kinetic study of the methanation process from individual bio-oil compounds and realistic surrogate bio-oil mixtures conversion can also be considered in order to provide a better understanding of the LTSR mechanism when using real bio-oil as feedstock. The kinetic rate expression and simulation study should also be carried in order to verify the kinetic behaviour of the  $\text{CH}_4$  production from bio-oil compounds conversion via the LTSR process. Then, it is suggested to use the obtain kinetic data to simulate the methanation reactor by using a kinetic reactor model which is available in Aspen Plus software, where it will give more accurate results in terms of the amount of gaseous production and the energy released from the methanation process. Techno-economic analysis and the life cycle analysis would then further the case for support of uptake of the technology to demonstrate social, economic and environmental gains.

## List of References

1. Goldemberg, J. The promise of clean energy. *Energy policy*. 2006, **34**(15), pp.2185-2190.
2. Oh, T.H., Pang, S.Y. and Chua, S.C. Energy policy and alternative energy in Malaysia: issues and challenges for sustainable growth. *Renewable and Sustainable Energy Reviews*. 2010, **14**(4), pp.1241-1252.
3. Ong, H., Mahlia, T. and Masjuki, H. A review on energy scenario and sustainable energy in Malaysia. *Renewable and Sustainable Energy Reviews*. 2011, **15**(1), pp.639-647.
4. Victor, D.G., Jaffe, A.M. and Hayes, M.H. *Natural gas and geopolitics*. Cambridge University Press Cambridge, 2006.
5. Hub, E.C.M.E.I. *Primary Energy Supply*. [Online]. 2011. [Accessed April 2017]. Available from: <http://meih.st.gov.my/>
6. Peebles, M.W. *Natural gas fundamentals*. Twayne Publishers, 1992.
7. Commission, E. *National Energy Balance 2014*. Putrajaya, Malaysia, 2016.
8. Kelly-Yong, T.L., Lee, K.T., Mohamed, A.R. and Bhatia, S. Potential of hydrogen from oil palm biomass as a source of renewable energy worldwide. *Energy Policy*. 2007, **35**(11), pp.5692-5701.
9. Mahlia, T. Emissions from electricity generation in Malaysia. *Renewable Energy*. 2002, **27**(2), pp.293-300.
10. Pearce, F. Methane: the hidden greenhouse gas. *New Scientist*. 1989, **122**, pp.37-41.
11. Tom Boden, B.A., Gregg Marland. *Global CO2 emissions from fossil-fuel burning, cement manufacture and gas flaring: 1751-2014*. [Online]. 2017. [Accessed May 2017]. Available from: [http://cdiac.esd.ornl.gov/trends/emis/meth\\_reg.html#](http://cdiac.esd.ornl.gov/trends/emis/meth_reg.html#)

12. Moss, A.R. *Methane: global warming and production by animals*. Chalcombe Publications, 1993.
13. Lim, S. and Teong, L.K. Recent trends, opportunities and challenges of biodiesel in Malaysia: an overview. *Renewable and Sustainable Energy Reviews*. 2010, **14**(3), pp.938-954.
14. LLC, M. *Crude Oil Prices-70 Year Historical Chart*. [Online]. May 2017. [Accessed October 2017]. Available from: <http://www.macrotrends.net/1369/crude-oil-price-history-chart>
15. BP. *BP Statistical Review of World Energy June 2016*. [Online]. 2016. [Accessed May 2017]. Available from: <http://www.bp.com/>
16. Kopyscinski, J., Schildhauer, T.J. and Biollaz, S.M.A. Production of synthetic natural gas (SNG) from coal and dry biomass - A technology review from 1950 to 2009. *Fuel*. 2010, **89**(8), pp.1763-1783.
17. (US), N.R.E.L. *Energy analysis biogas potential in the United States. Colorado (US)*. U.S. Department of Energy (US), 2013.
18. AEBIOM, A. biogas road map for Europe. *European Biomass Association*. 2009.
19. Environmental, K. *Canadian Biogas Study: Benefits to the Economy, Environment and Energy* 2013.
20. Commission, E. *National Energy Balance 2013*. Putrajaya, Malaysia, 2014.
21. McLeay, I., Harris, K. and Annut, A. *Digest of United Kingdom Energy Statistics 2014*. London, 2014.
22. A, B. *The German biogas experience: Opportunities and key experiences for US deployment*. 2011.
23. Hosseini, S.E. and Wahid, M.A. Feasibility study of biogas production and utilization as a source of renewable energy in Malaysia. *Renewable & Sustainable Energy Reviews*. 2013, **19**, pp.454-462.
24. Subramaniam, V., MaAn, N., ChooYuen, M. and Nik Meriam, N. Environmental performance of the milling process of Malaysian palm oil

- using the life cycle assessment approach. *American Journal of Environmental Sciences*. 2008, **4**(4), pp.310-315.
25. Prasertsan, S. and Prasertsan, P. Biomass residues from palm oil mills in Thailand: an overview on quantity and potential usage. *Biomass and Bioenergy*. 1996, **11**(5), pp.387-395.
  26. Huber, G.W., Iborra, S. and Corma, A. Synthesis of transportation fuels from biomass: chemistry, catalysts, and engineering. *Chemical reviews*. 2006, **106**(9), pp.4044-4098.
  27. USDA United State of Department Agriculture, E.R.S. *All Crops Yearbook 2017*. [Online]. 2017. [Accessed July]. Available from: <http://www.ers.usda.gov/data-products/oil-crops-yearbook.aspx>
  28. Basiron, Y. Palm oil production through sustainable plantations. *European Journal of Lipid Science and Technology*. 2007, **109**(4), pp.289-295.
  29. Plantation, S.D. *Palm Oil Facts and Figures*. [Online]. 2014. [Accessed July]. Available from: [www.simedarby.com/upload/Palm\\_Oil\\_Facts\\_and\\_Figures.pdf](http://www.simedarby.com/upload/Palm_Oil_Facts_and_Figures.pdf)
  30. Carter, C., Finley, W., Fry, J., Jackson, D. and Willis, L. Palm oil markets and future supply. *European Journal of Lipid Science and Technology*. 2007, **109**(4), pp.307-314.
  31. Mielke, T. *Oil World: World Supply, Demad and Price Forecasts for Oilseeds, Oils and Meals*. Hamburg, Germany, 2017.
  32. Initiative, U.S.A. *Sustainable palm oil: Good agriculture practice guidelines*. 2014.
  33. Yusoff, S. Renewable energy from palm oil–innovation on effective utilization of waste. *Journal of cleaner production*. 2006, **14**(1), pp.87-93.
  34. Husain, Z., Zainal, Z. and Abdullah, M. Analysis of biomass-residue-based cogeneration system in palm oil mills. *Biomass and Bioenergy*. 2003, **24**(2), pp.117-124.



35. Abas, R., Kamaruddin, M., Nordin, A. and Simeh, M. A study on the Malaysian oil palm biomass sector—supply and perception of palm oil millers. *Oil Palm Industry Economic Journal*. 2011, **11**(1), pp.28-41.
36. Sumathi, S., Chai, S. and Mohamed, A. Utilization of oil palm as a source of renewable energy in Malaysia. *Renewable and Sustainable Energy Reviews*. 2008, **12**(9), pp.2404-2421.
37. Ahmad, S., Ab Kadir, M.Z.A. and Shafie, S. Current perspective of the renewable energy development in Malaysia. *Renewable and Sustainable Energy Reviews*. 2011, **15**(2), pp.897-904.
38. Shuit, S.H., Tan, K.T., Lee, K.T. and Kamaruddin, A. Oil palm biomass as a sustainable energy source: A Malaysian case study. *Energy*. 2009, **34**(9), pp.1225-1235.
39. Mohammed, M., Salmiaton, A., Azlina, W.W., Amran, M.M., Fakhru'l-Razi, A. and Taufiq-Yap, Y. Hydrogen rich gas from oil palm biomass as a potential source of renewable energy in Malaysia. *Renewable and Sustainable Energy Reviews*. 2011, **15**(2), pp.1258-1270.
40. Qader, S.A. Natural gas substitutes from coal and oil. 1985.
41. Gao, J. COAL, OIL SHALE, NATURAL BITUMEN, HEAVY OIL, AND PEAT. 2009.
42. Yi, L., Feng, J., Qin, Y.-H. and Li, W.-Y. Prediction of elemental composition of coal using proximate analysis. *Fuel*. 2017, **193**, pp.315-321.
43. Henry Jr, J. and Louks, B. *Economic study of pipeline gas production from coal.[Critical analysis of several processes]*. Stanford Res. Inst., Stanford, CA, 1971.
44. Shimekit, B. and Mukhtar, H. Natural gas purification technologies-major advances for CO<sub>2</sub> separation and future directions. In: *Advances in Natural Gas Technology*. InTech, 2012.
45. Rudolph, P.F. *The Lurgi Process: The Route to SNG from Coal*. Lurgi Mineralöltechnik, 1972.
46. MCLEAN, V. HANDBOOK OF GASIFIERS AND GAS-TREATMENT SYSTEMS. 1982.

47. Marten, J., Banchik, I. and Subramanian, T. Winkler technology for clean fuels from coal. In: *Synthetic Fuels Processing: Comparative Economics*, 1977, pp.251-285.
48. Archer, D., Vidt, E., Keairns, D., Morris, J. and Chen, J. Coal Gasification for Clean Power Production. In: *Proceedings of the Third International Conference on Fluidized Bed Combustion, Hueston Woods, Ohio*, 1972.
49. Simbeck, D., Dickenson, R. and Oliver, E. *Coal-gasification systems: a guide to status, applications, and economics. Final report.* Synthetic Fuels Associates, Inc., Mountain View, CA (USA), 1983.
50. Twigg, M.V. *Catalyst handbook.* CRC, 1989.
51. Eisenlohr, K.-H. and Moeller, F. Effect of certain reaction parameters on methanation of coal gas to SNG. In: ACS Publications, 1975.
52. Panek, J. and Grasser, J. Practical experience gained during the first twenty years of operation of the great plains gasification plant and implications for future projects. *DOE Office of Fossil Energy: Technical Report.* 2006.
53. Moeller, F., Roberts, H. and Britz, B. Methanation of coal gas for SNG. *Chemischer Informationsdienst.* 1974, **5**(31).
54. Topsoe, H. *Methanation Catalyst PK-7R.* 2008.
55. Höhle, B., Menzer, R. and Range, J. High temperature methanation in the long-distance nuclear energy transport system. *Applied Catalysis.* 1981, **1**(3-4), pp.125-139.
56. Topsoe, H. From coal to substitute natural gas using TRESP. *Haldor Topsoe.* 2008.
57. Harms, H., Höhle, B. and Skov, A. Methanisierung kohlenmonoxidreicher Gase beim Energie-Transport. *Chemie Ingenieur Technik.* 1980, **52**(6), pp.504-515.
58. White, G., Roszkowski, T. and Stanbridge, D. The RMPProcess. In: ACS Publications, 1975.

59. White, G. The RMProcess–A methanation system. In: *Proceedings of ninth synthetic pipeline gas symposium, Chicago, American Gas Association, 1977*, pp.129-135.
60. Hohlein, B., Niessen, H., Range, J., Schiebahn, H.J.R. and Vorwerk, M. METHANE FROM SYNTHESIS GAS AND OPERATION OF HIGH-TEMPERATURE METHANATION. *Nuclear Engineering and Design*. 1984, **78**(2), pp.241-250.
61. Er-Rbib, H. and Bouallou, C. Methanation catalytic reactor. *Comptes Rendus Chimie*. 2014, **17**(7), pp.701-706.
62. Bartholomew, C.H. Mechanisms of catalyst deactivation. *Applied Catalysis A: General*. 2001, **212**(1), pp.17-60.
63. Götz, M., Lefebvre, J., Mörs, F., Koch, A.M., Graf, F., Bajohr, S., Reimert, R. and Kolb, T. Renewable Power-to-Gas: A technological and economic review. *Renewable Energy*. 2016, **85**, pp.1371-1390.
64. Porubova, J., Bazbauers, G. and Markova, D. Modeling of the adiabatic and Isothermal methanation process. *Scientific Journal of Riga Technical University. Environmental and Climate Technologies*. 2011, **6**(1), pp.79-84.
65. Sudiro, M., Zanella, C., Bressan, L., Fontana, M. and Bertucco, A. Synthetic natural gas (SNG) from petcoke: model development and simulation. In: *AIDEC conference series*, 2009, pp.309-318.
66. Klemm, M., Ortwein, A., Zeymer, M., Rönsch, S. and Schmersahl, R. Gasreinigung undkonditionierung-Stand der Technik und Gesamtkonzepte für Methanisierungsanlagen. 1. In: *International Biomass Conference, Leipzig, 2010*.
67. Schaaf, T., Grünig, J., Schuster, M.R., Rothenfluh, T. and Orth, A. Methanation of CO<sub>2</sub>-storage of renewable energy in a gas distribution system. *Energy, Sustainability and Society*. 2014, **4**(1), p.2.
68. Götz, M. *Methanisierung im Dreiphasen-Reaktor*. thesis, Karlsruhe, Karlsruher Institut für Technologie (KIT), Diss., 2014, 2014.

69. Puertas, J. Renewable gas: the sustainable energy solution. *Program Committee on Sustainability, International Gas Union*. 2009, **2012**, p.31.
70. Petersson, A. and Wellinger, A. Biogas upgrading technologies—developments and innovations. *IEA Bioenergy*. 2009, **20**.
71. Luis, P. Use of monoethanolamine (MEA) for CO<sub>2</sub> capture in a global scenario: consequences and alternatives. *Desalination*. 2016, **380**, pp.93-99.
72. Grande, C.A. *Biogas upgrading by pressure swing adsorption*. INTECH Open Access Publisher, 2011.
73. Sircar, S. and Golden, T. Purification of hydrogen by pressure swing adsorption. *Separation Science and Technology*. 2000, **35**(5), pp.667-687.
74. MS, C. *Biogas upgrading with the highest performance level*. [Online]. [Accessed Jun 2017]. Available from: <http://methanesys.com/wp-content/uploads/DMT-Carborex>
75. Hoyer, K., Hulteberg, C., Svensson, M., Jernberg, J. and Nörregård, Ö. Biogas Upgrading-Technical Review. 2016.
76. Persson, M., Jönsson, O. and Wellinger, A. Biogas upgrading to vehicle fuel standards and grid injection. In: *IEA Bioenergy task*, 2006, pp.1-34.
77. Lems, R., Langerak, J. and Dirkse, E. Next generation biogas upgrading using highly selective gas separation membranes—showcasing the Poundbury project. In: *17th European Biosolids & Organic Resources Conference. 19th–21th November, 2012*.
78. Vijay, V. *Water scrubbing based biogas enrichment technology by IIT Delhi*. [Online]. [Accessed June 2017]. Available from: [http://www.google.co.uk/url?sa=t&rct=j&q=&esrc=s&frm=1&source=web&cd=1&ved=0ahUKEwjRytHb36TUAhWKLsAKHWFzBz4QFggpMAA&url=http%3A%2F%2Fwww.valorgas.soton.ac.uk%2FPub\\_docs%2FDeIhi\\_Aug\\_2013%2FBiogas%2520Vehicle%25203%2Fbiogas%2520upgrading8-13.pdf&usg=AFQjCNHoiJAfni7z2wt88c6dpM\\_JqdHeuA](http://www.google.co.uk/url?sa=t&rct=j&q=&esrc=s&frm=1&source=web&cd=1&ved=0ahUKEwjRytHb36TUAhWKLsAKHWFzBz4QFggpMAA&url=http%3A%2F%2Fwww.valorgas.soton.ac.uk%2FPub_docs%2FDeIhi_Aug_2013%2FBiogas%2520Vehicle%25203%2Fbiogas%2520upgrading8-13.pdf&usg=AFQjCNHoiJAfni7z2wt88c6dpM_JqdHeuA)

79. Rasi, S., Läntelä, J. and Rintala, J. Upgrading landfill gas using a high pressure water absorption process. *Fuel*. 2014, **115**, pp.539-543.
80. Eze, J. and Agbo, K. Maximizing the potentials of biogas through upgrading. *Am. J. Sci. Ind. Res.* 2010, **1**(3), pp.604-609.
81. Kapdi, S., Vijay, V., Rajesh, S. and Prasad, R. Biogas scrubbing, compression and storage: perspective and prospectus in Indian context. *Renewable Energy*. 2005, **30**(8), pp.1195-1202.
82. Lombardi, L. and Carnevale, E. Economic evaluations of an innovative biogas upgrading method with CO<sub>2</sub> storage. *Energy*. 2013, **62**, pp.88-94.
83. Ofori-Boateng, C. and Kwofie, E. Water scrubbing: a better option for biogas purification for effective storage. *World Applied Sciences Journal*. 2008, **5**(5 Special Issue), pp.122-125.
84. Ni, M., Leung, D.Y., Leung, M.K. and Sumathy, K. An overview of hydrogen production from biomass. *Fuel processing technology*. 2006, **87**(5), pp.461-472.
85. Phillips, S., Aden, A., Jechura, J., Dayton, D. and Eggeman, T. *Thermochemical ethanol via indirect gasification and mixed alcohol synthesis of lignocellulosic biomass*. National Renewable Energy Laboratory (NREL), Golden, CO., 2007.
86. Fendt, S., Tremel, A., Gaderer, M. and Spliethoff, H. The potential of small-scale SNG production from biomass gasification. *Biomass Conversion and Biorefinery*. 2012, **2**(3), pp.275-283.
87. Göransson, K., Söderlind, U., He, J. and Zhang, W. Review of syngas production via biomass DFBGs. *Renewable and Sustainable Energy Reviews*. 2011, **15**(1), pp.482-492.
88. Thunman, H. and Seemann, M. Advanced intrinsic syngas cleaning and increased bioSNG efficiency. In: *REGATEC 2017, May 2017, Pacengo (Verona), Italy*. Sweden: Renewable Energy Technology International AB, 2017.
89. Fang, Z. *Pretreatment techniques for biofuels and biorefineries*. Springer, 2013.

90. Zhang, W., He, J., Engstrand, P. and Björkqvist, O. Economic evaluation on bio-synthetic natural gas production integrated in a thermomechanical pulp mill. *Energies*. 2015, **8**(11), pp.12795-12809.
91. van der Meijden, C.M., Veringa, H.J. and Rabou, L.P. The production of synthetic natural gas (SNG): A comparison of three wood gasification systems for energy balance and overall efficiency. *Biomass and bioenergy*. 2010, **34**(3), pp.302-311.
92. Gassner, M. and Maréchal, F. Thermo-economic process model for thermochemical production of Synthetic Natural Gas (SNG) from lignocellulosic biomass. *Biomass and bioenergy*. 2009, **33**(11), pp.1587-1604.
93. Bridgwater, A.V. Review of fast pyrolysis of biomass and product upgrading. *Biomass and bioenergy*. 2012, **38**, pp.68-94.
94. Zhang, R., Cummer, K., Suby, A. and Brown, R.C. Biomass-derived hydrogen from an air-blown gasifier. *Fuel processing technology*. 2005, **86**(8), pp.861-874.
95. Sulaiman, F., Abdullah, N., Gerhauser, H. and Shariff, A. An outlook of Malaysian energy, oil palm industry and its utilization of wastes as useful resources. *Biomass and bioenergy*. 2011, **35**(9), pp.3775-3786.
96. Badger, P.C. and Fransham, P. Use of mobile fast pyrolysis plants to densify biomass and reduce biomass handling costs—A preliminary assessment. *Biomass and bioenergy*. 2006, **30**(4), pp.321-325.
97. Balat, M. Mechanisms of thermochemical biomass conversion processes. Part 1: reactions of pyrolysis. *Energy Sources, Part A*. 2008, **30**(7), pp.620-635.
98. Sulaiman, F. and Abdullah, N. Optimum conditions for maximising pyrolysis liquids of oil palm empty fruit bunches. *Energy*. 2011, **36**(5), pp.2352-2359.
99. Mohan, D., Pittman, C.U. and Steele, P.H. Pyrolysis of wood/biomass for bio-oil: a critical review. *Energy & fuels*. 2006, **20**(3), pp.848-889.
100. Czernik, S. and Bridgwater, A. Overview of applications of biomass fast pyrolysis oil. *Energy & fuels*. 2004, **18**(2), pp.590-598.

101. Naik, S.N., Goud, V.V., Rout, P.K. and Dalai, A.K. Production of first and second generation biofuels: a comprehensive review. *Renewable and Sustainable Energy Reviews*. 2010, **14**(2), pp.578-597.
102. Bridgwater, A. and Peacocke, G. Fast pyrolysis processes for biomass. *Renewable and sustainable energy reviews*. 2000, **4**(1), pp.1-73.
103. Lehto, J., Oasmaa, A., Solantausta, Y., Kyto, M. and Chiaramonti, D. Fuel oil quality and combustion of fast pyrolysis bio-oils. *VTT Technology*. 2013, **87**, p.79.
104. Wang, S., Guo, X., Wang, K. and Luo, Z. Influence of the interaction of components on the pyrolysis behavior of biomass. *Journal of Analytical and Applied Pyrolysis*. 2011, **91**(1), pp.183-189.
105. Zhu, X.-f. and Lu, Q. *Production of chemicals from selective fast pyrolysis of biomass*. INTECH Open Access Publisher, 2010.
106. Părpăriță, E., Brebu, M., Uddin, M.A., Yanik, J. and Vasile, C. Pyrolysis behaviors of various biomasses. *Polymer Degradation and Stability*. 2014, **100**, pp.1-9.
107. Abdullah, N., Sulaiman, F. and Gerhauser, H. Characterisation of oil palm empty fruit bunches for fuel application. *J. Phys. Sci.* 2011, **22**(1), pp.1-24.
108. Sukiran, M.A., Chin, C.M. and Bakar, N.K. Bio-oils from pyrolysis of oil palm empty fruit bunches. *American Journal of Applied Sciences*. 2009, **6**(5), pp.869-875.
109. Auta, M., Ern, L. and Hameed, B. Fixed-bed catalytic and non-catalytic empty fruit bunch biomass pyrolysis. *Journal of Analytical and Applied Pyrolysis*. 2014, **107**, pp.67-72.
110. Zin, R.M., Lea-Langton, A., Dupont, V. and Twigg, M.V. High hydrogen yield and purity from palm empty fruit bunch and pine pyrolysis oils. *International Journal of Hydrogen Energy*. 2012, **37**(14), pp.10627-10638.
111. Abdullah, N., Gerhauser, H. and Bridgwater, A. Bio-oil from fast pyrolysis of oil palm empty fruit bunches. *Journal of Physical Science*. 2007, **1**(1), pp.57-74.

112. Abdullah, N. and Gerhauser, H. Bio-oil derived from empty fruit bunches. *Fuel*. 2008, **87**(12), pp.2606-2613.
113. Rostrup-Nielsen, J.R. *Steam reforming catalysts: an investigation of catalysts for tubular steam reforming of hydrocarbons: a contribution from the Research Laboratory of Haldor Topsøe A/S*. Teknisk Forlag, 1975.
114. Bond, G.C. *Catalysis by metals*. Academic Press, 1962.
115. Richardson, J. SNG catalyst technology. *Hydrocarbon Processing*. 1973, **52**(12), pp.91-95.
116. Trimm, D.L. *Design of industrial catalysts*. distributors for the US and Canada, Elsevier/North-Holland, 1980.
117. Hughes, R. *Deactivation of catalysts*. Academic Pr, 1984.
118. Seemann, M.C., Schildhauer, T.J. and Biollaz, S.M. Fluidized bed methanation of wood-derived producer gas for the production of synthetic natural gas. *Industrial & engineering chemistry research*. 2010, **49**(15), pp.7034-7038.
119. Li, J., Zhou, L., Li, P.C., Zhu, Q.S., Gao, J.J., Gu, F.N. and Su, F.B. Enhanced fluidized bed methanation over a Ni/Al<sub>2</sub>O<sub>3</sub> catalyst for production of synthetic natural gas. *Chemical Engineering Journal*. 2013, **219**, pp.183-189.
120. Schlesinger, M., Demeter, J. and Greyson, M. Catalyst for producing methane from hydrogen and carbon monoxide. *Industrial & Engineering Chemistry*. 1956, **48**(1), pp.68-70.
121. Kiendl, I., Klemm, M., Clemens, A. and Herrman, A. Dilute gas methanation of synthesis gas from biomass gasification. *Fuel*. 2014, **123**, pp.211-217.
122. Allegue, L.B. and Hinge, J. Biogas upgrading: Evaluation of methods for H<sub>2</sub>S removal. *Danish Technological Institute*. 2014.
123. Manolis, M.T., Merilyn, L. and Howell, H.H. Use of Molecular Sieves to Remove H<sub>2</sub>S and CO<sub>2</sub> from Landfill Gas, Producing a High-Energy Content Methane Stream. In: *The 2006 Spring National Meeting*, 2006.



124. Kim, K., Jeon, S., Vo, C., Park, C.S. and Norbeck, J.M. Removal of hydrogen sulfide from a steam-hydrogasifier product gas by zinc oxide sorbent. *Industrial & engineering chemistry research*. 2007, **46**(18), pp.5848-5854.
125. Abbasian, J., Rehmat, A., Leppin, D. and Bannerjee, D. H<sub>2</sub>S REMOVAL FROM FUEL GAS DURING COAL GASIFICATION. *Argonne National Laboratory*. 1990.
126. Hufton, J., Mayorga, S. and Sircar, S. Sorption-enhanced reaction process for hydrogen production. *AIChE Journal*. 1999, **45**(2), pp.248-256.
127. Lopez Ortiz, A. and Harrison, D.P. Hydrogen production using sorption-enhanced reaction. *Industrial & engineering chemistry research*. 2001, **40**(23), pp.5102-5109.
128. Balasubramanian, B., Ortiz, A.L., Kaytakoglu, S. and Harrison, D. Hydrogen from methane in a single-step process. *Chemical Engineering Science*. 1999, **54**(15-16), pp.3543-3552.
129. Gu, H., Song, G., Xiao, J., Zhao, H. and Shen, L. Thermodynamic analysis of the biomass-to-synthetic natural gas using chemical looping technology with CaO sorbent. *Energy & Fuels*. 2013, **27**(8), pp.4695-4704.
130. Wu, S., Beum, T., Yang, J. and Kim, J. Properties of Ca-base CO<sub>2</sub> sorbent using Ca(OH)<sub>2</sub> as precursor. *Industrial and Engineering Chemistry Research*. 2007, **46**(24), pp.7896-7899.
131. Zeleznik, F.J. and Gordon, S. An analytical investigation of three general methods of calculating chemical-equilibrium compositions. 1960.
132. Gordon, S. and McBride, B.J. Computer program for calculation of complex chemical equilibrium compositions and applications. Part 1: Analysis. 1994.
133. Vitasari, C.R., Jurascik, M. and Ptasiniski, K.J. Exergy analysis of biomass-to-synthetic natural gas (SNG) process via indirect gasification of various biomass feedstock. *Energy*. 2011, **36**(6), pp.3825-3837.

134. Begum, S., Rasul, M.G., Akbar, D. and Ramzan, N. Performance analysis of an integrated fixed bed gasifier model for different biomass feedstocks. *Energies*. 2013, **6**(12), pp.6508-6524.
135. Tremel, A., Gaderer, M. and Spliethoff, H. Small-scale production of synthetic natural gas by allothermal biomass gasification. *International journal of energy research*. 2013, **37**(11), pp.1318-1330.
136. Peters, J.F., Petrakopoulou, F. and Dufour, J. Exergetic analysis of a fast pyrolysis process for bio-oil production. *Fuel Processing Technology*. 2014, **119**, pp.245-255.
137. Ward, J., Rasul, M. and Bhuiya, M. Energy recovery from biomass by fast pyrolysis. *Procedia Engineering*. 2014, **90**, pp.669-674.
138. Onarheim, K., Solantausta, Y. and Lehto, J. Process simulation development of fast pyrolysis of wood using aspen plus. *Energy & Fuels*. 2014, **29**(1), pp.205-217.
139. Sharma, A., Shinde, Y., Pareek, V. and Zhang, D. Process modelling of biomass conversion to biofuels with combined heat and power. *Bioresource Technology*. 2015, **198**, pp.309-315.
140. Isahak, W.N.R.W., Hisham, M.W., Yarmo, M.A. and Hin, T.-y.Y. A review on bio-oil production from biomass by using pyrolysis method. *Renewable and sustainable energy reviews*. 2012, **16**(8), pp.5910-5923.
141. Tech, A. Aspen Physical Property System 11.1. *Aspen Technology, Inc., Cambridge, MA, USA*. 2001.
142. Cozma, P., Wukovits, W., Mămăligă, I., Friedl, A. and Gavrilăscu, M. Modeling and simulation of high pressure water scrubbing technology applied for biogas upgrading. *Clean Technologies and Environmental Policy*. 2015, **17**(2), pp.373-391.
143. Görling, M., Larsson, M. and Alvfors, P. Bio-methane via fast pyrolysis of biomass. *Applied energy*. 2013, **112**, pp.440-447.
144. Dupont, V., Twigg, M.V., Rollinson, A.N. and Jones, J.M. Thermodynamics of hydrogen production from urea by steam reforming

- with and without in situ carbon dioxide sorption. *International Journal of Hydrogen Energy*. 2013, **38**(25), pp.10260-10269.
145. Wang, Q., Luo, J., Zhong, Z. and Borgna, A. CO<sub>2</sub> capture by solid adsorbents and their applications: current status and new trends. *Energy & Environmental Science*. 2011, **4**(1), pp.42-55.
  146. Blamey, J., Manovic, V., Anthony, E.J., Dugwell, D.R. and Fennell, P.S. On steam hydration of CaO-based sorbent cycled for CO<sub>2</sub> capture. *Fuel*. 2015, **150**, pp.269-277.
  147. Remon, J., Broust, F., Volle, G., Garcia, L. and Arauzo, J. Hydrogen production from pine and poplar bio-oils by catalytic steam reforming. Influence of the bio-oil composition on the process. *International Journal of Hydrogen Energy*. 2015, **40**(16), pp.5593-5608.
  148. Cheng, C.B., Shen, D.K., Xiao, R. and Wu, C.F. Methanation of syngas (H<sub>2</sub>/CO) over the different Ni-based catalysts. *Fuel*. 2017, **189**, pp.419-427.
  149. Guo, C.L., Wu, Y.Y., Qin, H.Y. and Zhang, J.L. CO methanation over ZrO<sub>2</sub>/Al<sub>2</sub>O<sub>3</sub> supported Ni catalysts: A comprehensive study. *Fuel Processing Technology*. 2014, **124**, pp.61-69.
  150. Gao, J.J., Jia, C.M., Zhang, M.J., Gu, F.N., Xu, G.W. and Su, F.B. Effect of nickel nanoparticle size in Ni/ $\alpha$ -Al<sub>2</sub>O<sub>3</sub> on CO methanation reaction for the production of synthetic natural gas. *Catalysis Science & Technology*. 2013, **3**(8), pp.2009-2015.
  151. Garbarino, G., Riani, P., Magistri, L. and Busca, G. A study of the methanation of carbon dioxide on Ni/Al<sub>2</sub>O<sub>3</sub> catalysts at atmospheric pressure. *International Journal of Hydrogen Energy*. 2014, **39**(22), pp.11557-11565.
  152. Bette, N., Thielemann, J., Schreiner, M. and Mertens, F. Methanation of CO<sub>2</sub> over a (Mg,Al)O<sub>x</sub> Supported Nickel Catalyst Derived from a (Ni,Mg,Al)-Hydrotalcite-like Precursor. *Chemcatchem*. 2016, **8**(18), pp.2903-2906.
  153. Abu Bakar, W.A.W., Ali, R. and Toemen, S. Catalytic methanation reaction over supported nickel-rhodium oxide for purification of

- simulated natural gas. *Journal of Natural Gas Chemistry*. 2011, **20**(6), pp.585-594.
154. Abello, S., Berruenco, C. and Montane, D. High-loaded nickel-alumina catalyst for direct CO<sub>2</sub> hydrogenation into synthetic natural gas (SNG). *Fuel*. 2013, **113**, pp.598-609.
  155. Yun, H.A.H. and Dupont, V. Thermodynamic analysis of methanation of palm empty fruit bunch (PEFB) pyrolysis oil with and without in situ CO<sub>2</sub> sorption. *AIMS Energy*. 2015, **3**(4), pp.774-797.
  156. Machinery, A. *Supply EFB (Empty Palm Fruit Bunch) Pellet Production Line*. [Online]. 12 January 2015. [Accessed 12 May 2016]. Available from: <https://www.linkedin.com/pulse/supply-efb-empty-palm-fruit-bunch-pellet-production-line-bella-wu>
  157. Zhengzhou Azeus Machinery Co., L. *Biopellet Machines*. [Online]. [Accessed 12 May 2016]. Available from: <http://biopelletmachine.com/product/sawdust-making-machine/EFB-shredder-crushing-machine.html>
  158. Amos, W.A. *Report on Biomass Drying Technology*. Colorado, U.S.: Midwest Research Institute, 1998.
  159. Fagernäs, L., Brammer, J., Wilén, C., Lauer, M. and Verhoeff, F. Drying of biomass for second generation synfuel production. *Biomass and Bioenergy*. 2010, **34**(9), pp.1267-1277.
  160. Hebi Yidafeng Industrial Co., L. *EFB shredder--machine to crush empty fruit bunches into fiber quickly--exported to Malaysia, Thailand and Indonesia* [Online]. [Accessed 12 May 2016]. Available from: [http://hbydf.en.alibaba.com/product/60263725709-801183376/EFB\\_shredder\\_machine\\_to\\_crush\\_empty\\_fruit\\_bunches\\_in\\_to\\_fiber\\_quickly\\_exported\\_to\\_Malaysia\\_Thailand\\_and\\_Indonesia.html](http://hbydf.en.alibaba.com/product/60263725709-801183376/EFB_shredder_machine_to_crush_empty_fruit_bunches_in_to_fiber_quickly_exported_to_Malaysia_Thailand_and_Indonesia.html)
  161. Zhengzhou Azeus Machinery Co., L. *Biopellet Machines*. [Online]. [Accessed 12 May 2016]. Available from: <http://biopelletmachine.com/product/sawdust-making-machine/wood-chipper-drum-type.html>

162. Solantausta, Y. and Asplund, D. *Puunkäyttö polttoaineena II. Polttoaineominaisuudet*. Poltto-ja voiteluainelaboratorio: VTT: Espoo, Finland, 1979.
163. Rensfelt, E., Lindman, N., Bjerle, S. and Kelen, T. *Raport inom NE-området Syntetiska drivmedel*. KTH Royal Institute of Technology: Stockholm, Sweden, 1980.
164. Sukiran, M.A., Kheang, L.S., Bakar, N.A. and May, C.Y. Production and characterization of bio-char from the pyrolysis of empty fruit bunches. *American Journal of Applied Sciences*. 2011, **8**(10), p.984.
165. Pimenidou, P. and Dupont, V. Characterisation of palm empty fruit bunch (PEFB) and pinewood bio-oils and kinetics of their thermal degradation. *Bioresource technology*. 2012, **109**, pp.198-205.
166. Jones, S.B., Valkenburg, C., Walton, C.W., Elliott, D.C., Holladay, J.E., Stevens, D.J., Kinchin, C. and Czernik, S. *Production of gasoline and diesel from biomass via fast pyrolysis, hydrotreating and hydrocracking: a design case*. 2009.
167. Dupont, V., Yun, H.A.H., White, R. and Tande, L. High methane conversion efficiency by low temperature steam reforming of bio-feedstock. In: *REGATEC 2017, May 2017, Pacengo (Verona), Italy*. Sweden: Renewable Technology International AB, 2017.
168. Garcia-Perez, M., Chaala, A., Pakdel, H., Kretschmer, D. and Roy, C. Characterization of bio-oils in chemical families. *Biomass and Bioenergy*. 2007, **31**(4), pp.222-242.
169. Jecht, U. *Flue Gas Analysis in Industry: Practical guide for Emission and Process Measurements*. testo, 2004.
170. ENERGY.GOV. *Energy Tips-Process Heating*. November 2007 ed. U.S. Department of Energy Washington: Industrial Technologies Program Energy Efficiency and Renewable Energy, 2007.
171. Woodward, C. High-temperature methanation catalyst for SNG applications. *Am. Chem. Soc., Div. Fuel Chem., Prepr.:(United States)*. 1976, **21**(4).

172. Perkins, E. and Innovates, A. Fundamental Geochemical Processes Between CO<sub>2</sub>, Water and Minerals. *Alberta Innovates–Technology Futures*.
173. Lind, F., Heyne, S. and Johnsson, F. What is the efficiency of a biorefinery? 2012.
174. Channiwala, S. and Parikh, P. A unified correlation for estimating HHV of solid, liquid and gaseous fuels. *Fuel*. 2002, **81**(8), pp.1051-1063.
175. Duret, A., Friedli, C. and Maréchal, F. Process design of Synthetic Natural Gas (SNG) production using wood gasification. *Journal of cleaner production*. 2005, **13**(15), pp.1434-1446.
176. Kerdsuwan, S. and Laohalidanond, K. *Renewable energy from palm oil empty fruit bunch*. INTECH Open Access Publisher, 2011.
177. Yang, H., Yan, R., Chen, H., Lee, D.H., Liang, D.T. and Zheng, C. Pyrolysis of palm oil wastes for enhanced production of hydrogen rich gases. *Fuel Processing Technology*. 2006, **87**(10), pp.935-942.
178. Ruengvilairat, P., Tanatavikorn, H. and Vitidsant, T. Bio-oil production by pyrolysis of oil palm empty fruit bunch in nitrogen and steam atmospheres. *Journal of Sustainable Bioenergy Systems*. 2012, **2**(4), p.75.
179. Mohammed, M., Salmiaton, A., Azlina, W.W. and Amran, M.M. Gasification of oil palm empty fruit bunches: a characterization and kinetic study. *Bioresource technology*. 2012, **110**, pp.628-636.
180. Shariff, A., Aziz, N.S.M. and Abdullah, N. Slow pyrolysis of oil palm empty fruit bunches for biochar production and characterisation. *Journal of Physical Science*. 2014, **25**(2), p.97.